LOS ALAMOS SCIENTIFIC LABORATORY
of the
University of California

LOS ALAMOS • NEW MEXICO

Biological and Medical Research Group (H-4) of the Health Division -- Annual Report July 1965 Through June 1966

UNITED STATES
ATOMIC ENERGY COMMISSION
CONTRACT W-7405-ENG. 36

Printed in USA. Price ~~$6.00~~. Available from the Clearinghouse for Federal Scientific and Technical Information, National Bureau of Standards, United States Department of Commerce, Springfield, Virginia

LA-3610-MS
UC-48, BIOLOGY
AND MEDICINE
TID-4500

LOS ALAMOS SCIENTIFIC LABORATORY
of the
University of California
LOS ALAMOS • NEW MEXICO

Report written: July 1966

Report distributed: November 18, 1966

Biological and Medical Research Group (H-4) of the Health Division -- Annual Report July 1965 Through June 1966

Group Leader, W. H. Langham
Division Leader, T. L. Shipman

CONTENTS

	Page
CHAPTER 1 - INTRODUCTION	13
CHAPTER 2 - CELLULAR RADIOBIOLOGY SECTION	17
1. Premitotic Radiosensitivity of Mammalian Cells. I. Timing and Dose Dependency of the Radiation-Induced G_2 Delay R. A. Walters and D. F. Petersen	17
2. Premitotic Radiosensitivity of Mammalian Cells. II. Radiation Effects on Terminal Protein Synthesis Essential for Division R. A. Walters and D. F. Petersen	24
3. Methylation of Mammalian RNA A. G. Saponara, M. D. Enger, and J. L. Hanners	28
4. Effects of Inhibitors of Protein and RNA Synthesis on Regeneration of Surface Sialic Acid of Cells in Culture P. M. Kraemer	37
5. Energy Metabolism of Cultured Mammalian Cells W. D. Currie and C. T. Gregg	41
6. Automatic Cell Counter for Mammalian Cells in Suspension Culture E. C. Anderson, D. L. Carlson, R. B. Glascock, J. H. Larkins, J. D. Perrings, and R. A. Walters	44

7. Intercellular Control of Development of Competence in Cultures of Hemophilus Influenzae by a Cell-Free Product of Cell Metabolism 50

B. J. Barnhart and S. H. Cox

8. Studies of Horse Liver Alcohol Dehydrogenase: Structural Changes during Acid Inactivation 54

C. H. Blomquist

Abstracts of Cellular Radiobiology Section Publications and Manuscripts Submitted

1. Inhibition of the Respiration of Cultured Mammalian Cells by Oligomycin 61

W. D. Currie and C. T. Gregg

2. Rapid Estimation of Fast-Neutron Doses following Radiation Exposure in Criticality Accidents: The $S^{32}(n,p)P^{32}$ Reaction in Body Hair 61

D. F. Petersen

3. Mengovirus Replication. III. Virus Reproduction in Chinese Hamster Ovary Cells 61

R. A. Tobey and E. W. Campbell

4. Mengovirus Replication. IV. Inhibition of Chinese Hamster Ovary Cell Division as a Result of Infection with Mengovirus 62

R. A. Tobey, D. F. Petersen, and E. C. Anderson

5. Kinetics of Bacteriophage λ Deoxyribonucleic Acid Infection of Escherichia Coli 62

B. J. Barnhart

6. Sialic Acid and the Trypsin Barrier 62

P. M. Kraemer

7. Incorporation of [^{3}H]Uridine and [Me-^{14}C]-Methionine into Chinese-Hamster Cell Ribonucleic Acid 63

A. G. Saponara and M. D. Enger

8. Neutron Activation of Sulfur in Hair: Application in a Nuclear Accident Dosimetry Study 63

D. F. Petersen and W. H. Langham

9. Sialic Acid of Mammalian Cell Lines 64

P. M. Kraemer

10. Regeneration of Sialic Acid on the Surface of Chinese Hamster Cells in Culture. I. General Characteristics of the Replacement Process 64

P. M. Kraemer

11. Life Cycle Analysis of Mammalian Cells. III. The Inhibition of Division in Chinese Hamster Cells by Puromycin and Actinomycin 64

R. A. Tobey, D. F. Petersen, E. C. Anderson, and T. T. Puck

12. Preparation and Assay of Phosphorylating Submitochondrial Particles: Particles from Rat Liver Prepared by Drastic Sonication 65

C. T. Gregg

13. Configuration Change of Surface Sialic Acid during Mitosis 65

P. M. Kraemer

14. Effects of Uncouplers of Oxidative Phosphorylation on the Infection of Escherichia Coli K12 by Phage-λ DNA 66

B. J. Barnhart

CHAPTER 3 - MOLECULAR RADIOBIOLOGY SECTION 67

1. Purification of Ribonucleic Acid Polymerase from Escherichia Coli 67

R. L. Ratliff, T. T. Trujillo, and D. A. Smith

2. Enzymatic Synthesis of Short Polydeoxyribonucleotides 74

F. N. Hayes and V. E. Mitchell

3. Simultaneous Use of Two or More Deoxynucleotide 5'-Triphosphates for Polydeoxynucleotide Synthesis with Terminal Deoxynucleotidyl Transferase from Calf Thymus Glands 79

R. L. Ratliff, T. T. Trujillo, D. G. Ott, and D. E. Hoard

4. P^1, P^2-Pyrophosphates as Initiators in the Terminal Deoxyribonucleotide Transferase Reaction 83

A. W. Schwartz

5. Synthesis of Oligo- and Polydeoxynucleotides by Enzymatic Means 90

D. E. Hoard and W. B. Goad

6. Investigation of the Mode of Action of Nucleases Using Defined Polydeoxynucleotide Substrates 95

D. E. Hoard

7. Chemical Synthesis of Oligodeoxyribonucleotides 102

D. L. Williams

8. Deoxyribonucleoside Triphosphate Derivatives 115

E. Hansbury and D. G. Ott

9. Oligonucleotide Chromatography 118

A. Murray

10. Organometallic Compounds in Nucleic Acid Chemistry 135

V. N. Kerr

11. Computer Analysis of Ultraviolet Spectra 138

G. T. Fritz

Abstracts of Molecular Radiobiology Section Publications and Manuscripts Submitted

1. High-Resolution Disc Electrophoresis of Histones I. An Improved Method 142

G. R. Shepherd and L. R. Gurley

2. High-Resolution Disc Electrophoresis of Histones II. Application to Whole and Fractionated Preparations from Various Laboratories 142

L. R. Gurley and G. R. Shepherd

3. Unprimed Synthesis of Polyadenylate and Polyuridylate Catalyzed by Ribonucleic Acid Polymerase 143

D. A. Smith, R. L. Ratliff, T. T. Trujillo, D. L. Williams, and F. N. Hayes

4. Disc Electrophoresis of Bovine Thymus Histones 143

G. R. Shepherd and L. R. Gurley

5. Nuclear Histones and Early Embryogenesis of the Chick 143

C. W. Kischer, L. R. Gurley, and G. R. Shepherd

6. The Synthesis and Evaluation of Some New Trans-1,2-Diarylethylenes as Liquid Scintillators 144

G. H. Daub, F. N. Hayes, J. L. Schornick, D. W. Holty, and L. G. Ionescu

CHAPTER 4 - MAMMALIAN RADIOBIOLOGY SECTION 145

1. Dose Rate-Total Dose Effect on Survival in Mice 145

J. F. Spalding, O. S. Johnson, and R. F. Archuleta

2. Injury and Recovery of Bone Marrow during and following Continuous Low-Intensity Gamma Irradiation 149

J. F. Spalding, N. J. Basmann, and R. F. Archuleta

3. Comparative Aftersurvival Times of Mice following Graded First and Graded but Reversed Second Exposures 155

J. F. Spalding and O. S. Johnson

4. A Test of the Effective Residual Dose Concept of Radiation Injury in Mice 159

J. F. Spalding, N. J. Basmann, and R. F. Archuleta

Abstracts of Mammalian Radiobiology Section Publications and Manuscripts Submitted

1. Acute Radio-Sensitivity as a Function of Age in Mice 164

J. F. Spalding, O. S. Johnson, and R. F. Archuleta

2. Reduction in Life Expectancy as a Measure of Radiation-Induced Genetic Damage in Mice 164

J. F. Spalding and M. R. Brooks

3. Heritable Radiation Effects on Mouse Body and Organ Weights, Fat Deposition, Cellular Enzymes, and Blood 164

R. R. J. Chaffee, J. C. Hensley, and J. F. Spalding

4. Comparative Repopulation Recovery of Circulating Erythrocytes following Graded Second Gamma-Ray Exposures in Mice 165

J. F. Spalding

5. Reproductivity and Life Span of Mouse Populations from 25 Generations of Irradiated Sires 165

J. F. Spalding, M. R. Brooks, and P. McWilliams

CHAPTER 5 - MAMMALIAN METABOLISM SECTION 166

1. Residence Time of Fallout Cesium-137 in a Control Population following the July 1964 Peak 166

C. R. Richmond and J. E. London

2. Cesium-137 Content of New Mexico Control Subjects: July 1965 through June 1966 170

C. R. Richmond, J. E. London, and J. S. Wilson

3. Loss of Whole-Body Cesium-137 in Humans 177

J. E. Furchner, J. E. London, G. A. Drake, and C. R. Richmond

4. Retention of Cesium-137 by the White-Tailed Rat 181

J. E. Furchner, G. A. Drake, and C. R. Richmond

5. Retention of Silver-110 by Mice 186

J. E. Furchner, G. A. Drake, and C. R. Richmond

6. Effective Retention of Silver-110 by Dogs after Oral Administration 191

J. E. Furchner, G. A. Drake, and C. R. Richmond

7. Whole-Body Retention of Cadmium-109 by Mice following Oral, Intraperitoneal, and Intravenous Administration 195

C. R. Richmond, J. S. Findlay, and J. E. London

8. Whole-Body Retention of Barium-133 by Monkeys 201

C. R. Richmond and J. E. London

9. Evaluation of Detector Variance 206

J. E. Furchner, G. A. Drake, and P. C. McWilliams

Abstracts of Mammalian Metabolism Section Publications and Manuscripts Submitted

1. Enhancement of Cesium-137 Excretion by Rats Maintained Chronically on Ferric Ferrocyanide 210

C. R. Richmond and D. E. Bunde

2. Half-Life of Iodine-125 210

C. R. Richmond and J. S. Findlay

3. Comparative Metabolism of Radionuclides in Mammals. III. Retention of Manganese-54 by Four Mammalian Species 211

J. E. Furchner, C. R. Richmond, and G. A. Drake

4. Long-Term in vivo Retention of Cerium-144 by Beagles 211

C. R. Richmond and J. E. London

5. Cesium-137 Body Burdens in Man: 1956-1966 212

C. R. Richmond

6. Movement of Discrete Particles in the 100- to 200-Micron Diameter Range through the Gastrointestinal Tract of Laboratory Animals and Man 212

C. R. Richmond and J. E. Furchner

CHAPTER 6 - BIOPHYSICS SECTION 214

1. In vivo Measurement of Plutonium-239 Lung Burdens in Humans 214

P. N. Dean and J. H. Larkins

2. Further Development of the Cell Separator 222

M. J. Fulwyler

3. Detection of Biological Cells by Light-Scattering 225

M. A. Van Dilla

4. Volume Distribution of Normal Human Erythrocytes and Leucocytes 234

M. A. Van Dilla and J. M. Hardin

5. Volume Distribution of Mouse Bone Marrow Cells 239

M. A. Van Dilla, J. M. Hardin, and C. F. Bidwell

6. Amino Acid Analysis by Computer 248

P. N. Dean and C. N. Roberts

Abstracts of Biophysics Section Publications and Manuscripts Submitted

1. Some Biological Aspects of Radioactive Microspheres 262

   W. H. Langham, C. R. Richmond, J. C. Hensley, P. N. Dean, and M. A. Van Dilla

2. Computer Reduction of Metabolic Data Obtained from Scintillation Counters 262

   P. N. Dean

3. Electronic Separation of Biological Cells by Volume 262

   M. J. Fulwyler

4. Automatic Data Acquisition, Reduction and Analysis 262

   P. N. Dean and C. R. Richmond

5. Computer Analysis of Cell Volume Distributions 263

   P. N. Dean

6. Isolation of Normal and Abnormal Circulating Cells by an Electronic Particle Separator 263

   I. U. Boone, M. J. Fulwyler, and M. W. Stewart

7. The Cell Separator -- Design and Usage 264

   M. J. Fulwyler

8. Erythrocyte Volume Distribution during Recovery from Radiation-Induced Bone Marrow Arrest 264

   M. A. Van Dilla and J. F. Spalding

9. Volume Distribution and Separation of Normal Human Leucocytes 265

   M. A. Van Dilla, M. J. Fulwyler, and I. U. Boone

CHAPTER 1

INTRODUCTION

The increased emphasis over the past 5 years on attempts to contribute to the understanding of radiation effects at the cellular- and molecular-levels has been primarily responsible for expansion of the biological and medical research program at Los Alamos. These investigations have largely taken the direction of studying some of the detailed processes of information transfer in in vitro biological systems and the sequential biochemistry of phased mammalian cells grown in culture medium. The eventual objective of these investigations is to determine the influence of radiation, radioactive materials, and drugs of known biological effect on the previously established cellular and molecular processes. The purpose of studying drug effects is to observe whether there is parallelism between radiation effects and the known action of the drug. As an example, is there similarity between cycloheximide inhibition of synthesis of essential protein for cell division and inhibition of cell division by irradiation?

Many of these new projects are now yielding sufficient results to justify beginning of radiation studies which will be reflected in future program direction. Expansion of the more fundamental aspects of the program has essentially leveled off insofar as staff-level personnel are concerned. At the present time, however, the staff-to-technician plus research assistant personnel ratio is about 0.9. Some expansion in the latter category is needed and contemplated to increase the efficiency of utilization of staff-level scientists.

Past emphasis of the cellular radiobiology aspect of the program has resulted in increased emphasis on biophysics and instrumentation, largely along the lines of developing electronic means of quantitatively monitoring the rate of growth of cells in culture medium and on means of actually separating living cells electronically on the basis of their volume. Other means of studying the properties of

cells and cell populations and separating living cells electronically (e.g., fluorescence and light absorption and scattering) are being investigated.

Although over 50 percent of the present effort is devoted to more fundamental studies at the cellular- and molecular-levels, the applied aspects of the program are being re-emphasized, particularly along the lines of potential risks of radiation exposure and contamination from space applications of nuclear energy in rocket propulsion systems and auxiliary power supplies. The nuclear weapons incident in Spain in January 1966 has focused programmatic attention on the need for development of methods of diagnosing plutonium exposure to replace or to supplement the standard urine analysis method, which appears inadequate for inhalation exposures to insoluble radioactive particulates. Sophisticated proportional counters and solid-state detector systems are being considered for this purpose.

A summary of the past year's research effort can be seen in the Table of Contents in the preceding pages.

The present group organization and personnel are shown in the Table of Organization. New personnel are as follows:

Staff Members

C. H. Blomquist, Ph.D., Cellular Radiobiology Section
L. M. Holland, D.V.M., Mammalian Radiobiology Section
P. F. Mullaney, Ph.D., Biophysics Section
K. D. Munkres, Ph.D., Cellular Radiobiology Section
B. R. Burchill, Ph.D., LASL Postdoctoral Appointment, Cellular Radiobiology Section

Research Assistant

E. L. Martinez, Jr., B.S., Molecular Radiobiology Section

Clerk-Typist

J. H. Montague

Technicians

M. T. Butler, Biophysics Section
E. Mueller, Cellular Radiobiology Section
E. C. Wilmoth, Cellular Radiobiology Section

Animal Caretaker

F. Benavidez, Mammalian Metabolism Section

The following terminations occurred:

Staff Members

R. R. J. Chaffee, Ph.D., Cellular Radiobiology Section
J. C. Hensley, D.V.M., Mammalian Radiobiology Section

Research Assistant

F. Sapir, M.S., Cellular Radiobiology Section

Technician

V. M. Gibbs, Cellular Radiobiology Section

Animal Caretaker

R. C. Adams, Mammalian Radiobiology Section

The previous annual report of the Biological and Medical Research Group (July 1964 through June 1965) appeared as Los Alamos Scientific Laboratory Report LA-3432-MS (1965).

BIOMEDICAL RESEARCH GROUP

W. H. Langham, Ph.D., Group Leader
D. G. Ott, Ph.D., Alternate Group Leader
O. S. Johnson, B.S., Administrative Deputy
E. M. Sullivan, Secretary
J. H. Montague, Clerk-Typist

CELLULAR RADIOBIOLOGY SECTION

D. F. Petersen, Ph.D., Section Leader

Staff Members

E. C. Anderson, Ph.D.
B. J. Barnhart, Ph.D.
C. H. Blomquist, Ph.D.
I. U. Boone, M.D.
M. D. Enger, Ph.D.
C. T. Gregg, Ph.D.
E. A. Hyatt, Ph.D.
P. M. Kraemer, Ph.D.
K. D. Munkres, Ph.D.
A. G. Saponara, Ph.D.
R. A. Tobey, Ph.D.

Research Assistants

E. W. Campbell, B.S.
S. G. Carpenter, B.A.
S. H. Cox, B.A.
P. M. LaBauve, B.A.
P. C. Sanders, M.S.

Technicians

J. L. Hanners
E. Mueller
E. C. Wilmoth

Postdoctoral Appointees

B. R. Burchill, Ph.D.
W. D. Currie, Ph.D.

ARMU Doctoral Candidate

R. A. Walters

MOLECULAR RADIOBIOLOGY SECTION

F. N. Hayes, Ph.D., Section Leader

Staff Members

L. R. Gurley, Ph.D.
D. E. Hoard, Ph.D.
V. N. Kerr, M.A.
A. Murray, M.S.
R. L. Ratliff, Ph.D.
G. R. Shepherd, Ph.D.
D. A. Smith, Ph.D.
T. T. Trujillo, B.S.
D. L. Williams, M.S.

Research Assistants

G. T. Fritz, B.S.
E. Hansbury, M.A.
E. H. Lilly, B.S.
A. M. Martinez, B.S
E. L. Martinez, Jr., B.S.
B. J. Noland, B.A.
C. N. Roberts, B.A.

Technician

V. E. Mitchell

Postdoctoral Appointee

A. W. Schwartz, Ph.D.

MAMMALIAN RADIOBIOLOGY SECTION

J. F. Spalding, Ph.D., Section Leader

Staff Member

L. M. Holland, D.V.M.

Research Assistants

C. F. Bidwell, M.S.
M. R. Brooks, B.Ch.E.

Technicians

R. F. Archuleta
N. J. Basmann

Animal Caretakers

F. Archuleta
J. E. Atencio
S. Cordova
L. Ortiz
A. Trujillo
F. Valdez
J. G. Valdez
E. A. Vigil

MAMMALIAN METABOLISM SECTION

C. R. Richmond, Ph.D., Section Leader

Staff Member

J. E. Furchner, Ph.D.

Research Assistants

G. A. Drake, B.S.
J. E. London, B.S.
J. S. Wilson, B.S.

Animal Caretakers

F. Benavidez
R. Martinez

BIOPHYSICS SECTION

M. A. Van Dilla, Ph.D., Section Leader

Staff Members

P. N. Dean, M.A.
M. J. Fulwyler, B.S.
J. H. Larkins, B.S.*
P. F. Mullaney, Ph.D.
J. D. Perrings

Research Assistant

J. M. Hardin, M.S.

Electronics Technicians

M. T. Butler
L. J. Carr

*Casual employee.

CHAPTER 2

CELLULAR RADIOBIOLOGY SECTION

PREMITOTIC RADIOSENSITIVITY OF MAMMALIAN CELLS. I. TIMING AND DOSE DEPENDENCY OF THE RADIATION-INDUCED G_2 DELAY (R. A. Walters* and D. F. Petersen)

INTRODUCTION

Improved techniques for life-cycle analysis (1) have permitted the accurate description of several temporal markers in the G_2 segment of the life cycle of mammalian cells. These markers locate terminal RNA and protein synthesis essential for cell division and indicate that several necessary features of cell division involve biosynthesis of macromolecules late in the life cycle (1). The precise timing afforded by automated cell counting equipment developed in this Laboratory (2) has allowed examination of the well established radiation-induced G_2 delay of mammalian cells (3-5) in terms of both onset and duration as a function of radiation dose. The results indicate that the onset of G_2 delay is dose-independent, is characteristic for specific cell lines, and occurs late in G_2. The duration of G_2 delay is directly proportional to dose in the region from 25 to 800 rads. The results do not substantiate several previous claims that radiosensitivity measured by division delay varies with position of the cell in the life cycle (6,7).

MATERIALS AND METHODS

Three cell lines were employed for these studies: Chinese hamster ovary (CHO), HeLa S-3, and the murine lymphoma of

---

*Associated Rocky Mountain Universities, Inc., Predoctoral Fellow, Colorado State University.

the mouse (L5178-Y). CHO cells were grown in Ham's F-10 medium supplemented with 10 percent calf and 5 percent fetal calf sera; HeLa S-3 were cultured in Eagle's basal medium plus 5 percent calf serum, and L5178-Y were grown in Manson's L-1 modification of Fischer's medium plus 5 percent calf serum. All growth media contained antibiotics. Automated counting equipment capable of providing routine population estimates to + 0.4 percent at intervals as frequent as every 4 minutes is described elsewhere in this report (2). Synchrony in CHO populations was induced as reported previously (8) using a single blockade with 10 mM thymidine. X-radiation exposures were performed at 37°, 250 KVP, 30 ma, with Thoraeus II filtration. All dose values expressed have been converted to absorbed dose at dose rates of 50 and 150 rads/min.

RESULTS AND DISCUSSION

A detailed discussion of the theory of life-cycle analysis by cell counting and a comparison with other methods have been presented (1). Briefly, cells are allowed to complete division, and the cell concentration is determined at frequent intervals. If, at any time (t_0), an inhibitor is introduced which impedes progress of the cells through the life cycle at a point (t_1) before completion of mitosis, the population would increase normally from t_0 to t_1. The logarithm of the cell number would increase linearly from t_0 to t_1 and then flatten to zero slope. The point of action is thus precisely defined by the intersection of the growth curve and the horizontal line.

Results shown in Fig. 1 demonstrate that cell division continued normally for a measurable amount of time following irradiation and then ceased. These results are typical and provide the basis for calculations of division delay for all three cell lines following radiation doses ranging from 25 to 800 rads summarized in Table 1. These data clearly demonstrate that in each case the onset of division delay is dose-independent.

A characteristic of division delay in mammalian cells which has been described repeatedly is the spontaneous recovery exhibited following irradiation. Figure 1 also demonstrates the typical recovery pattern following exposure to a wide range of doses and indicates the dose-dependence of division delay. Complete data for the three cell lines are summarized

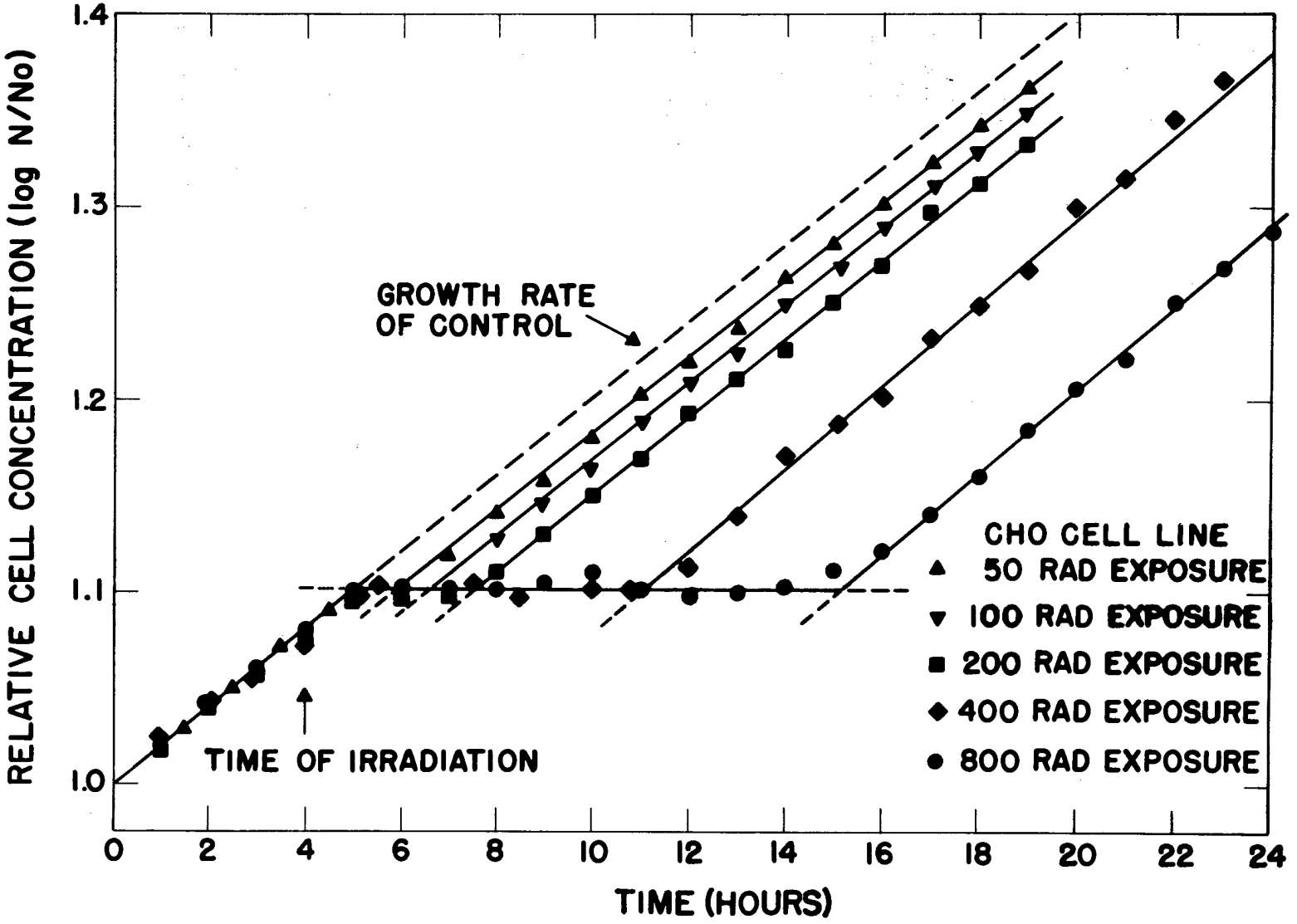

Fig. 1. Time of action and duration of division delay of a random CHO cell population exposed to varying doses of X irradiation.

TABLE 1. TIME OF ACTION OF X IRRADIATION ON DIVISION OF THREE MAMMALIAN CELL LINES

Cell Line	Dose (rads)	Time from Irradiation to Cessation of Division (hours)	Average Effective Lag Time ± S. D. (Mean) (hours)
CHO (T_G = 15.2 ± 0.2 hours)	25	0.91*	
	50	0.95	
	200	0.91	
	400	0.97	
	800	1.02	0.95 ± 0.06 (pooled data)
HeLa S-3 (T_G = 18.3 ± 0.2 hours)	25	1.10	
	50	1.18	
	100	1.10	
	200	1.23	
	300	1.22	1.18 ± 0.10 (pooled data)
L5178-Y (T_G = 9.2 ± 0.3 hours)	50	1.04	
	100	0.92	
	200	0.97	
	400	0.99	
	600	1.04	1.02 ± 0.09 (pooled data)

*Each value is the mean of a minimum of 4 separate experiments.

in Table 2. Over the dose range studied here, duration of delay increased linearly with dose, yielding delay values of 0.012 hr/rad for CHO, 0.024 hr/rad for HeLa S-3, and 0.011 hr/rad for L5178-Y.

The data in Fig. 2 show a clearly defined growth curve, a measurable delay, and resumption of the preirradiation division rate following recovery, with no evidence that a particular segment of the population traversed the life cycle at an appreciably faster or slower rate than any other. The data indicate that radiosensitivity as measured by division delay does not necessarily vary with position of the cell in the life cycle.

REFERENCES

(1) R. A. Tobey, D. F. Petersen, E. C. Anderson, and T. T. Puck, Biophys. J. (in press).

(2) E. C. Anderson, D. L. Carlson, R. B. Glascock, J. H. Larkins, J. D. Perrings, and R. A. Walters, this report, p. 44.

(3) L. S. Kelly, Prog. Biophys. Biophys. Chem. 8, 144 (1957).

(4) A. C. Upton, Exp. Cell Res., Suppl. 9, 538 (1963).

(5) L. J. Tolmach, Ann. N. Y. Acad. Sci. 95, 743 (1961).

(6) S. Mak and J. E. Till, Radiation Res. 20, 600 (1963).

(7) T. Terasima and L. J. Tolmach, Biophys. J. 3, 11 (1963).

(8) D. F. Petersen and E. C. Anderson, Nature 203, 642 (1964).

TABLE 2. DURATION OF RADIATION-INDUCED DIVISION DELAY IN THREE MAMMALIAN CELL LINES

Cell Line	Dose (rads)	Division Delay (hours)
CHO (T_G = 15.2 ± 0.2 hours)	25	0.63*
	50	0.83
	100	1.33
	200	2.20
	400	5.74
	800	9.60
HeLa S-3 (T_G = 18.3 ± 0.2 hours)	25	0.79
	50	1.61
	100	2.80
	200	4.70
	400	7.52
L5178-Y (T_G = 9.2 ± 0.3 hours)	50	1.03
	100	1.52
	200	2.86
	400	5.05
	600	6.87

*Each value is the mean of a minimum of 4 separate experiments.

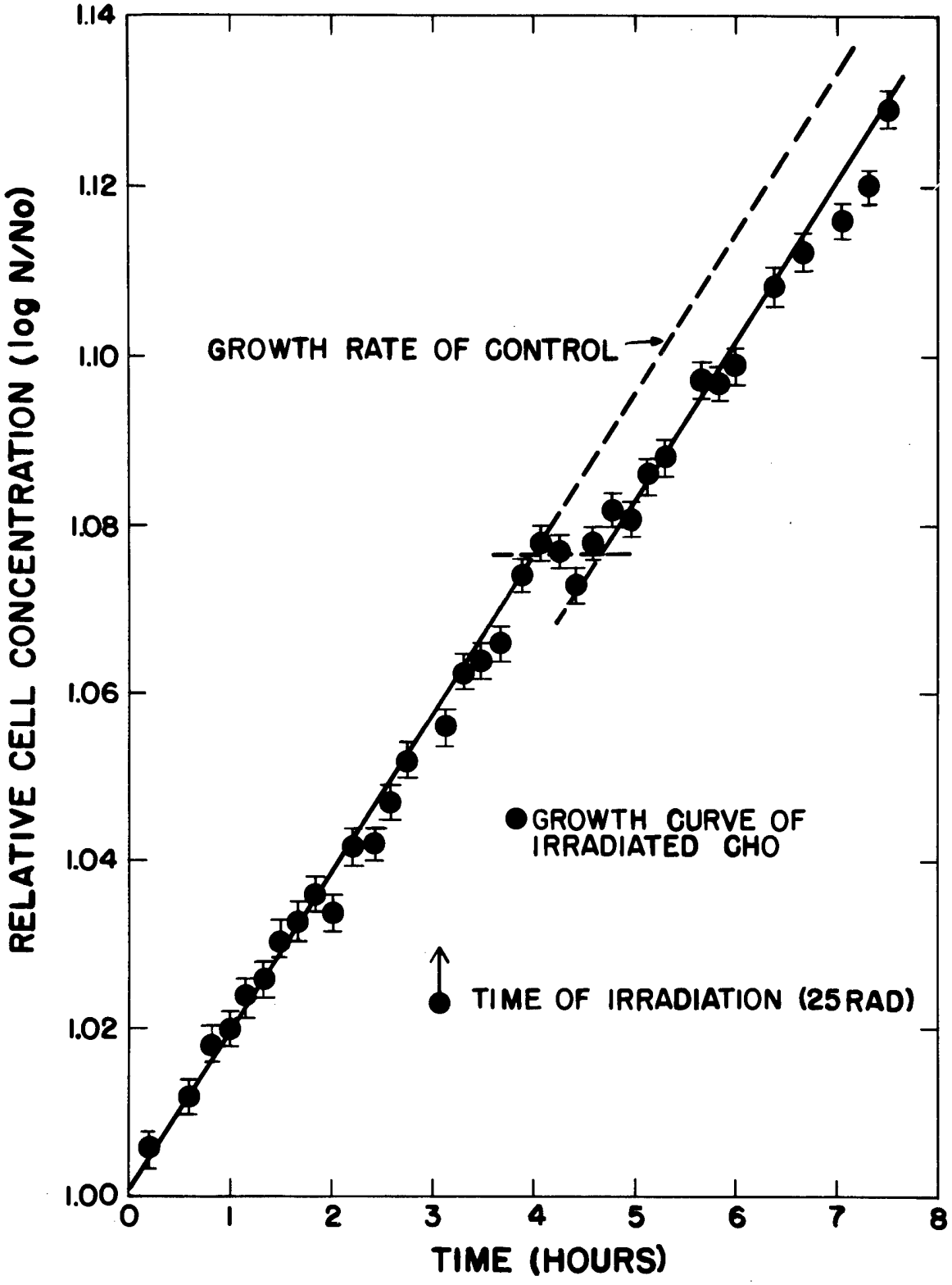

Fig. 2. Influence of small doses of X rays on the growth and division delay in CHO cells.

PREMITOTIC RADIOSENSITIVITY OF MAMMALIAN CELLS. II. RADIATION EFFECTS ON TERMINAL PROTEIN SYNTHESIS ESSENTIAL FOR DIVISION (R. A. Walters* and D. F. Petersen)

INTRODUCTION

The timing of the terminal radiosensitive event of G_2 in mammalian cells has been described (1). This point, 0.95 $\pm$ 0.06 hour prior to division in CHO cells, is experimentally indistinguishable from the point of action of cycloheximide, an inhibitor of protein synthesis (2). The similarity of the times of action of radiation and inhibition of protein synthesis raised the question of possible involvement of terminal protein synthesis in radiation-induced G_2 delay. Experiments were designed, therefore, to test this hypothesis. The results indicate that no recovery from radiation-induced division delay occurs in the presence of the protein inhibitor and that upon release from the influence of cycloheximide the normal pattern of recovery of untreated cells is duplicated.

MATERIALS AND METHODS

Chinese hamster ovary (CHO) cells (3) were cultivated in Ham's F-10 medium as described previously (2). All cell counting was performed by an automatic cell counter (4) which routinely provided data to + 0.5 percent precision. Radiation exposures were performed at 37°, 250 KVP, 30 ma, with Thoraeus II filtration, at absorbed dose rates of 150 rads/min. Cycloheximide (Actidione, Upjohn) was added at final concentrations of 2 μg/ml, and cells were released into prewarmed, conditioned medium to ensure a minimum lag time before resumption of growth. Details of the time sequence of radiation, cycloheximide addition, and resuspension in growth medium are described in the figure legend (Fig. 1).

RESULTS AND DISCUSSION

The control growth curve of Fig. 1 indicates the continued stable growth of the culture in the absence of intervention.

---

*Associated Rocky Mountain Universities, Inc., Predoctoral Fellow, Colorado State University.

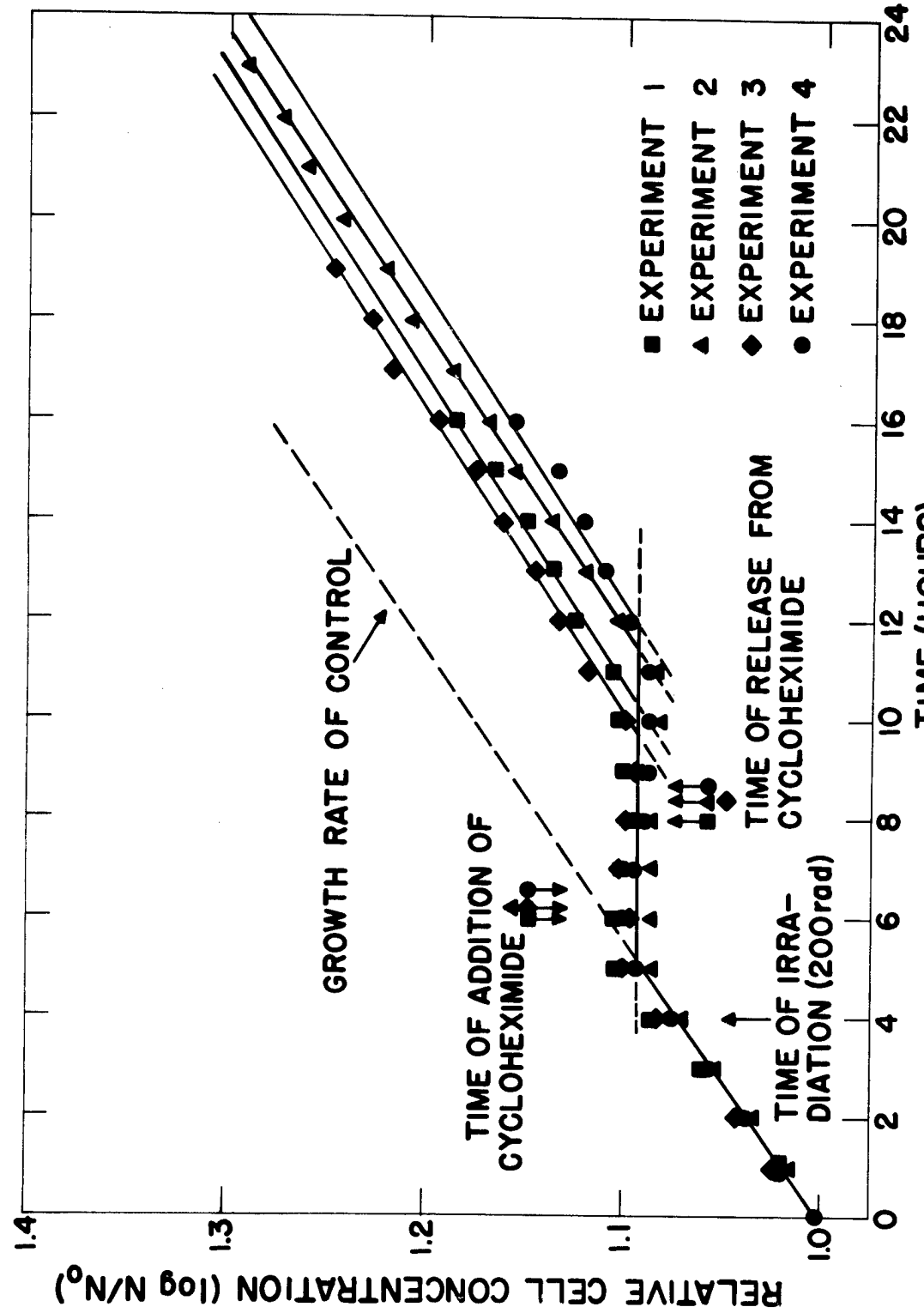

Fig. 1. Influence of time of addition of cycloheximide on recovery from X irradiation in CHO cells.

The irradiated culture exhibited the typical G_2 lag 60 minutes after exposure to 200 rads and the typical resumption of growth at the preirradiated rate 3 hours later. Unirradiated cells treated with cycloheximide for a 2-hour interval and then released by centrifugation, washing, and resuspension in prewarmed, conditioned medium resumed growth at the normal rate 70 minutes after release. Cells exposed to 200 rads were allowed to enter G_2 lag and then were inhibited for 2 hours with cycloheximide, as shown in Fig. 1. Under these conditions, the subsequent recovery interval was additive as though the radiation defect could not be repaired in the presence of the protein synthesis inhibitor but could resume the recovery process at the normally expected rate after removal of cycloheximide.

At their present stage of development, these experiments do not provide rigorous proof but do suggest that one of the immediate biosynthetic defects involved in radiation-induced G_2 lag is an effect on terminal protein synthesis essential for division. However, the method is sensitive only to the last of a potential series of defects suggested by the absence of a differential sensitivity of cells at various stages of development pointed out in the previous report (1).

It must be emphasized that our concern here is centered on biochemical events occurring within the generation in which a cell is exposed and involves radiation doses which may eventually impair colony formation but which are much lower than doses required for interphase death. Moreover, we are in agreement that, even after much larger doses, irradiated cells divide once before they die (1,5). These experiments are being continued to determine how late in the recovery process the inhibition of protein synthesis will arrest division.

REFERENCES

(1) R. A. Walters and D. F. Petersen, this report, p. 17.

(2) R. A. Tobey, D. F. Petersen, and E. C. Anderson (manuscript in preparation).

(3) J. H. Tjio and T. T. Puck, J. Exp. Med. 108, 259 (1958).

(4) E. C. Anderson, D. L. Carlson, R. B. Glascock, J. H. Larkins, J. D. Perrings, and R. A. Walters, this report, p. 44.

(5) I. Watanabe and S. Okada, Radiation Res. 27, 290 (1966).

METHYLATION OF MAMMALIAN RNA (A. G. Saponara, M. D. Enger, and J. L. Hanners)

INTRODUCTION

Ribosomal and transfer RNA's from all sources examined to date are methylated. These methyl groups are derived from methionine and are found either on the nucleic acid purine or pyrimidine bases or on the 2'-position of ribose. The functional significance of RNA methylation is not at present understood. As a working hypothesis, we have suggested that methylation allows cellular enzymes to distinguish messenger RNA (which will act as a template for protein synthesis and will subsequently be degraded) from the stable cellular RNA's (which are rejected as messengers by protein-synthesizing systems). The following work presents some analytical data on the methylation of RNA in Chinese hamster ovary cells growing in tissue culture.

METHODS AND RESULTS

Alkaline hydrolysis of RNA proceeds via a 2',3'-cyclic phosphate intermediate. The presence of a 2'-substituent which is stable to base will, therefore, prevent hydrolysis at such a position. We have utilized this property to discriminate base methylation from ribose methylation.

In our initial work, RNA was labeled in vivo with methionine-methyl-^{14}C and was isolated with phenol as previously described (1). The RNA was hydrolyzed with 0.3 N potassium hydroxide at 37° for 18 hours, neutralized with perchloric acid, and applied to a DEAE-cellulose column at pH 8.3. Fractions of 3 ml were collected, evaporated to dryness under a heat lamp, and counted in a liquid scintillation counter after addition of 1.25 ml of water and 10 ml Bray's scintillation mixture. Figures 1, 2, and 3 show the elution patterns of 4S RNA and the 18S and 30S RNA's of ribosomes separated by sucrose gradient centrifugation. The order of elution of the main constituent bases from the column is 2'(3')-uridylate 2'(3')-cytidylate, 3'-adenylate, 2'-adenylate, and 2'(3')-guanylate. If, as an approximation, we assume that the species eluting after guanylate are dinucleotides (or higher oligomers), it can be seen that most of the methyl groups of 4S RNA occur on the bases, while 18S

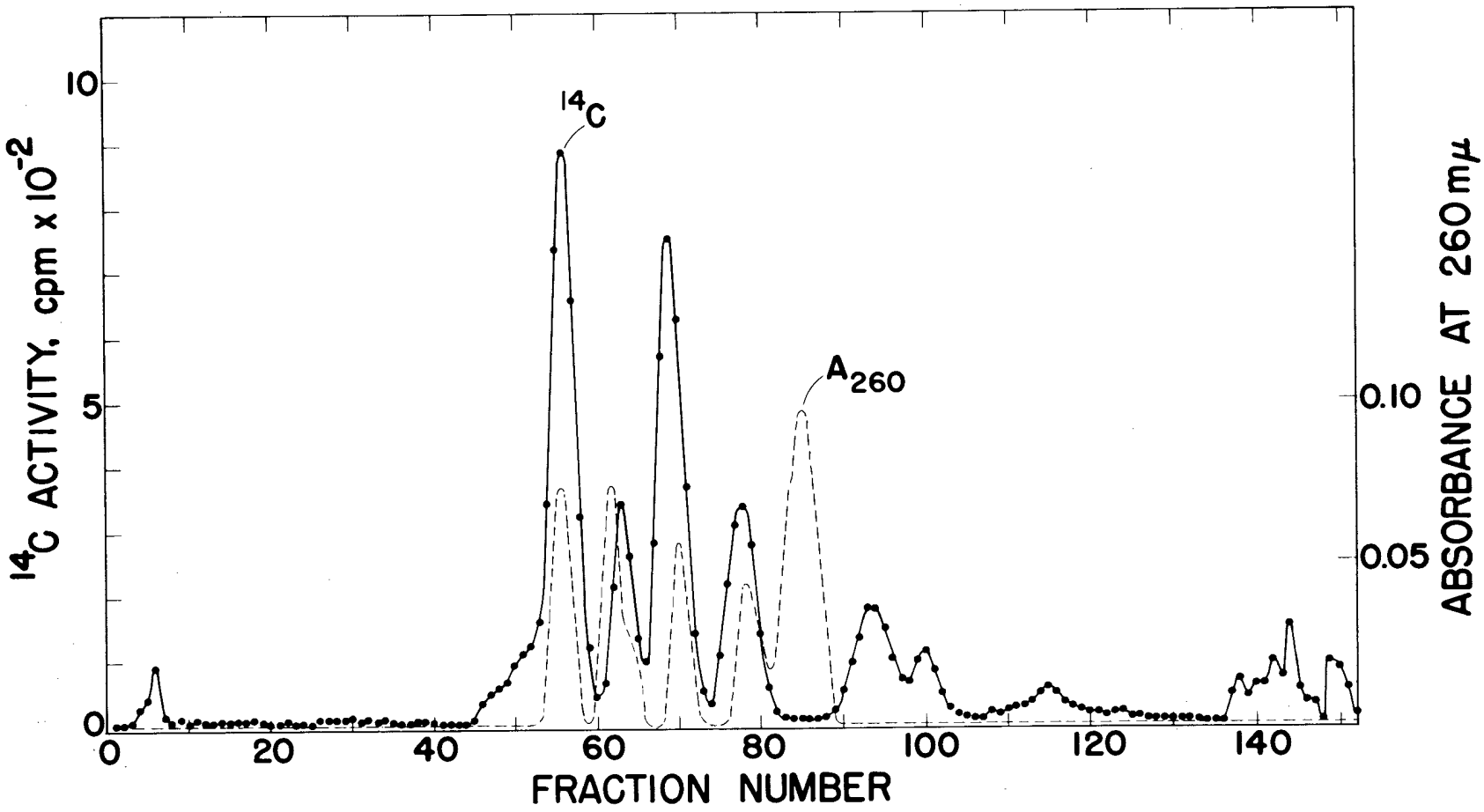

Fig. 1. Elution pattern of an alkaline digest of 4S RNA labeled with methionine-methyl-^{14}C from DEAE-cellulose (1 x 25 cm). The gradient of ammonium bicarbonate (pH 8.3) was linear and varied from 0.001 to 0.40 M.

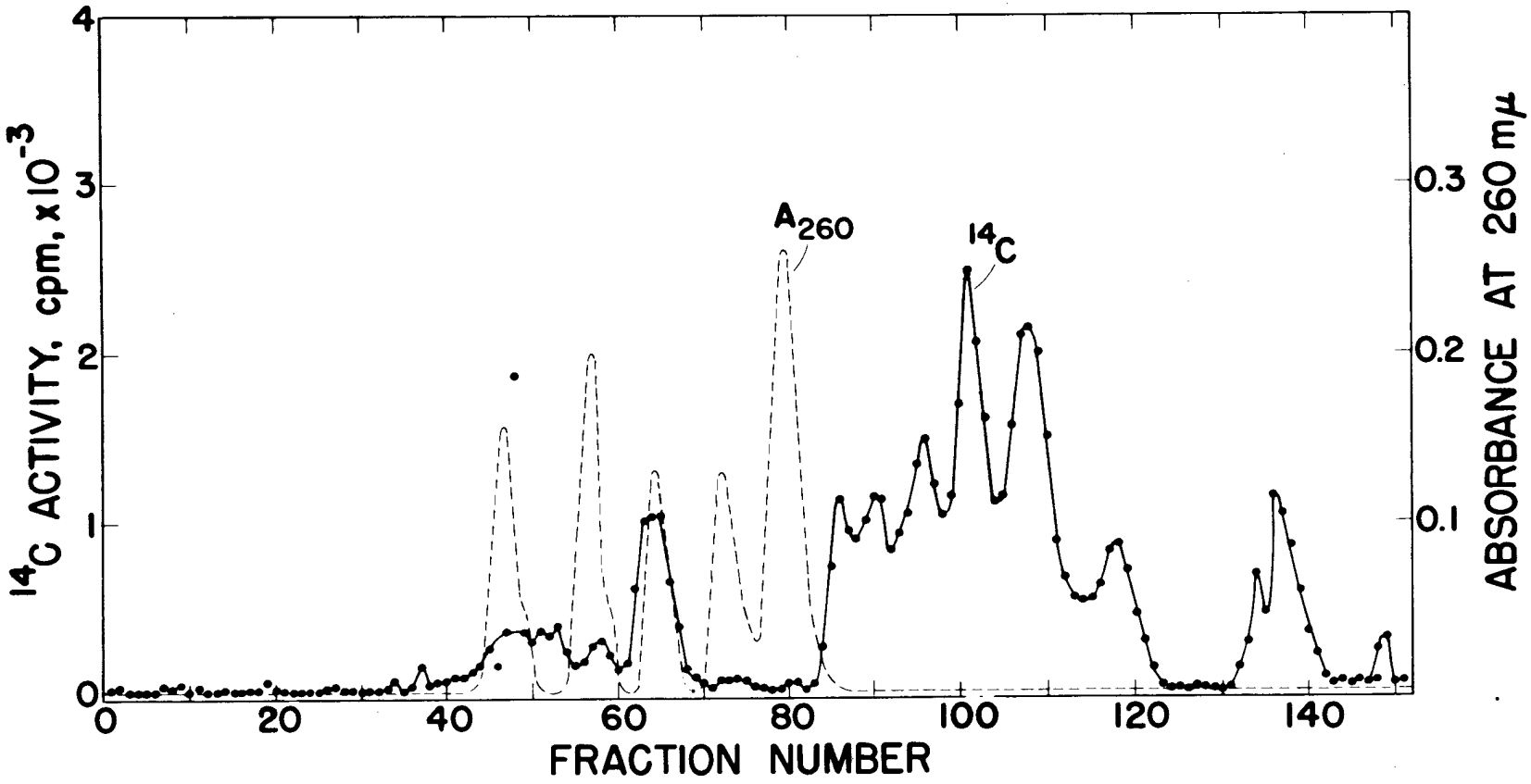

Fig. 2. Elution pattern of an alkaline digest of 18S RNA labeled with methionine-methyl-^{14}C from DEAE-cellulose. The experimental conditions were the same as for Fig. 1.

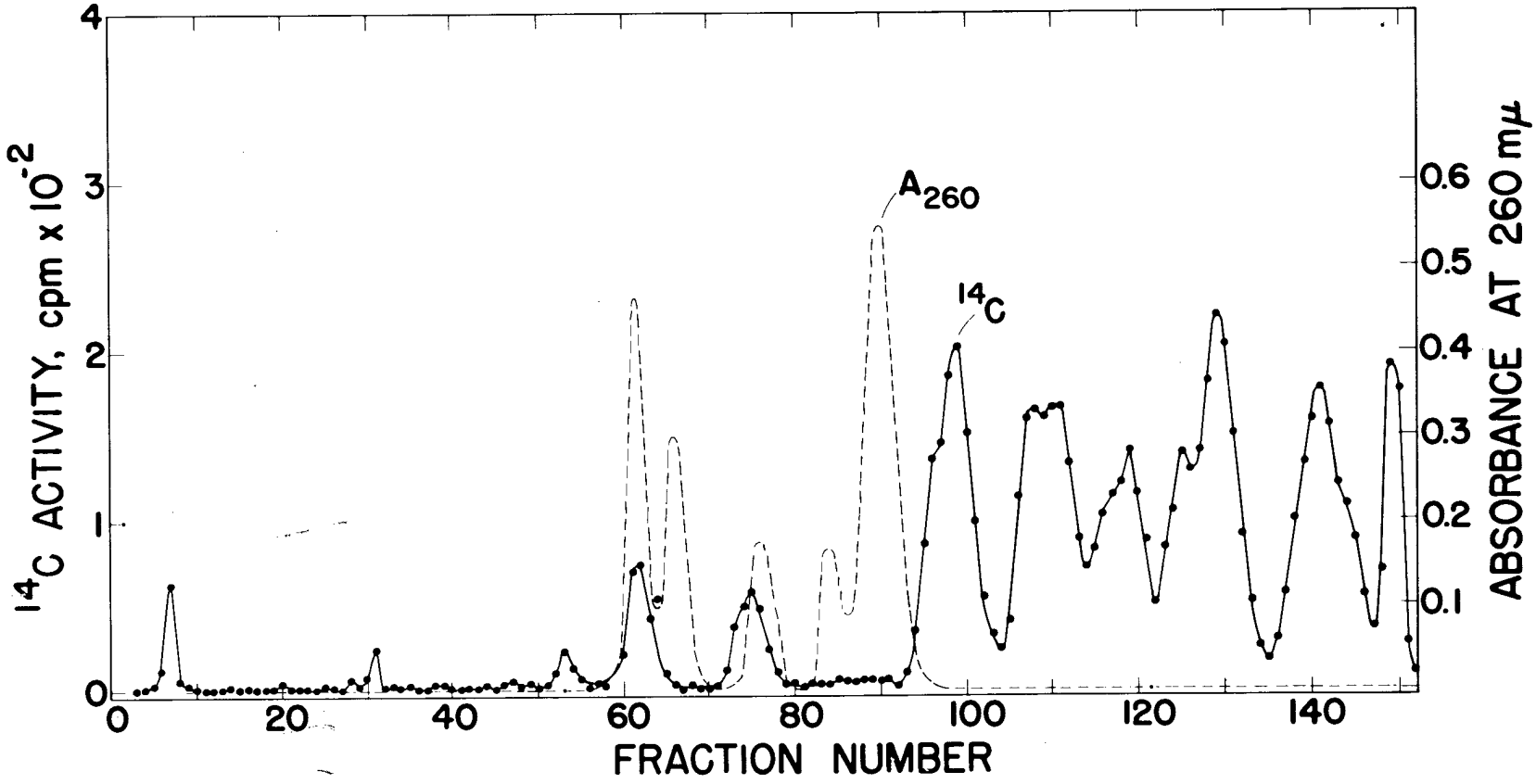

Fig. 3. Elution pattern of an alkaline digest of 30S RNA labeled with methionine-methyl-^{14}C from DEAE-cellulose. The experimental conditions were the same as for Figs. 1 and 2.

and 30S ribosomal RNA is chiefly 2'-O-methylated. The percentages of methyl groups in dinucleotides are 24.8, 80.0, and 87.0 percent, respectively, for the 4S, 18S, and 30S species.

A much simpler profile of methylation is obtained if the 2'- and 3'-phosphates are removed prior to chromatography. Such a procedure also has the advantage of separating dinucleotides from contaminating methylated mononucleotides eluting from DEAE at higher salt concentration than guanylate. For this purpose the alkaline digest was adjusted to pH 8.3. Bacterial alkaline phosphatase was then added, and the mixture was incubated for 5 hours at 37°. Incubation was repeated after an additional aliquot of the enzyme was added. The hydrolysate was then titrated to pH 5.0 with perchloric acid and applied to a DEAE-cellulose column at pH 5.0. The nucleosides which were not retained by DEAE were collected, lyophilized, and separated on a phosphocellulose column at pH 3.75. The sample shown in Fig. 4 was labeled with ^{3}H-cytidine and methionine-methyl-^{14}C and is a typical separation of nucleosides on such a column. The order of elution of the major nucleosides is uridine, guanosine, adenosine, and cytidine. Figure 5 shows a typical separation of the dinucleoside monophosphates on DEAE-cellulose at pH 5.0. The RNA was obtained from cells labeled with ^{3}H-cytidine and methionine-methyl-^{14}C. Since cytidine is not readily converted to uridine by Chinese hamster ovary cells (the ratio of tritium in cytidine to that in uridine was 26 to 1), the ratio of tritium to carbon-14 indicates the analytical composition of some of the methylated dinucleotides. Thus, peak I is probably CpC and peak II CpX or XpC. Peaks III, IV, V, and VI are various dinucleotides lacking cytidine and probably lacking uridine as well. Peak VII, which is stripped off with molar buffer, may represent higher oligomers containing more than one 2'-O-methyl on adjacent sugars. Experiments utilizing combinations of the other three ^{3}H-nucleosides with methionine-methyl-^{14}C are in progress.

A comparison of the methylation pattern in 30S RNA with that in 18S RNA was made by labeling cells in vivo with either methionine-methyl-^{3}H or methionine-methyl-^{14}C. RNA was isolated and separated on a sucrose gradient; 30S RNA labeled with tritium was mixed with 18S RNA labeled with carbon-14. The mixture was hydrolyzed and treated with alkaline phosphatase. Fraction II is heterogeneous (Fig. 6). Similar experiments are being run with a longer column in an attempt to resolve these species better. Peaks VI and VII seem to

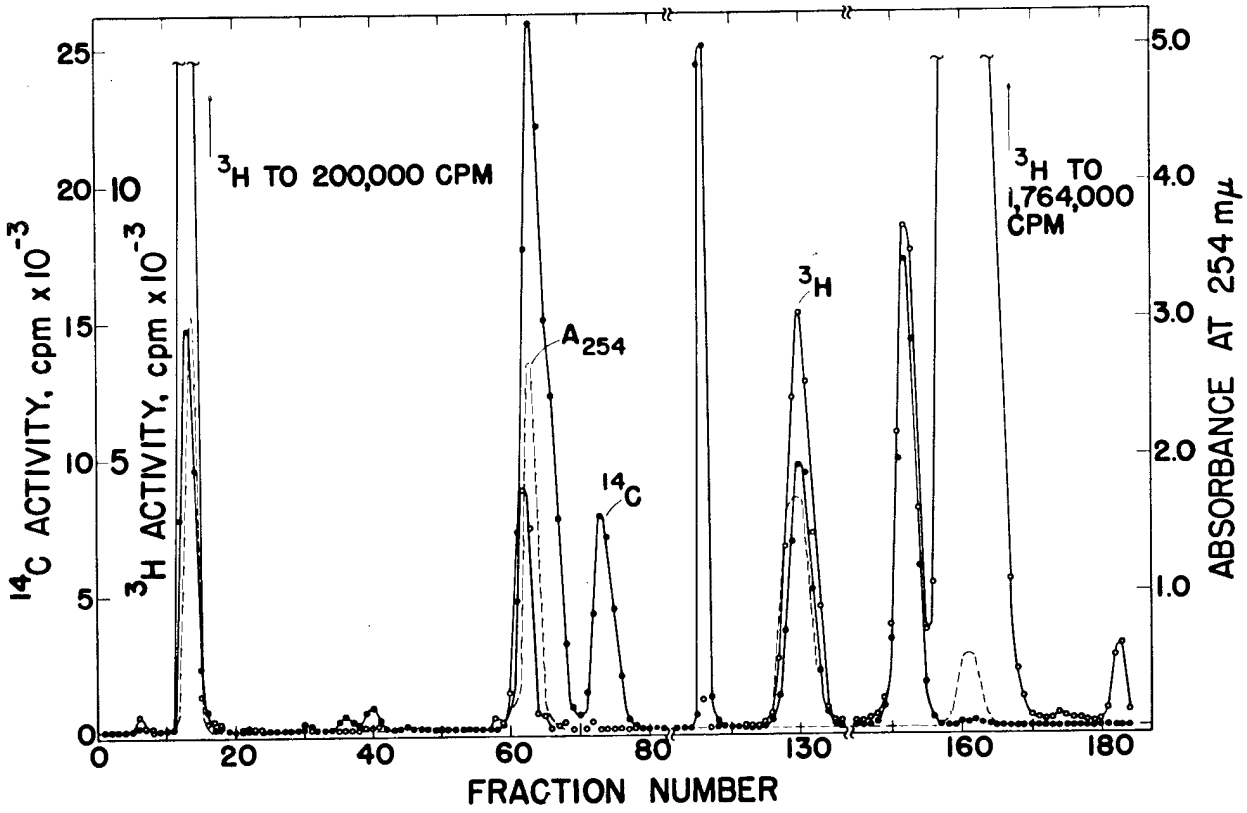

Fig. 4. Elution pattern of mononucleosides from a total RNA preparation. Cells were labeled with ^{3}H-cytidine and methionine-methyl-^{14}C for 24 hours (1.5 generation times). Phenol-isolated RNA was hydrolyzed with alkali and alkaline phosphatase as described in the text. The digest was applied to a DEAE-cellulose column at pH 5.0. The unadsorbed mononucleosides were collected, lyophilized, taken up in 0.005 M ammonium formate (pH 3.75), and applied to a phosphocellulose column. The nucleosides were eluted with a linear gradient of ammonium formate, varying from 0.005 to 0.20 M over a total volume of 400 ml.

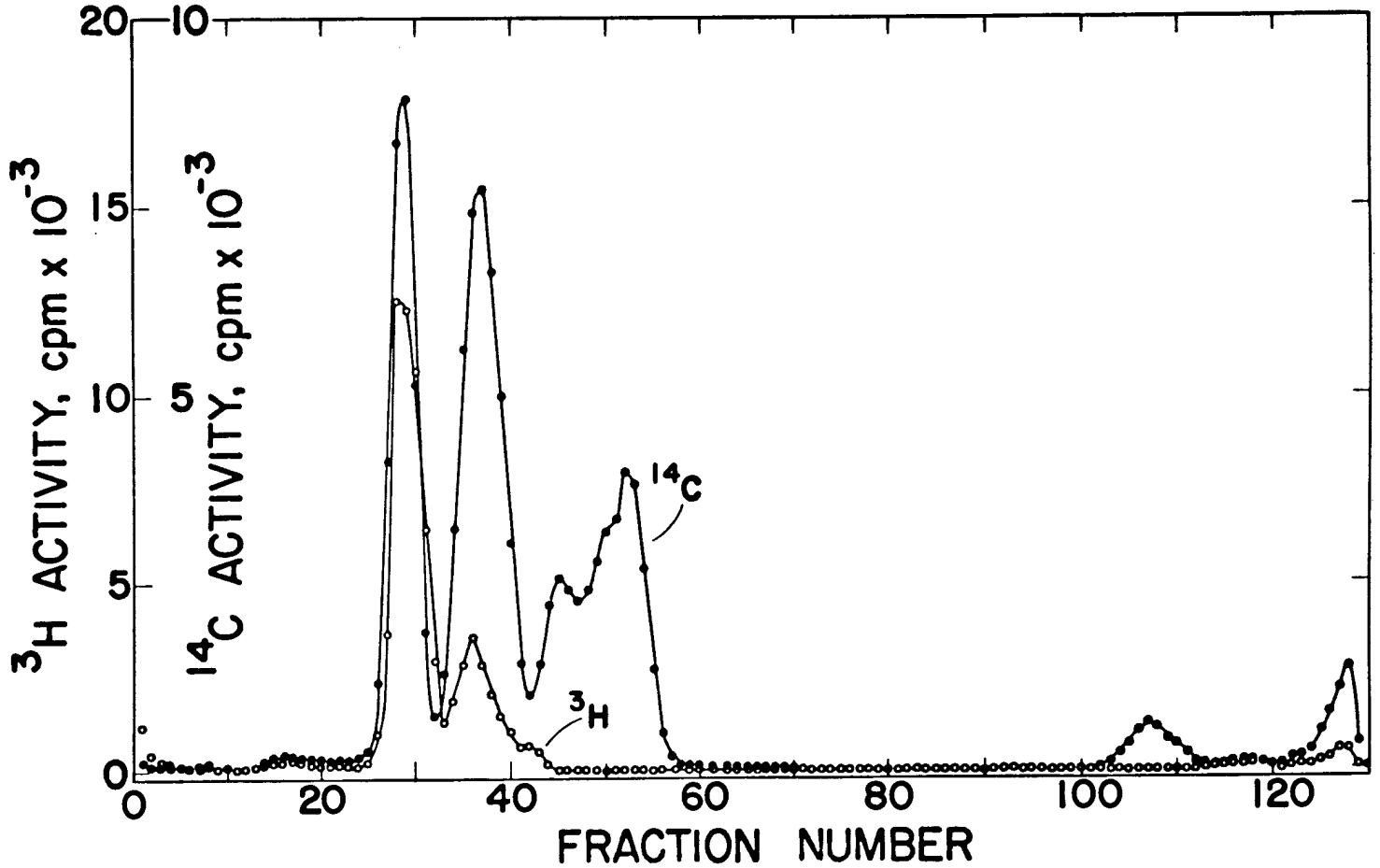

Fig. 5. Elution pattern of dinucleoside monophosphates from a total RNA preparation. The sample was prepared as described for Fig. 4, except for the labeling time which was 18 hours (1 generation time). The digest was applied to a DEAE-cellulose column at pH 4.0. Sampling was begun after the nucleosides had been eluted. The column (1 x 70 cm) was eluted with ammonium acetate, varying linearly from 0.005 to 0.10 M over a volume of 200 ml, and then from 0.10 to 0.40 M over an additional 200 ml.

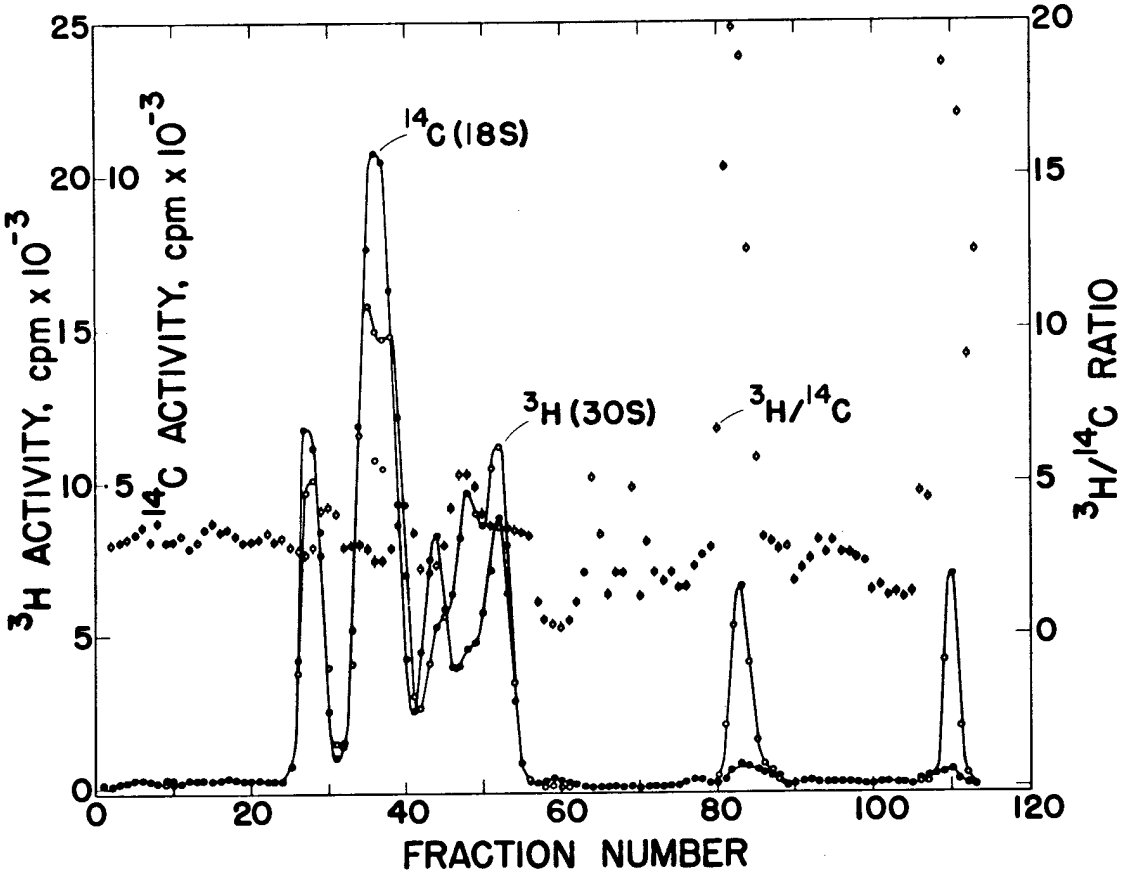

Fig. 6. Comparisons of the dinucleoside monophosphate patterns of 18S and 30S RNA's. Cells were labeled and the RNA was prepared as described in the text. The experimental conditions were the same as for Fig. 5. Carbon-14 label corresponds to 18S and tritium label to 30S RNA.

be unique to 30S RNA. The small amount of carbon-14 label very likely derives from 30S RNA, which partially overlaps the 18S species in our sucrose gradient cuts. The differences observed here are significant, since a sample of total RNA labeled simultaneously with methionione-methyl-^{3}H and methionine-methyl-^{14}C and processed as above showed on chromatography a constant ratio of tritium to carbon-14 in all peaks. Such constancy also indicates that very little, if any, methyl label gets into purine rings since, in this event, some tritium would be lost.

Experiments are currently in progress making comparisons of mono- and dinucleotides in other methylated species. Such comparisons are contemplated with 35S and 50S species, which are thought to represent precursors to ribosomal RNA.

REFERENCE

(1) A. G. Saponara and M. D. Enger, Biochim. Biophys. Acta 119, 492 (1966).

EFFECTS OF INHIBITORS OF PROTEIN AND RNA SYNTHESIS ON REGENERATION OF SURFACE SIALIC ACID OF CELLS IN CULTURE (P. M. Kraemer)

INTRODUCTION

Previous studies of surface sialic acid regeneration (1) utilized mass data from cells treated with neuraminidase to remove surface sialic acid, returned to growth medium, and treated a second time with neuraminidase at various times thereafter for assay of removable sialic acid. These studies indicated that puromycin (50 μg/ml) inhibited the regeneration process, while cells treated with actinomycin D (6 μg/ml) were indistinguishable from controls. The present studies were directed toward the same end, using incorporation data of precursor glucosamine-1-^{14}C rather than assay of surface sialic acid mass.

METHODS

The methods used for growth culture of Chinese hamster ovary (CHO) cells, cell counting, hydrolysis with neuraminidase, and use of inhibitors of protein and RNA synthesis were the same as previously described (1,2). Glucosamine-1-^{14}C was obtained from Nuclear Science and Engineering Corporation at a specific activity of 1.2 mC/mM. Treatments were routinely performed with cells suspended in Earle's balanced salt solution, containing 0.3 percent crystalline bovine albumin and adjusted to pH 7.0 (BSS-A).

RESULTS AND DISCUSSION

Glucosamine-1-^{14}C was rapidly incorporated into CHO cells in culture, but when prelabeled cells were transferred to unlabeled medium or to any of a variety of physiological salt solutions, a progressive transfer of radioactivity from cells to diluent resulted. This transfer, presumably in part representing a labile UDP-N-acetylhexosamine pool (3), complicated measurement of surface sialic acid label, since part of the radioactivity released from cells upon neuraminidase treatment occurred with buffer alone. However, the kinetics of release of label from cells incubated in BSS-A, compared

with release from cells incubated in BSS-A plus neuraminidase, provided a reproducible measure of radioactivity of surface sialic acid (Fig. 1).

When cells pretreated with neuraminidase were returned to growth medium containing glucosamine-1-^{14}C, total incorporation of label into cells and incorporation into surface sialic acid were both linear for at least 8 hours. Radioactivity of surface sialic acid accounted for about 10 percent of the total throughout the regeneration experiment. Similar experiments to which actinomycin D (6 μg/ml), puromycin (50 μg/ml), or cycloheximide (10 μg/ml) were added showed almost unimpaired overall incorporation for at least 5 hours, after which puromycin- and cycloheximide-blocked (but not actinomycin D-treated) cells ceased further incorporation. However, no radioactivity was detectable at any time in surface sialic acid in the presence of any of the three inhibitors.

The apparent discrepancy between mass data and incorporation data of cells treated with actinomycin D was resolved as follows. Cells pretreated with neuraminidase were prelabeled with glucosamine-1-^{14}C, then treated again with neuraminidase, and returned to unlabeled medium or unlabeled medium containing the inhibitors. Under these conditions, radioactivity appeared in the surface sialic acid fraction of control and actinomycin D-treated cells but was inhibited by the protein synthesis inhibitors, puromycin and cycloheximide (Fig. 2).

These data suggest that the regeneration process requires both protein and RNA synthesis for formation of a labile intracellular precursor, which can then be incorporated onto the outer surface of the plasma membrane without further RNA synthesis. This final step does, however, require protein synthesis.

REFERENCES

(1) P. M. Kraemer, J. Cell. Physiol. (1966), in press.

(2) P. M. Kraemer, J. Cell. Physiol. 67, 23 (1966).

(3) S. Kornfeld and V. Ginsburg, Exp. Cell Res. 41, 592 (1966).

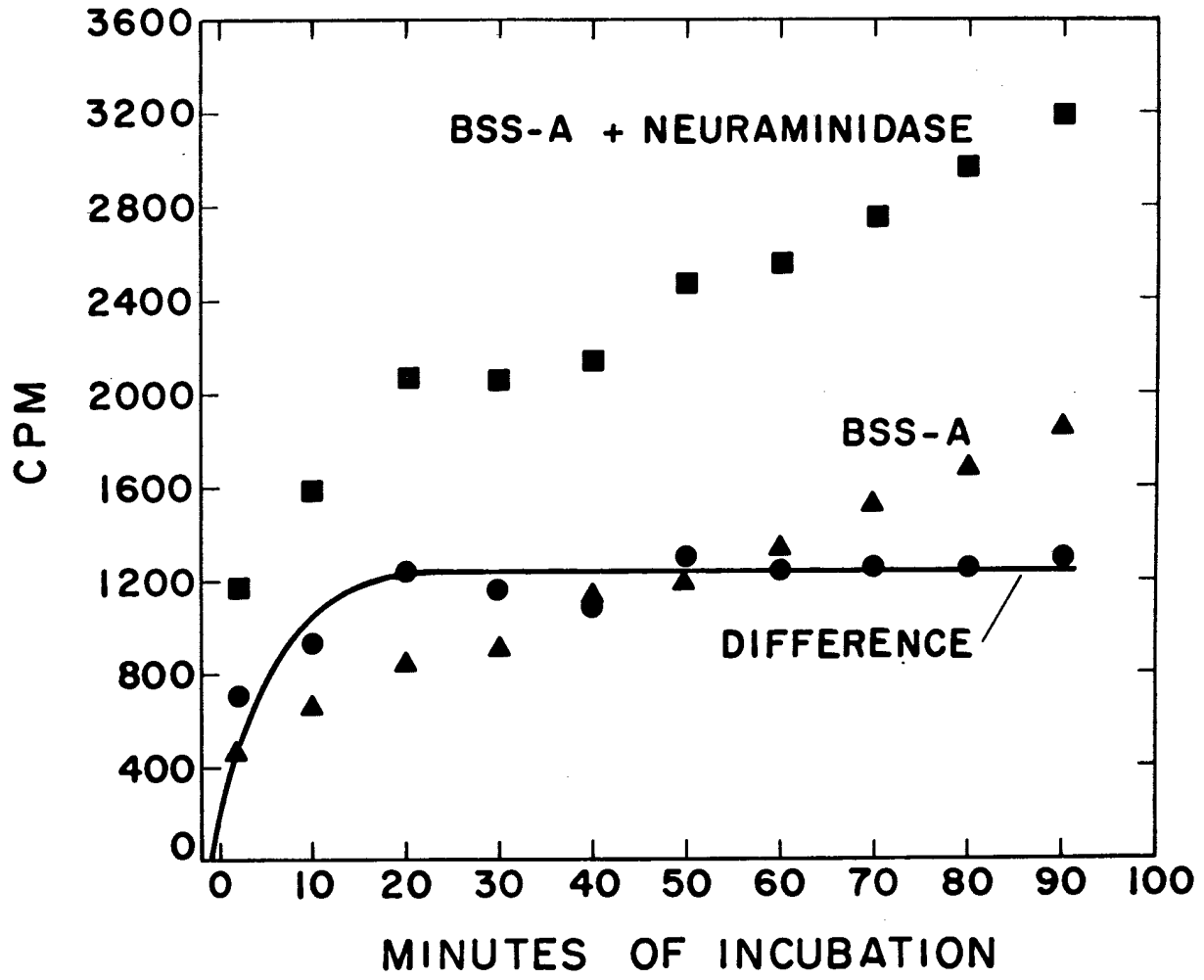

Fig. 1. Carbon-14 activity appearing in supernatant solution from cells pre-labeled with glucosamine-1-^{14}C, harvested, suspended in BSS-A or BSS-A plus 25 units/ml neuraminidase, and incubated at 37 °C.

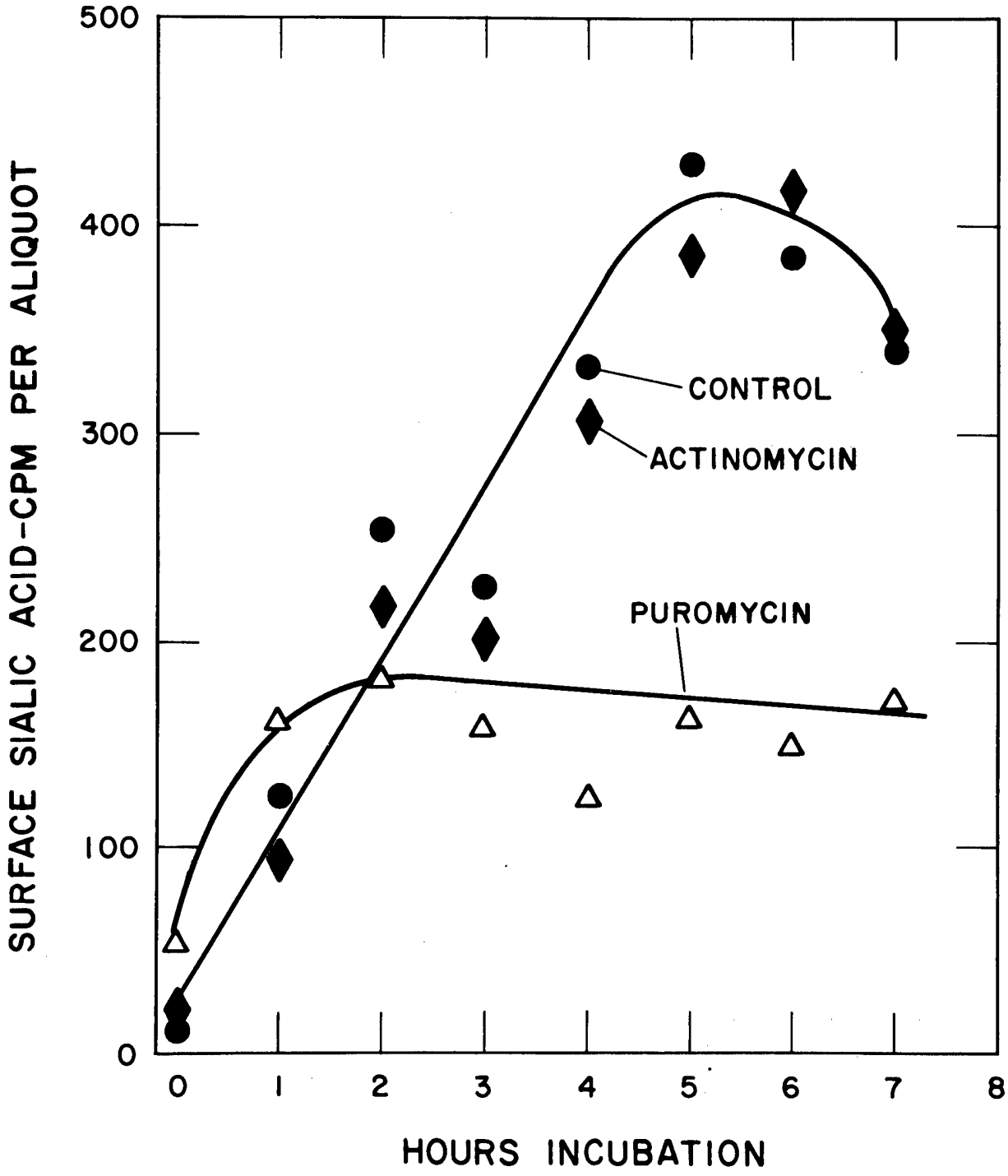

Fig. 2. Emergence of sialic acid counts onto the surface of cells prelabeled with glucosamine-1-^{14}C, treated with neuraminidase, and returned to control culture medium or medium containing 6 μg/ml actinomycin D or 50 μg/ml puromycin.

ENERGY METABOLISM OF CULTURED MAMMALIAN CELLS (W. D. Currie and C. T. Gregg)

INTRODUCTION

Previous studies on energy metabolism of cultured mammalian cells were mainly concerned with determining the respiratory properties of randomly- and synchronously-growing cell populations and with the effects of various inhibitors on these properties. Our attention is currently focused on the relative importance of glycolysis, respiration, and intracellular ATP concentration to growth and division. Synchronized cell cultures described by Petersen and Anderson (1) provide a tool for determining the importance of the various energy-providing pathways at various times in the life cycle of the cell.

METHODS

Cell growth (1), isolation (2), and measurement of respiration (3) in randomly- and synchronously-growing suspension cultures were carried out as previously described. Glycolytic activity in washed cells resuspended in saline-phosphate was determined under aerobic and anaerobic conditions by enzymatic determination of lactic acid levels in TCA-soluble aliquots (4).

RESULTS AND DISCUSSION

Initial studies using respiratory inhibitors and uncouplers of oxidative phosphorylation indicated that cells grown in culture have basically the same complement of enzymes catalyzing electron transport and oxidative phosphorylation as do other mammalian tissues. In addition, experiments with synchronized cells showed that respiratory inhibitors at appropriate concentrations delayed or inhibited cell division. Since all phases of the cell cycle were equally affected by these inhibitors, these experiments were consistent with the hypothesis that a constant supply of energy from respiratory chain phosphorylation was necessary for growth and division.

Experiments were also conducted to determine the glycolytic capacity of cultured cells and the contribution of this pathway at various points of the cell life cycle. As shown in Table 1, five different lines of cultured cells exhibited the high rate of aerobic glycolysis characteristic of malignant tissue. Glycolytic activity in all cell lines, with the exception of Chinese hamster ovary (CHO) cells, was greatly stimulated under anaerobic conditions.

Studies on synchronized cultures in which glycolysis and respiratory activity were measured simultaneously demonstrated that both pathways operate continuously throughout the life cycle of CHO cells. Oxygen consumption per cell by synchronized cultures was constant throughout 2 generation times except for a burst of respiratory activity preceding the first mitotic wave. This "burst" of respiration was not observed in random populations, nor was it seen prior to the second wave of mitosis in a synchronized population. Thus, it is tentatively concluded that the "burst" of respiratory activity is due to a metabolic perturbation caused by the thymidine block used to achieve synchronous growth. Lactic acid production per cell also proceeded at a relatively constant rate throughout 2 generation times, with lactic acid accumulating in the medium to final concentrations of approximately millimolar. Current experiments are designed to determine the ATP levels throughout the life cycle of CHO cells in the presence and absence of respiratory inhibitors.

REFERENCES

(1) D. F. Petersen and E. C. Anderson, Nature 203, 642 (1964).

(2) C. T. Gregg, Los Alamos Scientific Laboratory Report LA-3132-MS (1964), p. 224.

(3) W. D. Currie and C. T. Gregg, Los Alamos Scientific Laboratory Report LA-3432-MS (1965), pp. 153-157.

(4) H. Adams, in Methods of Enzymatic Analysis (H. V. Bergmeyer, ed.), Academic Press, New York (1963), p. 266.

TABLE 1. GLYCOLYSIS UNDER AEROBIC AND ANAEROBIC CONDITIONS*

Cell Line	Lactate to Protein Ratio (μg/mg)	
	Aerobic	Anaerobic
CHO	27.3	27.7
L5178-Y	29.5	42.3
C-13	12.6	20.7
P-183	28.7	31.8
Ascites	20.0	33.4

*Incubation time 10 minutes.

AUTOMATIC CELL COUNTER FOR MAMMALIAN CELLS IN SUSPENSION CULTURE

(E. C. Anderson, D. L. Carlson, R. B. Glascock,* J. H. Larkins, J. D. Perrings, and R. A. Walters**)

INTRODUCTION

The objectives of this development were: (a) the automatic measurement of concentrations of mammalian cells at frequent intervals (5 to 15 minutes) from several (up to 4) parallel suspension cultures in spinner flasks; (b) a precision of measurement of $\pm$ 0.5 percent or better for each determination; (c) rapid response to transients; and (d) the potential for expansion to include automatic cell spectrometry and chemostat operation.

A Coulter probe was chosen as the sensing element because of the precise volume spectrometry possible with this transducer. The automatic system of James and Anderson (1) was considered but was rejected because it was feared that the continuous-flow rate-meter method would not yield the desired precision and because the thin aperture required would not permit cell volume spectrometry. In addition, direct digital output was desired for computer processing.

METHODS AND RESULTS

In preference to continuous-flow systems using in-line apertures, an intermittent batch-sampling method with adjustable sample dilution was chosen. This choice offered considerable flexibility, with ease of changing the dilution factor as well as sampling frequency and volume. Cell concentration in the counting solution could be regulated to avoid coincidence losses over a large dynamic range, and long apertures (e.g., 90 x 300 microns) could be used for spectrometry. Volumetric syringes were readily available with a precision of better than 0.1 percent, and counts could be taken on 10^6 cells, reducing the statistical error to 0.1 percent.

---

*Group P-1 of the Physics Division, Los Alamos Scientific Laboratory.

**Associated Rocky Mountain Universities, Inc., Predoctoral Fellow, Colorado State University.

The basic unit of the electronic control circuitry was a "logics control chassis," which initiated performance of each operation, received the "operation complete" signal from the mechanical system, and initiated the following step. A relay system originally, the logics control was redesigned with transistorized plug-in logical units. The steps in the logics cycle were: (a) "ready" -- cycle completed and waiting for an elapsed time signal to initiate the next round; (b) "select" -- a rotary selector valve advances to sample the next culture in sequence; (c) "empty" -- previous sample removed from the counting beaker by opening a solenoid valve to vacuum drain, followed after 2 seconds by a saline rinse; (d) "drop Hg" -- solenoid valve opens, applying vacuum to the Coulter probe to lower the mercury in the manometer below the volumetric contacts; (e) "set" -- solenoid valve closes as mercury reaches "set" position, and scaler is reset; (f) "count" -- rising mercury reaches lower volumetric contact, beginning the count; and (g) "readout" -- mercury reaches upper volumetric contact, stops count, and initiates printing of flask number, count number, time of day, and total cell count. Completion of printing returns cycle to either position "5" for a replicate count (1 to 4) or to position "1" to await next time signal.

Figure 1 shows the front panel of the "logics" chassis of the control system. The status of the system at any time is indicated by lights which show the conditions of the various valves and syringes, as well as of the current stage of the logical cycle and subcycles. The "start" and "stop" controls in the upper right permit the independent setting of times at which the "rinse," "flush," "set," and "empty" valves are opened or closed during the "empty" cycle. These times are interpreted as positions of the "Y register," which advance at 2-second intervals.

The selector valve ("flask number") is a rotary stopcock (stainless Kel F) driven by a 1-RPM Bodine motor with microswitch positioning. The diluent syringe is a commercial pneumatic dispenser (Research Specialties Company), modified to be driven by laboratory vacuum and pressure supplies. The sample syringe is a glass hypodermic type (5-ml capacity) driven by a 3-RPM motor through a "walking beam" mechanical coupling. Volume is continuously variable by setting a micrometer stop to limit the intake stroke.

Each culture flask is fitted with a special sampling valve designed to minimize hold-up in the system by permitting the saline diluent to be injected at the sampling point. The

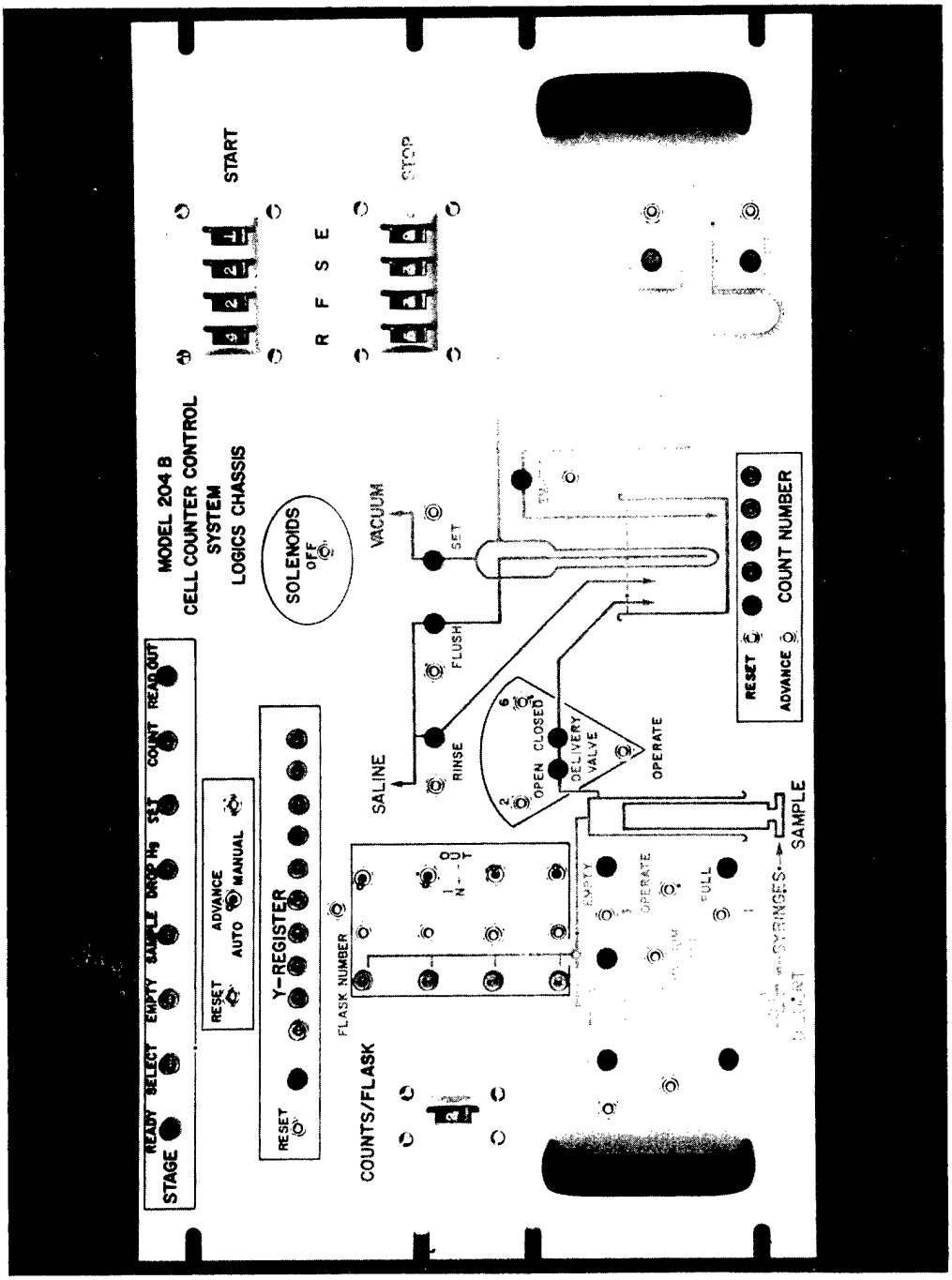

Fig. 1. Logics control chassis.

entire sampling line is thus swept out by the saline, and there is minimal "memory" from sample to sample. Tubing diameter does not have to be kept extremely small, and thus pumping pressures are not excessive. A cross section of a sampling valve is shown in Fig. 2. It consists of a central tube of 1/8-in. diameter stainless steel, which is moved up and down through a pair of O-ring seals by application of a vacuum or pressure to the piston at the top. In the "down" position the filling port in the side is exposed to the culture medium, and a sample can be drawn into the sample syringe. In the "up" position the filling port is above the lower O-ring, and the sample is delivered into the counting beaker from the sample syringe. The saline diluent then passes into the outer tube of the sampling valve, enters the filling port, and flushes all the plumbing (including the empty sample syringe) into the counting beaker. "Memory" of the preceding sample was found to be less than 3 percent.

Immediately before entering the counting beaker, the solutions are passed through a Swinney filter unit containing only the 100-micron mesh plate. The mesh alone was of proper porosity to trap large foreign objects which could clog the aperture. No interference with passage of cells was noted, and very few instances of plugging were noted after addition of the filter. Occasional difficulties were due to such things as airborne lint falling directly into the beaker, and frequency of occlusions was greatly reduced by keeping the beaker covered at all times.

Cell suspensions were grown in jacketed spinner flasks of 250- to 1000-ml capacity with access tubes in the lid rather than in the sides to reduce interference between sampling probe and spinner. Temperature was regulated by a thermostated circulating water bath.

The sampling probes were sterilized by immersion in 70 percent alcohol at all times when not in use. Successful runs extended over a period of several days without bacterial contamination.

The Coulter probe was of conventional design except for replacement of manual stopcocks with solenoid valves to set the mercury manometer and to flush the interior. "Long" apertures (90 x 100 to 90 x 300 microns) were used.

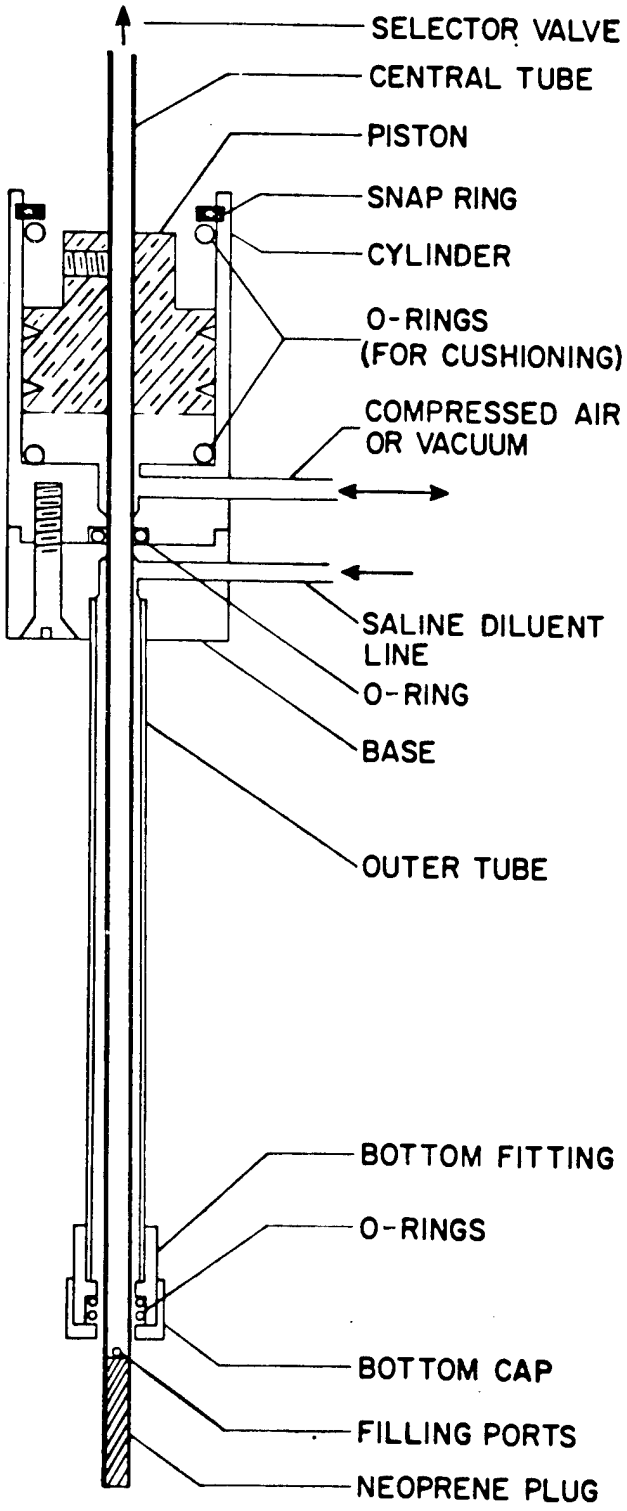

Fig. 2. Sampling valve.

DISCUSSION

The instrument has operated to design specifications for extended periods of 24 hr/day without failures, but also without complete freedom from servicing the somewhat complicated plumbing and valving. The difficulties were primarily leaking stopcocks and sticking valves and were largely eliminated by preventive maintenance and a few design changes.

The precision of the system was estimated from scatter of the data about a least-squares regression line for cultures in exponential growth and for cultures with constant cell number (as a result of thymidine blockade). Under the best conditions, standard deviations of 0.4 to 0.6 percent were observed, compared with counting statistical errors of 0.3 percent. Unexpectedly, the growth rate of a supposedly "random" culture often varied, sometimes by as much as a factor of 2, over periods of a number of hours. Manual counting indicated this to be a true variation and not an error in the automatic system.

This device has been in use for a number of months in experiments to determine the effects of radiation and drugs on random and synchronized mammalian cell cultures. Its principal shortcomings are inherent complexities of the electronic control and plumbing system and the finite sample size requirement. A sample of 2 ml (typical) taken every 4 minutes removes 30 ml/hr. If this depletion rate is not to exceed the growth rate of the culture, then a 500-ml initial volume is required for a culture with a generation time of 12 hours and proportionately more for slower growing cultures. Work is currently underway on a simplified model which counts the sample without dilution and returns it to culture after measurement, thereby significantly reducing culture volume requirements. Coincidence losses are significant at high cell concentrations, and volume spectrometry is not possible; however, the resulting system should be far simpler and more economical to build and to operate.

REFERENCE

(1) T. W. James and N. G. Anderson, Science 142, 1183 (1963).

INTERCELLULAR CONTROL OF DEVELOPMENT OF COMPETENCE IN CULTURES OF HEMOPHILUS INFLUENZAE BY A CELL-FREE PRODUCT OF CELL METABOLISM

(B. J. Barnhart and S. H. Cox)

INTRODUCTION

Control of development of competence (i.e., physiological state necessary for transformation) in several bacterial transformation systems by macromolecular cellular products has been described in recent years (1-3). Several published reports, however, have presented data showing that no such control system could be detected with Hemophilus influenzae (4,5). A systematic reappraisal of the latter transformation system has revealed that indeed an intercellular control of competence is operational.

METHODS

A streptomycin-sensitive (Sm^S) strain of H. influenzae Rd is grown in a medium which does not allow development of high-level competence in the culture. These cells are resuspended in either supernatants taken from cultures grown in a rich medium which allows development of a high level of competence or from fresh rich medium. After incubation at 37°C without aeration, the cells are exposed to an excess of DNA extracted from a streptomycin-resistant (Sm^r) mutant of H. influenzae Rd. The mixture is aerated for 30 minutes at 35°C, and the pancreatic DNase is added to terminate the cell-DNA interaction. The Sm^S cells are diluted and plated for transformation to Sm^r and for viable center titers.

RESULTS

When cells of low-level competence are resuspended in sterile supernatants taken from cultures of competent cells, the former bacteria are stimulated to develop competence with a shorter initial delay period, a faster rate once development starts, and a high frequency of competent cells at optimal development when compared with cells resuspended in supernatants taken from low-level competent cultures or from fresh medium (Fig. 1). Cultured bacteria from the early to mid-log phases of growth are the most sensitive to stimulation. The stimulation process

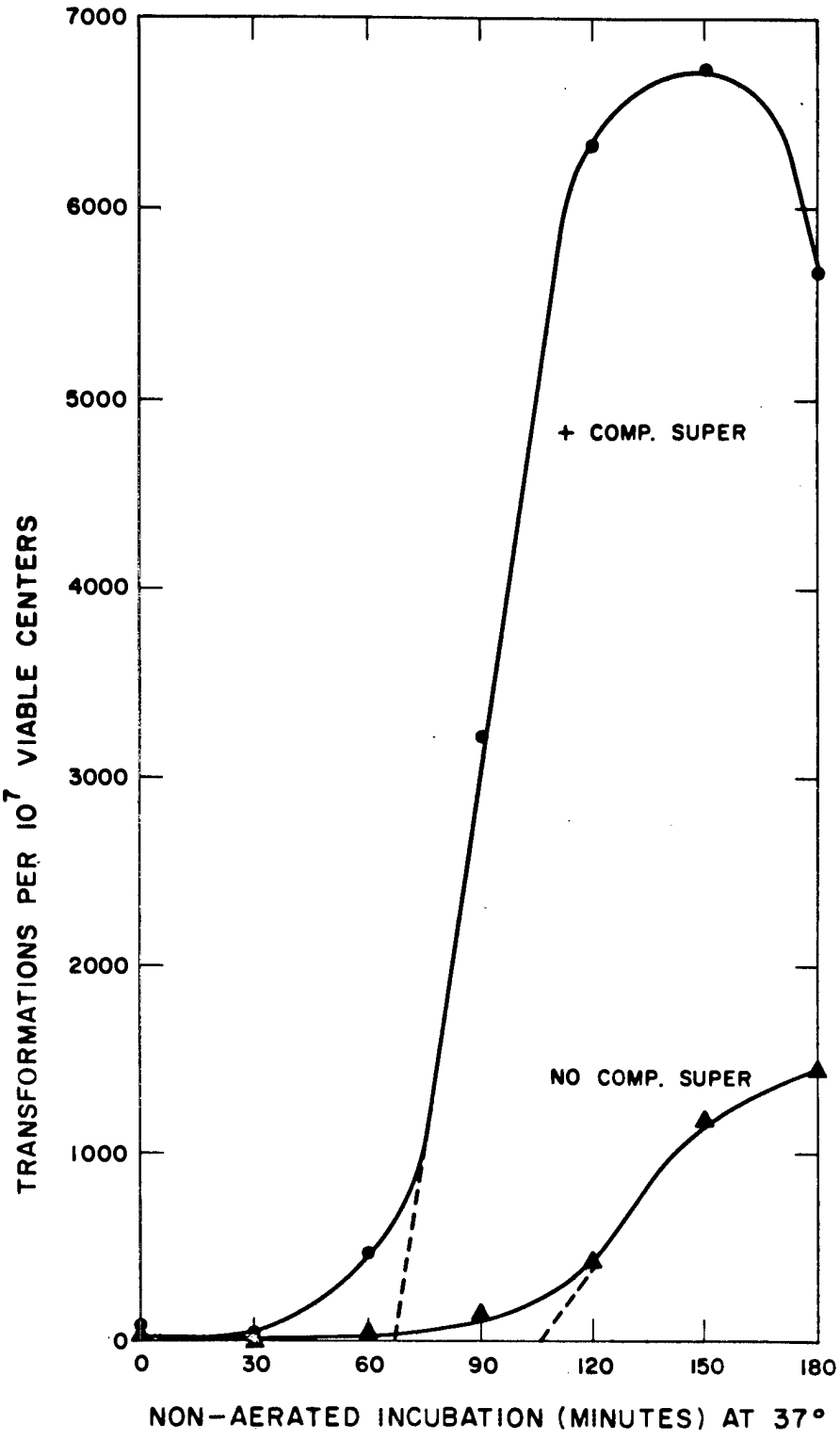

Fig. 1. Stimulation of development of competence.

is temperature-sensitive, being reduced from 27 to 2 fold when the temperature is reduced from 37° to 27°C. Puromycin (4 μg/ml), which was added to the cells concomitantly with the competent cell supernatant, completely inhibited stimulation.

Identification of the competent stimulating factor(s) in cell supernatants is being pursued. The factor(s) is resistant to trypsin, pronase, and RNase. It is heat-stable at 135°C for 45 minutes and can be dialyzed. Over 60 percent of the stimulating activity can be recovered from the dialyzate, while the corresponding retentate contains less than 0.5 percent of the original activity. Recombination of the two fractions does not result in a higher level of activity.

DISCUSSION

In three other bacterial transformation systems (1-3), development of cellular competence is under the control of macromolecular protein-like factors produced exclusively by competent cells. When the factor is contacted by noncompetent neighboring cells in the culture, they are stimulated to develop competence. It is concluded that an intercellular control of competence exists in those systems. The intercellular control of competence development in H. influenzae is described in this report. Competence-stimulating activity is found in the supernatants of competent cultures, and preliminary evidence indicates the activity is present to a lesser extent in supernatants of logarithmically-growing cells. Thus, contrary to the competence factors described in the systems mentioned above, the Hemophilus factor(s) is not produced exclusively by competent cells but is present in direct proportion to the cell concentration during the logarithmic phase of growth. The competence of cells in this phase is relatively quite low. In addition, the Hemophilus factor(s) is unlike that of the other transformable bacteria in that it is heat-stable, is resistant to the action of proteolytic enzymes, and is dialyzable. This factor appears to be a low molecular-weight nonprotein-like metabolic product of growing cells.

These results give rise to the notion that within a growing culture of H. influenzae, under the proper conditions, the cells produce a factor(s) -- perhaps a nutrient -- which can be utilized by cells in that culture such that metabolism favoring competence development is initiated. Isolation

and/or identification of the competence-stimulating factor of H. influenzae is being pursued by two different approaches. Amino acids and other nutrients are being added to fresh medium and to cell supernatants to determine which, if any, stimulate competence. The other approach involves concentration and fractionation of active supernatants using column and paper chromatographic methods.

REFERENCES

(1) R. Pakula and A. H. W. Hauschild, Canad. J. Microbiol. 11, 823 (1965).

(2) A. Tomasz and J. L. Mosser, Proc. Natl. Acad. Sci., U. S. 55, 58 (1966).

(3) M. Charpak and M. R. Dedonder, Compt. rend. Acad. Sc. (Paris) 260, 5638 (1965).

(4) S. H. Goodgal and R. M. Herriott, J. Gen. Physiol. 44, 1201 (1961).

(5) H. T. Spencer and R. M. Herriott, J. Bacteriol. 90, 911 (1965).

STUDIES OF HORSE LIVER ALCOHOL DEHYDROGENASE: STRUCTURAL CHANGES DURING ACID INACTIVATION (C. H. Blomquist)

INTRODUCTION

Horse liver alcohol dehydrogenase (ADH) is unstable in acid or alkaline medium. Catalytic activity is rapidly lost upon exposure of the enzyme at room temperature (23 to 25°C) to media of pH less than 5.0 or greater than 11.5 (1-3). Observed changes in optical rotation and in fluorescence emission spectrum of the enzyme protein under conditions where catalytic activity is lost imply that structural changes do occur (3). The relative stability of enzyme-coenzyme binary complexes and enzyme-coenzyme-inhibitor ternary complexes under conditions where the free native enzyme is inactivated (2), release of zinc during inactivation, and inhibition of release of the metal ion by binary or ternary complex formation (4) imply that part of the total structural change in the molecule occurs at the "active center."

To characterize the structural changes which accompany acid inactivation, the acid difference spectrum of ADH has been determined. Studies have been made of the activity loss as a function of pH and time in an attempt to differentiate structural effects occurring at the "active center" from those occurring elsewhere in the molecule.

MATERIALS AND METHODS

Crystalline horse liver alcohol dehydrogenase was obtained from Worthington Biochemicals, Inc. It was recrystallized 2 times from 10 percent ethanol and stored as a crystalline suspension at 4°C in 50 percent saturated ammonium sulfate. Before use, the enzyme was suspended in 0.1 M phosphate-ammonia (pH 9.5) and dialyzed against 0.1 M phosphate buffer (pH 7.0) for 24 to 48 hours. The molecular weight was taken as 84,000, and using an absorbancy of 0.455 mg^{-1} cm^2, purity estimated by NAD titration of ADH in the presence of excess pyrazole was 100 percent. For acid inactivation studies, the enzyme was further dialyzed at 4°C for 12 hours against water. Insoluble material was removed by centrifugation.

Acid difference spectra were determined using 10 x 10-mm matched cuvettes in a tandem cell arrangement in a Cary Model 14 recording spectrophotometer.

Enzyme activity was measured using the method of Dalziel (5), as modified by Theorell and McKinley-McKee (6).

RESULTS

The acid difference spectrum of horse liver alcohol dehydrogenase is given in Fig. 1. The reference solution contained ADH in 0.1 M glycine (pH 2.7), and the sample contained an equal concentration of ADH in 0.1 M phosphate buffer (pH 6.9). Three maxima at 234, 287, and 294 mμ characterized the spectrum and represented decreases in molar absorbance, as indicated in the ordinate of Fig. 1. The difference spectrum further exhibited peaks in the 258- to 270-mμ region and a broad shoulder in the 298- to 305-mμ region. The spectrum was recorded in the 310- to 280-mμ region approximately 3 minutes after addition of the stock enzyme solution to the acid medium. It was constant for at least 3 hours at 23°C. No catalytic activity was detected in the pH-2.7 sample.

At higher pH values (7.0 versus 4.5), the difference spectrum is time-dependent, as indicated in Fig. 2. It can be seen that both the absolute values of $-\Delta\epsilon_{287}$ mμ and $-\Delta\epsilon_{294}$ mμ and their relative values are clearly time-dependent. The change in extinction at 287 mμ is essentially complete after approximately 20 minutes, whereas the change at 294 mμ approaches completion after 180 minutes.

Similar results were obtained when catalytic activity as a function of time was measured at various pH values. Samples of ADH were incubated at 23.5°C in acidic media, and aliquots were withdrawn at time intervals for activity measurements (5, 6). The results of such an experiment are given in Fig. 3. Phosphate buffer was used for pH $\geq$ 5.0 and glycine buffer for pH $<$ 4.0. Both the rate of activity loss and extent of inactivation are pH-dependent.

DISCUSSION

The principal chromophores contributing to the absorption by proteins in the 250- to 310-mμ region are the aromatic amino

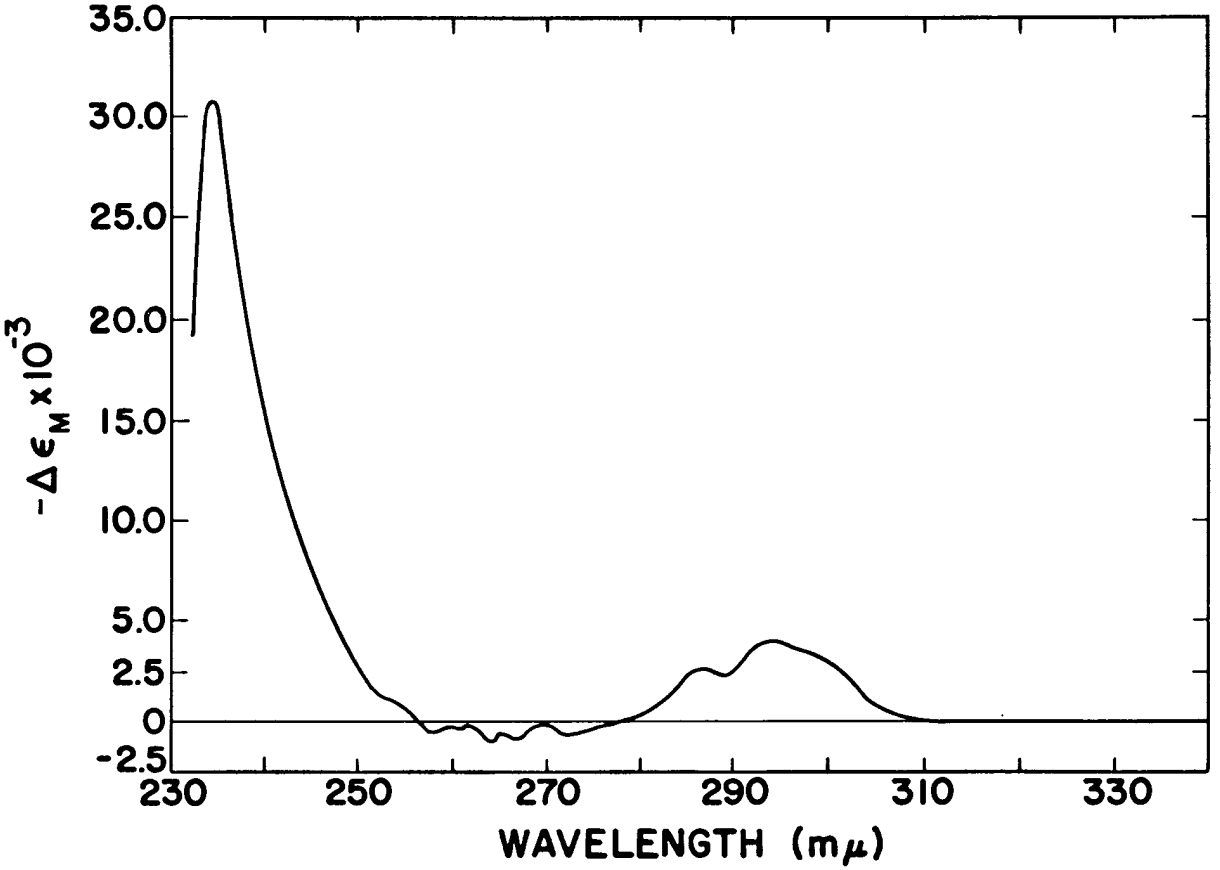

Fig. 1. Acid difference absorption spectrum of liver alcohol dehydrogenase. Spectrum recorded using 10 x 10-mm cuvettes in tandem arrangement with reference solution in 0.1 M glycine (pH 2.7) and sample in 0.1 M phosphate buffer (pH 6.9).

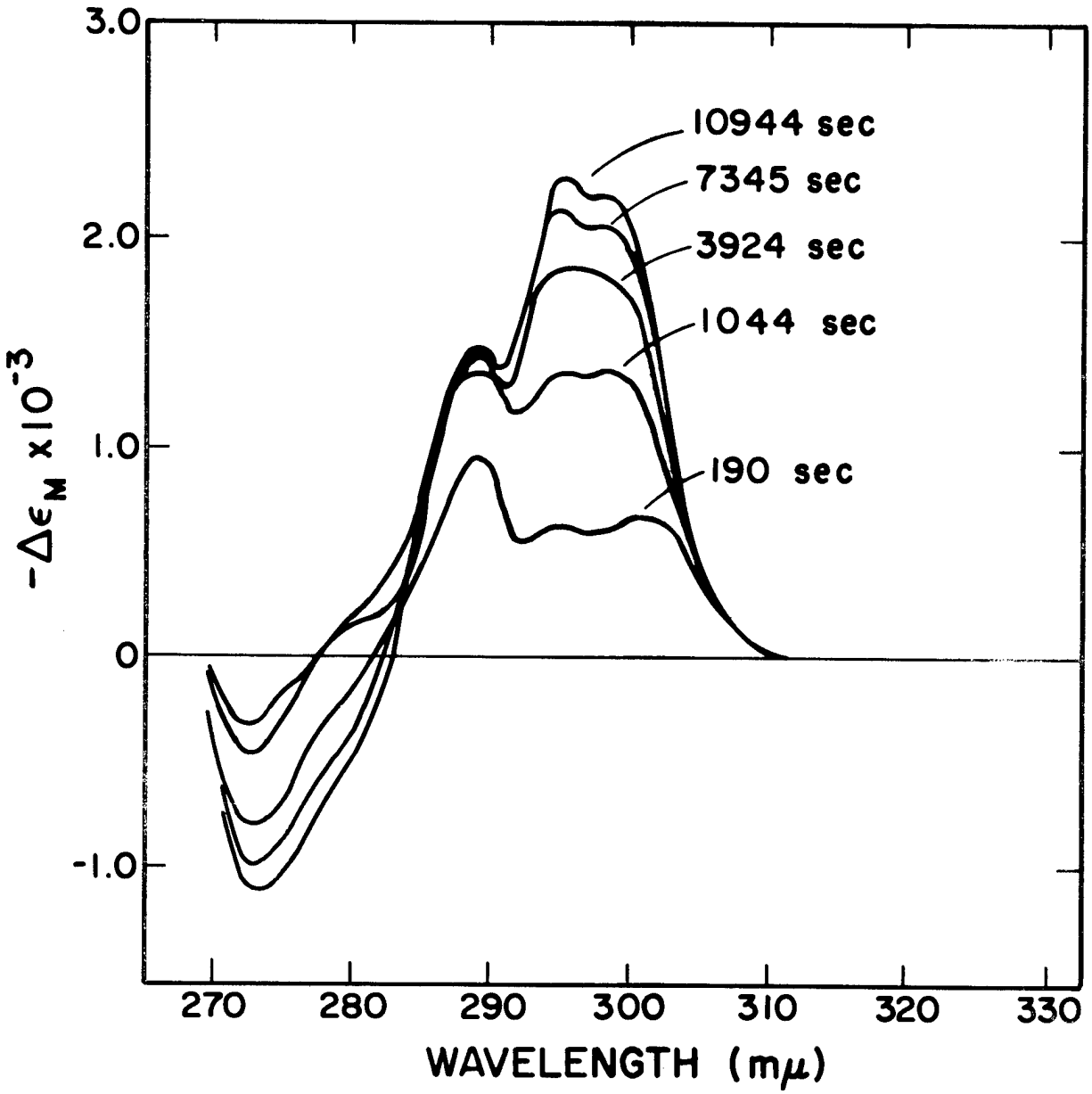

Fig. 2. Acid difference absorption spectrum of horse liver alcohol dehydrogenase. Alcohol dehydrogenase was 10 μM in 0.1 M acetate (pH 4.5) in reference solution and 10 μM in 0.1 M phosphate (pH 7.0) in sample solution.

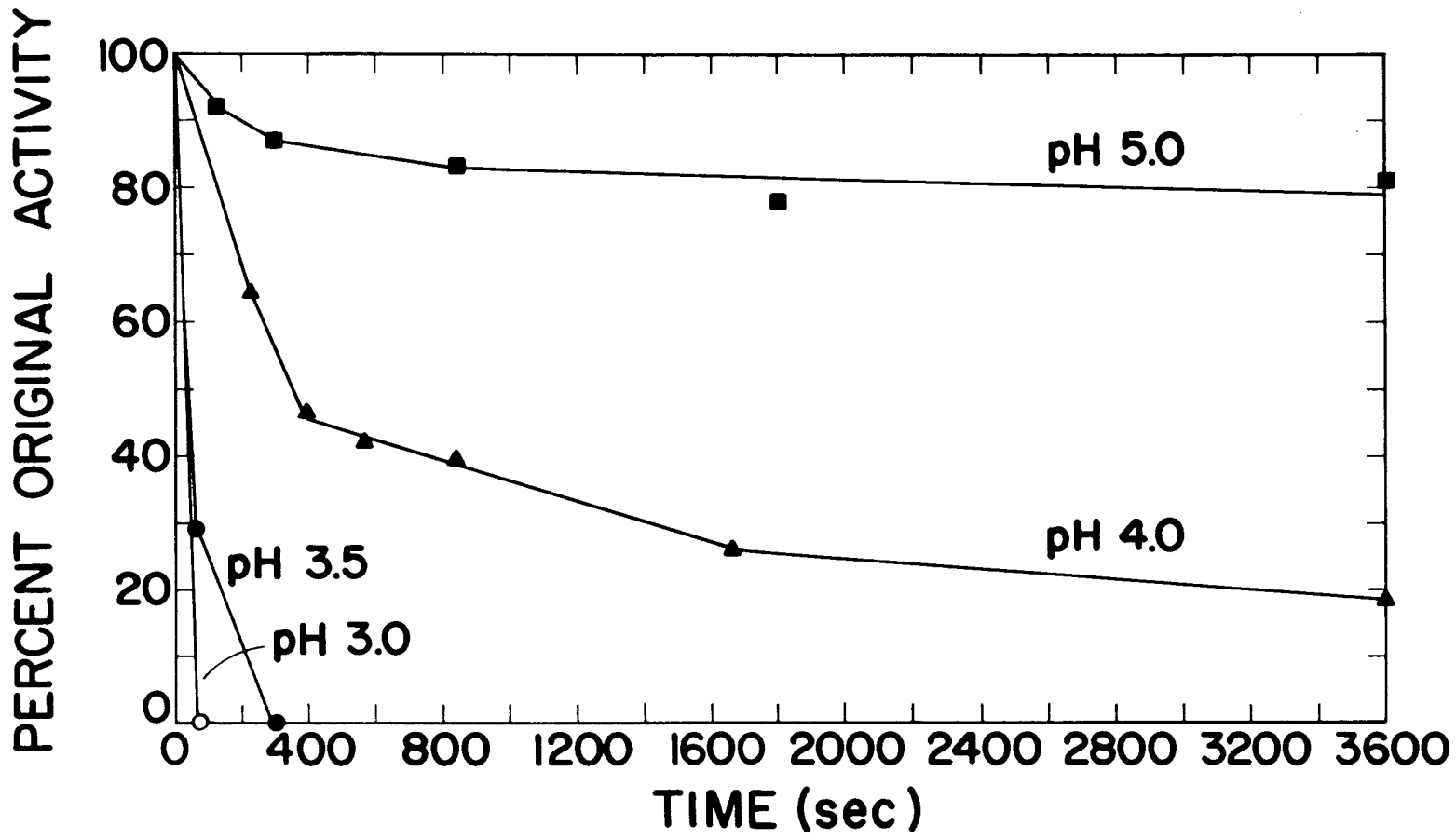

Fig. 3. Activity of horse liver alcohol dehydrogenase as a function of time at various pH values.

acids tyrosine and tryptophan. There is also a smaller contribution by phenylalanine residues (7). In general, the absorption spectrum of an aromatic amino acid is shifted to slightly longer wavelengths ("red shift") when the chromophore is incorporated into a protein molecule. The possible reasons for this "red shift" has received detailed consideration (7-9). It is a characteristic also of these aromatic amino acids that the absorption spectrum is shifted to shorter wavelengths ("blue shift") on exposure of the chromophore to acidic medium, and a similar result is observed on exposure of proteins to acidic conditions (7,8). Acid difference spectra with maxima at 287 and 294 mμ have been observed for numerous proteins (7) and are similar, in a general way, to that given for liver alcohol dehydrogenase (Fig. 1). The 287-mμ peak can be assigned to tyrosine and the maximum at 294 mμ to tryptophan. (These peaks actually represent decreases in absorbance but appear as maxima in the difference spectrum recorded with the acid solution in the reference cell and the neutral solution in the sample compartment.)

Of particular interest is the observation of not only the time-dependence of the difference spectrum but the result that the changes at 287 and 294 mμ, involving tyrosine and tryptophan residues, occur at different rates. These data indicate a structural change (or structural changes) in the protein molecule under acidic conditions and further that the changes involving tryptophan residues differ from those involving the tyrosine residues.

These structural changes are accompanied by a loss of catalytic activity of the enzyme molecule. The rate of activity loss is more closely correlated with the tryptophan peak at 294 mμ. However, no conclusion can be drawn as to the possible involvement of tryptophan at the "active center." The data more strongly support the conclusion that tyrosine is not a part of the "active center," although there apparently are changes in solvent environment of this chromophore when ADH is exposed to acidic conditions.

REFERENCES

(1) H. Sund and H. Theorell, In The Enzymes, Vol. 7 (P. D. Boyer, H. Lardy, and K. Myrbäck, editors), Academic Press, New York (1963), p. 25.

(2) T. Yonetani and H. Theorell, Arch. Biochem. Biophys. 99, 433 (1962).

(3) L. Brand, J. Everse, and N. O. Kaplan, Biochemistry 1, 423 (1962).

(4) R. Druyan and B. L. Vallee, Biochemistry 3, 944 (1964).

(5) K. Dalziel, Acta Chem. Scand. 11, 397 (1957).

(6) H. Theorell and J. S. McKinley-McKee, Acta Chem. Scand. 15, 1797 (1961).

(7) D. B. Wetlaufer, Adv. Prot. Chem. 17, 304 (1962).

(8) S. Yanari and F. A. Bovey, J. Biol. Chem. 235, 2818 (1960).

(9) S. J. Leach and H. A. Scheraga, J. Biol. Chem. 235, 2827 (1960).

CELLULAR RADIOBIOLOGY SECTION

PUBLICATIONS AND ABSTRACTS OF MANUSCRIPTS SUBMITTED

INHIBITION OF THE RESPIRATION OF CULTURED MAMMALIAN CELLS BY OLIGOMYCIN, W. D. Currie and C. T. Gregg. Biochem. Biophys. Res. Commun. 21, 9-15 (1965).

Abstracted in Los Alamos Scientific Laboratory Report LA-3432-MS (1965), p. 173.

RAPID ESTIMATION OF FAST-NEUTRON DOSES FOLLOWING RADIATION EXPOSURE IN CRITICALITY ACCIDENTS: THE $S^{32}(n,p)P^{32}$ REACTION IN BODY HAIR, D. F. Petersen. In: Personnel Dosimetry for Radiation Accidents, International Atomic Energy Agency, Vienna (1965), pp. 217-233.

Abstracted in Los Alamos Scientific Laboratory Report LA-3432-MS (1965), p. 176.

MENGOVIRUS REPLICATION. III. VIRUS REPRODUCTION IN CHINESE HAMSTER OVARY CELLS, R. A. Tobey and E. W. Campbell. Virology 27, 11-16 (1965).

Abstracted in Los Alamos Scientific Laboratory Report LA-3432-MS (1965), p. 173.

MENGOVIRUS REPLICATION. IV. INHIBITION OF CHINESE HAMSTER OVARY CELL DIVISION AS A RESULT OF INFECTION WITH MENGOVIRUS, R. A. Tobey, D. F. Petersen, and E. C. Anderson. Virology 27, 17-22 (1965).

Abstracted in Los Alamos Scientific Laboratory Report LA-3432-MS (1965), p. 173.

KINETICS OF BACTERIOPHAGE λ DEOXYRIBONUCLEIC ACID INFECTION OF ESCHERICHIA COLI, B. J. Barnhart. J. Bacteriol. 90, 1617-1623 (1965).

The kinetics of Escherichia coli K-12 infection by phage λ deoxyribonucleic acid (DNA) were determined. An initial lag of 55 to 80 seconds was found to be the time required for infecting DNA to become deoxyribonuclease-insensitive at 33 C. When cell-DNA interactions were stopped by washing away unbound DNA, the already bound DNA continued to infect the cell at rates described by linear kinetics with no apparent lag. Whereas the lag period was relatively insensitive to DNA and cell concentrations, both the lag and the subsequent linear portions of the rate curves were temperature-sensitive. Cell and DNA dose-response curves prescribed hyperbolic functions. Similarities between λ DNA infection of E. coli and bacterial transformation systems are discussed.

SIALIC ACID AND THE TRYPSIN BARRIER, P. M. Kraemer. J. Cell Biol. 27, 55A (1965), Abstract No. 106.

The relationship of the "trypsin barrier" to sialic acid (SA) localization was investigated in a variety of cultured cells, including C13 Syrian hamster and its polyoma-transformed derivative P183, HeLa, L929, L-5178Y, Chinese hamster ovary, and whole mouse embryo secondary cultures, and also in human erythrocytes (RBC). Two-thirds of the SA of cultured cells was removed by neuraminidase without loss of viability, suggesting that this fraction was on the external cell surface. The remaining third was demonstrated with neuraminidase treatment of frozen-thawed cell pellets or with mild acid hydrolysis. Preliminary evidence indicates that this intracellular fraction is not bound to membranes. Prolonged trypsinization of intact cells failed to remove detectable

amounts of either fraction. Thus the SA of cultured cells is entirely within the trypsin barrier. Neuraminidase treatment of RBC released all SA. Trypsinization removed 60 percent of the SA without any hemolysis, suggesting that, unlike that in cultured cells, a majority of the SA was outside the trypsin barrier. RBC had much less surface SA per unit surface area than cultured cells (1.57×10^5 molecules per μ^2 vs. 5.4 to 16.1 x 10^5 molecules per μ^2 for the various cell lines).

Further studies with cultured cells confirmed that disulfide bridge-reducing agents that permeate the cell (e.g., 2-mercaptoethanol) render cells susceptible to tryptic digestion [Shepherd and Sanders, J. Cell Biol. 14, 346 (1962)]. However, cells treated with disulfide-reducing agents that cannot enter the cell (e.g., mercaptoethylgluconamide) were unaffected. Cells rendered permeable to trypan blue by freeze-thawing or hypotonic treatments were almost instantly digested upon trypsin addition. Experiments designed to show an indirect trypsin effect (e.g., activation of lysosomal enzymes of trypsin-susceptible cells) had uniformly negative results. Thus the trypsin barrier apparently represents differences between the inside and outside surfaces of the external cell membrane. Possible implications of contrasting localizations of SA in cultured cells and RBC were discussed in the context of the trypsin barrier.

INCORPORATION OF [^{3}H]URIDINE AND [Me-^{14}C]METHIONINE INTO CHINESE-HAMSTER CELL RIBONUCLEIC ACID, A. G. Saponara and M. D. Enger. Biochim. Biophys. Acta 119, 492-500 (1966).

Abstracted in Los Alamos Scientific Laboratory Report LA-3432-MS (1965), p. 174.

NEUTRON ACTIVATION OF SULFUR IN HAIR: APPLICATION IN A NUCLEAR ACCIDENT DOSIMETRY STUDY, D. F. Petersen and W. H. Langham. Health Phys. 12, 381-384 (1966).

Abstracted in Los Alamos Scientific Laboratory Report LA-3432-MS (1965), p. 174.

SIALIC ACID OF MAMMALIAN CELL LINES, P. M. Kraemer. J. Cell. Physiol. 67, 23-34 (1966).

Abstracted in Los Alamos Scientific Laboratory Report LA-3432-MS (1965), p. 175.

REGENERATION OF SIALIC ACID ON THE SURFACE OF CHINESE HAMSTER CELLS IN CULTURE. I. GENERAL CHARACTERISTICS OF THE REPLACEMENT PROCESS, P. M. Kraemer. J. Cell. Physiol. (in press).

Treatment of cultured CHO cells with neuraminidase reduced the mean surface sialic acid density to less than 10 percent of pretreatment values. Upon return to culture, the mean density returned to pretreatment values within 12 to 16 hours. During the period of surface sialic acid deficiency, no effect on cell volume, cell division, or attachment and spreading of cells on glass could be discerned. Surface sialic acid regeneration occurred at the same rate in suspension and monolayer cultures. Cells treated with neuraminidase, then with 10 mM thymidine or 6 μg/ml actinomycin D, ceased division yet replaced their surface sialic acid at the usual rate. By contrast puromycin (50 μg/ml), while stopping cell division, caused rapid inhibition of the regeneration process. Puromycin did not prevent cells untreated with neuraminidase from maintaining their control amount of surface sialic acid per cell.

LIFE CYCLE ANALYSIS OF MAMMALIAN CELLS. III. THE INHIBITION OF DIVISION IN CHINESE HAMSTER CELLS BY PUROMYCIN AND ACTINOMYCIN, R. A. Tobey, D. F. Petersen, E. C. Anderson, and T. T. Puck. Biophys. J. (in press).

Analysis of the effects of actinomycin and puromycin on the G_2 and mitotic parts of the life cycle in Chinese hamster ovary cells grown in suspension and synchronized by thymidine treatment has been carried out. Rates of division of partially synchronized cell populations were measured in the presence and absence of the drugs, and various controls were performed to test for absence of complex side effects. Actinomycin produces a block 1.9 hours before completion of division, while puromycin produces a block almost coinciding with the initiation of mitosis. Evidence is presented that the puromycin block may be a double one, inhibiting one kind of

protein synthesis that virtually coincides with the beginning of mitosis and another that occurs about 8 minutes earlier. The data are interpreted in terms of the time interval between messenger formation and its associated protein synthesis in this region of the life cycle. The various events studied have been provisionally mapped in the G_2 and mitotic periods of the life cycle.

PREPARATION AND ASSAY OF PHOSPHORYLATING SUBMITOCHONDRIAL PARTICLES: PARTICLES FROM RAT LIVER PREPARED BY DRASTIC SONICATION, C. T. Gregg. In Methods in Enzymology, Oxidation and Phosphorylation Section, Academic Press, New York (in press).

Sonication of rat liver mitochondria in a hypotonic medium for up to 60 minutes yields particles which carry out oxidative phosphorylation (P/O ratio approximately 1.0), the 2,4-dinitrophenol-stimulated ATPase (DNP-ATPase) reaction, and the ATP-Pi and ATP-ADP exchange reactions. The particles are obtained in good yield and possess a specific respiratory activity comparable to other submitochondrial preparations. These preparations are noteworthy because of their stability to freezing and thawing, the peculiar behavior of the partial reactions, and the fact that they show very pronounced reverse acceptor control of respiration. The preparation of these particles by two different procedures is described in detail, as are the procedures for carrying out assays for oxidative phosphorylation and the DNP-ATPase and exchange reactions.

CONFIGURATION CHANGE OF SURFACE SIALIC ACID DURING MITOSIS, P. M. Kraemer. Submitted to J. Cell Biol.

The well known increase in cell electrophoretic mobility accompanying cell division has recently been shown to be related to neuraminidase-susceptible groups on the cell surface [Mayhew, J. Gen. Physiol. 49, 717 (1966)]. Mayhew's observation, which utilized parasynchronous suspension-cultured cells, raised the question of whether the neuraminidase-sensitive elevation of electrophoretic mobility indicated a shift in mass of surface sialic acid accompanying the division wave. Surface sialic acid, cell count, and mean

cell surface area were followed in parasynchronous Chinese hamster cells released from thymidine block. When surface sialic acid was expressed as a function of mean cell surface area, the data indicated that no shift in mass accompanies the division wave. Hence, it is concluded that the transient elevation of electrophoretic mobility is probably due to conformational or terminal complex changes of sialoglycolipids or sialoglycopeptides.

EFFECTS OF UNCOUPLERS OF OXIDATIVE PHOSPHORYLATION ON THE INFECTION OF ESCHERICHIA COLI K12 BY PHAGE-λ DNA, B. J. Barnhart. Submitted to J. Bacteriol.

Some effects of two uncouplers of oxidative phosphorylation on the infection of Escherichia coli K12 by bacteriophage-λ deoxyribonucleic acid (DNA) are described. The initial lag in the λ-DNA infection kinetics was sensitive to 2,4-dinitrophenol and carbonyl cyanide m-chlorophenylhydrazone. It was shown that the action of these agents was most probably due to uncoupling of oxidative phosphorylation, thus limiting the successful infection of already bound DNA rather than to interference with the initial cell-free DNA interaction. The results support the conclusion that the process of infection is coupled to cellular metabolism.

CHAPTER 3

MOLECULAR RADIOBIOLOGY SECTION

PURIFICATION OF RIBONUCLEIC ACID POLYMERASE FROM ESCHERICHIA COLI (R. L. Ratliff, T. T. Trujillo, and D. A. Smith)

INTRODUCTION

Several procedures for purification of RNA polymerase from bacteria have been described (1-5). Most procedures are limited to processing a few hundred grams of cells because of the need for a high-speed centrifugation as one of the early steps. The present paper describes a purification procedure for preparation of RNA polymerase from an extract of 1.36 kg of cell paste. The extraction and streptomycin precipitation procedure of Chamberlin and Berg (5) was adopted because of its suitability for isolation of RNA and DNA polymerases from a single preparation.

METHODS AND RESULTS

Frozen cells of Escherichia coli B were obtained from the Grain Processing Company of Muscatine, Iowa. The $(pt)_6$ and $(pt)_{13}$ were prepared in this Laboratory. The $(pt)_{13}(pa)_{100}$ was prepared using terminal deoxynucleotidyl transferase from calf thymus (6), $(pt)_{13}$, and dATP. The assay mixture has been described previously (1). The reaction was stopped by spotting the mixture on glass filter paper, soaking in a mixture of 5 percent trichloroacetic acid and 0.01 M sodium pyrophosphate, washing several times with 5 percent trichloroacetic acid-0.01 M sodium pyrophosphate and 95 percent ethanol, and drying in an oven before counting in a Packard Model 3324 liquid scintillation spectrometer.

All reagents were prepared using twice-distilled deionized water. Buffer A consisted of 0.01 M Tris, 0.01 M $MgCl_2$,

0.01 M 2-mercaptoethanol, and 0.1 mM EDTA. The ammonium sulfate solutions were prepared in 0.05 M potassium phosphate, and pH was adjusted with 1 M ammonium hydroxide at 5°. All buffers used contained 0.01 M 2-mercaptoethanol unless otherwise noted.

Partially thawed cells (1.36 kg) were mixed with 1.36 l. of buffer A in a 2-gallon Lourdes Volu Mix homogenizer at 5°. The mixture was blended at low speed (setting 30) for several minutes, and 3.4 kg of glass beads (200 μ) was added to the suspension. The suspension was then blended for 15 minutes at high speed (setting 70). An additional 1.3 l. of buffer A was added, and the mixture was blended for 5 minutes. After allowing the mixture to settle, the supernatant was decanted, and the residue was extracted with 1.3 l. more of buffer A. The supernatant solutions were combined and stirred for 5 minutes before centrifuging at 15,000 x g for 30 minutes.

The protein concentration of the supernatant liquid (fraction 1) was determined, and 1 g of streptomycin sulfate as a 10 percent (w/v) solution in buffer A was added with stirring for each 2.4 g of protein. After 20 minutes, the solution was centrifuged. The precipitate was suspended in 0.05 M potassium phosphate, pH 7.4 (1/10th volume of extract), was stored at -20° until at least 10 pounds of cell paste had been processed to this point, and was then used for isolation of DNA polymerase (7). The supernatant fluid (fraction 2) was used for isolation of RNA polymerase and was concentrated by adding 95 percent ethanol (chilled to -20°) to a concentration of 30 percent. The precipitate was collected by centrifugation and dissolved in 0.05 M ammonium citrate-0.05 M EDTA, pH 8.0, giving a final volume of 600 ml (fraction 3).

Fraction 3 was centrifuged in a Spinco Model L preparative ultracentrifuge for 4 hours at 30,000 RPM in a No. 30 rotor. The supernatant fluid (fraction 4) was fractionated with ammonium sulfate by addition of solid $(NH_4)_2SO_4$ to 0.40 saturation and then to 0.50 saturation. The 0.50-saturated precipitate was dissolved in 0.05 M potassium phosphate, pH 7.5 (fraction 5). The protein concentration was determined, and the solution was then diluted to 5 mg/ml using the same buffer.

The 5 mg/ml-protein solution was added to hydroxylapatite (950 ml settled volume equilibrated with 0.05 M potassium phosphate, pH 7.5) in a 4-l. beaker and stirred for 30 minutes. The suspension was poured into a 69-cm^2 by 30-cm

column and allowed to run until all of the diluted protein solution had passed through. The column was washed with 200 ml of phosphate buffer, and a linear gradient of 0.05 M potassium phosphate, pH 7.5, and 1 M ammonium sulfate, pH 7.5 (total volume 4 l.), was used to elute the enzyme. The fractions which contained the majority of the enzyme were concentrated with 80 percent ammonium sulfate. After centrifuging, the precipitate was dissolved in 0.05 M K_2HPO_4 (fraction 6) and diluted to 1 mg/ml of protein with the same buffer.

The diluted protein solution was absorbed onto a DEAE-cellulose column (chloride form) using 30 mg/mg of protein and was equilibrated with 0.05 M K_2HPO_4. After absorption of the enzyme, a linear gradient of 0.05 M K_2HPO_4 and 1 M ammonium sulfate, pH 8.4 (total volume 4 l.), was used. The flow rate was adjusted to 1 ml/minute, and the eluate was collected in 15-ml fractions. The active fractions were combined (fraction 7) and concentrated by addition of solid ammonium sulfate to 80 percent saturation. The precipitate was collected by centrifugation, washed twice with 150 ml of 60 percent $(NH_4)_2SO_4$, pH 7.8, and extracted with 50 ml of 40 percent ammonium sulfate, pH 7.8, and with 50 ml of 30 percent ammonium sulfate, pH 7.8. The 30 percent extract (fraction 8) was dialyzed overnight against 50 volumes of 0.05 M K_2HPO_4 using dialysis tubing which had been boiled in 0.05 M ammonium citrate-0.05 M EDTA, pH 8.0.

Amberlite CG-50, which had been prepared according to the procedure of Hirs (8), was equilibrated with 0.05 M K_2HPO_4 and was adjusted to pH 7.5 with 1 N KOH over a 2-hour period. A column of 250 mg resin/mg protein was prepared, and the dialyzed solution was passed through the Amberlite. A gradient of 0.05 M K_2HPO_4 and 1 M $(NH_4)_2SO_4$, pH 8.4 (total volume 2 l.), was used to elute the RNA polymerase from the resin. Tubes which contained the peak of activity were combined and concentrated with 0.80-saturated ammonium sulfate. After centrifuging, the precipitate was dissolved in 0.05 M potassium phosphate, pH 7.5 (no 2-mercaptoethanol was added to this buffer), giving a final protein concentration of 10 to 15 mg/ml (fraction 9), which was stored in liquid nitrogen.

A summary of the data obtained from the average of 11 preparations is given in Table 1. The RNA polymerase is obtained after a 120-fold purification with 16 percent overall yield and has an A_{280}/A_{260} of 1.70.

TABLE 1. STEPS IN THE PURIFICATION OF RNA POLYMERASE

Fraction Number		Total Activity (units x 10^{-5})	Protein (mg/ml)	Specific Activity (units/mg protein)	Recovery (percent)
1	Extract	17.70	24.5	19	--
2	Streptomycin Supernatant	9.15	11.8	17	51.60
3	Alcohol Precipitate	6.54	39.6	26	36.80
4	4-Hour Spinco Supernatant	5.73	32.7	26	32.30
5	$(NH_4)_2SO_4$ 0.50-Saturation	7.89	29.6	77	4.45
6	Concentrated Hydroxyl-apatite Fractions	5.40	11.9	178	30.40
7	Pooled DEAE-Cellulose Fractions	4.77	1.0	370	26.90
8	0.30-Saturation $(NH_4)_2SO_4$ Extract	4.29	11.8	840	24.20
9	Concentrated Amberlite CG-50 Eluate	2.85	10.8	2237	16.10

Figure 1 gives the time-course of enzymatic reaction using $(pt)_6$, $(pt)_{13}$, and heat-denatured calf thymus DNA as templates and ATP-8-^{14}C as the nucleotide substrate. Curve 4 shows the reaction rate with all four ribonucleoside triphosphates. The ATP reaction rates with heat-denatured DNA and $(pt)_{13}$ are linear over a 30- to 45-minute period. The short oligonucleotide, $(pt)_6$, will not prime the synthesis of poly-A at 37°.

SUMMARY

RNA polymerase from E. coli has been purified 120-fold over the initial extract. The RNA polymerase has been found to be practically free of both DNA and RNA nucleases and other polymerases. Some preliminary studies on the properties of the enzyme have been published (9,10).

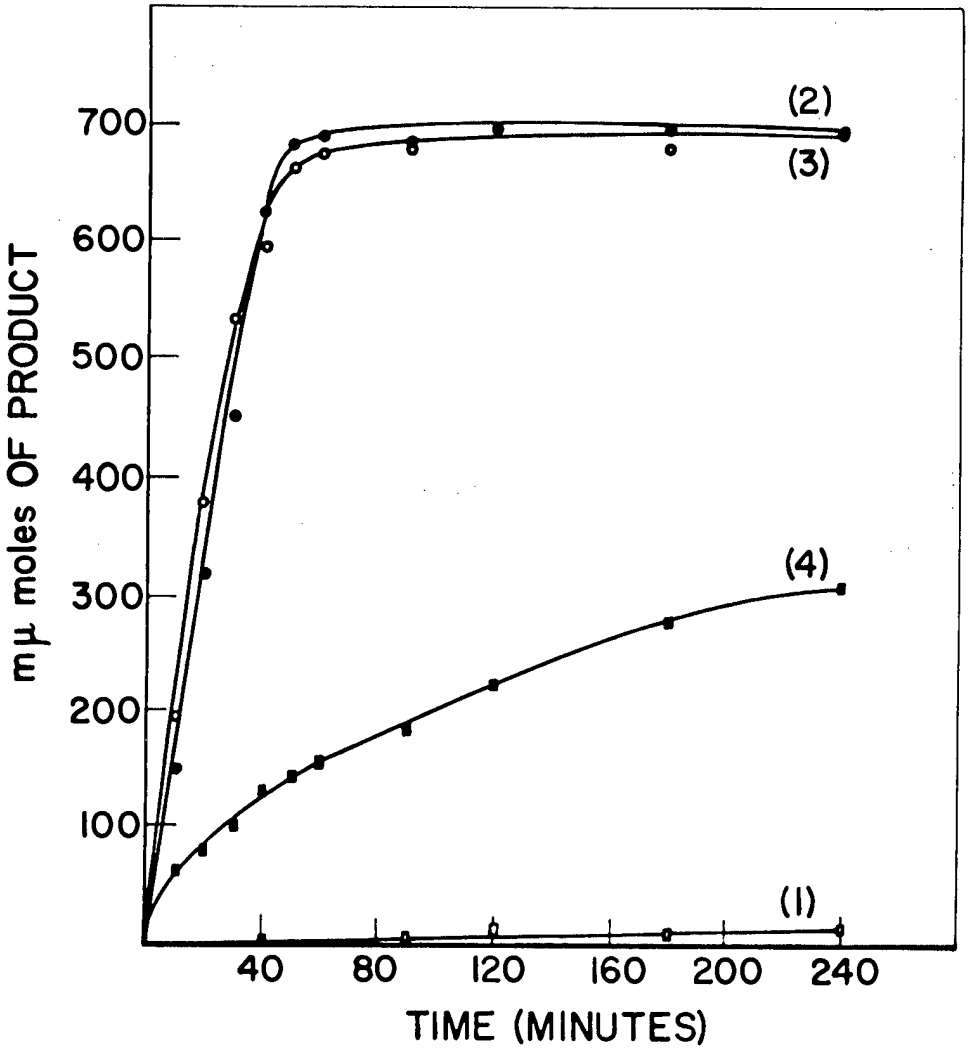

Fig. 1. Kinetics of RNA polymerase reaction using various primers. The reaction mixture contained in 1 ml 30 μmoles Tris, pH 7.9, 3 μmoles $MgCl_2$, 0.75 μmole $MnCl_2$, 10 μmoles 2-mercaptoethanol, 0.7 μmole ATP-8-^{14}C, and the following primers: 0.03 μmole $(pt)_6$ (curve 1); 0.03 μmole $(pt)_{13}$ (curve 2); 0.45 μmole heat-denatured calf thymus DNA (curve 3); and 0.6 μmole each ATP, GTP, UTP, and CTP-^{14}C and 0.45 μmole calf thymus DNA (curve 4). Each reaction contained 85 μg of enzyme. The reaction mixture was incubated at 37°, and 0.1 ml was removed for each assay.

REFERENCES

(1) T. Nakamoto, C. F. Fox, and S. B. Weiss, J. Biol. Chem. 239, 167 (1964).

(2) A. Stevens and J. Henry, J. Biol. Chem. 239, 196 (1964).

(3) J. J. Furth, J. Hurwitz, and M. Anders, J. Biol. Chem. 237, 2611 (1962).

(4) E. Fuchs, W. Zielig, P. H. Hofschneider, and A. Preuss, J. Mol. Biol. 10, 546 (1964).

(5) M. Chamberlin and P. Berg, Proc. Natl. Acad. Sci., U. S. 48, 81 (1962).

(6) M. Yoneda and F. G. Bollum, J. Biol. Chem. 240, 3385 (1965).

(7) R. L. Ratliff and T. T. Trujillo, Los Alamos Scientific Laboratory Report LA-3132-MS (1964), pp. 236-239.

(8) C. H. W. Hirs, S. Moore, and W. H. Stein, J. Biol. Chem. 200, 493 (1953).

(9) D. A. Smith, R. L. Ratliff, T. T. Trujillo, D. L. Williams, and F. N. Hayes, J. Biol. Chem. 241, 1915 (1966).

(10) D. A. Smith, R. L. Ratliff, D. L. Williams, and A. Martinez (in preparation).

ENZYMATIC SYNTHESIS OF SHORT POLYDEOXYRIBONUCLEOTIDES (F. N. Hayes and V. E. Mitchell)

INTRODUCTION

Oligo- and polydeoxyribonucleotides of varied and known structures are miniature models of DNA and as such are useful for studies of the chemistry and radiobiology of DNA. In addition to purely chemical approaches to synthesis of such compounds (1), combined chemical and enzymatic methods have been applied with great success (2,3). The calf thymus-derived enzyme, terminal deoxyribonucleotidyl transferase (hereafter referred to as addase), has been used to effect synthesis of polydeoxyribonucleotides of 100 monomer units length or greater (2). In this report its applicability toward synthesis of short polymers is described.

The addase reaction uses an oligodeoxyribonucleotide initiator and involves repetitive grafting of mononucleotide units from a deoxyribonucleoside 5'-triphosphate onto the 3'-terminal hydroxyl function of a growing single-stranded polymer. For addase reaction product polymer mixtures with average length greater than 20, there are no effective methods for fractionation of the individual molecular species according to length. Therefore, such products are handled as mixtures and described as average structures. However, in the less than 20-nucleotide unit range, fractionation can be accomplished with anion exchange resins such as DEAE-cellulose. We have successfully applied this methodology to obtain individual oligomers from addase reactions involving only a few additions to the initiator.

MATERIALS AND METHODS

Oligo-5'-thymidylic acids, $(pt)_n$, were synthesized by the method of Khorana and Vizsolyi (4) from pt and ^{3}H-pt (5). Deoxyribonucleoside 5'-triphosphates were obtained from Pabst Laboratories and Schwarz BioResearch, Inc. Addase was isolated from calf thymus according to the procedure of Yoneda and Bollum (6,7).

Where it was desired to recover residual addase from completed polymerizations, the reaction mixture was run through phosphocellulose (Whatman P-70), 100 mg/mg protein, which

passed the polynucleotide but retained the protein. Protein was subsequently removed from the column with 0.3 M potassium phosphate (pH 6.9). When the addase was not to be recovered, it was heat-denatured and spun down. The deproteinized reaction mixture was then fractionated either on Bio-Gel P-60 for long polymers or on an anion exchange resin, after desalting on Bio-Gel P-2, for short polymers.

Homogeneous liquid scintillation counting, spectrophotometric measurements, and phosphorus analyses were carried out on the addase-derived products and on the oligodeoxyribonucleotide initiators.

EXPERIMENTS AND RESULTS

Reaction to Add Fifty 2'-Deoxyadenylate Units onto the Tetramer of 5'-Thymidylic Acid

The mixture containing 0.25 mM p3a, 5.1 μM (^{3}H-pt)$_4$, 8 mM $MgCl_2$, 1 mM 2-mercaptoethanol, and 7,140 units of addase made up to 16 ml with 0.05 M potassium phosphate (pH 6.9) was incubated at 35° for 3 hours, whereupon 31 percent hypochromicity had occurred. The yield of polymer was 3.9 mono-μmoles (90 percent), and its average structure was calculated from isotopic dilution to be (^{3}H-pt)$_4$(pa)$\overline{58}$.

Reaction to Add Ten 2'-Deoxyadenylate Units onto the Pentamer of 5'-Thymidylic Acid

The mixture containing 83 μM p3a, 8.3 μM (^{3}H-pt)$_5$, 8 mM $MgCl_2$, 1 mM 2-mercaptoethanol, and 75,000 units of addase made up to 60 ml with 0.05 M potassium phosphate (pH 6.9) was incubated at 35° for 2 hours. After desalting on Bio-Gel P-2, the product was fractionated on DEAE-cellulose with a lithium chloride gradient at pH 5.0. The larger molecules did not separate into individual species, but the broad peak of product was cut into two major fractions: one analyzing for (^{3}H-pt)$_5$(pa)$\overline{10.5}$ and the other for (^{3}H-pt)$_5$(pa)$\overline{19.9}$.

Reaction to Add Three 2'-Deoxycytidylate Units onto the Pentamer of 5'-Thymidylic Acid

The mixture containing 0.194 mM p_3c, 64.6 μM $(pt)_5$, 8 mM $MgCl_2$, 1.4 mM 2-mercaptoethanol, and 680,000 units of addase made up to 100 ml with 0.1 M glycerol was incubated at 10° for 7 hours. The reaction was 0.01 M in potassium phosphate. After the reaction was terminated, it was passed through phosphocellulose from which was later recovered 323,000 units of addase. The eluted nucleotide containing solution was desalted on Bio-Gel P-2 giving, after concentration, 5 ml containing 350 A_{267} units. This was fractionated on ECMOR-SF-1 [(8), 1 x 10 cm, 0 to 0.3 M LiCl (pH 5.0), 6 l.) producing an elution profile, part of which is reproduced in Fig. 1. Each of the fractions numbered I through VI was desalted on Bio-Gel P-2 and then spectrophotometrically analyzed. Fraction VI, thought to contain the highest percentage of pc, was analyzed at both pH 7.0 and pH 2.0, showing a pronounced hypsochromic shift on λ_{max} from 267 mμ (pH 7.0) to 273 mμ (pH 2.0), while its A_{280}/A_{260} ratio changed from 0.78 to 1.15. This agrees qualitatively with that expected from a mixed spectrum of pc and pt. Further work on characterizing these fractions is in progress. Preliminary evidence indicates that fraction IV may be $(pt)_5(pc)_3$.

DISCUSSION

It has been found practical to add less than 100 nucleotide units to an initiator in the addase reaction. In an extreme case just a few were added, and the products were separated by anion exchange chromatography. Thus, the range of usefulness of the addase reaction is extended, and we will be able to effect enzymatic synthesis of more varied sequences than possible from a single-step, single-base addase reaction.

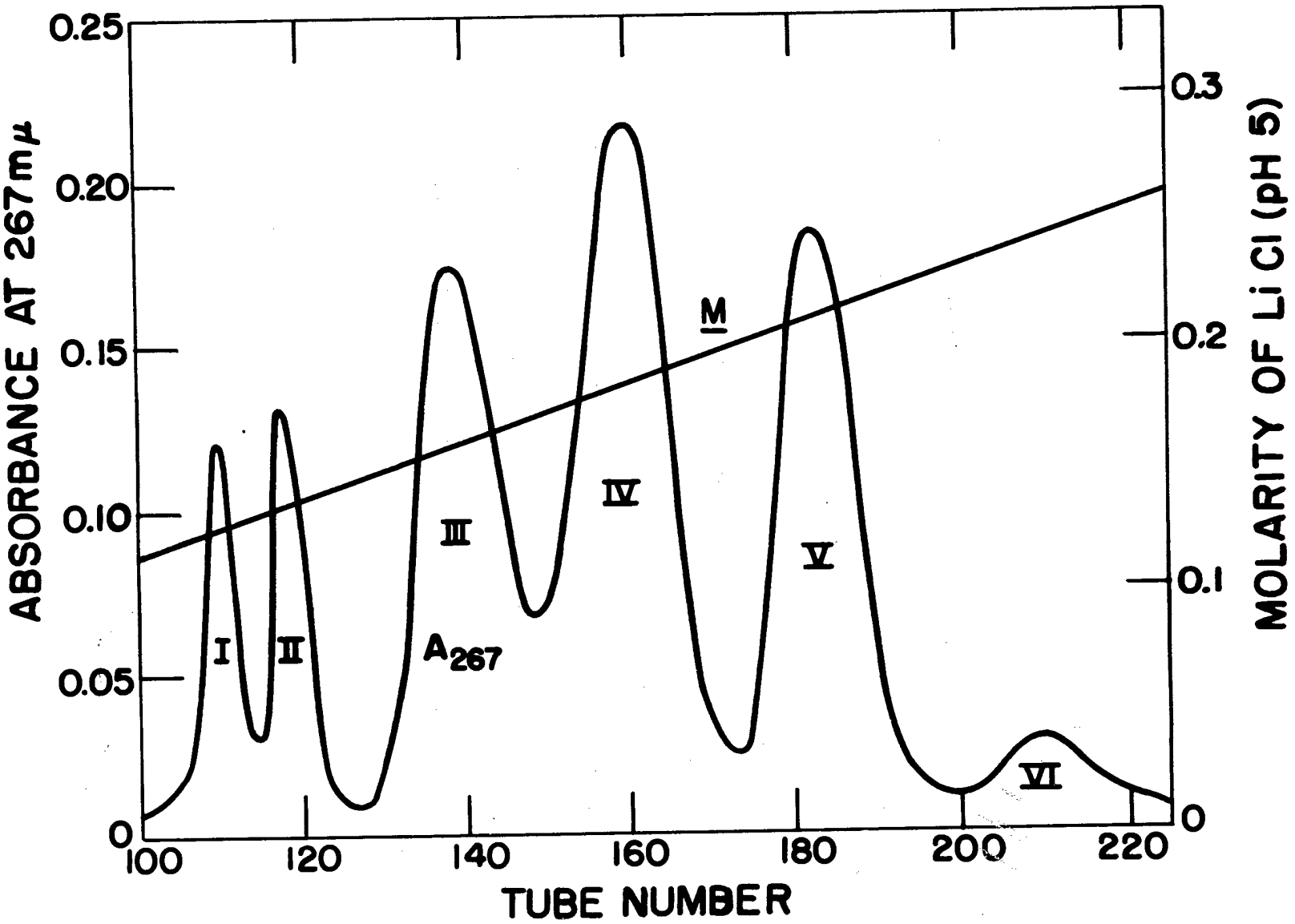

Fig. 1. Elution profile of major products from $(pt)_5$ plus p_3c reaction.

REFERENCES

(1) T. M. Jacob and H. G. Khorana, J. Am. Chem. Soc. 87, 2971 (1965).

(2) F. J. Bollum, E. Groeniger, and M. Yoneda, Proc. Natl. Acad. Sci., U. S. 51, 853 (1964).

(3) C. Byrd, E. Ohtsuka, M. W. Moon, and H. G. Khorana, Proc. Natl. Acad. Sci., U. S. 53, 79 (1965).

(4) H. G. Khorana and J. P. Vizsolyi, J. Am. Chem. Soc. 83, 675 (1961).

(5) D. L. Williams, this report, p. 102.

(6) M. Yoneda and F. J. Bollum, J. Biol. Chem. 240, 3385 (1965).

(7) R. L. Ratliff and T. T. Trujillo, Los Alamos Scientific Laboratory Report LA-3432-MS (1965), p. 241.

(8) A. Murray, Los Alamos Scientific Laboratory Report LA-3432-MS (1965), p. 215.

SIMULTANEOUS USE OF TWO OR MORE DEOXYNUCLEOTIDE 5'-TRIPHOSPHATES FOR POLYDEOXYNUCLEOTIDE SYNTHESIS WITH TERMINAL DEOXYNUCLEOTIDYL TRANSFERASE FROM CALF THYMUS GLANDS

(R. L. Ratliff, T. T. Trujillo, D. G. Ott, and D. E. Hoard)

INTRODUCTION

The synthesis of polydeoxynucleotides using an oligodeoxyribonucleotide with a chain length of 3 or more, a deoxynucleoside 5'-triphosphate, and the terminal deoxynucleotidyl transferase (addase) has been reported previously by Bollum (1) and Hayes (2). The present experimental work was designed to determine if 2 or more nucleoside triphosphates could be utilized simultaneously in the synthesis of copolymers or mixtures of homopolymers.

MATERIALS AND METHODS

Addase was purified according to the procedure of Bollum (1). The oligodeoxyribonucleotide, $(pt)_6$, was prepared in this Laboratory. The reaction mixture contained 40 mM potassium phosphate (pH 7.0), 8 mM $MgCl_2$, and 1 mM 2-mercaptoethanol. The deoxynucleoside triphosphate, $(pt)_6$, and enzyme concentrations are given in the various reactions (Tables 1 and 2).

All combinations of 2, 3, as well as single, and all 4 nucleoside triphosphates were incubated with initiator and enzyme at 37° for the time specified. One of the nucleoside triphosphates in each reaction was labeled with carbon-14, and the degree of polymerization of each labeled nucleotide was determined from the radioactivity of acid-insoluble product. Table 1 gives the results for incorporation of each carbon-14 labeled nucleoside triphosphate. The superior substrate when only one nucleotide is present is dATP; however, when 2 or more nucleotides are included in the incubation mixture, dGTP is the best substrate.

Following reaction the polymers were isolated, deproteinized, and dialyzed. Absorbance versus temperature profiles (Table 2) were determined in 0.15 M NaCl, 0.015 M sodium citrate [pH 7.0 (3)] with an automated recording apparatus providing a temperature change rate of 0.4°/minute.

TABLE 1. INCORPORATION RESULTS FROM ADDASE REACTIONS

Nucleoside Triphosphates Added	Incorporation of Nucleotides (mμmoles)*			
	^{14}C-dAMP	^{14}C-dCMP	^{14}C-dGMP	^{14}C-TMP
dATP	512 (979)			
dCTP		7 (461)		
dGTP			146 (185)	
TTP				23 (45)
dATP, dCTP	39 (349)	34 (444)		
dATP, dGTP	278 (516)		323 (553)	
dATP, TTP	109 (208)			77 (257)
dCTP, dGTP		55 (370)	128 (441)	
dCTP, TTP		8 (256)		10 (141)
dGTP, TTP			106 (248)	31 (97)
dATP, dCTP, dGTP	49 (179)	51 (270)	108 (325)	
dATP, dCTP, TTP	18 (191)	16 (243)		19 (240)
dATP, dGTP, TTP	88 (276)		134 (323)	50 (238)
dCTP, dGTP, TTP		25 (173)	66 (271)	18 (106)
dATP, dCTP, dGTP, TTP	41 (142)	35 (196)	78 (236)	25 (160)

*Separate incubations were used for each reaction, each containing a different carbon-14 labeled nucleotide. The amount of initiator used was 0.01 μmole $(pt)_6$, the total nucleoside triphosphate concentration was 1 μmole, and the reaction time was 1 hour. Each incubation contained 60 μg of addase; all other conditions were those given for a standard assay. The final volume was 1.5 ml, the reactions were incubated at 37°, and 0.1 ml was removed for each assay. The mμmoles of nucleoside triphosphate incorporated are for total volume. The values in parentheses are for 24 hours.

TABLE 2. THERMAL HYPERCHROMICITY DATA

Polymer	Hyperchromicity (percent)	T_m (°C)*	Temperature Range (°C)
d-A,G	24	--	22 - 90
d-A,T	23	42	25 - 75
d-C,G	21	86	30 - 103
d-A,G,T	17	--	30 - 92
d-A,C,G	13	--	23 - 95
d-A,C	11	--	25 - 67
d-A,C,G,T	7	--	29 - 74
d-G,T	6	--	26 - 95
d-C,G,T	6	--	23 - 84
d-A,C,T	5	--	23 - 100
d-C,T	2	--	27 - 100
d-AT:d-AT**	52	64.5	23 - 100
d-A,T:d-A,T+	44	64	26 - 93
d-A:d-T‡	48	65.5	30 - 90

*No value given indicates no inflection over this temperature range.

**Copolymer synthesized de novo with E. coli DNA polymerase.

+Synthesized with calf thymus DNA polymerase and poly d-A,T as template.

‡Synthesized with calf thymus DNA polymerase and poly d-A as template.

RESULTS AND DISCUSSION

Analysis of the poly d-A,T by the Burton degradation (4) gave oligothymidylate sequences of various lengths and adenine. Studies are being done on other mixed polymers to determine the length of various nucleotide sequences, as well as the effect of changing the ratio of deoxynucleotide triphosphates thereon.

REFERENCES

(1) M. Yoneda and F. G. Bollum, J. Biol. Chem. 240, 3385 (1965).

(2) F. N. Hayes, A. W. Schwartz, R. L. Ratliff, V. N. Kerr, and T. T. Trujillo, Biochemistry (submitted).

(3) J. Marmur and P. Doty, J. Mol. Biol. 5, 109 (1962).

(4) K. Burton and G. B. Petersen, Biochem. J. 75, 17 (1960).

P^1,P^2-PYROPHOSPHATES AS INITIATORS IN THE TERMINAL DEOXYRIBONUCLEOTIDE TRANSFERASE REACTION (A. W. Schwartz)

INTRODUCTION

In order to synthesize oligo- and polynucleotides of known sequence by means of the enzyme calf thymus terminal deoxynucleotidyl transferase (addase), it is desirable to utilize dinucleotides as initiators as well as trinucleotides and higher oligomers. Although Bollum (1) has not found it possible to incorporate dimeric initiators under standard conditions, there was some preliminary evidence (2) that $(pt)_2$ might serve as an initiator when in the form of the P^1,P^2-symmetrical pyrophosphate, II (Fig. 1). Various pyrophosphates were consequently synthesized, and their activities as initiators in terminal polymerization were studied.

METHODS AND RESULTS

The procedure of Smith, Moffatt, and Khorana (3) was utilized to synthesize the symmetrical pyrophosphates I, II, and III (Fig. 1). For synthesis of the mixed pyrophosphate of pt and $(pt)_2$, IV, a 10 fold excess of pt was employed in order to favor the synthesis of the unsymmetrical product at the expense of the symmetrical pyrophosphate II. A yield of 82 percent was obtained, based on incorporation of $(pt)_2$ into the final unsymmetrical pyrophosphate. The reaction products were purified by chromatography on DEAE-cellulose with a linear gradient of triethylammonium bicarbonate, and the identity of the pyrophosphates was substantiated by paper chromatography of the products of acetic anhydride cleavage (4).

Figure 2 illustrates the rate of incorporation of dATP using various initiators. It is apparent that incorporating $(pt)_2$ into a pyrophosphate does indeed appear to increase its ability to act as an initiator; however, the efficiency of incorporation was extremely low. In two polymerizations using the unsymmetrical pyrophosphate IV, incorporation of initiator was 0.9 and 1.5 percent. Similarly, only 0.7 percent of II was incorporated in another experiment (Table 1). It appears that this approach to incorporating dimer as initiator in the addase reaction is particularly inefficient;

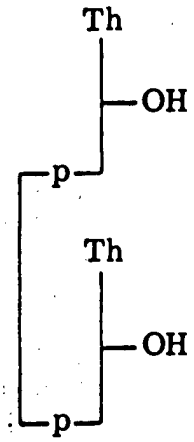

I

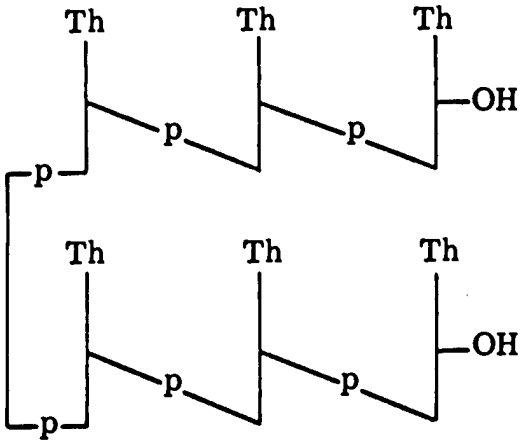

III

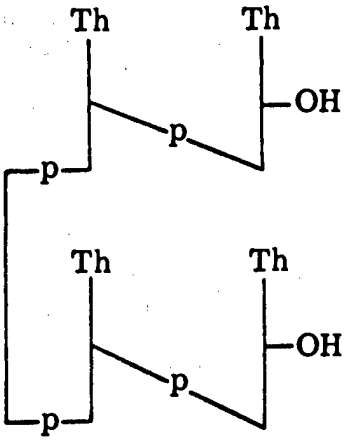

II

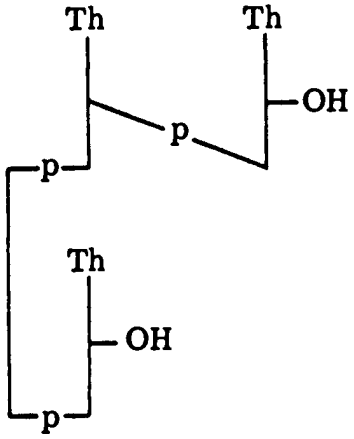

IV

Fig. 1. Pyrophosphates tested as initiators.

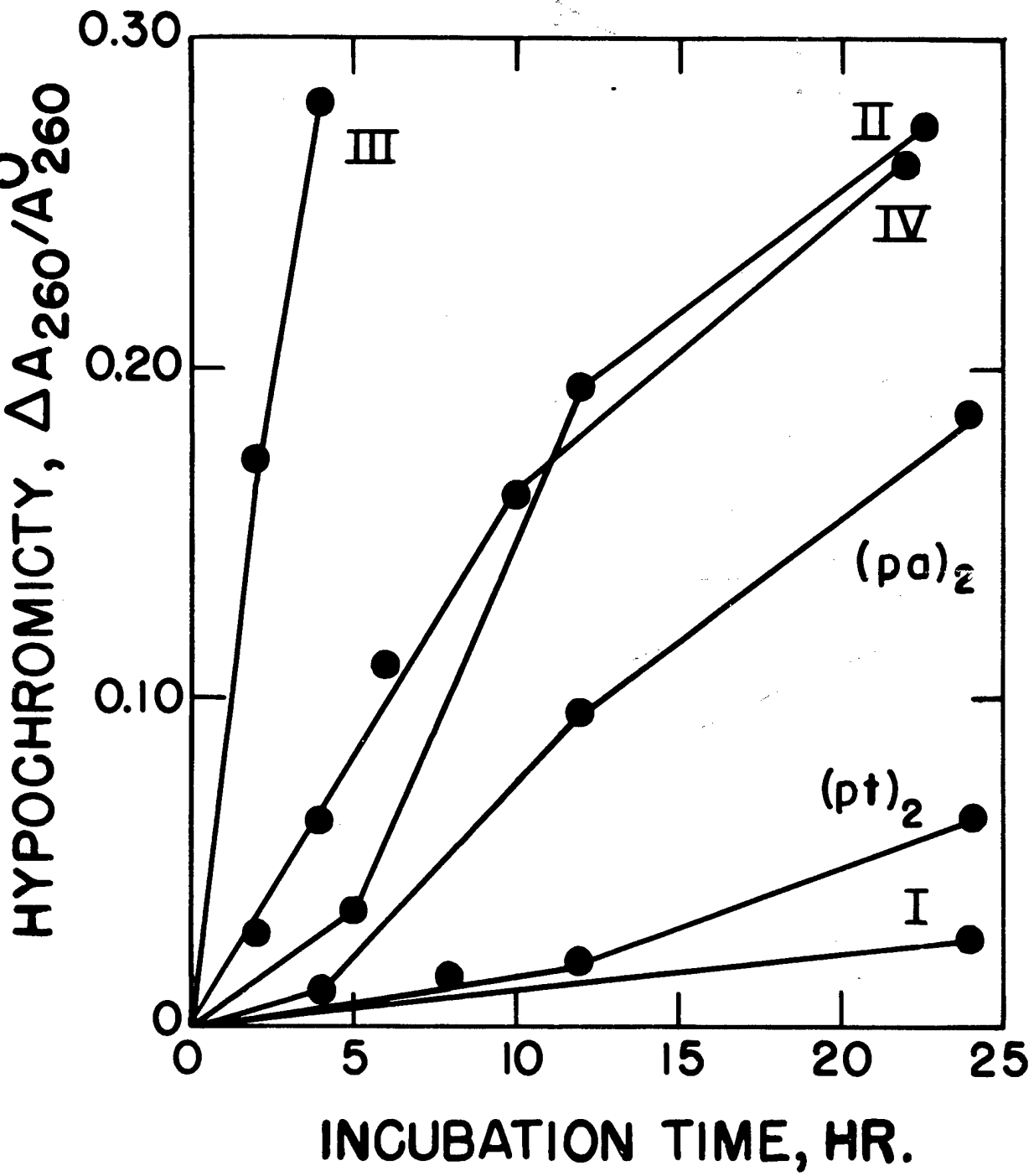

Fig. 2. Kinetics of incorporation of dATP with various initiators. All solutions 1.0 mM dATP, 0.01 mM initiator. I, $(pt)_2$, $(pa)_2$, and IV contained 1000 addase units/ml; II contained 1500 units/ml; III contained 655 units/ml.

TABLE 1. SUMMARY OF POLYMERIZATIONS*

Polymer	Initiator	Initiator (μmoles/ml)	dATP (μmoles/ml)	Addase (units/ml)	Hours	Polymer Yield (percent)	Initiator Incorporation (percent)	n**	S_{obs}
A	^{3}H-$(pt)_5$	0.0005	1.0	1500	12	82	100	1600	6.0
B	^{3}H-$(pt)_3$	0.04	1.0	1200	1.5	90	49	52	-
C		0.01	1.0	655	6	45	28	170	-
D		0.002	1.0	655	6	85	81	514	-
E		0.002	0.2	655	6	92	37	245	-
F		0.001	1.0	1100	4	69	72	951	-
G	$(pt)_2$	0.01	1.0	1000	24	19	--	--	-
H	$(pa)_2$	0.01	1.0	1000	24	58	--	--	-
I	I	0.01	1.0	1000	24	9	--	--	-
J	IV	0.01	1.0	1000	22	78	--	--	-
K	^{14}C-IV	0.01	1.0	1000	24	23	0.9	4000	6.0
L		0.01	1.0	350	48	26	1.5	1300	8.7
M	^{3}H-II	0.01	1.0	1500	23	81	0.7	11,000	4.2
N	III	0.01	1.0	655	4	85	--	--	-
O	^{3}H-III	0.002	1.0	340	21	82	67	676	-
P		0.01	1.0	1390	4	97	37	267	3.0

*All polymerizations in 0.05 M potassium phosphate (pH 6.9), 1 mM 2-mercaptoethanol, 8 mM $MgCl_2$; incubated at 35°.

**Calculated from specific activity.

in fact, there is some doubt as to their actual incorporation. There is no correlation between the S_{obs} and specific activities of the products. In the case of polymer L, when refractionated on a column of P-300 in the presence of urea, the specific activity dropped from 9.8 to 7.8 x 10^6 disintegrations/minute/A_{260} unit. Recently discovered conditions for increased utilization of small initiators (5) have not as yet been applied to these poorly incorporated pyrophosphates.

Incorporation of the symmetrical pyrophosphate III is on considerably firmer ground. Since the initiating pyrophosphate was exclusively pyrimidine in nature and the remainder of the polymer consisted of acid-labile pa residues, a Burton degradation (6) was employed to isolate the initiator segment of the polymer molecule obtained with III (polymer O, Table 1 and Fig. 3). It can be seen that degradation of a polyadenylic acid chain will leave a 3'-phosphate end group on the original initiator. Therefore, if all available 3'-hydroxyl groups of the incorporated initiator had been utilized in polymerization, Burton degradation of the product would produce the di-substituted fragment V. Fractionation of the products of the Burton degradation of polymer O gave peaks corresponding to 8 and 10 charges from a DEAE-cellulose column [1 x 10 cm, 0.005 to 0.5 M triethylammonium bicarbonate (pH 7.8), 1 l.], suggesting structures VI and V, respectively. The recovered label was distributed 21 percent to VI and 74 percent to V. These products were treated with E. coli alkaline phosphatase, and the dephosphorylated products were each shown to be identical with the original pyrophosphate initiator by paper chromatography. It can be concluded, therefore, that most of the polymer molecules are substituted at both ends by pa residues. Formation of a minor proportion of VI may indicate the presence of some unsymmetrically polymerized species or perhaps partial dephosphorylation of V.

DISCUSSION

Although it is apparently possible to utilize $(pt)_2$ as an initiator in the addase reaction by its incorporation into a pyrophosphate, there appears to be little practical value to the method. Efficiency is very low, and it has thus far not been possible to cleave selectively the pyrophosphate bond in such products. The polymer which was produced from

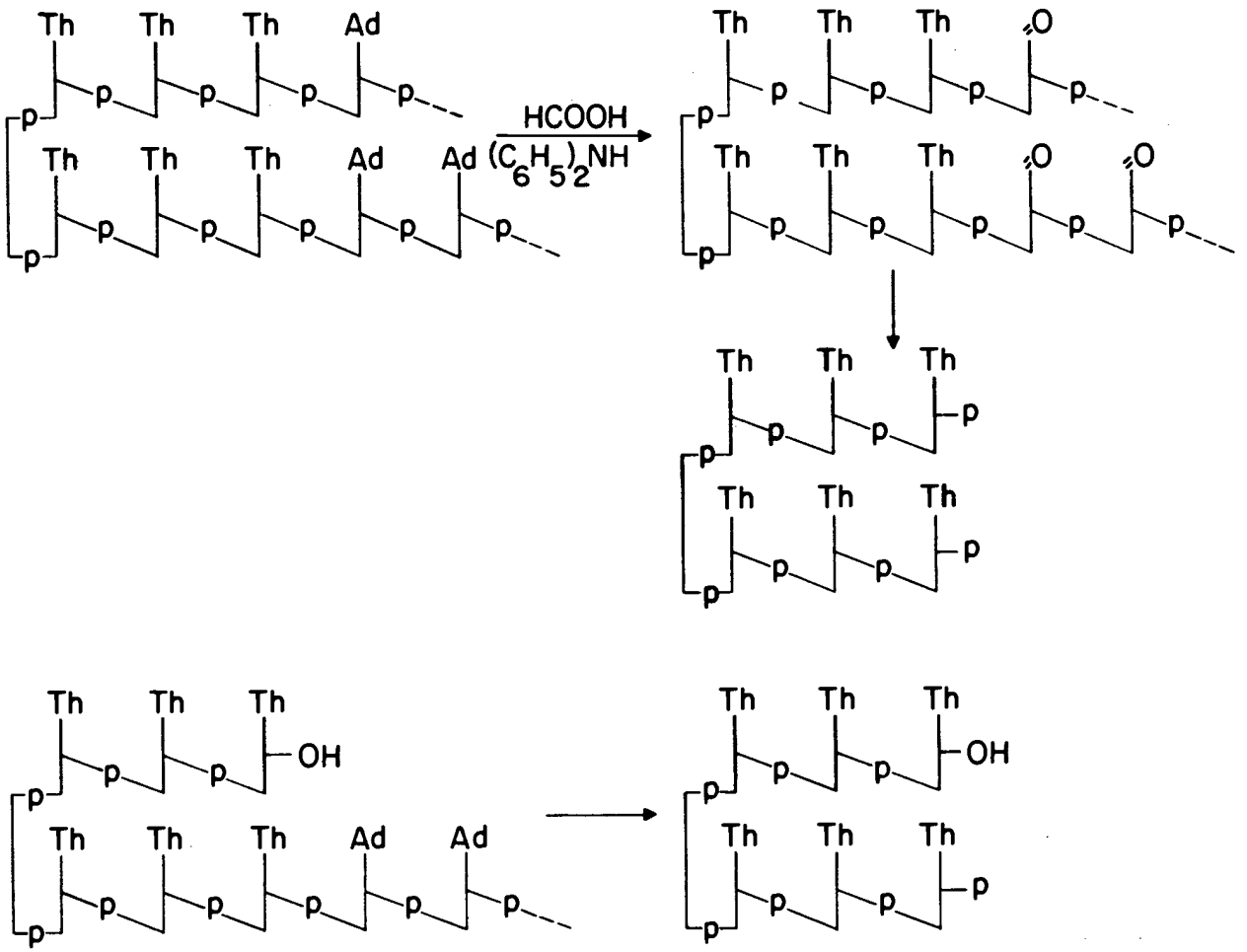

Fig. 3. Possible reactions in Burton degradation of polymer O.

the symmetrical pyrophosphate of (pt)3 and which was shown to possess predominantly adenylate end groups was also originally sought as a model for pyrophosphate cleavage studies. Recent work of Moon and Khorana (7) indicates that conventional chemical methods are not adequate for cleavage of such materials. No further synthetic work in this direction is planned, although the addase product derived from II will be used as template in DNA- and RNA-polymerase reactions. These studies are to determine whether information can be read out in two directions at the same time from the same strand.

REFERENCES

(1) F. J. Bollum, E. Groeniger, and M. Yoneda, Proc. Natl. Acad. Sci., U. S. 51, 853 (1964).

(2) A. W. Schwartz and V. N. Kerr, Los Alamos Scientific Laboratory Report LAMS-3034 (1965), p. 211.

(3) M. Smith, J. G. Moffatt, and H. G. Khorana, J. Am. Chem. Soc. 80, 6204 (1958).

(4) H. G. Khorana, J. P. Vizsolyi, and R. T. Ralph, J. Am. Chem. Soc. 84, 414 (1962).

(5) F. N. Hayes, V. E. Mitchell, R. L. Ratliff, A. W. Schwartz, and D. L. Williams, Biochemistry (submitted).

(6) K. Burton and G. B. Petersen, Biochem. Biophys. Acta 26, 667 (1957).

(7) M. W. Moon and H. G. Khorana, J. Am. Chem. Soc. 88, 1798 (1966).

SYNTHESIS OF OLIGO- AND POLYDEOXYNUCLEOTIDES BY ENZYMATIC MEANS (D. E. Hoard and W. B. Goad*)

INTRODUCTION

Long-chain polydeoxynucleotides which cannot be prepared by purely chemical procedures are easily synthesized in reactions mediated by the purified terminal deoxyribonucleotidyl transferase (addase) from calf thymus (1,2). Treatment of addase-synthesized homopolymers with nucleases (3) enables one to prepare the corresponding series of oligomers; one advantage of such a procedure is that properly chosen conditions ought to afford better yields of the oligonucleotides of chain-length greater than 4 mononucleotide residues than purely chemical procedures. The ability of addase to attach a long homopolynucleotide single strand to an oligonucleotide initiator can then be employed for synthesis of a chain in which a piece of differing sequence information is present at the 5'-end or, as in the present instance, a radioactively-labeled segment of known length. Such products are useful, for example, in further defining the specificities of various nucleases (4).

METHODS AND RESULTS

Polydeoxyadenylate Syntheses Catalyzed by Addase

These reactions were carried out at 35° in 0.005 M potassium phosphate buffer (pH 6.9) in the presence of magnesium chloride (0.01 M) and 2-mercaptoethanol (0.001 M), with deoxyadenosine 5'-triphosphate at a concentration of 1 mM and addase at a ratio of 500 to 600 units (5) per μmole triphosphate. The presence of oligonucleotide initiator was always found to be necessary for a reaction to take place; the concentration chosen was dictated by the ultimate chain-length desired in the product. The course of the reaction was followed spectrophotometrically. Reaction was judged to be complete when the A_{260} of the reaction mixture had fallen to 67 to 70 percent of its initial value.

---

*Group T-4 of the Theoretical Division, Los Alamos Scientific Laboratory.

Uniformly Tritium-Labeled Polydeoxyadenylate

This material was synthesized under the conditions described above employing ^{3}H-deoxyadenosine 5'-triphosphate (100 μ-moles) with unlabeled deoxyadenylyl(5':3')deoxyadenylyl-(5':3')deoxy-5'-adenylic acid, $(pa)_3$ (0.33 μmole), as initiator. (The concentration of initiator was kept low in this instance to minimize the possibility of unequal labeling in oligomers derived from the polymer due to the presence of an unlabeled trimer segment at the 5'-end.) After 48 hours, the polymer was isolated by repeated precipitation from 0.5-M sodium chloride solution with alcohol and was finally de-salted by passage through a column of Bio-Gel P-2 polyacryl-amide gel (4.5 x 60 cm). The ultimate product comprised 73 μg-atoms esterified phosphorus (73 percent), specific activity 2.54 x 10^6 disintegrations/minute/μg-atom P.

The Polynucleotide ^{3}H-$(pa)_6(pa)_{124}$

This polynucleotide was synthesized with addase employing as initiator uniformly-labeled ^{3}H-$(pa)_6$ (0.3 μmole, isolated as described below) and unlabeled deoxyadenosine 5'-triphosphate (29 μmoles). On this scale the product was most conveniently purified by a single passage of the reaction mixture (0.5 M in sodium chloride) through a column of Bio-Gel P-60 (2 x 30 cm) using 0.005 M triethylammonium bicarbonate as developer, followed by removal of the bicarbonate by volatilization. The purified product comprised 30 μg-atoms organic phosphorus (114,750 disintegrations/minute/μg-atom P). The dilution of specific activity indicated an average chain-length of 130 deoxyadenylate residues.

Uniformly-Labeled Oligodeoxyadenylates

These oligodeoxyadenylates were isolated after partial digestion of uniformly-labeled polydeoxyadenylate (72 μg-atom P) by crystalline DNase I (4.2 mg) at 7.9 and 35° in a pH stat. In addition to the above substances, the solution contained magnesium acetate (120 μmoles) and sodium acetate (450 μ-moles) in an initial volume of 13 ml. Within 1 hour the instrument had delivered 170 μl. 0.1 N KOH in holding the pH to its initial value. Protein was separated from the reaction mixture by heating for 5 minutes on a steam bath, followed

by centrifugation; the deproteinized supernatant solution was applied to a column of DEAE-cellulose (bicarbonate form, 3.1 x 38 cm). After washing with water, the column was eluted with a linear gradient of triethylammonium bicarbonate (pH 7.5, 0 to 0.5 M, 8 l.). This elution schedule gave the recovery of some 35 percent of the initial nucleotide material in 8 well-resolved peaks [pa through $(pa)_8$] plus $(pa)_9$ and $(pa)_{10}$, the latter two being only partially separated from each other (Table 1). The remaining ultraviolet-absorbing material, which must have represented oligonucleotides of chain-length in excess of 10 residues but considerably smaller than the original polynucleotide, was quantitatively recovered upon eluting the column with 800 ml of 1.6 M triethylammonium bicarbonate solution. Fractions comprising individual peaks were pooled and concentrated in vacuo at low temperature or were lyophilized, and triethylammonium bicarbonate was removed by repeated evaporation of ethanol solutions of the residual material.

DISCUSSION

The principal disadvantage of the above procedure for preparation of homodeoxynucleotide oligomers is the requirement for substantial quantities of the purified addase enzyme. Once this requirement has been met, however, the procedure offers considerable advantages. Of these the most compelling is probably that the scale of reaction and, more particularly, the simplicity of the steps required make the procedure ideally suited for the synthesis of radioactively-labeled materials. The degradation of the addase-synthesized polydeoxyadenylic acid by DNase I was purposely terminated at a point where only an estimated 24 percent of the total phosphodiester bonds of the substrate had been cleaved; mathematical calculations based on a simplified model of the specificity of DNase I had indicated that the hexamer would occur at optimal concentration in the mixture of oligonucleotide products when the digestion was carried out to this extent. From Table 1 it is apparent that the number of monomer units found in hexamer exceeded the corresponding numbers recovered in the remaining identified fractions from monomer through decamer, in accord with the prediction. Although the bulk of the oligonucleotides in the digest was still of chain-length greater than 10 units, it is possible to recover more of the shorter oligomers by further digestion of this fraction with DNase I.

TABLE 1. ION EXCHANGE FRACTIONATION OF UNIFORMLY-LABELED OLIGODEOXYADENYLATES

Peak	Compound	Percent of Applied A_{260}
I	pa	0.64
II	$(pa)_2$	1.63
III	$(pa)_3$	2.42
IV	$(pa)_4$	2.70
V	$(pa)_5$	2.91
VI	$(pa)_6$	3.26
VII	$(pa)_7$	2.84
VIII	$(pa)_8$	2.68
IX, X	$(pa)_9$, $(pa)_{10}$	5.52

REFERENCES

(1) F. J. Bollum, E. Groeniger, and M. Yoneda, Proc. Natl. Acad. Sci., U. S. 51, 853 (1964).

(2) F. N. Hayes and V. E. Mitchell, Los Alamos Scientific Laboratory Report LA-3432-MS (1965), p. 178.

(3) F. J. Bollum, J. Biol. Chem. 240, 2599 (1965).

(4) D. E. Hoard, this report, p. 95.

(5) R. L. Ratliff and T. T. Trujillo, Los Alamos Scientific Laboratory Report LA-3432-MS (1965), p. 247.

INVESTIGATION OF THE MODE OF ACTION OF NUCLEASES USING DEFINED POLYDEOXYNUCLEOTIDE SUBSTRATES (D. E. Hoard)

INTRODUCTION

Most knowledge currently available on the modes of action of various nucleases in the deoxyribonucleotide field has resulted from studies which employed short, chemically-synthesized oligodeoxynucleotides of known sequence as substrates (1-3). A limitation of such studies is the fact that features of nuclease activity having profound influence during the initial stages of degradation of the enormous polynucleotide molecules found in nature may be discovered through digestion of only such low molecular-weight materials. Comparatively long-chained polydeoxynucleotides, either homopolymeric (4) or containing a limited amount of other sequence information at the 5'-ends of the chains (5), are readily synthesizable with the aid of terminal deoxyribonucleotidyl transferase (addase) of calf thymus. Partial digestions of one such material by various nucleases have been undertaken in hope of further defining the modes of attack of these enzymes on high molecular-weight polydeoxynucleotides.

METHODS

Polydeoxyadenylate

Polydeoxyadenylate of average chain length of 130 nucleotide residues, the 5'-terminal hexamer segment tritium-labeled (114,750 disintegrations/minute/μg-atom P on day of assay), was prepared as described elsewhere in this report (6).

Nuclease Digestions

These were carried out at 37° in a Metrohm pH stat. In addition to enzyme, each solution (1.1 to 1.2 ml) contained 4.6 to 4.8 μg-atoms substrate P, 44 μmoles sodium acetate, and 11 μmoles magnesium acetate. Upon addition by the instrument of an amount of alkali corresponding to the desired degree of enzymatic hydrolysis (10 to 50 percent of the substrate

phosphodiester bonds, depending on the nuclease being studied), the reaction was terminated by heating on a steam bath. Denatured protein was separated by low-speed centrifugation.

Characterization of Digests

Characterization of digests was by gel filtration chromatography on a column of Bio-Gel P-60 polyacrylamide gel (1 x 120 cm). Deproteinized digest (1 ml) was applied to the column, the column was eluted with 0.047 M aqueous triethylammonium bicarbonate solution, and the effluent was collected in fractions of approximately 5 ml. The elution positions of the undegraded polymer, a representative oligomer [$(pa)_8$], the monomer (pa), and the base adenine were established in calibration runs. Eluate fractions were analyzed spectrophotometrically; in instances where no established $\epsilon(P)$ value existed, the phosphorus content of fractions was determined directly. Fractions with demonstrable nucleotide content and, in some instances, fractions corresponding in elution position to a molecular species of interest but exhibiting no ultraviolet absorption were assayed for radioactivity by liquid scintillation counting.

RESULTS AND DISCUSSION

In Fig. 1 are shown the distributions of nucleotide products obtained after (a) cleavage of an estimated 50 percent of the phosphodiester bonds of the substrate with purified crotalus adamanteus venom diesterase at pH 9.0 (enzyme amount sufficient to hydrolyze completely 4 μmoles of thymidylyl(3':5')-thymidine 5'-phosphate in 1 hour), or (b) after cleavage of an estimated 20 percent of the substrate phosphodiester bonds by 0.28 mg of crystalline DNase I at pH 7.8. The contrast in patterns of the products of exo- and endonuclease activities is obvious; similar results have been reported by Birnboim (7). The radioactivity derived from the 6 nucleotide residues adjacent to the 5'-terminus (dashed lines in the figure) affords further insight into the modes of attack of both enzymes. As would be predicted from the known mode of attack of the venom diesterase (1), most of the radioactivity was recovered in the peak corresponding to partially degraded polymer. The increase in specific activity of this material (25 percent over that of the original substrate) is, however,

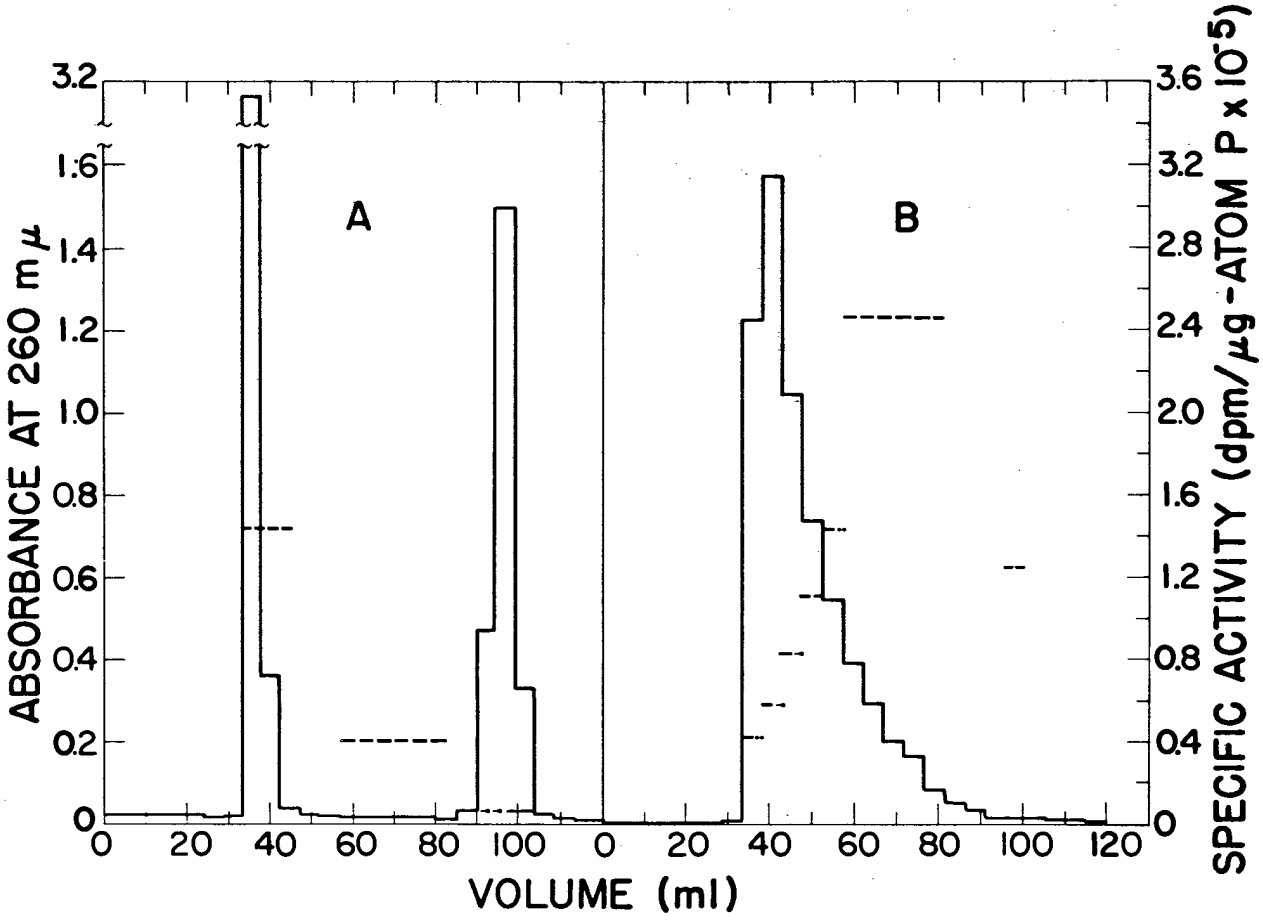

Fig. 1. Gel filtration chromatograms of partial digests of the polymer (^{3}H-pa)6(pa)$\overline{124}$ by (A) venom diesterase, and (B) DNase I. Specific activities of tritium in various fractions are indicated by the dashed lines (right-hand ordinate).

below what would be expected were mononucleotide residues being removed at equal rates from the 3'-ends of a more or less homogeneous population of long polynucleotide chains. The presence of radioactivity (2 percent of the applied sample) in the monomer fraction likewise indicates that significant exonucleolytic degradation has occurred near the 5'-terminus of a fraction of the substrate molecules.

These data alone do not provide an explanation for this finding; the presence initially of a small population of labeled chains significantly shorter than 130 nucleotide residues cannot be absolutely ruled out. Alternatively, a few such chains could have been formed during the course of the degradation by occasional endonucleolytic hits by the enzyme. If the rate of attack by the enzyme increases once the substrate chain has been reduced below a certain "critical" length, the results could have been produced by exonucleolytic action alone. No oligonucleotide intermediates were detectable in the chromatogram by ultraviolet absorption measurement. Radioactivity was detected in the oligonucleotide region but at such a marginal level as to preclude interpretation. Examination of the radioactivity of the fractions obtained after partial digestion with DNase I affords the rather startling result that the specific activity of the fragments bears an inverse relationship to their length. Since only 6 residues (out of an average of 130) adjacent to the 5'-end were labeled, a very marked preference on the part of the enzyme for diester bonds in the vicinity of the 5'-end must exist. Purely random endonucleolytic attack would produce oligonucleotide fragments of different lengths with similar specific activity to the original substrate, at least during early stages in the digestion.

In Fig. 2 are portrayed results obtained by partial digestion of the substrate with spleen diesterase at pH 6.5, either (a) after pretreatment with E. coli alkaline phosphatase (still present during the diesterase experiment), or (b) without phosphatase treatment. In experiment (a) digestion was continued until an estimated 40 percent of the phosphodiester bonds had been cleaved; in (b) substrate was exposed to diesterase alone for an identical time interval before denaturing the enzyme. In conformity with expectation, the bulk of the radioactivity under the conditions in (a) was recovered in the monomer fractions (deoxyadenosine 3'-phosphate plus deoxyadenosine derived from the former by dephosphorylation); only a vestige remained in the polymer. Possible oligomer intermediates were undetectable by either ultraviolet absorption or radioactivity; this suggests that

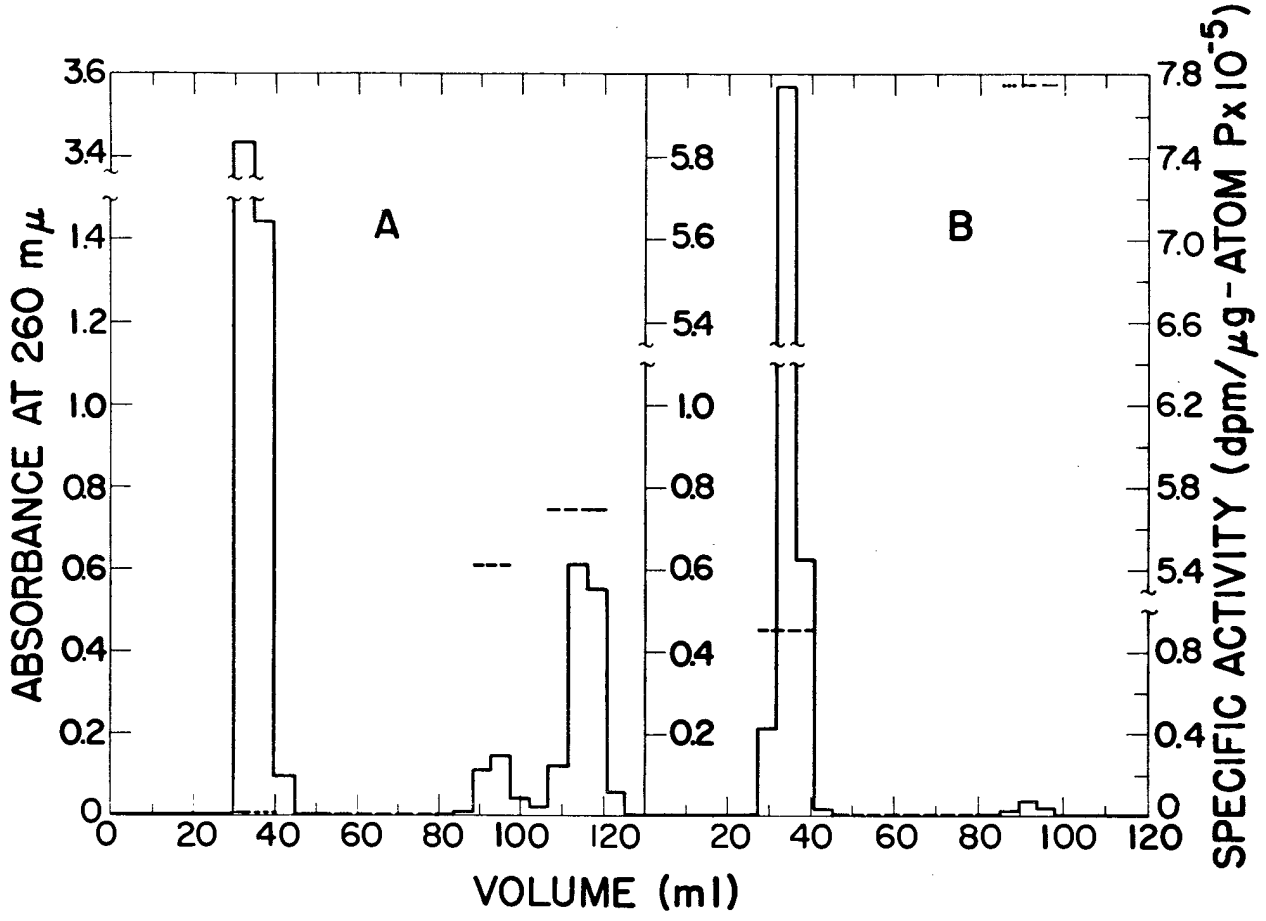

Fig. 2. Gel filtration chromatograms of spleen diesterase partial digests of $(^3H\text{-pa})_6(pa)_{\overline{124}}$: (A) with, and (B) without alkaline phosphatase. Specific activities of tritium in various fractions are indicated by the dashed lines (right-hand ordinate).

the spleen diesterase, even more than the venom diesterase, degrades short oligomers at a more rapid rate than long polynucleotide chains. The result of the experiment depicted in Fig. 2B seems to rule out the hypothetical possibility that attack, once begun on a given polynucleotide chain, is preferentially continued on that chain. Exonucleolytic attack is strongly (but not completely) inhibited by the presence of 5'-terminal phosphomonoester groups; such attack once begun does not give monomer with specific activity the same as the undegraded polymer chain (as would result if a slow first exonucleolytic cleavage were followed by a rapid complete degradation of each once-hit chain to monomer).

The results described above agree, in general, with published conclusions regarding exo- or endonucleolytic modes of attack of the various nucleases. The use of higher molecular-weight substrates containing sequence information of the type described has already permitted further conclusions to be drawn concerning these reactions, particularly in the case of DNase I. It is anticipated that further knowledge can be gained by use as substrates of other polydeoxynucleotides which can be synthesized with the aid of addase. As an example, substrates in which a labeled pyrimidine oligodeoxynucleotide segment is followed by a polydeoxyadenylate chain can be used to detect a preference of a nuclease for nucleoside sequences containing purine or pyrimidine bases. Incorporation of only slightly more sophisticated sequence information into the polymeric substrates should likewise permit the demonstration of possible preferential attack of certain internucleotide linkages by nucleases.

REFERENCES

(1) W. E. Razzell and H. G. Khorana, J. Biol. Chem. 234, 2114 (1959).

(2) W. E. Razzell and H. G. Khorana, J. Biol. Chem. 236, 1144 (1961).

(3) R. K. Ralph, R. A. Smith, and H. G. Khorana, Biochemistry 1, 131 (1962).

(4) F. J. Bollum, E. Groeniger, and M. Yoneda, Proc. Natl. Acad. Sci., U. S. 51, 853 (1964).

(5) F. N. Hayes and V. E. Mitchell, Los Alamos Scientific Laboratory Report LA-3432-MS (1965), p. 178.

(6) D. E. Hoard and W. B. Goad, this report, p. 90.

(7) H. Birnboim, Biochem. Biophys. Acta 119, 198 (1966).

CHEMICAL SYNTHESIS OF OLIGODEOXYRIBONUCLEOTIDES (D. L. Williams)

INTRODUCTION

The synthesis of oligodeoxyribonucleotides with a variety of known base sequences is being continued (1). These chemically derived compounds, isotopically labeled as desired, are useful initiators for studies with calf thymus deoxyribonucleotidyl transferase (addase) (2). Certain repetitive oligodeoxyribonucleotides are also of use in in vitro studies with RNA polymerase (3). These compounds are most efficiently synthesized by one of two routes: (a) homopolymerization of a mononucleotide (4,5), and (b) stepwise synthesis with suitably protected intermediates (6). In the latter procedure, a 5'-terminal phosphate group may be introduced as a final step.

METHODS AND RESULTS

A. Oligonucleotides by Polymerization of Mononucleotides

Oligomers of ^{3}H-5'-Thymidylic Acid.--The chemical polymerization of ^{3}H-5'-thymidylic acid was essentially according to a published procedure (4). A solution of pyridinium ^{3}H-5'-thymidylate (5 mmoles, 0.87 mc/mmole) was thoroughly dried by evaporation of anhydrous pyridine. The residue in 5 ml of dry pyridine was treated with 25 mmoles of dicyclohexylcarbodiimide (DCC) for a period of 6 days, with shaking. Separation of the resulting tritium-labeled oligonucleotides on a 4.5 x 50-cm DEAE-cellulose column (bicarbonate form), after the cleavage of pyrophosphate linkages, gave the proportion of products shown in Table 1. The linear oligonucleotides were further purified by rechromatography of the individual peaks on DEAE-cellulose (Cl^-) at pH 5.5.

Oligomers of ^{3}H-2'-Deoxy-5'-cytidylic Acid.--A mixture of 0.3 mmole of pyridinium ^{3}H-N-acetyl-2'-deoxy-5'-cytidylate and 0.1 mmole of pyridinium ^{3}H-N,O$^{3'}$-diacetyl-2'-deoxy-5'-cytidylate (2.42 mc/mmole) was thoroughly dried by evaporation of pyridine. The residue was dissolved in 1 ml of dry pyridine and treated with 1.2 mmoles of DCC, with shaking,

TABLE 1. DISTRIBUTION OF PRODUCTS FROM POLYMERIZATION OF ^{3}H-5'-THYMIDYLIC ACID

Column Peak	Nucleotide Material (percent of total)	Composition of Peak
2	3.0	Pyridinium nucleotide compound
3 and 4	0.8	Unknown and 3',5'-cyclic-pt
5	19.7	pt and 3',5'-cyclic-$(pt)_2$
6	8.2	$(pt)_2$
7	5.6	Mainly 3',5'-cyclic-$(pt)_3$
8	7.9	$(pt)_3$
9	3.4	Mainly 3',5'-cyclic-$(pt)_4$
10	9.3	$(pt)_4$
11	2.1	Mainly 3',5'-cyclic-$(pt)_5$
12	8.7	$(pt)_5$
13	7.3	$(pt)_6$
14	5.7	$(pt)_7$
15	4.5	$(pt)_8$
16	3.8	$(pt)_9$
17	2.5	$(pt)_{10}$
18	1.9	$(pt)_{11}$
19	2.0	$(pt)_{12}$
20	0.9	$(pt)_{13}$
21	0.8	$(pt)_{14}$
22	0.5	$(pt)_{15}$
23	0.3	$(pt)_{16}$
24	1.2	Higher polymers removed with 1 M salt

for 6 days (5). After cleavage of pyrophosphate linkages and hydrolysis of protective groups, the oligonucleotides were separated on a 3 x 35-cm DEAE-cellulose (bicarbonate) column with the distribution of nucleotidic material as shown in Table 2. The linear oligonucleotides were further purified by rechromatography of individual peaks on DEAE-cellulose (Cl^-) at pH 5.5.

Hypochromicity of Oligonucleotides.--The purified oligonucleotides derived from 5'-thymidylic and 2'-deoxy-5'-cytidylic acids afford a means of evaluating the hypochromic effect on ultraviolet molar extinction coefficients, for the various species, due to interactions in aqueous medium. The pc oligomers of 25 and 52 units were addase-derived (7), as were the pt oligomers of 10 and 25 units.

A suitable solution of each species (lithium salt) was prepared in distilled water; the pH of all solutions was in the range 6.5 to 7.0. Ultraviolet absorption readings were made with a Unicam SP-800 spectrophotometer, and each solution was assayed for total phosphorus and checked for orthophosphate. Extinction coefficients per gram-atom of phosphorus, $\epsilon(P)$, were calculated at 267 mμ for 5'-thymidylic acid oligomers and at 271 mμ for the 2'-deoxy-5'-cytidylic acid oligomers (Fig. 1).

B. Stepwise Synthesis of Oligonucleotides

The Dimer, $MeOTrc^{An}pt$.*--A solution of N-anisoyl-$O^{5'}$-(methoxytrityl)-2'-deoxycytidine ($MeOTrc^{An}$, 1.5 mmoles) and pyridinium $O^{3'}$-acetyl-5'-thymidylate (ptAc, 0.874 mmole) in dry pyridine (4 ml) was treated with mesitylenesulfonyl chloride (329 mg, 1.5 mmoles) for 6 hours. An additional 1 mmole of the condensing agent was added, and after a total reaction time of 22 hours, the reaction was cooled in ice and diluted with water, and the pH was adjusted to 7.0 with 0.1 N triethylamine. The unreacted $MeOTrc^{An}$, which soon precipitated (0.774 mmole), was collected in a fritted funnel and washed with water. Extraction of the aqueous pyridine filtrate with chloroform (3 times with 100-ml amounts) completely removed the fully

*The abbreviated descriptive system presented previously (8) is used for representing nucleosides, nucleotides, oligonucleotides, and protective groups.

TABLE 2. DISTRIBUTION OF PRODUCTS FROM POLYMERIZATION OF ^{3}H-2'-DEOXY-5'-CYTIDYLIC ACID

Column Peak	Nucleotide Material (percent of total)	Composition of Peak
2	5.9	3',5'-cyclic-pc
4	43.9	pc
5	13.9	3',5'-cyclic-$(pc)_2$
6	14.8	$(pc)_2$
7	1.5	Mainly 3',5'-cyclic-$(pc)_3$
8	7.7	$(pc)_3$
9	0.5	Mainly 3',5'-cyclic-$(pc)_4$
10	4.1	$(pc)_4$
11	0.2	Mainly 3',5'-cyclic-$(pc)_5$
12	2.2	$(pc)_5$
13	1.1	$(pc)_6$
14	0.6	$(pc)_7$
15	0.5	$(pc)_8$
16	0.2	$(pc)_9$

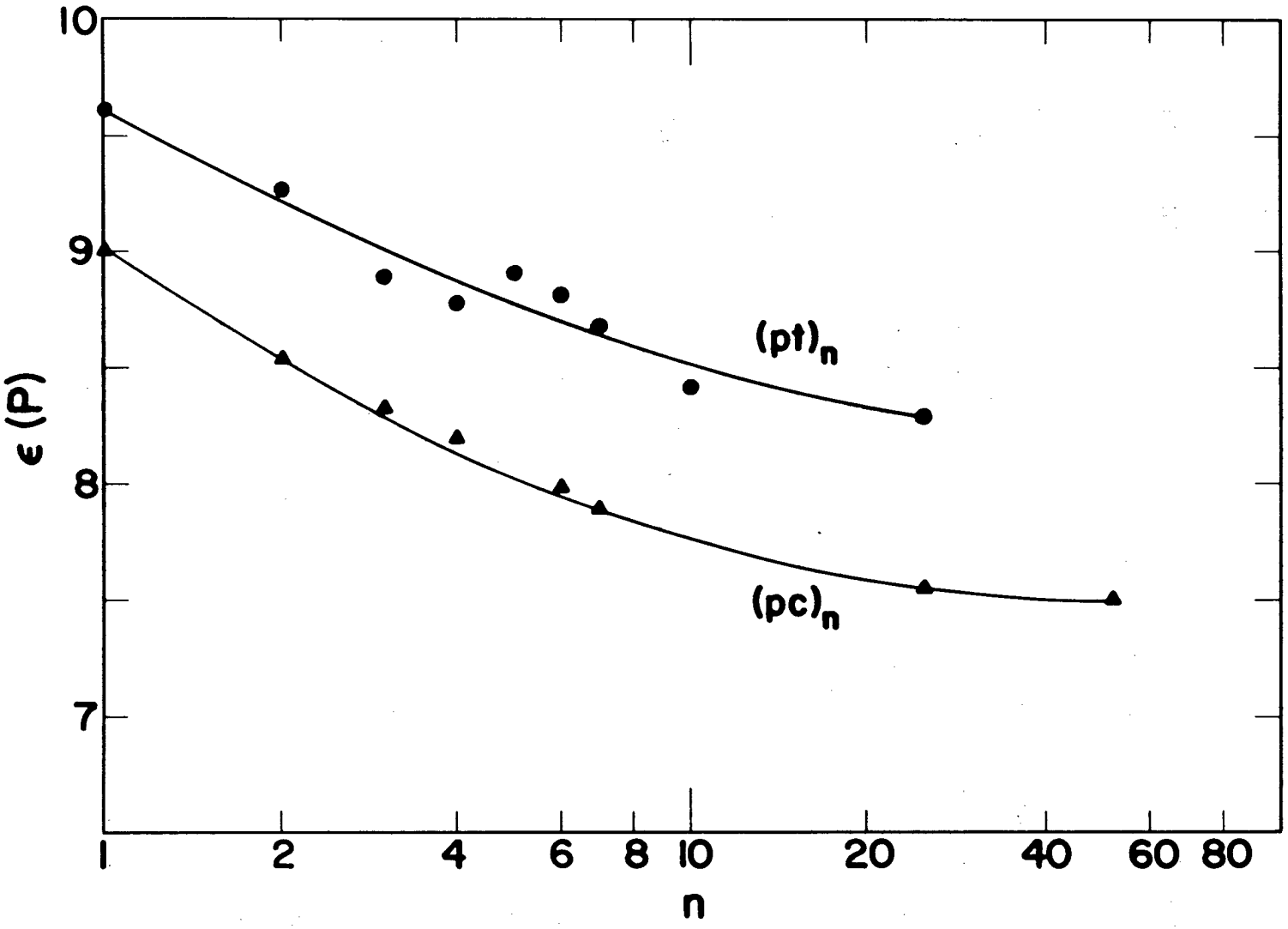

Fig. 1. Hypochromicity shown by oligomers of 5'-thymidylic acid, $(pt)_n$, (●), and 2'-deoxy-5'-cytidylic acid, $(pc)_n$, (▲).

protected dinucleotide (as indicated by checking the aqueous mother liquor for the characteristic ultraviolet absorbance spectrum). The chloroform solution of the product was evaporated under vacuum with several additions of pyridine until final volume was 10 ml. To remove the $O^{3'}$-acetyl group, the pyridine solution was diluted with 5 ml of water, 15 ml of 2 N sodium hydroxide was added with ice cooling, and the solution was kept at about 2° for 12 minutes. Sodium ions were removed quickly by the addition of an excess of Dowex-50W-X4 pyridinium resin (30 ml of wet resin), and the solution was passed through a like amount of resin in a fritted funnel. All the resin was then washed several times with 25 percent pyridine. The entire filtrate was applied to a 3.5 x 35-cm column of DEAE-cellulose (bicarbonate form). A gradient of triethylammonium bicarbonate (0.005 M to 0.2 M in 2 l.) removed mesitylenesulfonic acid and unreacted pt (0.363 mmole, 41.5 percent). The MeOTrc^{An}pt was then eluted from the column with a linear gradient of triethylammonium bicarbonate (0.005 M to 0.2 M in 2 l.) in 30 percent ethanol. All the tubes in the major peak which gave a constant A_{270}/A_{302} ratio of 1.1* were pooled; total volume 2.76 l. with A_{302} of 3.43; calculated yield 0.42 mmole (48.2 percent based on pt).** Ultraviolet spectral characteristics are given in Table 3.

The Trimer, MeOTrc^{An}ptpt.--A solution of pyridinium MeOTrc^{An}pt (0.374 mmole) and pyridinium ptAc (1.5 mmoles) in 5 ml of dry pyridine, containing 0.5 g of dry pyridinium Dowex-50W-X4 resin, was treated with 7.5 mmoles of DCC for 46 hours. Water (5 ml) was added, the dicyclohexylurea (DCU) and Dowex-50W were collected in a fritted funnel and washed thoroughly with

---

*For pc^{An}, the value for ϵ_{270} is 15,000 and that for ϵ_{302} is 22,450. For pt ϵ_{270} is 9300, with no significant absorbance at 302 mμ (6).

**In a recent preparation of MeOTrtpt and in earlier preparations of MeOTrc^{An}ptAc and MeOTrc^{An}pcAc$_2$, high yields (> 90 percent), based on the nucleotide, were obtained with a nucleoside to nucleotide ratio of 2.

25 percent pyridine. The combined filtrate was evaporated to small volume with additions of pyridine. The final volume was adjusted to 10 ml with pyridine. Water (5 ml) was added, followed, with cooling in ice, by 15 ml of 2 N sodium hydroxide. After the solution remained in ice for 13 minutes, 31 ml of wet pyridinium Dowex-50W-X4 resin was added at once to remove sodium ions, and the solution was passed through a like amount of wet resin.

The resin was washed thoroughly with 25 percent pyridine, and the pH of the filtrate was raised from 6.9 to 7.4 with 0.1 N triethylamine. The entire solution was applied to a 2.4 x 40-cm column of DEAE-cellulose. To remove pyridine, pt, and small amounts of nontritylated material, an aqueous gradient (0.005 M to 0.2 M in 2 l.) of triethylammonium bicarbonate (pH 7.5) was first passed through the column. After 1.7 l., a linear gradient (0.005 M to 0.2 M in 4 l.) of triethylammonium bicarbonate (pH 7.5) in 30 percent ethanol was used to elute unreacted dimer and the product, MeOTrc^{An}ptpt (Fig. 2). The yield was 0.376 mmole (90 percent); the recovered MeOTrc^{An}pt from peak VII amounted to 0.032 mmole (7.7 percent). Ultraviolet spectral characteristics are given in Table 3.

The Tetramer, MeOTrc^{An}ptptpcAc$_2$.--A solution of pyridinium MeOTrc^{An}ptpt (0.168 mmole) and pyridinium pcAc$_2$ (1.02 mmoles) in 3.6 ml of dry pyridine, containing 0.5 g of dry pyridinium Dowex-50W-X4 resin, was treated with 1.055 g (5.1 mmoles) of DCC for 4-1/2 days, with shaking. With ice-cooling, the pyridine reaction mixture was diluted with 10 ml of water, unchanged DCC was extracted with petroleum ether, and the aqueous solution was filtered to remove DCU and the Dowex resin, which were washed thoroughly with 25 percent pyridine. The aqueous filtrate was adjusted to pH 7.5 with 0.1 N triethylamine and applied to a 2.4 x 40-cm DEAE-cellulose column (acetate form). Pyridine, unreacted pcAc2, and small amounts of other nontritylated material were washed from the column with a linear aqueous gradient (0.005 M to 0.2 M in 2 l.) of triethylammonium acetate (pH 7.0). A second linear gradient (0.005 M to 0.2 M in 4 l.) of triethylammonium acetate (pH 7.0) in 50 percent ethanol was used to elute unreacted trimer and the completely protected product as illustrated in Fig. 3. The yield of MeOTrc^{An}ptptpcAc$_2$ was 0.0414 mmole (24.6 percent).*

*The yield in a second preparation with DCC, in which extreme care was taken to eliminate moisture, was 24.2 percent. This is less than hoped for from the literature (6), but this particular tetramer has not been reported.

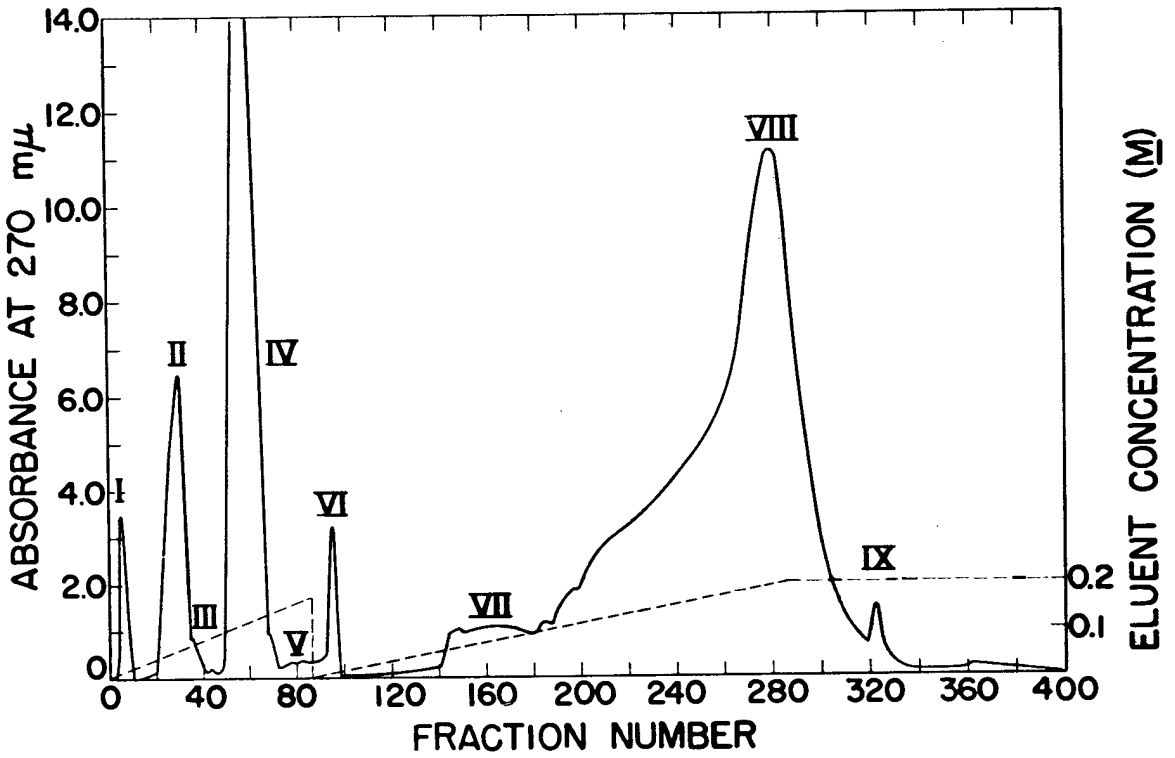

Fig. 2. Isolation of MeOTrc^{An}ptpt on a DEAE-cellulose column with a triethylammonium bicarbonate gradient in 30 percent ethanol (see text). Peak I, pyridine; II, presumably pyridinium nucleotide; III, unknown with λ_{max} at 260 mμ; IV, pt and pyro-pt; V, unknown with λ_{max} at 262 mμ; VI, presumably (pt)2 with λ_{max} at 267 mμ; VII, a mixture of MeOTrc^{An}pt$_{An}$ (A_{270}/A_{302} ratio of 1.1) and a small amount of (pt)2; VIII, MeOTrc^{An}ptpt (A_{270}/A_{302} ratio of 1.4 to 1.5); and IX, unidentified, MeOTr-positive with acid (A_{270}/A_{302} ratio of 1.3 to 1.7). The broken line denotes the triethylammonium bicarbonate gradient.

TABLE 3. ULTRAVIOLET ABSORPTION CHARACTERISTICS

Compound	Solvent	Maxima		Minima	
		λ (mμ)	ε (10^{-3})	λ (mμ)	ε (10^{-3})
MeOTrc^{An}pt (Et_3NH)	50% EtOH	301.0 275.0	22.6 26.5	246.5	19.5
MeOTrc^{An}ptpt ($Et_3NH)_2$	H_2O, pH 7.0	303.0 271.0	24.2 34.1	297.0 243.5	23.4
MeOTrc^{An}ptptpcAc$_2$ ($Et_3NH)_3$	H_2O, pH 7.5	302.0* 270.0	30.2 39.6	239.5	35.8
cptptpc($NH_4)_3$	H_2O, pH 7.0	267.5	33.6	236.5	18.9
pcptptpc($NH_4)_5$	H_2O, pH 7.0	267.5	33.6	236.5	18.9

*Shoulder.

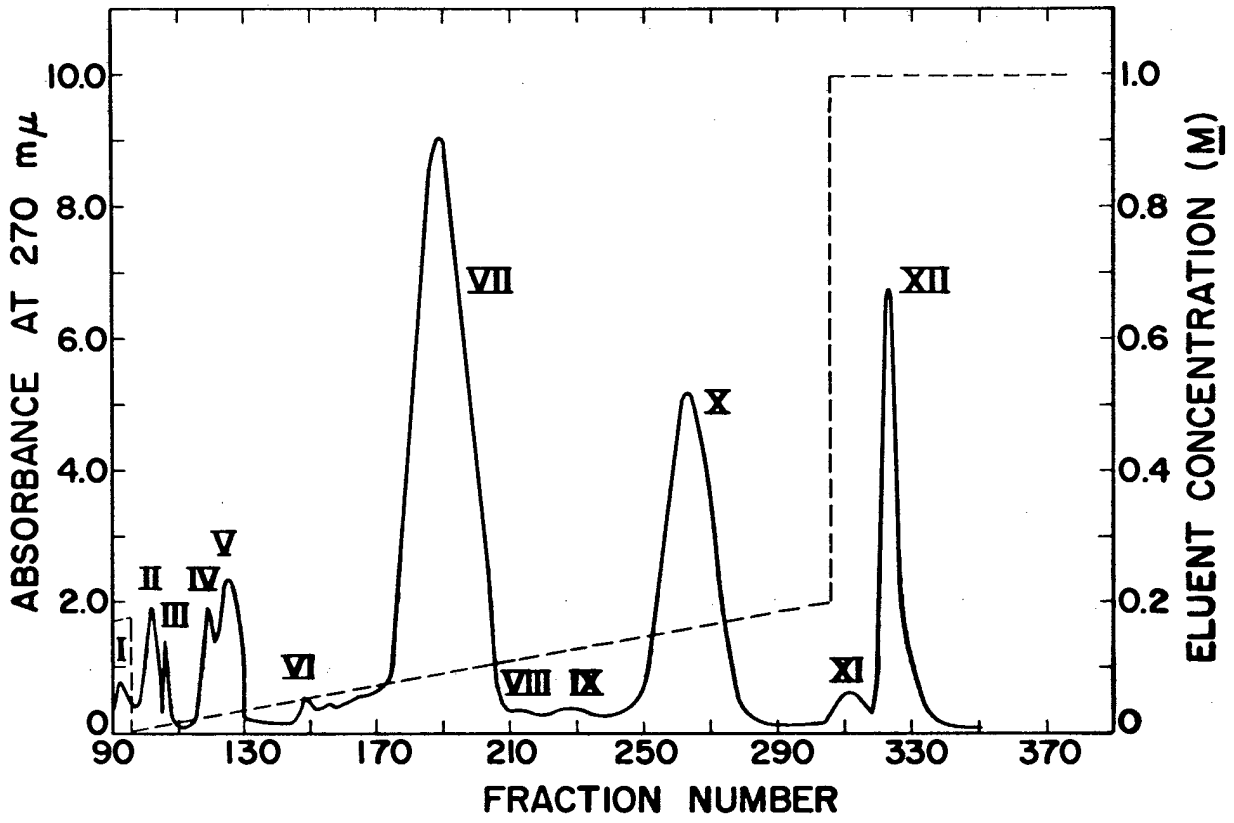

Fig. 3. Isolation of MeOTrc^{An}ptptpcAc$_2$ on a DEAE-cellulose column with a triethylammonium acetate gradient in 50 percent ethanol. Peak I, spectrum of N-acetyl pc; II, (pc)$_2$; III, colored material insoluble in water; IV and V, MeOTr-positive and with N-anisoyl group; VI, the spectrum and A_{270}/A_{302} ratio indicated mainly MeOTrc^{An}ptpt; VII, unreacted MeOTrc^{An}ptpt; VIII and IX, unidentified; X, MeOTrc^{An}ptptpcAc$_2$; XI, unidentified; and XII, according to Ref. 6, this is material which results from phosphorylation of pyrimidine ring nitrogen in either the starting trimer or the product tetramer, or both.

Ultraviolet spectral characteristics are given in Table 3. The unreacted protected trinucleotide recovered from peak VII amounted to 0.08 mmole (47.6 percent).

$c^{An}ptptpcAc_2$.--To ensure complete acetylation of the $O^{3'}$-hydroxyl group, 41 μmoles of pyridinium $MeOTrc^{An}ptptpcAc_2$ was dissolved in 2 ml of dry pyridine and treated with 1 ml of acetic anhydride for 16 hours. The solution was evaporated, and the residue was dissolved in 4 ml of 80 percent acetic acid for 4 hours to effect removal of the $O^{5'}$-methoxytrityl group. The solvent was evaporated to dryness, and the residue was dissolved in 5 ml of water and taken to dryness. The residue of $c^{An}ptptpcAc_2$ was dissolved in 4 ml of dry pyridine and 6 ml of dimethylformamide* (DMF) and evaporated to small volume under oil-pump vacuum. The residue was dissolved in 2 ml of DMF, and 3 ml of dry pyridine was added. The resulting solution was added dropwise to 40 ml of dry ether, cooled at 2° for 9 hours, and centrifuged to collect the precipitate which was then washed with dry ether. This process was repeated twice more, and the precipitate was dissolved in DMF. The amount of $c^{An}ptptpcAc_2$ was 35.1 μmoles.

Phosphorylation of $c^{An}ptptpcAc_2$.--The $c^{An}ptptpcAc_2$ (35.1 μmoles) solution in DMF was evaporated to 1 ml, and 2 ml of dry pyridine was added, followed by 0.5 g of dry Dowex-50W-X4 pyridinium resin. The mixture was thoroughly dried by the repeated evaporation of 2-ml amounts of dry pyridine. Pyridinium 2-cyanoethyl phosphate (0.44 mmole) in 5 ml of dry pyridine was added, and the volume was reduced to 1 ml. The mixture was thoroughly dried by the repeated addition and evaporation of dry pyridine. Finally, 5 ml of dry pyridine was added, the volume was reduced to 4 ml, and 2.2 mmoles of DCC was added in a desiccator over P_2O_5. After 4-1/2 days, water was added, unchanged DCC was extracted with petroleum ether, and the aqueous solution was filtered to remove DCU and the Dowex resin, which were washed with 25 percent pyridine. The filtrate was reduced to 2 ml volume, 10 ml of concentrated ammonium hydroxide was added, and the solution was warmed at 60° for 2 hours. The cooled solution was filtered, evaporated to small volume, and applied to a 2.4 x 35-cm DEAE-cellulose column (bicarbonate form). The product and unphosphorylated cptptpc were separated, as shown in Fig. 4, with a linear gradient of

*This compound was only slightly soluble in dry pyridine.

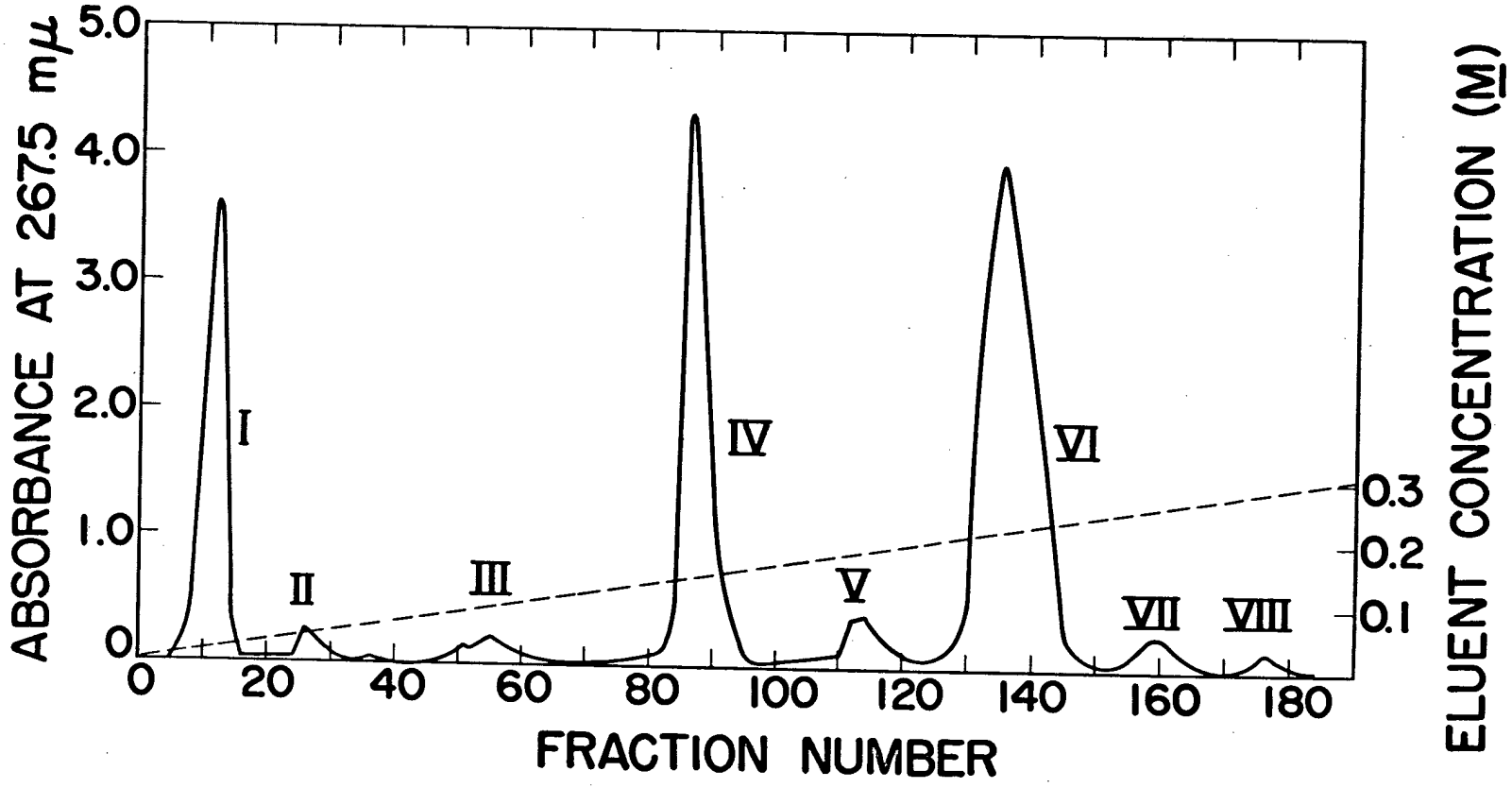

Fig. 4. Separation of cptptpc and pcptptpc on a DEAE-cellulose column, triethylammonium bicarbonate gradient (see text). Peak I, pyridine and anisamide; IV, cptptpc; VI, pcptptpc; II, III, V, VII, and VIII, small amounts of unidentified byproducts, all of which had ultraviolet spectra similar to cptptpc, with maxima at 267.5 mμ.

triethylammonium bicarbonate (0.005 M to 0.3 M in 4 l.) at pH 7.5. The yield of pcptptpc was 20.8 μmoles (59.3 percent), and 10.6 μmoles (30.2 percent) of cptptpc was recovered. Ultraviolet spectral characteristics are given in Table 3. Material in other peaks with an ultraviolet spectrum similar to that of cptptpc amounted to 10.5 percent of the total.

DISCUSSION

The feasibility of preparing oligodeoxyribonucleotides of defined structure, with or without a 5'-terminal phosphate and with appropriate carbon-14 or tritium labeling, is apparent from these and previous results. Stepwise synthesis of oligonucleotides of definite base sequences will be continued and extended to longer oligomers.

REFERENCES

(1) D. L. Williams, D. E. Hoard, V. N. Kerr, E. Hansbury, E. H. Lilly, and D. G. Ott, Los Alamos Scientific Laboratory Report LA-3432-MS (1965), p. 187.

(2) F. N. Hayes, V. E. Mitchell, R. L. Ratliff, A. W. Schwartz, and D. L. Williams, Biochemistry (submitted).

(3) D. A. Smith, R. L. Ratliff, T. T. Trujillo, D. L. Williams, and F. N. Hayes, J. Biol. Chem. 241, 1915 (1966).

(4) H. G. Khorana and J. P. Vizsolyi, J. Am. Chem. Soc. 83, 675 (1961).

(5) H. G. Khorana, A. F. Turner, and J. P. Vizsolyi, J. Am. Chem. Soc. 83, 686 (1961).

(6) T. M. Jacob and H. G. Khorana, J. Am. Chem. Soc. 87, 2971 (1965).

(7) F. N. Hayes and V. E. Mitchell, this report, p. 74.

(8) D. L. Williams, V. N. Kerr, and R. E. Hine, Los Alamos Scientific Laboratory Report LA-3132-MS (1964), p. 263.

DEOXYRIBONUCLEOSIDE TRIPHOSPHATE DERIVATIVES (E. Hansbury and D. G. Ott)

INTRODUCTION

5'-Triphosphates of oligonucleotides and of mononucleosides with blocked 3'-hydroxyl function should be interesting substrates in polynucleotide syntheses with addase (1). The choice of synthetic method for the particular triphosphates depends on the nature of the desired product, as well as on the relative availability of starting materials. Syntheses are presented for $O^{3'}$-acetyl-2'-deoxyadenosine 5'-triphosphate and 2'-deoxyadenylyl-(5':3')-2'-deoxyadenosine 5'-triphosphate.

METHODS AND RESULTS

$O^{3'}$-Acetyl-2'-deoxyadenosine 5'-Triphosphate (p_3aAc)

To 10 μmoles of disodium 2'-deoxyadenosine 5'-triphosphate in 10 ml of water was added dropwise 1.4 ml of acetic anhydride while the stirred solution was maintained near pH 7.0 by addition of 4 N sodium hydroxide from a pH-stat. The mixture was cooled during the reaction and for 1/2 hour following, then treated with excess Dowex-50 (pyridinium) and evaporated. The product was isolated by preparative-scale paper chromatography (Whatman No. 31 paper, solvent 1), R_f 0.78 (R_f 0.61 for p3a). Further purification was effected by column chromatography on DEAE-cellulose with an ammonium bicarbonate gradient. Ultraviolet analysis ($\epsilon_{259\ m\mu}$ 15,400) and phosphorus determination gave 2.87 g-atoms P/mole (no detectable inorganic phosphate). Treatment of an aliquot with 4 N ammonium hydroxide at room temperature for 2 hours gave complete conversion to p_3a. Chromatography data are given in Table 1.

2'-Deoxyadenylyl-(5':3')-2'-deoxyadenosine 5'-Triphosphate (p_3apa)

The general procedure (2) for conversion of an oligonucleotide, papa (3), through pyrophosphorylation of its

TABLE 1. THIN LAYER CHROMATOGRAPHY R_f VALUES[a]

Compound	Solvent 1[b]	Solvent 2[c]
a	0.89	0.64
pa	0.73	0.37
paAc	0.87	--
p_2a	0.65	--
p_2aAc	0.78	--
p_3a	0.59	0.24
p_3aAc	0.73	--
papa	0.72	0.22
p_2apa	0.62	--
p_3apa	0.52	0.14
p	0.44	0.47
p_2	0.30	0.33

[a]Cellulose plates, Analtech, Inc., No. MN-300.

[b]Isobutyric acid:1 M ammonium acetate:0.1 M EDTA (100:60:1.6, v/v).

[c]1 M Ammonium acetate:95 percent ethanol (1:1, v/v), pH 7.5.

imidazolidate was modified by the use of hexamethylphosphoric triamide (HMP) as a solvent in place of N,N-dimethylformamide (DMF). Insolubility of the bis(tributylammonium) salt of papa appeared to affect the yield of imidazolidate. The product was purified by column chromatography (DEAE-cellulose, bicarbonate gradient) and by paper chromatography (Whatman No. 31 paper, solvent 1, R_f 0.62). Ultraviolet absorption ($\epsilon_{258\ m\mu}$ 12,600) and phosphorus analysis gave 1.85 g-atoms P/mole (no detectable inorganic phosphate). R_f values are given in Table 1.

DISCUSSION

Other nucleoside 5'-triphosphates with acylated 3'-function can undoubtedly be prepared by direct acylation of the triphosphates. Acetylation of mononucleotides by this procedure (4) showed no interference from substituent amino groups, and preparation of p_3aAc above has shown that the triphosphate group is stable toward the reaction conditions. This procedure is simpler than the alternative of preparing the compounds by addition of the triphosphate group to acylated precursors.

The synthesis of p_3apa presented a difficulty not previously encountered (i.e., solubility of the oligonucleotide tributylammonium salt in dimethylformamide). It appears that hexamethylphosphoric triamide is a satisfactory solvent; this will be studied further in reactions on a larger scale in which visible evidence of solubility is possible.

REFERENCES

(1) F. N. Hayes and V. E. Mitchell, this report, p. 74.

(2) D. E. Hoard and D. G. Ott, J. Am. Chem. Soc. 87, 1785 (1965).

(3) D. L. Williams, D. E. Hoard, V. N. Kerr, E. Hansbury, E. H. Lilly, and D. G. Ott, Los Alamos Scientific Laboratory Report LA-3432-MS (1965), p. 187.

(4) A. Stuart and H. G. Khorana, J. Biol. Chem. 239, 3885 (1964).

OLIGONUCLEOTIDE CHROMATOGRAPHY (A. Murray)

INTRODUCTION

The object of this continuing study with oligo-5'-thymidylic acids is four fold: (a) to screen and to characterize 50 new cellulosic anion exchange media of varying weak-base strengths (pK_b 5.0 to 8.5); (b) to optimize chromatography elution gradients; (c) to evaluate the contribution of base strength to the ion exchange process; and (d) to develop resins with improved resolution over the currently employed DEAE-cellulose for separating oligonucleotides in the size range of decamer and beyond.

METHODS AND RESULTS

Characterization of DEAE column separation of oligonucleotides was established with a standard assay sample (1) [containing 20 A_{267}-units each of $(pt)_{1-10}$ and 10 each of $(pt)_{11}$ and $(pt)_{13}$] before proceeding with the resin screening program. All columns contained approximately 1 g of ion exchanger (1 x 12 cm) and were eluted at a flow rate of 1.2 ml/min, temperature 20°.

DEAE

A column from which $(pt)_{1-5}$ had been eluted by linear gradient (bicarbonate, pH 7.5) was sectioned for distribution analysis of the residual bound oligomers. The findings [fractional distances: 0 to 0.07, $(pt)_{11,13}$; 0.07 to 0.38, $(pt)_{8-10}$; 0.38 to 0.69, $(pt)_{7-8}$; 0.69 to 1.00, $(pt)_6$] demonstrate that polyion distribution coefficients decrease in orderly fashion down the column, with elution proceeding by classical differential migration rather than by fractional extraction as with macromolecules.

Since gradient elution theory cannot yet predict the most useful concentration and volume relationships for optimizing band resolution, these values are determined empirically. Three parameters investigated were (a) eluent ion and pH -- as they affect solute charge rather than column efficiency (bicarbonate, 7.5; chloride, 4 and 7.5); (b) slope of linear

gradients; and (c) gradient shape. Resolution with chloride at pH 7.5 was generally poor; it is desirable to avoid operating in the vicinity of the pK of the resin. Convex and concave gradients were generated with open vessels of unequal sectional areas and were calibrated spectrophotometrically for both concentration and total salt. These shapes appear to offer little immediate advantage over any extended range of oligomers for a screening program. Separation resolution -- that relationship of band-width and band-spacing in the elution profile -- was evaluated by two complementary numerical indices useful in critically comparing a number of profiles: (a) the A_{267} ratio (peak-to-valley) and (b) the differential eluent volume separating adjacent peaks (normalized to percentage of the profile volume). Table 1 relates gradient slope and resolution for bicarbonate and Table 2 for chloride. In any homologous series, where the energy of sorption tends to vary linearly with structure, optimum separation is attained by uniform spacing.

In a linear gradient (slope, S, in molarity units/l. and origin zero), the total quantity of salt, Q (in mmoles), is proportional to concentration squared:

$$Q = \frac{500}{S} M^2.$$

The observed values of oligomer charge, eluent molarity, and mmoles for a number of slopes of bicarbonate and chloride gradients are presented in Figs. 1 and 2, respectively. It is significant that, as linear gradients flatten, an oligomer is characterized by release from the exchanger at reduced eluent concentration but at higher total amount of salt. The improved resolution found in these homologous separations with flatter gradients correlates with the increased number of eluent moles competing for the fixed binding sites and reaching a limit in the optimum separation of two related components usually achieved with a fixed concentration eluent.

At a given slope the incremental relationship between solute charge and eluent concentration or total amount was found to be an inverse one, placing ever-increasing restrictions upon the band-spacing of higher oligomers (see Figs. 1 and 2 and Tables 1 and 2). No significant integral nor differential correlation between the ratio (mmoles/molarity) and

TABLE 1. RESOLUTION OF THYMIDYLATE OLIGOMERS, $(pt)_n$, ELUTED AT pH 7.5 FROM DEAE AS A FUNCTION OF LINEAR BICARBONATE GRADIENT SLOPE

Oligomer (n)	Differential Elution Volume (percent of profile volume)			Peak-to-Valley Ratio		
	Slope (M/l.)			Slope (M/l.)		
	0.5	0.25	0.1	0.5	0.25	0.1
1	12.5	10.2	10.4	236	∞	228
2	14.8	13.4	12.3	86	∞	137
3	10.6	10.6	11.9	24	71	48
4	9.9	9.8	11.6	8.5	32	24
5	8.3	8.6	10.7	4.7	10.3	11.5
6	7.6	8.3	9.7	4	5.1	9.7
7	6.6	8	9	2.2	3.3	4.2
8	6	6.7	8	1.9	2.8	3.5
9	5.2	5.9	8	1.7	2.7	2.8
10	5.4	5.2	8.4	1.6	2.4	2.3
11	4.4	5	0	1.5	1.8	0
13	8.6	8.3	0	2.7	3.4	0
Optimum Value	7.7	7.7	10		maximum	
Total Volume (ml)	929	1705	1361			

TABLE 2. RESOLUTION OF THYMIDYLATE OLIGOMERS, $(pt)_n$, ELUTED AT pH 4 FROM DEAE AS A FUNCTION OF LINEAR CHLORIDE GRADIENT SLOPE*

Oligomer (n)	Differential Elution Volume (percent of profile volume)				Peak-to-Valley Ratio			
	Slope (M/l.)				Slope (M/l.)			
	0.5	0.25	0.125	0.05	0.5	0.25	0.125	0.05
1	19.3	14.1	13.5	10.9	355	131	45	30
2	11.8	10.9	11.5	8.8	137	34	32	12
3	10.4	8.8	10.1	3.5	25	6.8	33	17
4	9.4	8	9.1	11.4	8.1	4.5	15	16
5	7.9	8	7.7	10.4	4.3	6.3	13	12
6	6.7	8.6	7.1	9.5	2.7	5.8	13	10
7	6.2	8	7.9	8.7	1.8	3	4.3	5.8
8	5.3	7.1	6.4	7.4	1.6	2.3	3.2	5
9	4.8	6.3	6.4	7	1.6	2	2.7	3.8
10	4.3	5.3	5.7	6.5	1.4	1.6	2.2	3.1
11	4.3	5.5	5.4	5.8	1.4	1.5	2.5	3
13	7	9.6	9.2	10	1.9	1.9	2.5	2.2
Total Volume (ml)	773	1358	2564	5770				

*BioRad DEAE, 0.74 meq/g, 1 x 12 cm, ~1 g, 60 ml/hr, 67°F, optimum spacing 7.7.

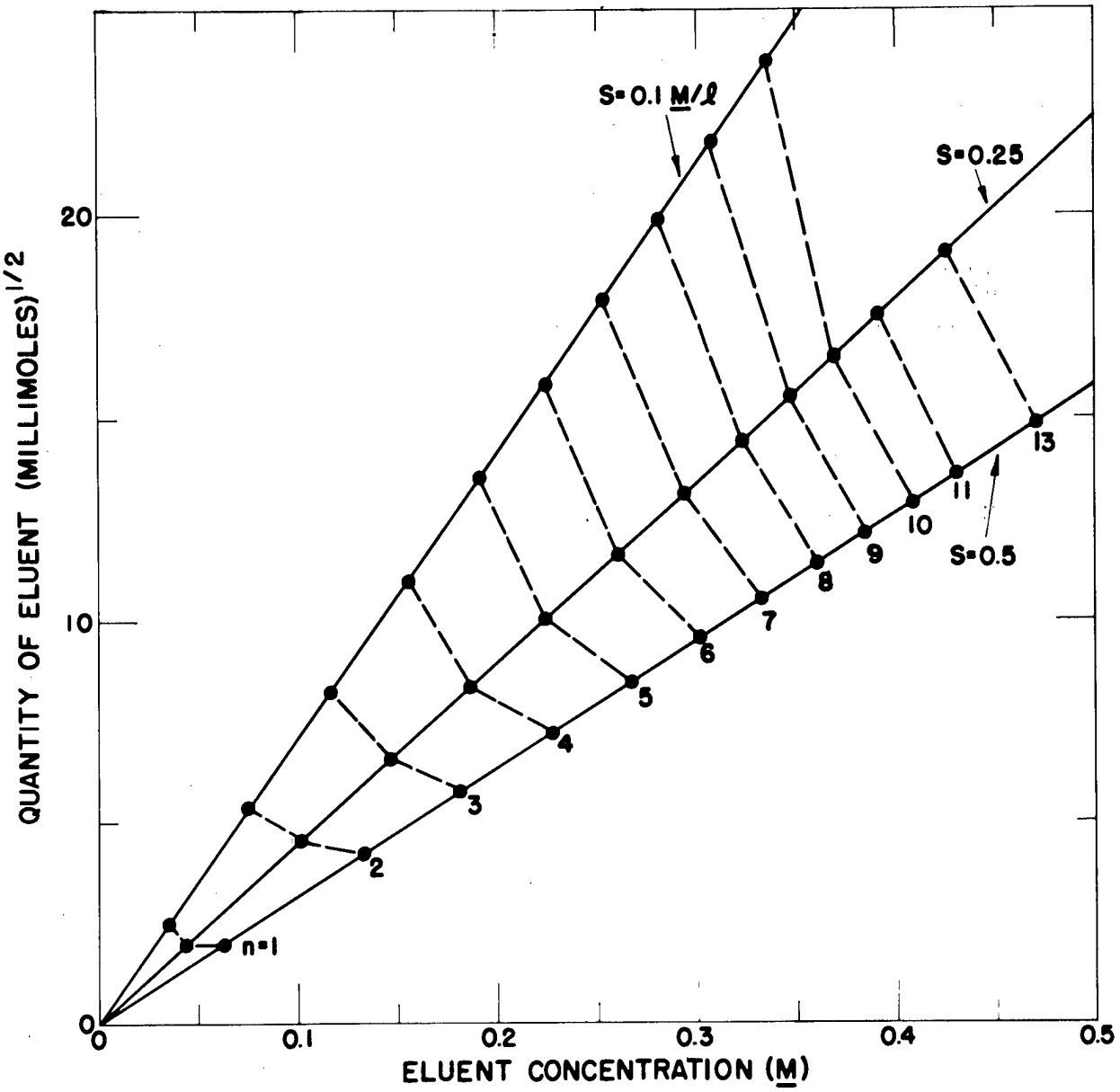

Fig. 1. Eluent quantity and concentration characterizing thymidylate oligomers, $(pt)_n$, eluted by linear bicarbonate gradients at pH 7.5 from DEAE (0.74 meq/g, 1 x 12-cm column, 1 ml/min).

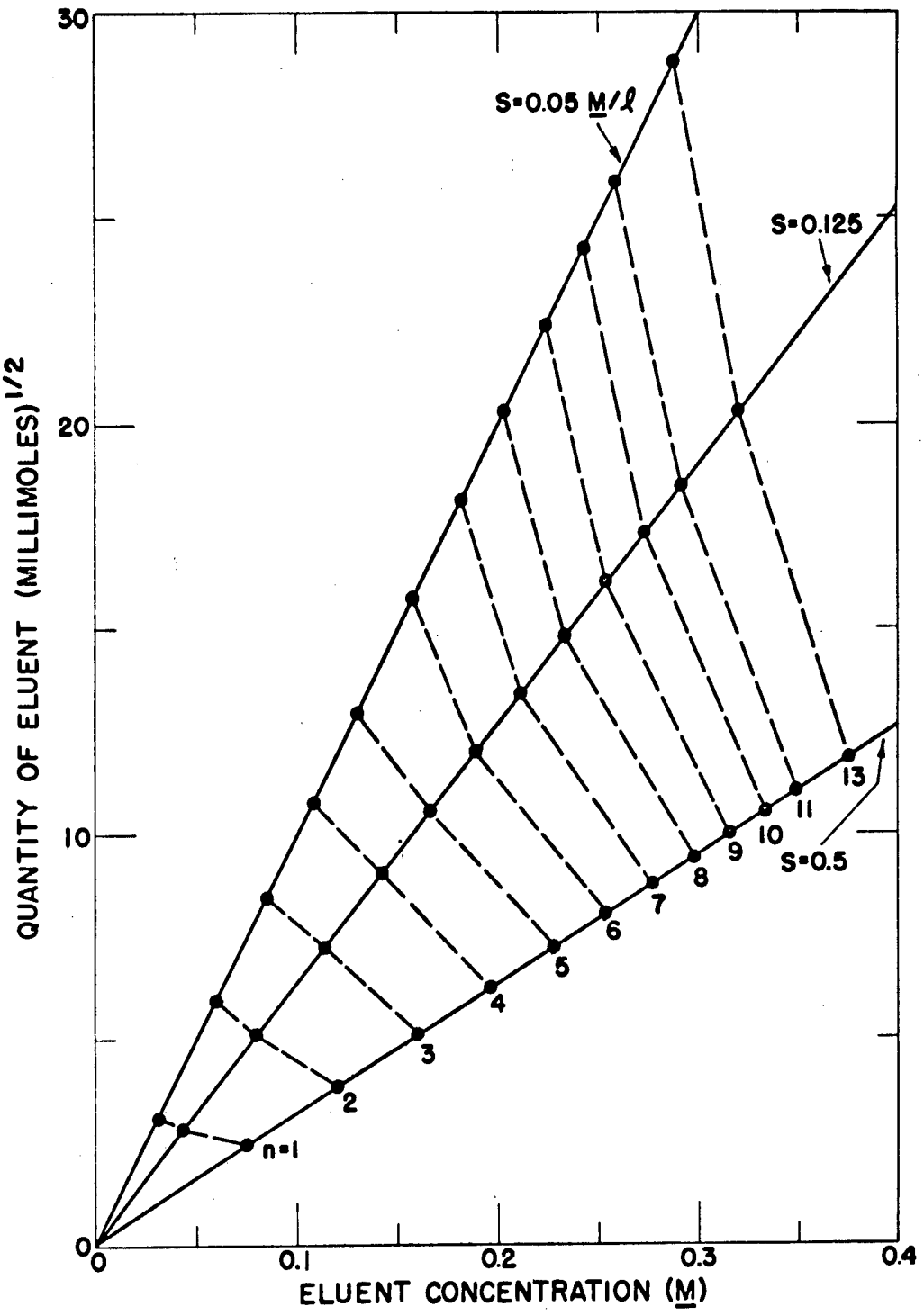

Fig. 2. Eluent quantity and concentration characterizing thymidylate oligomers, $(pt)_n$, eluted by linear chloride gradients of different slopes at pH 4.0 from DEAE.

charge was observed. Figure 3A illustrates the capacity of DEAE to resolve the standard assay mixture with a chloride gradient at pH 4 (the anomolous crowding of dimer and trimer is not representative).

Other Resins

Twelve new resins have been screened with relatively flat chloride gradients for capability to separate the assay mixture. Tables 3 and 4 evaluate selected, but not necessarily optimum, resolution powers of these media at arbitrary pH 5. Base strength, exchange capacity, slope, and generally decreasing incremental relationship between charge and resolution indices are correlated for comparison with reference DEAE. The influence of base strength and steric factors upon the exchange process is perhaps more apparent among the last half of the resins listed, since constant exchange capacity and column size might be expected, at a first approximation, to provide the same number of theoretical plates. Gradient slope cannot be reduced indefinitely, for optimum values do exist. Although most resins evidenced the usual increasing crowding of higher charge bands, ECAMPDOL and ECP1Z apparently do not.

Tests on 3 new resins with triethylammonium bicarbonate gradients at pH 7.5 were not encouraging. ECMOR released pt and $(pt)_2$ in fixed eluent fashion with the loading buffer (0.005 M), ECDEA (0.07 meq/g, pK_b 5.0) slipped $(pt)_{1-3}$, and B-ECTEOLA separated only half the sample with gentle concave, convex, and linear gradients.

ECMOR.--One outstanding new resin (ECMOR) has emerged from this study, and a comparison of its elution profile (Fig. 3B) with that of DEAE (Fig. 3A) reveals a unique ability reproducibly to resolve secondary components previously unsuspected in the assay sample. A freshly synthesized specimen of the resin displayed the same properties with a freshly dissolved sample of the assay mixture (DEAE control).

Elution band centers of $(pt)_{4-8}$, taken from DEAE (bicarbonate, pH 7.5) and rechromatographed on ECMOR (chloride, pH 5), displayed the leading secondary peaks (yield 20 percent), all with one less charge than the major peaks n. The origin of these chromatographically stable species with one reduced charge is uncertain; their appearance persisted after repeated

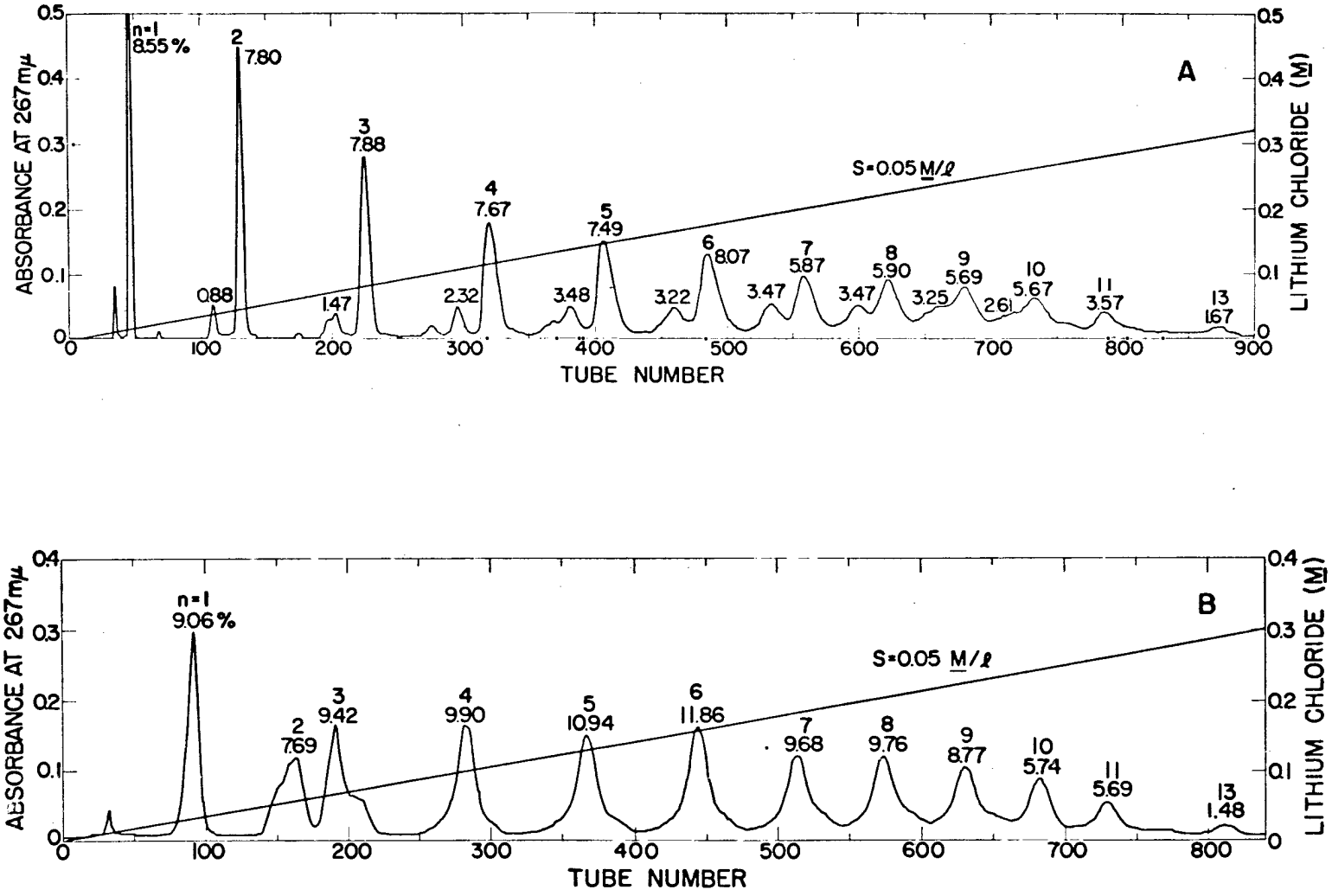

Fig. 3. Chromatographic elution profiles of thymidylate oligomers, $(pt)_n$, with linear chloride gradients at slope 0.05 M/l. and 7.15-ml fractions. (A) DEAE, pH 4; and (B) ECMOR, pH 5 (1.11 meq/g, 1 x 12-cm column, 1 ml/min). The percentage values pertain to absorbance unit distribution.

TABLE 3. BAND-SPACING OF THYMIDYLATE OLIGOMERS, $(pt)_n$, ELUTED AT pH 5 FROM DIFFERENT RESINS BY A LINEAR CHLORIDE GRADIENT

Resin	Capacity (meq/g Cl^-)	pK_b	Gradient Slope (M/l.)	Profile Volume (ml)	Differential Elution Volume (percent of profile volume) Oligomer (n) 1	2	3	4	5	6	7	8	9	10	11	13
ECTEPA	2.65	6.7	0.5	1309	17	13.5	11.8	9.9	8.5	7.4	6.2	5.4	4.7	5.2	*	*
ECMOR	1.11	8.5	0.05	6213	4.8	9.6	11	10.9	10	9	8.5	7.3	6.7	6.2	6	10.2
B-ECTEOLA	0.78	7	0.062	3168	11.3	11.4	10.6	10.1	8.5	7.6	7.6	5.2	5.4	5.1	5.6	11.6
DEAE	0.74	4.5	0.05	5770	10.9	8.8	3.5	11.4	10.4	9.5	8.7	7.4	7	6.5	5.8	10
ECAAPY-W	0.33	7.2	0.1	2433	10.7	10	9.7	9.8	8.9	8.2	8	7	6.8	7.1	7.4	*
ECAHMPDOL	0.19	7.2	0.05	2757	9.5	7.5	6.7	7	7.1	7.2	7.5	8.8	samples lost			
ECAMPDOL	0.16	6.2	0.062	2240	13.3	9.8	7.5	7.8	6.8	6	6.6	4.9	6.1	8.3	9.1	13
ECP1Z	0.14	6.7	0.062	3275	5.3	4.2	3.3	4.5	3.1	4.8	5	7.2	11.1	15.9	*	*
ECPID	0.12	5	0.025	3800	9.6	7.6	6.1	8.4	8.3	8.7	9	*	*	*	*	*
ECPYROLD	0.12	4.9	0.1	1411	15.5	9.6	8.3	7.6	6.5	6	6.5	6.2	4.8	*	*	*

*Poor band resolution.

TABLE 4. PEAK RESOLUTION OF THYMIDYLATE OLIGOMERS, $(pt)_n$, ELUTED AT pH 5 FROM DIFFERENT RESINS BY LINEAR CHLORIDE GRADIENT

Resin	Capacity (meq/g Cl^-)	pK_b	Gradient Slope (M/l.)	Profile Volume (ml)	Fraction Volume (ml)	Peak-to-Valley Ratio											
						Oligomer (n)											
						1	2	3	4	5	6	7	8	9	10	11	13
ECTEPA	2.65	6.7	0.5[a]	1309	7	59	18	12.5	7.7	3.8	2.4	1.6	1.4	1.3	1.2	1.1	1
ECMOR	1.11	8.5	0.05	6213	7	∞	150	94	36	15	10	4.9	3.3	2.9	2.3	2.5	1.8
B-ECTEOLA	0.78	7	0.062	3168	16	140	60	35	17	11.9	8.4	4.2	2.9	2.7	2.1	1.8	1.8
DEAE	0.74	4.5	0.05	5770	7	30	12	16	16.3	11.7	10.2	5.8	5	3.8	3.1	3	2.2
ECAAPY-W	0.33	7.2	0.1[b]	2433	7	96	35	33	9.4	4.9	3.1	2.1	1.8	2.1	1.4	1.2	1
ECAHMPDOL	0.19	7.2	0.05	2757	7	36	27	14.3	7.2	3.5	2.5	1.7	1.5	1.2	1.3	1	1
ECAPRMOR	0.18	7.4	0.062[c]	--	7	50	12.1	3.4	2.2	1.9	1.8	1.9	1.9	samples lost			
ECAMPDOL	0.16	6.2	0.062[d]	2240	16	88	47	9.3	3.8	2.3	2.3	2	1.7	1.6	1.5	1.3	1.2
ECP1Z	0.14	6.7	0.062	3275	16	52	16	3.8	2	1.9	1.3	1.3	1.9	1.8	1.4	1	1
ECPID	0.12	5	0.025	3800	16	20	6.6	5.2	3.8	2.2	1.9	1.4	1.2	1	1	1	1
ECPYROLD	0.12	4.9	0.1[e]	1411	7	40	6.7	2.5	1.8	1.6	1.5	1.3	1.2	1.1	1	1	1

TABLE 4 (continued)

FOOTNOTES:

[a]Slope 0.05 yielded good resolution through n = 8 (20, 5.9, 5.8, 4.5, 5.7, 3.3, 1.9, and 1.5), which then deteriorated badly after 8 1. Secondary peaks were resolved at n = 2-4.

[b]Discontinuous slope 0.05 (0.1 to 0.3 M/4 1., stressing molarity at the expense of mmoles) improved later resolution: 3.4, 2.9, 2.5, 2.4, 2.5, 1.7, and 1.3 at n = 6-13, respectively.

[c]Slope 0.031 eluted nothing beyond n = 5.

[d]Slope 0.016 eluted nothing beyond n = 3.

[e]Slope 0.02 resolved nothing beyond n = 8.

chromatography under "sterile conditions" of chloroform saturation to control microbial growth, washing of the resins with strong acid and alkali, and solution storage in the frozen state. Subsequent to purification (3 times on DEAE bicarbonate and 2 times on DEAE chloride), aliquots of $(pt)_5$ with DEAE (chloride, pH 4) and ECMOR (chloride, pH 5) gave identical results: separation of a compound of charge 4 in 18 to 19 percent yield. An elevated $\epsilon(P)$ value of 10.4, compared to the accompanying $(pt)_5$ value of 8.5, suggests possible dephosphorylation. Further study of this phenomenon is in progress.

Table 5 relates oligomer resolving power of ECMOR with chloride gradient slope at pH 5. As with DEAE, separability with chloride deteriorates at pH 7.5. Figure 4 correlates eluent molarity, mmoles, and gradient slope with the charge characterizing pt oligomers.

It is noteworthy that, although DEAE and ECMOR have quite different exchange capacity and base strength, the same size columns, in each of 3 cases of common gradient slope, disclose a striking parallelism in elution profile parameters: resolution of oligomer charge, summated distribution of absorbance units by charge, and integral and differential relationships of charge-to-eluent molarity and total moles.

The contribution to elution profile by the interplay of concentration and amount of eluent, which narrow bands and compress peaks, respectively, is illustrated by a comparison of the parameters characterizing the oligomers eluted by continuous and discontinuous linear chloride gradients of the same slope. Figure 5 illustrates the lag in mmoles when molarity has no zero intercept, and Table 6 presents the significant improvement in resolution of the higher oligomers realized by starting the eluent gradient at an appropriate intermediate value.

Application of ECMOR to the separation of hetero-oligomers $[(pt)_5(pc)_n]$ is treated elsewhere in this report (2).

DISCUSSION

A major problem of chromatographic separation of oligonucleotides is the resolution of complex series members. In a satisfactorily designed gradient elution system each solute distribution coefficient, for equilibrium partitioning

TABLE 5. RESOLUTION OF THYMIDYLATE OLIGOMERS, $(pt)_n$, ELUTED AT pH 5 FROM ECMOR AS A FUNCTION OF LINEAR CHLORIDE GRADIENT SLOPE*

Oligomer (n)	Differential Elution Volume (percent of profile volume)			Peak-to-Valley Ratio		
	Slope (M/l.)			Slope (M/l.)		
	0.25	0.125**	0.05	0.25	0.125**	0.05
1	7.8	10.8	4.8	90	∞	∞
2	12.5	8.2	9.6	64	63	150
3	11.4	9.9	11	42	49	94
4	10.5	9.8	10.9	16	18	36
5	9.2	9.1	10	6.8	8.9	15
6	8	8.3	9	3.8	6.5	10
7	7.6	7.6	8.5	3.3	3.6	4.9
8	6.3	6.9	7.3	3.1	2.7	3.3
9	6.1	6.7	6.7	3	2.5	2.9
10	5.9	6.8	6.2	2.8	2	2.3
11	5.8	6.6	6	2.7	2.4	2.5
13	8.8	11.6	10.2	1.9	2.5	1.8
Total Volume (ml)	1376	2673	6213			

*Resin capacity 1.11 meq/g, column 1 x 12 cm, ~ 1 g, 60 ml/hr, 67°F, optimum spacing 7.7 percent per unit charge.

**pH 4.

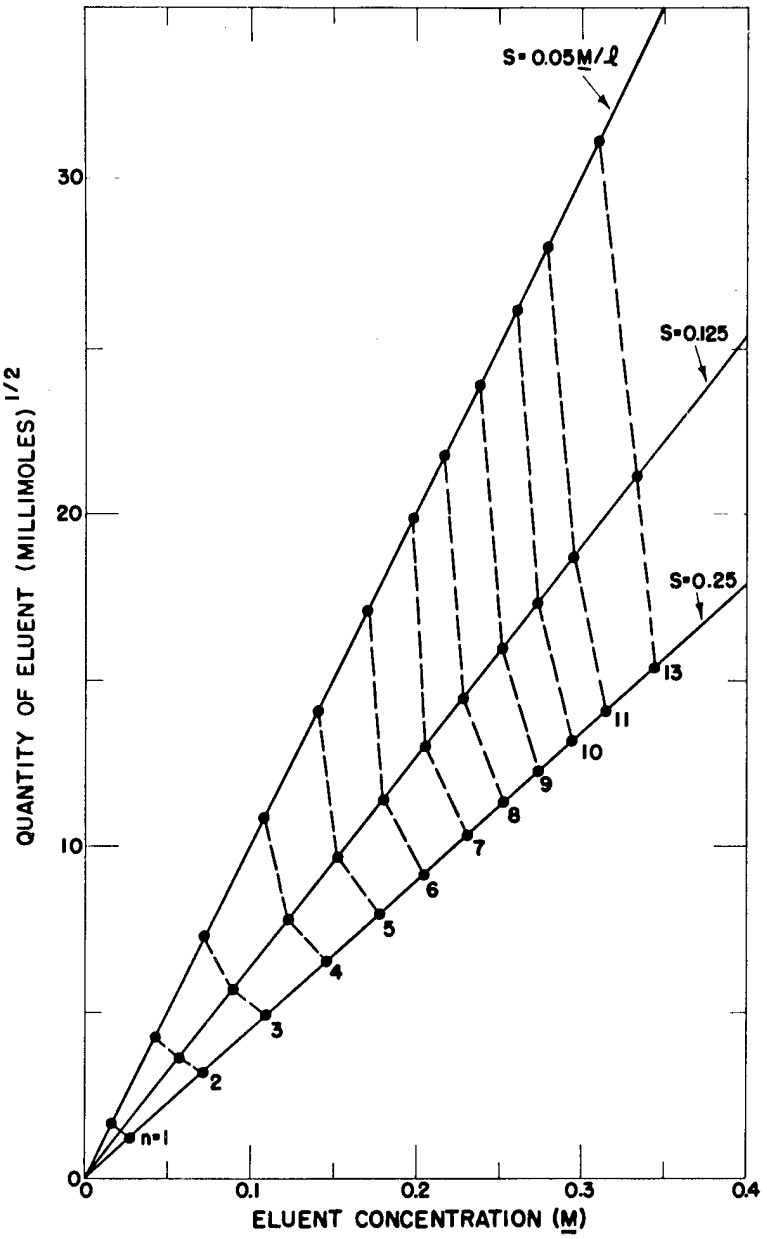

Fig. 4. Eluent quantity and concentration characterizing thymidylate oligomers, $(pt)_n$, eluted from ECMOR by linear chloride gradients of different slopes at pH 5.0.

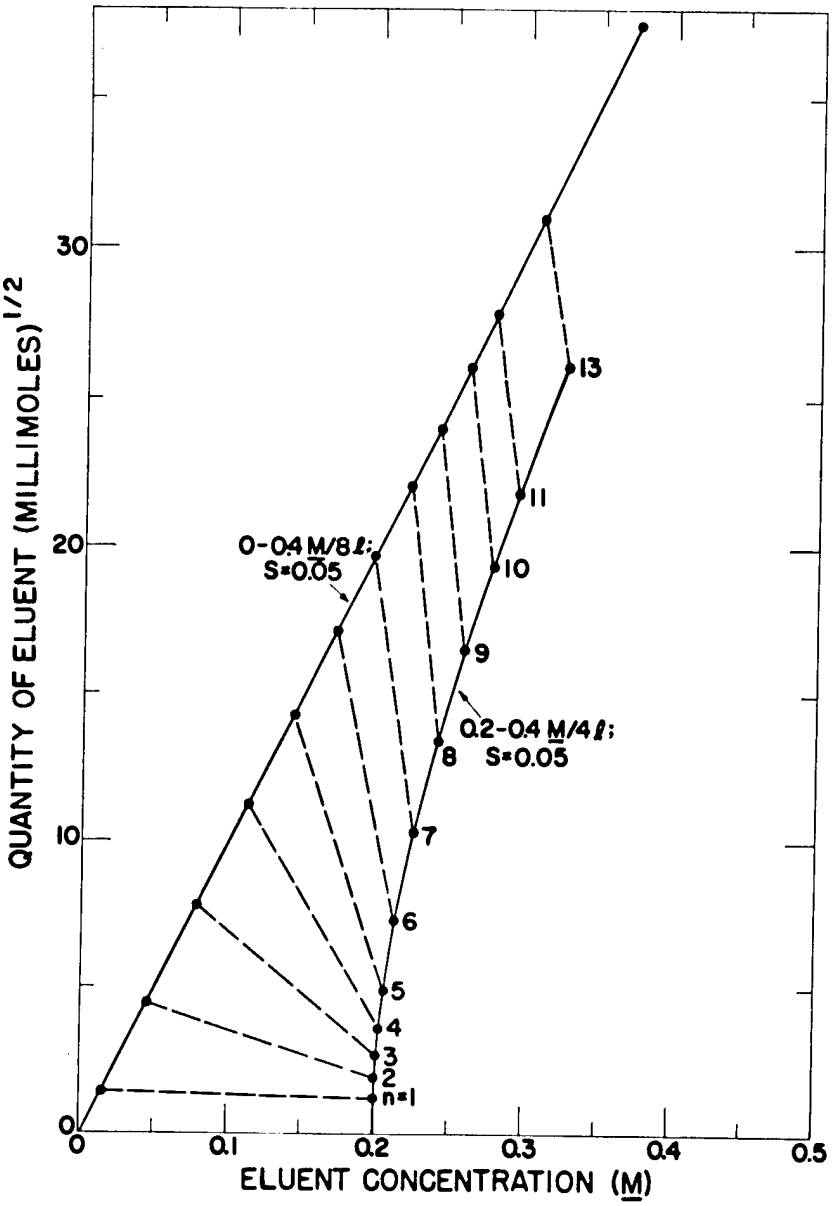

Fig. 5. Eluent quantity and concentration characterizing thymidylate oligomers, $(pt)_n$, eluted from ECMOR by continuous and discontinuous linear chloride gradients of the same slope at pH 5.0.

TABLE 6. RESOLUTION OF THYMIDYLATE OLIGOMERS, $(pt)_n$, ELUTED AT pH 5 FROM ECMOR BY CONTINUOUS AND DISCONTINUOUS LINEAR CHLORIDE GRADIENTS OF THE SAME SLOPE (0.05)

Oligomer (n)	Differential Elution Volume (percent of profile volume)	Peak-to-Valley Ratio
Continuous Gradient (0 to 0.4 M/8 l.)		
1	4.8	∞
2	9.6	150
3	11	94
4	10.9	36
5	10	15
6	9	10
7	8.5	4.9
8	7.3	3.3
9	6.7	2.9
10	6.2	2.3
11	6	2.5
13	10.1	1.8
Total Volume (ml)	6213	
Discontinuous Gradient (0.2 to 0.4 M/4 l.)		
1	0.31	-
2	0.43	-
3	0.7	-
4	1.2	4.3
5	2.1	6.7
6	5.3	7.8
7	9.3	9.3
8	12.4	7.6
9	14.3	5.9
10	14.3	4.5
11	14	3.4
13	25.6	2.7
Total Volume (ml)	2571	

between the stationary and moving phases within the column, must be reduced successively with time into a limited optimum range at the critical period of elution from the column, but with avoidance of excessive band retention volumes which cause a proportionate band broadening and peak compression. Constant band-width assures optimum separation and a comparable detection sensitivity for all sample components. Solute separation is uniquely defined by column plate number and selectivity coefficient (ratio of solute distribution coefficients). The search for selective resins attempts to impart specificity by chemically modifying functional ion exchange groups to alter suitably the coulomb field forces of the binding sites. The availability of an extensive homologous oligonucleotide series provides a unique opportunity to investigate the role of systematically increasing unit charge in ion exchange binding.

The separation variables (absorbent and sample weights, column length, eluent linear flow rate, and gradient steepness) are initially dictated by experimental convenience, then improved by suitable adjustment. Column loading capacity, to retain linearity of adsorption isotherms and resolution, may be increased through scaling up (that is, proportionately increasing the weight of resin and volume of eluent in each gradient vessel to maintain the same relative retention volumes).

Equipment is being installed to permit simultaneous operation and automatic recording of up to 4 columns. An effort will be made to optimize the ability of ECTEPA to separate secondary peaks. A higher exchange capacity preparation of ECDEA is desired for comparison to the related DEAE. Information regarding changes in exchange capacity, effected through hetero- and homo-dilution, is desired. Development of resin capability to resolve hetero-oligonucleotides is of prime importance.

REFERENCES

(1) A. Murray, Los Alamos Scientific Laboratory Report LA-3432-MS (1965), p. 215.

(2) F. N. Hayes and V. E. Mitchell, this report, p. 74.

ORGANOMETALLIC COMPOUNDS IN NUCLEIC ACID CHEMISTRY (V. N. Kerr)

INTRODUCTION

Some metallic salts and organometallic compounds have been found to be selective in binding to nucleic acids and nucleic acid components (1-3). This selectivity may be advantageous in staining for electron microscopy and in physical separation of various nucleic acid species.

METHODS AND RESULTS

A mercarbide (4) has been synthesized and applied as a stain

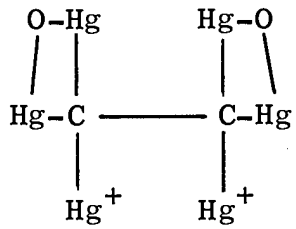

for collagen in an electron microscope preparation. The stain compared favorably with mercuric ion and presented greater resolution. The advantage of the mercarbide lies with the greater density of stain at a given site than is present with compounds containing only one mercury atom.

Mercuri-resins in column chromatography are being studied utilizing a mercurated organic polymer. The amounts of material absorbed on a mercuri-polystyrene resin were determined spectrophotometrically by measuring the absorbance of each solution before and after addition of the resin. It was found that this new resin was selective in taking up nucleosides. Preliminary experiments have shown that the amount of nucleoside absorbed on the resin is a function of pH and ionic species also present in the solution. Table 1 illustrates both effects. Further observations are that the nucleosides bind with the resin at a fast rate initially, followed by slower absorption. The reverse action, desorption, does not appear to be complete; however, it is possible

TABLE 1. NUCLEOSIDE BINDING ON CHLOROMERCURI-POLYSTYRENE

Salt	pH	Percent of Nucleoside Bound to Resin			
		Adenosine	Cytidine	Guanosine	Thymidine
NaCl (0.1 M)	4.8	4	2	3	2
NaH_2PO_4 (0.1 M)	5.4	15	35	63	35
Na_2HPO_4 (0.1 M)	8.9	25	17	68	82
NH_4OAc (0.1 M)	7.4	15	16	73	83
NH_4O_2CCHO (0.1 M)	7.4	18	19	75	83
$NaClO_3$ (0.05 M)	8.5	43	35	84	90
$NaO_2CCH_2NH_2$ (0.1 M)	9	7	0	58	69

that there is more than one absorption process taking place.

DISCUSSION

The successful application of the mercarbide as a collagen stain in electron microscopy suggests that, in light of the known affinity of mercury salts for nucleic acid, this compound can be used to provide greater resolution for nucleic acid preparations.

The chloromercuri-polystyrene resin shows promise for column chromatography separation of nucleic acid derivatives and is being investigated further.

REFERENCES

(1) A. M. Fiskin and M. Beer, Biochemistry 4, 1289 (1965).

(2) R. B. Simpson, J. Am. Chem. Soc. 86, 2059 (1964).

(3) N. Davidson, 151st National American Chemical Society Meeting, Pittsburgh, Pa. (1966).

(4) K. A. Hoffman, Ber. 33, 1328 (1900).

COMPUTER ANALYSIS OF ULTRAVIOLET SPECTRA (G. T. Fritz)

INTRODUCTION

Studies are being made to determine the best techniques to be used in computer analysis of ultraviolet spectra of multicomponent solutions of nucleic acid derivatives and to determine the limitations of the method. The spectra of 2'-deoxy-5'-adenylic acid (pa) and 5'-thymidylic acid (pt) at pH 7.0 were chosen for the study because their shapes are similar and, therefore, difficult to resolve.

METHODS

Spectra of stock solutions of pa and pt at pH 7.0 and concentrations of approximately 50 μM were used as the library for the computer analysis. Binary solutions were prepared using appropriate amounts of the stock solutions. Spectra were obtained on a Cary 14 recording spectrophotometer equipped with digital output. Absorbance readings were taken every 0.5 mμ. The region 310.5 to 220 mμ, a total of 180 points, was used for the calculations. In accordance with results of previous studies (1), the background spectrum was treated as a library spectrum, and a weighting factor of 1 was used.

RESULTS AND DISCUSSION

Figure 1 shows the variation of percent error with concentration in binary solutions in which the total concentration is approximately 50 μM. With one exception, the errors for concentrations greater than 20 μM are less than 1 percent. At a concentration of 1 μM, the error is about 50 percent. This means that, in a 5-ml sample, 5 nmoles (approximately 1.5 μg) can be determined to $\pm$ 2.5 nmoles in the presence of 250 nmoles of the second component.

Several aspects of the data indicate that the library can be improved. First, as seen in Fig. 1, the errors for pa and pt are positive and negative, respectively, with very few exceptions. Second, the fraction of background found to be present is always greater than the expected value of 1.00. Third, the plots of the residual spectra have a nonrandom character, indicating the poorest fit of the library to be

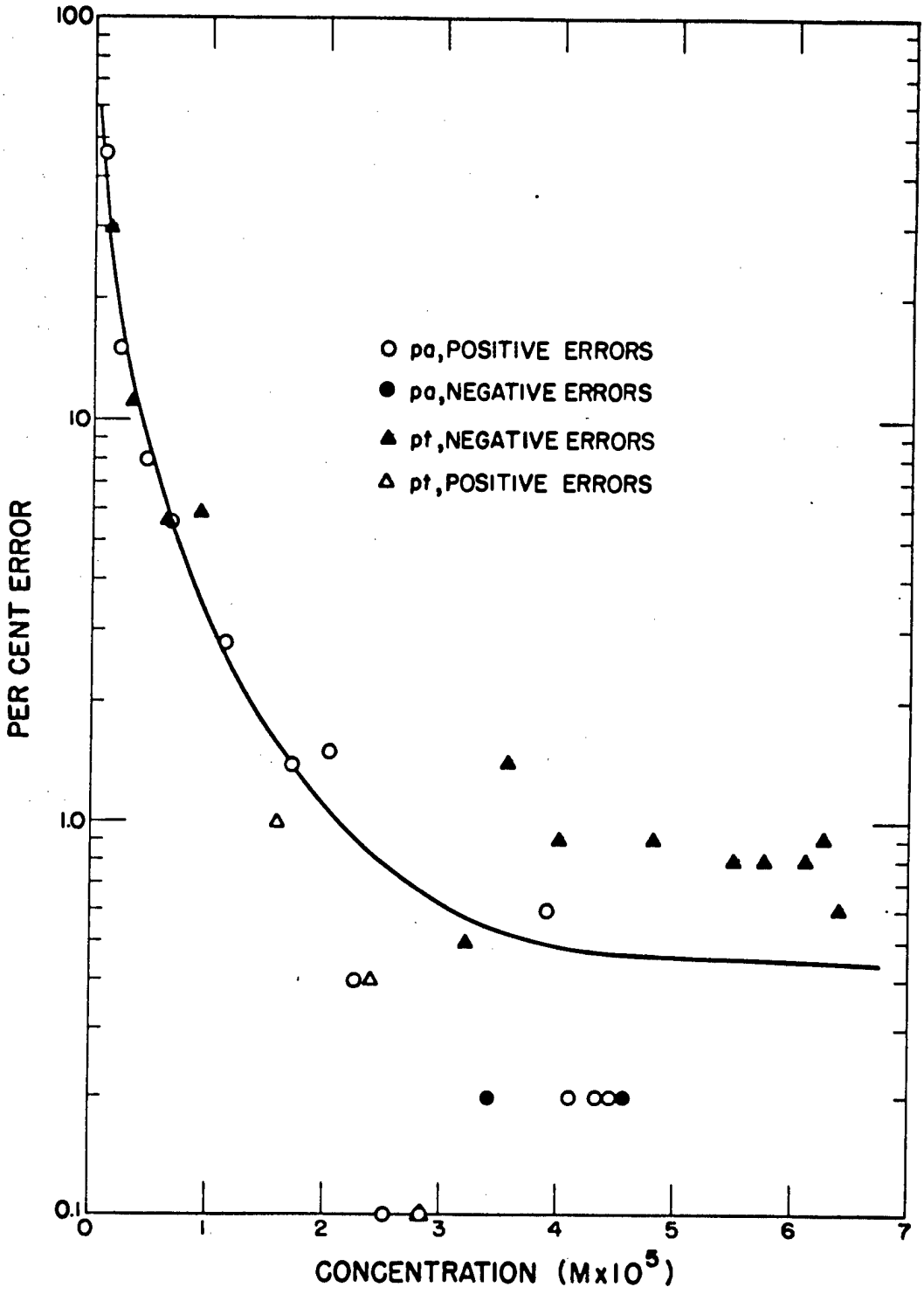

Fig. 1. Percent error as a function of concentration of pa and pt in binary solutions of total concentration 45 to 65 μM.

in the short wavelength region of the spectra. Fourth, analysis of solutions of 100 percent pt always indicates the presence of small amounts of pa (less than 1 percent), whereas no pt is found in solutions of pa. These difficulties are, in large part, a result of choosing the background for the library. The computer program is being changed to fit a polynomial to the background rather than using background spectrum in the library. Another cause of poor background fit in the short wavelength region is high sample background resulting from formation of tiny bubbles upon pouring solutions out of narrow-necked volumetric flasks. Pipetting the solutions from these flasks into the spectrophotometer cuvette overcomes this difficulty.

Computations were made with spectra averaged by the computer from several (2 to 5) individual scans and were compared to the average of results computed from the individual scans. There was no improvement in the percent error in the former case; however, the standard deviations of the computed mole fractions and the sum of the squares of the deviations were decreased by one-third to one-half, respectively, indicating a better fit of the library to the input data. Preliminary studies indicate that use of the averaging technique will permit use of the 0- to 0.1-absorbance slidewire on the Cary recorder and thus will lower the limit of analyzable concentration by a factor approaching 10.

The spectra of the solutions were redetermined at intervals of 1 week, 1 month, and 2 months after preparation. The solutions were stored in the refrigerator, but sterile techniques were not used. Table 1 shows the increase with time of the average percent error, the fraction of background found, and the sum of the squares of the deviations. Most of the significant increases in percent error up through 1 month occurred for concentrations less than 20 μM.

Since the spectra of pa and pt were chosen as being difficult to resolve, species with dissimilar spectral shapes should submit to analysis more easily. Use of the averaging technique, the 0.1-absorbance slidewire, and/or long path-length cuvettes should permit analysis of concentrations of 1 μM to $\pm$ 10 percent. The method is being applied to determination of base ratios in synthetic oligonucleotides.

REFERENCE

(1) G. T. Fritz, Los Alamos Scientific Laboratory Report LA-3432-MS (1965), p. 229.

TABLE 1. RESULTS OF COMPUTER ANALYSIS OF BINARY SOLUTIONS AS A FUNCTION OF TIME

	Weeks after Preparation			
	0	1	4	8
Percent Error*	1.600	2.300	3.200	13.500
Percent Error**	4.500	6.200	7.600	20.400
Fraction of Background Found	1.029	1.046	1.061	1.105
Sum of the Squares of the Deviations x 10^4	6.400	8.700	8.600	14.700

*Average for concentrations of 5 to 65 μM.

**Average for concentrations of 0.9 to 65 μM.

MOLECULAR RADIOBIOLOGY SECTION

PUBLICATIONS AND ABSTRACTS OF MANUSCRIPTS SUBMITTED

HIGH-RESOLUTION DISC ELECTROPHORESIS OF HISTONES I. AN IMPROVED METHOD, G. R. Shepherd and L. R. Gurley. Anal. Biochem. 14, 356-363 (1966).

An improved method for high-resolution polyacrylamide gel disc electrophoresis is presented. Electrophoretic patterns obtained by this technique for ribonuclease, trypsin, and a whole calf thymus histone preparation are displayed. The resolving power of this method is excellent, and its simplicity, sensitivity, and reproducibility recommend it for routine and analytical use.

HIGH-RESOLUTION DISC ELECTROPHORESIS OF HISTONES II. APPLICATION TO WHOLE AND FRACTIONATED PREPARATIONS FROM VARIOUS LABORATORIES, L. R. Gurley and G. R. Shepherd. Anal. Biochem. 14, 364-375 (1966).

An improved method of disc electrophoresis of histones on polyacrylamide gels has been applied to routine analysis of histones. Similar electrophoretic patterns of high complexity were obtained for unfractionated calf thymus histone prepared by different methods in several laboratories. Thus it would appear that the majority of the spectrum of histone bands demonstrated by this electrophoretic method may be isolated from calf thymus by each of the preparative techniques. All bands observed in unfractionated histone patterns corresponded with specific bands observed in the pattern of histone fractions, suggesting that the high degree of resolution obtained was not due to complexes of the various histone components.

All histone fractions were found to be heterogeneous, containing one or more major and several minor components. Lightly staining forerunner components observed in unfractionated

histones were found to be concentrated in the F_1 fraction and were preferentially removed from the nucleoprotein complex between pH 3.0 and pH 1.8 with H_2SO_4. These findings recommend polyacrylamide gel electrophoresis as a valuable technique for following the distribution of both major and minor components during fractionation studies.

UNPRIMED SYNTHESIS OF POLYADENYLATE AND POLYURIDYLATE CATALYZED BY RIBONUCLEIC ACID POLYMERASE, D. A. Smith, R. L. Ratliff, T. T. Trujillo, D. L. Williams, and F. N. Hayes. J. Biol. Chem. 241, 1915-1916 (1966).

When adenosine triphosphate and uridine triphosphate are incubated with ribonucleic acid polymerase in the absence of a template, polyadenylate and polyuridylate are formed. The reaction occurs after a lag period of variable length. Unprimed synthesis of polyadenylate and polyuridylate can be greatly inhibited through the use of sufficient amounts of templates of high molecular weight.

DISC ELECTROPHORESIS OF BOVINE THYMUS HISTONES, G. R. Shepherd and L. R. Gurley. Comp. Biochem. Physiol. (in press).

Whole bovine thymus histone preparations obtained from animals (Bos bovus) differing in age, sex, and breed were subjected to high-resolution polyacrylamide gel disc electrophoresis. No significant differences were observed between the resulting gel patterns. These data support the view that the variables of age, breed, and sex have no discernible effect on the observed properties of isolated bovine thymus histones.

NUCLEAR HISTONES AND EARLY EMBRYOGENESIS OF THE CHICK, C. W. Kischer, L. R. Gurley, and G. R. Shepherd. Nature (submitted).

Histones were extracted from purified nuclei of the whole chick embryo from gastrulation to 7 days of age. Electrophoretic patterns were identical for all such preparations,

while a gradual increase in the proportion of basic amino acid residues suggests a possible association of histones with acidic proteins in the early stages of maturation. It is concluded that the histone complement of chick embryo nuclear histones does not reflect the ontogenic changes in embryonic development.

THE SYNTHESIS AND EVALUATION OF SOME NEW TRANS-1,2-DIARYLETHYLENES AS LIQUID SCINTILLATORS, G. H. Daub, F. N. Hayes, J. L. Schornick, D. W. Holty, and L. G. Ionescu. J. Molecular Crystals (submitted).

As a continuation of fundamental studies on the relation of organic structure to scintillation performance, a series of derivatives of trans-stilbene have been synthesized and evaluated as to ultraviolet absorption, fluorescence, relative pulse height, and stability to ultraviolet damage. Maintaining the trans configuration by means of a 5- or 6-carbon bridge gives excellent performance. However, introduction of a methyl substituent on one carbon of the ethylenic double bond gives improved performance with the 6-membered bridge and drastically poorer performance with the 5-membered bridge. The implications of these observations are discussed along with ideas stemming from these for synthesis of better scintillators.

CHAPTER 4

MAMMALIAN RADIOBIOLOGY SECTION

DOSE RATE-TOTAL DOSE EFFECT ON SURVIVAL IN MICE (J. F. Spalding, O. S. Johnson, and R. F. Archuleta)

INTRODUCTION

Many simple dose rate effects studies (exposure to ionizing radiation at several dose rates with reduced survival time as the end point) have been reported in the past. Information is lacking, however, where both dose rate and total dose are variables. A study is nearing completion in which 12 dose rates (cobalt-60 gamma rays) within each of 12 total doses were used in an effort to establish a functional relationship between the variables of survival time, total dose, and dose rate. Data from 6 of the 12 total doses have been completed and are presented in this report.

METHODS

One thousand and forty RF strain virgin female mice 120 $\pm$ 14 days of age were randomly separated into 145 groups: 144 exposure groups (Table 1) with 7 mice per group and 1 control group with 32 mice. Each of the 144 experimental groups was assigned one of the dose rate-total dose exposures listed in Table 1. Each of the 144 different exposures was made by random selection, and all exposures were completed over a period of 6 weeks. Mice in each group were checked daily after exposure, and mean aftersurvival (MAS) times were calculated in an effort to derive a functional relationship between the variables of survival time, total dose, and dose rate. Data point comparisons were made by analysis of variance.

TABLE 1. DOSE RATE-TOTAL DOSE EFFECT

Total Dose (rads)	MAS (days) with Standard Error of the Mean (dose rate, rads/hr)												Test of Significance* (Dose rate within dose)	MAS (Data points combined)
	2.5	5	10	15	20	25	50	75	100	150	200	250		
100	-	-	-	-	-	-	-	-	-	-	-	-		
200	486 ± 39	470 ± 56	499 ± 29	426 ± 52	444 ± 40	338 ± 53	478 ± 52	304 ± 39	458 ± 67	448 ± 44	542 ± 38	433 ± 81	Yes	442 ± 16
300	-	-	-	-	-	-	-	-	-	-	-	-		
400	382 ± 63	302 ± 46	314 ± 50	368 ± 40	364 ± 48	251 ± 31	249 ± 36	333 ± 52	395 ± 41	302 ± 27	411 ± 71	404 ± 47	Yes	339 ± 14
500	-	-	-	-	-	-	-	-	-	-	-	-		
600	293 ± 47	206 ± 27	237 ± 40	341 ± 40	279 ± 27	401 ± 20	287 ± 37	337 ± 45	268 ± 36	371 ± 42	261 ± 26	316 ± 54	Yes	301 ± 12
700	-	-	-	-	-	-	-	-	-	-	-	-		
800	260 ± 32	232 ± 45	153 ± 55	191 ± 59	534 ± 50	263 ± 35	303 ± 74	168 ± 72	380 ± 37	162 ± 56	272 ± 30	312 ± 37	Yes	229 ± 17
900	-	-	-	-	-	-	-	-	-	-	-	-		
1000	341 ± 61	40 ± 27	11 ± 0.4	129 ± 51	330 ± 45	256 ± 58	211 ± 55	228 ± 58	423 ± 33	132 ± 72	201 ± 55	**	Yes	207 ± 20
1100	-	-	-	-	-	-	-	-	-	-	-	-		
1200	192 ± 33	49 ± 29	158 ± 68	11 ± 0.3	10 ± 2	35 ± 32	203 ± 91	319 ± 54	37 ± 3	8 ± 0.7	6 ± 0.7	100 ± 59	Yes	93 ± 16
Data Points Combined	322 ± 23	210 ± 28	221 ± 30	244 ± 29	233 ± 29	257 ± 23	289 ± 26	306 ± 26	237 ± 29	282 ± 32	313 ± 31	-		

*Duncan-Kramer multiple range test (5 percent level of significance).

**Point lost.

RESULTS AND DISCUSSION

Only 6 of the 12 total dose groups have been analyzed; several of the other groups await completion for MAS values. The data are tabulated in Table 1. Analysis of variance of dose rate within each total dose showed significant differences in MAS values in all total dose groups; however, differences shown were not dose rate-related. With the exception of the 400-rad dose group (which reversed with the 200-rad dose group), the number of dose rates differing from each other (in terms of MAS) increased with total dose. When dose rate data were pooled, disregarding total dose, analysis still showed no dose rate-related difference in MAS (Table 1). Since no dose rate-related differences were observed within each total dose group, the 12 dose rate groups were pooled to determine the relationship between total dose and reduction in life span. These figures are shown in the last column of Table 1 and are expressed in graph form in Fig. 1.

The dose rate-total dose effect data presented here show no dose rate effect on lethality (MAS) within the dose rate range of 2.5 to 250 rads/hr. Total dose data indicate that, within the dose rate range studied, MAS is reduced approximately 30 days/100 rads (Fig. 1). Assuming a mouse-to-man relationship of 1 day to 42.5 days, somewhat more than the value reported by Jones (1), similar exposure conditions in man might be expected to produce a reduction in MAS at the rate of approximately 3.5 years/100 rads.

REFERENCE

(1) H. Jones, In Hearings before the Special Subcommittee on Radiation of the Joint Committee on Atomic Energy, Congress of the United States, Eighty-Fifth Congress, First Session on the Nature of Radioactive Fallout and Its Effect on Man (June 4-7, 1957), Part 2 (1957), pp. 1103-1104.

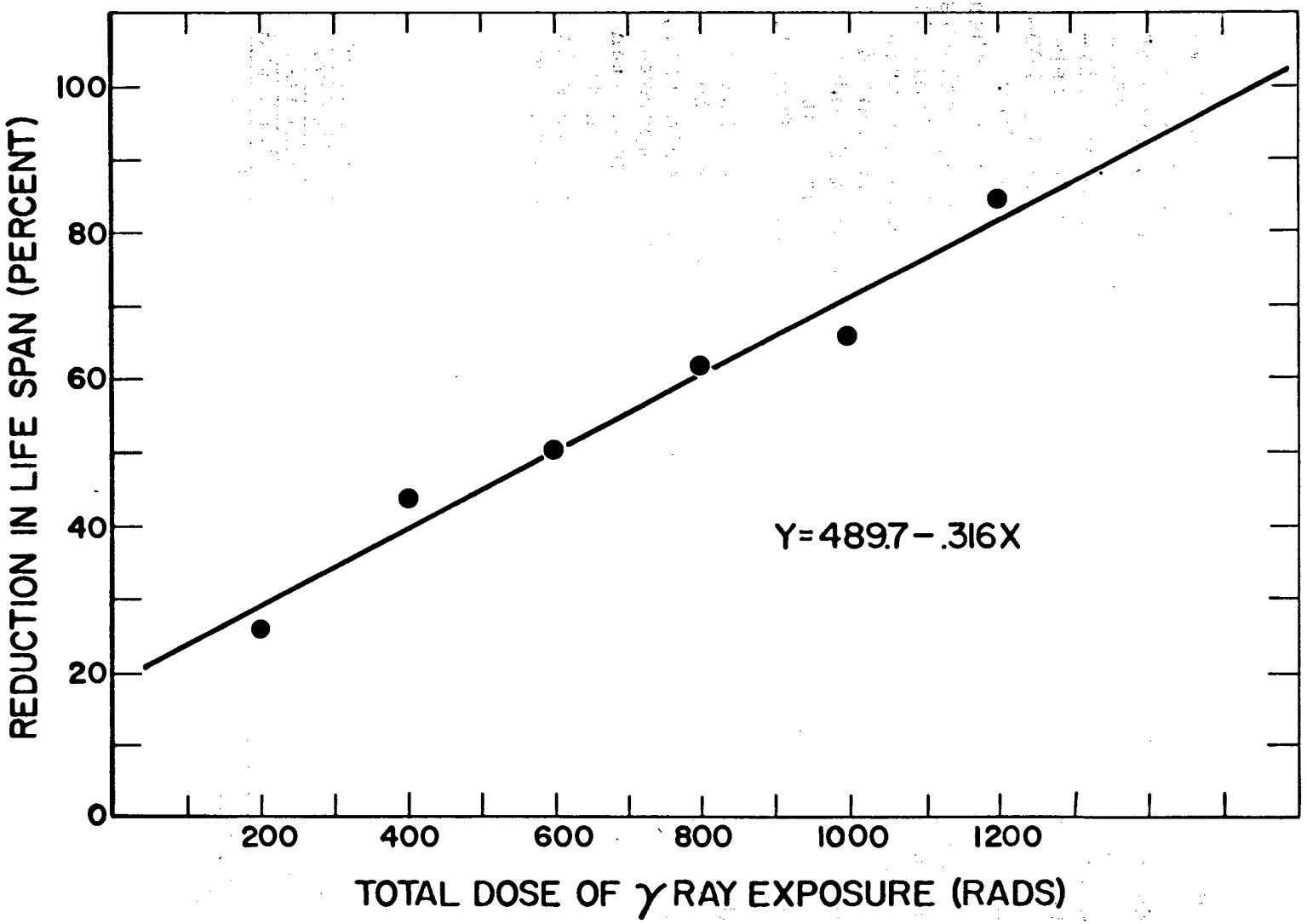

Fig. 1. Reduction in life span plotted as a function of total exposure dose with cobalt-60 gamma rays.

INJURY AND RECOVERY OF BONE MARROW DURING AND FOLLOWING CONTINUOUS LOW-INTENSITY GAMMA IRRADIATION (J. F. Spalding, N. J. Basmann, and R. F. Archuleta)

INTRODUCTION

Injury from continuous gamma-ray exposure appears to change from chronic to acute in the dose rate range of 2 to 5 rads/hr in RF strain mice (1). If bone marrow is the critical organ in low-intensity continuous exposure, bone marrow arrest should occur in this same dose rate range. This investigation was done to determine (a) whether or not bone marrow arrest does coincide with the acute effects dose rate, (b) to what level the erythrocyte count may be permitted to drop before lethality can be anticipated, and (c) if a progressive irreparable bone marrow disease or lesion is induced by continuous low-intensity gamma-ray exposure stopped short of a lethal dose.

METHODS

Four hundred and sixty RF strain female mice were randomized and divided into 4 groups of 150, 140, 140, and 30 mice each, respectively. Group I (150 mice) was exposed continuously to death with cobalt-60 gamma rays, Group II (140 mice) was exposed to gamma rays for 8 to 9 days, Group III (140 mice) was exposed to gamma rays for 15 days, and Group IV (30 mice) was retained as a nonirradiated control. The dose rate for all irradiated groups was 4.52 rads cobalt-60 gamma rays per hour. Group I was placed in the gamma-ray environment and irradiated continuously until death. Group II was exposed to continuous gamma rays for 188 hours, after which time the mice were removed for observation during the recovery period. Group III was given continuous gamma-ray exposure for 355 hours, and the mice were then removed for study during the recovery phase. Group IV mice were nonirradiated controls used to establish base line data. Blood samples were obtained by the orbital bleeding technique (2) from irradiated groups according to the schedule shown in Fig. 1. Erythrocyte numbers (red blood cells, RBC's), mean cell volumes (MCV's), and body weights (in g) were recorded for comparison with control values.

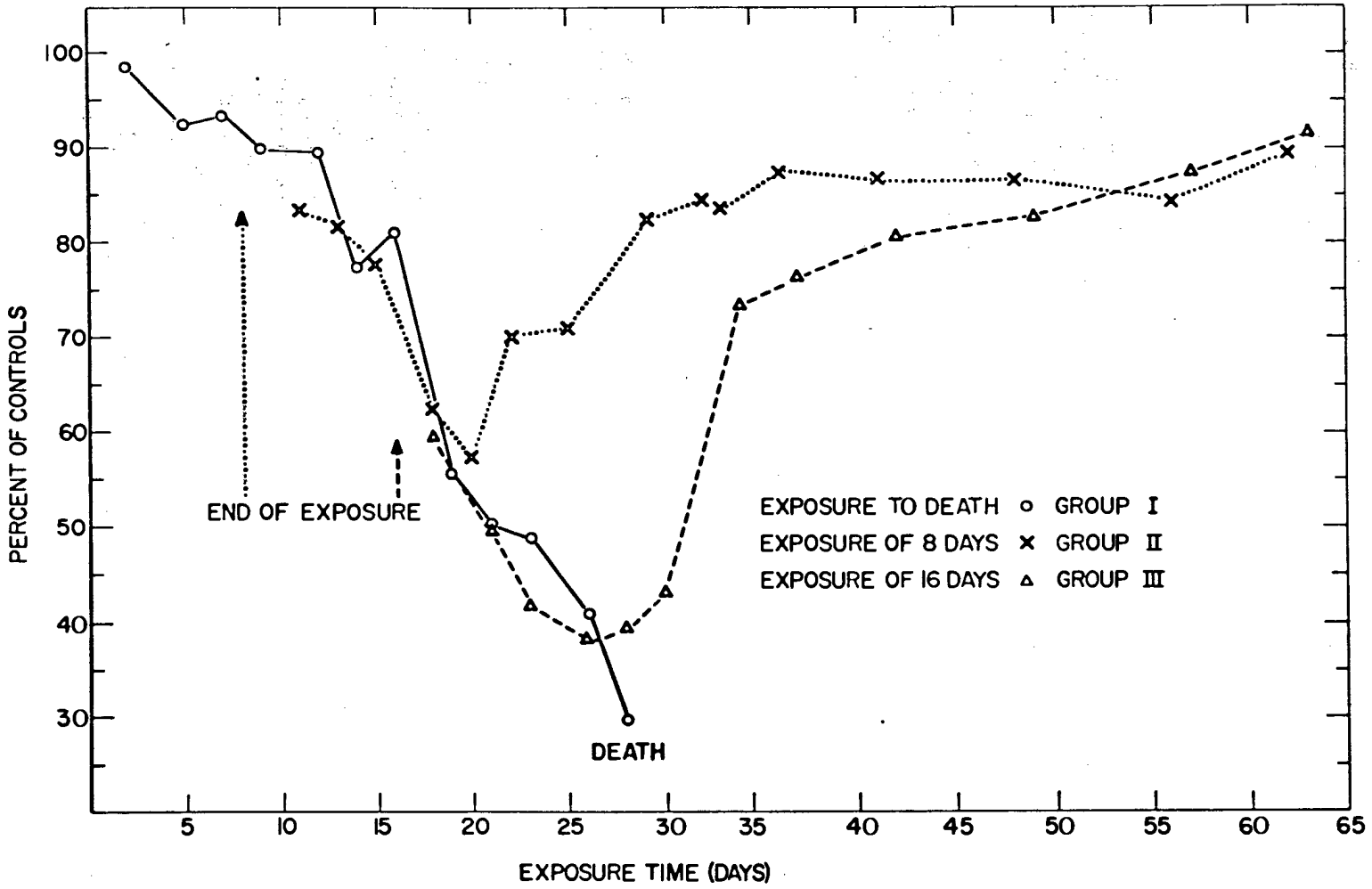

Fig. 1. Erythrocyte counts (percent of control) during exposure and recovery from continuous gamma-ray exposure at 4.52 rads/hr. Group I, continuous exposure to death; Group II, removed from gamma-ray environment after 8 to 9 days of exposure; and Group III, removed from gamma-ray environment after 15 days of exposure.

RESULTS AND DISCUSSION

RBC counts and MCV's, normalized to control values, are shown in Figs. 1 and 2, respectively. Body weights, expressed as percent of pre-exposure weights, are shown in Fig. 3.

In Group I (continuous exposure to death), RBC's started to drop at the first bleeding (2 days into the exposure) and continued downward until reaching 30 percent of control, after which death ensued. The more or less continuous drop in RBC in Group I suggests that the dose rate used (4.52 rads/hr) was sufficient to prevent erythropoiesis or to cause bone marrow arrest. This would be in agreement with the dose rate range within which radiation effects reportedly change from chronic to acute (1).

Group II mice showed a continuing post-exposure drop in RBC's for 12 days after receiving a total gamma-ray dose of 918 rads (Fig. 1), and the RBC level dropped to about 50 percent of the control value. This level was not critical, and 14 days after removing the bone marrow block (continuous gamma-ray exposure) erythropoiesis began to evidence rapid recovery, returning RBC's to near normal by the 54th day after irradiation.

Group III mice continued to lose erythrocytes for 10 days after gamma irradiation was stopped and after receiving a total gamma-ray exposure of 1604 rads. The RBC level reached a low of 38 percent of the control value (Fig. 1), and lethality followed in nearly 50 percent of the animals in Group III. Animals surviving the exposure showed a return of erythropoiesis, in terms of RBC recovery, 14 days after removal from the gamma-ray exposure field, and RBC's returned to near normal values by the 48th day after exposure (Fig. 1).

MCV's are plotted in Fig. 2 as percent of control for the 3 exposed groups. The blood-forming organs responded to radiation injury by pouring large numbers of reticulocytes into the bloodstream which, in turn, was reflected by an increased MCV. Group I mice showed little or no sign of bone marrow activity through increased MCV's, and during the last few days of exposure MCV's decreased to below control values (a characteristic shrinking of aging erythrocytes). When bone marrow arrest (gamma-ray exposure) was terminated in Groups II and III, recovery of erythropoiesis was evidenced by both a return to normal RBC values and an increase in MCV's above control values, returning to near normal approximately 40 to 50 days post-exposure.

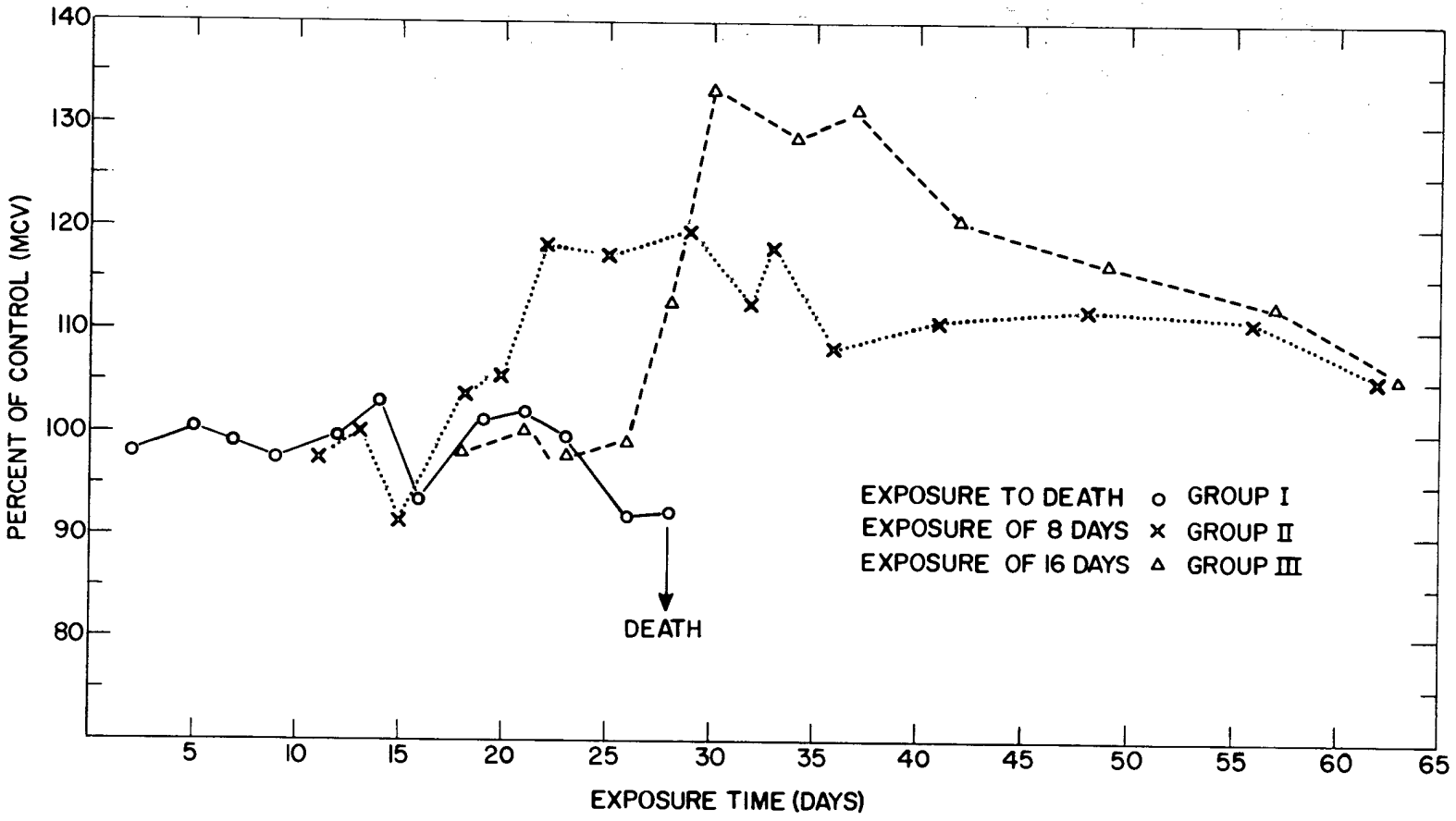

Fig. 2. Mean cell volume (percent of control) during exposure and recovery from continuous gamma-ray exposure.

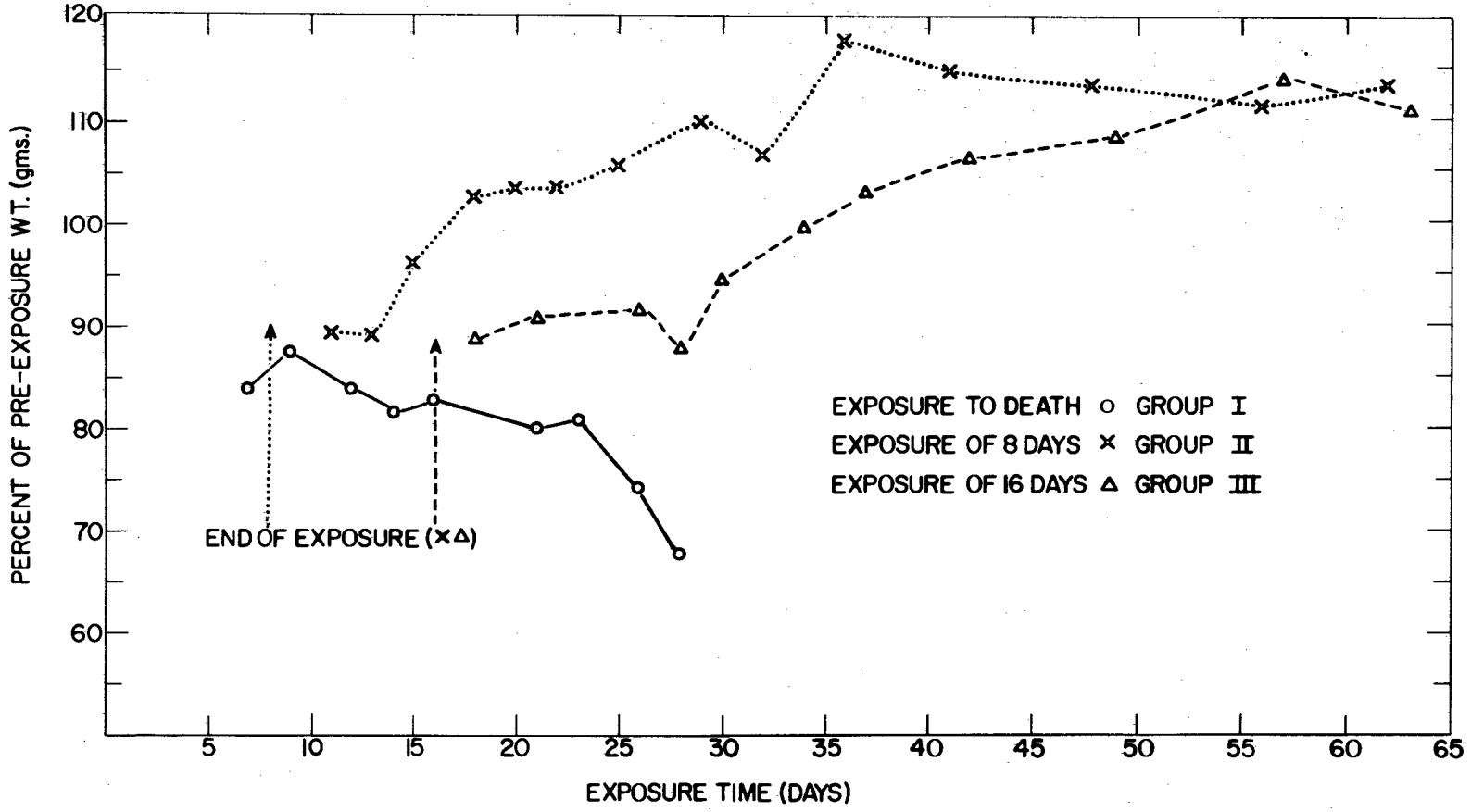

Fig. 3. Body weight (percent of control) during exposure and recovery from continuous gamma-ray exposure.

Body weights, plotted as percent pre-exposure weights, are shown in Fig. 3. Body weights of all exposed groups declined to about 85 percent of the pre-exposure level, and Group I (in which radiation was continued to death) continued a gradual weight loss until death. As soon as mice were removed from the gamma-ray environment, they began to recover from weight loss, and a normal weight gain with age followed (Groups I and II, Fig. 3). Weight loss and recovery followed a similar pattern to RBC decline and recovery, indicating general malaise associated with anemia.

These studies do indeed indicate that bone marrow arrest does coincide with the acute effects dose rate range. No progressive irreparable bone marrow lesion was evidenced in this study. The critical erythrocyte level before lethality may be anticipated was approximately 40 percent of control levels. Body weight loss and recovery, in general, followed the decline and rise in erythrocyte count. Studies in this general area will continue in conjunction with the Effective Residual Dose (ERD) concept program.

REFERENCES

(1) J. F. Spalding, T. T. Trujillo, and P. McWilliams, Health Phys. 10, 709 (1964).

(2) V. Riley, Proc. Soc. Exp. Biol. Med. 104, 751 (1960).

COMPARATIVE AFTERSURVIVAL TIMES OF MICE FOLLOWING GRADED FIRST AND GRADED BUT REVERSED SECOND EXPOSURES (J. F. Spalding and O. S. Johnson)

INTRODUCTION

Recovery from radiation injury in the mammal is the subject of considerable concern and attention. Several exposure parameters which may affect biological recovery have been investigated. Answers to such questions as to what extent do rate and size of a prompt dose affect repair rate and within what dose rate range do radiation effects change from chronic to acute have been sought in earlier investigations (1,2). Since the bone marrow is one of the critical organs in radiation injury, much attention is being turned in this direction. Tubiana (3), using 400 to 450 rads of gamma rays to lower the immunological defenses for kidney grafts in human subjects, found that 100-rad exposures 2 to 3-1/2 months later produced severe and long-lasting bone marrow aplasia, suggesting unexpected residual hematopoietic tissue damage from first exposures. Subsequent studies on comparative repopulation recovery of circulating erythrocytes following graded second gamma-ray exposures in mice failed to show any significant residual damage (4). Although no residual irreparable bone marrow lesion was indicated in the erythrocyte repopulation investigation, it was felt that mean aftersurvival time studies would reflect this damage, if present.

METHODS AND RESULTS

Two hundred and fifty RF strain virgin mice, 4 months + 2 weeks of age, were randomized and divided into 5 groups of 50 mice each. Groups I through IV were given whole-body gamma-ray (cobalt-60) exposures of 200, 400, 600, and 800 rads, respectively, at a dose rate of 6 rads/min. Group V was a non-irradiated control group. Ninety days following first exposures irradiated groups were given second whole-body gamma-ray exposures, reversed such that Groups I through IV received 800, 600, 400, and 200 rads, respectively. Following second exposures, all 4 test groups had received a total exposure of 1000 rads in two unequal fractions separated by 90 days. This method of exposure was used to test the possible residual effect [in terms of mean aftersurvival time (MAS)] of a wide range of exposure conditions (i.e., near-lethal doses followed

by relatively small second exposures versus small first exposures followed by near-lethal second exposures). If a threshold effect exists within the dose range used (200 to 800 rads), one would not expect complete additivity in response to such end points as repopulation of circulating erythrocytes (4) or MAS.

Survival data are shown in Table 1 and in Fig. 1. MAS data for the control group are not available at this time; however, assuming a control mean survival time of 600 days, 1000 rads of gamma rays delivered in two prompt fractions separated by 90 days caused an average reduction in life span of 304 days (Table 1). No significant difference in MAS among the 4 groups was observed. Figure 1 shows a plot of percent survival versus survival time in days. This plot shows similarity in death distribution with time after exposure and again fails to show significant differences among the 4 groups. Death distribution data are in agreement with results of erythrocyte repopulation studies (4). Residual irreparable damage was independent of exposure conditions within the range described.

REFERENCES

(1) J. F. Spalding, T. T. Trujillo, and W. L. LeStourgeon, Radiation Res. 15, 378 (1961).

(2) J. F. Spalding, T. T. Trujillo, and W. L. LeStourgeon, Health Phys. 10, 709 (1964).

(3) M. Tubiana, C. M. Lalanne, and J. Surmont, In Diagnosis and Treatment of Acute Radiation Injury, World Health Organization, Geneva (1961), pp. 237-263.

(4) J. F. Spalding, Radiation Res. (in press).

TABLE 1. COMPARATIVE MEAN AFTERSURVIVAL TIME OF MICE FOLLOWING GRADED FIRST AND GRADED BUT REVERSED SECOND EXPOSURES (TOTALING 1000 RADS OF GAMMA RAYS)

Exposure Group (first dose/second dose)	MAS* (days)	Standard Error
200/800	299	± 14.5
400/600	292	± 18.0
600/400	309	± 14.1
800/200	285	± 16.0

*No significant difference in MAS at 0.05 level.

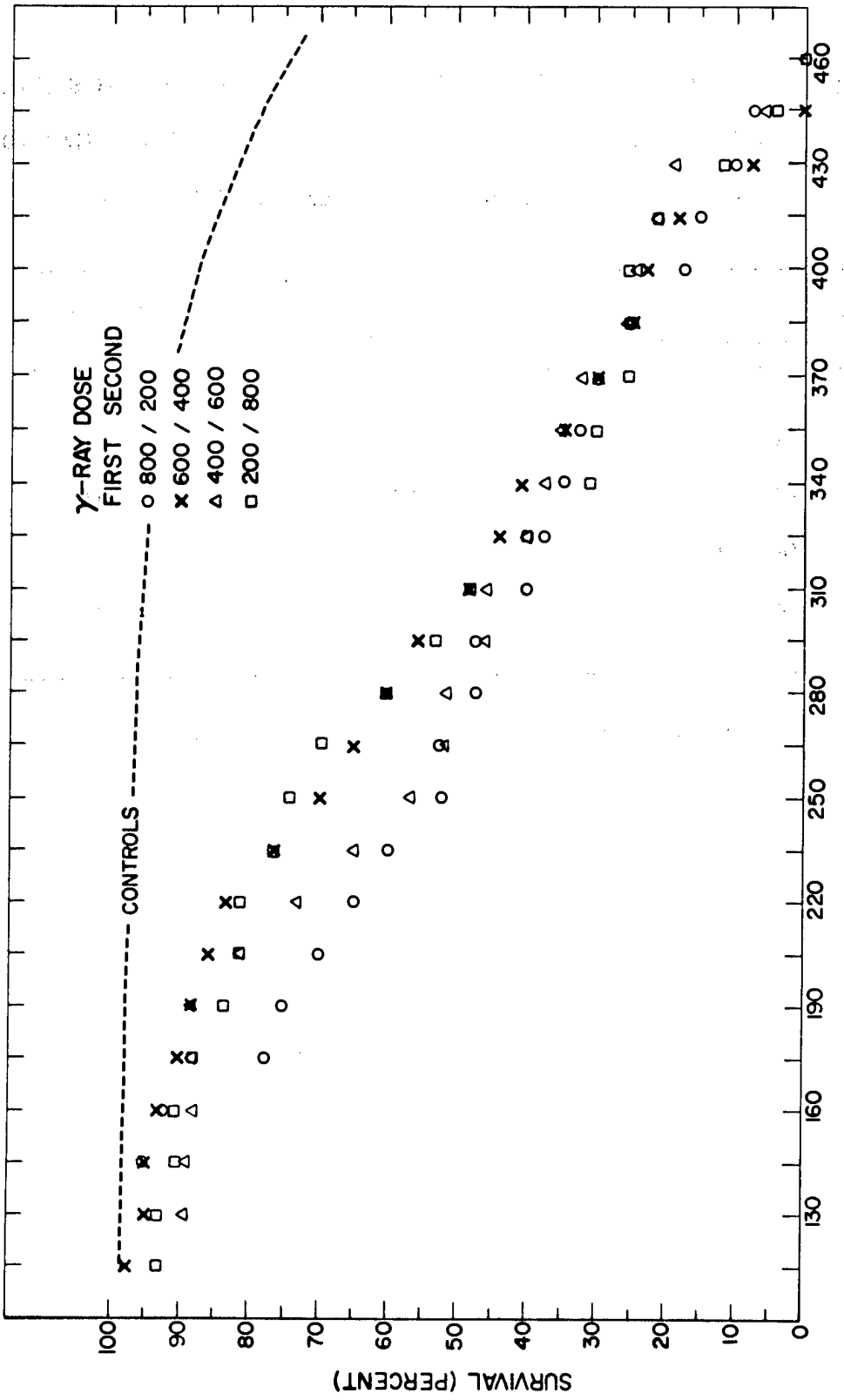

Fig. 1. Comparative MAS (percent) of 4 groups of mice following graded first and graded but reversed second exposures totaling 1000 rads of gamma rays.

A TEST OF THE EFFECTIVE RESIDUAL DOSE CONCEPT OF RADIATION INJURY IN MICE (J. F. Spalding, N. J. Basmann, and R. F. Archuleta)

INTRODUCTION

The residual dose concept of radiation injury is presently used in recommended procedures for exposure to radiation in an emergency (1). However, there is little experimental evidence that the validity of this concept has been tested in mammals. A program is in progress to test and to modify mathematical models which may be useful in describing and predicting biological injury from exposure to ionizing radiations. The following is a report on the first of a series of tests now under study.

METHODS

Two hundred RF strain virgin female mice 90 $\pm$ 7 days of age were randomly assigned to 4 groups of 50 mice each. Groups I, II, and III were assigned to effective residual exposure test conditions in which they would receive but never exceed effective residual doses (ERD's) of 100, 200, and 300 rads, respectively, throughout their entire life span. These exposure conditions were determined with the assumptions that injury from radiation repairs with a 7-day repair half time, RT_{50} (2), and that 5 percent of any given gamma- or X-ray dose results in irreparable damage (3). Each group was started on its exposure schedule with a single exposure of gamma rays equaling its assigned maximum permissible effective residual dose, MP ERD (i.e., 100, 200, or 300 rads). At random time intervals (from 1/2 to 2 RT_{50}'s) throughout the life of the mice, additional gamma-ray exposures were administered to each group to bring its injury level up to its respective MP ERD. All gamma-ray exposures were made using cobalt-60 and were given at an initial dose rate of 27 rads/hr. The fourth group of 50 mice was a sham-exposed control group.

RESULTS AND DISCUSSION

Much of the blood work was reported earlier (4). In general,

during the first 360 days of exposure the red blood cell (RBC) count dropped below control values after each exposure, and reduction in RBC number was a function of ERD level, with the higher level causing the greatest drop. No serious irreparable bone marrow lesion was evidenced in terms of a permanent reduction in RBC number at any ERD level studied.

Survival (in percent) plotted against time (in days) is shown in Fig. 1. Mean survival times for ERD levels of 100, 200, and 300 rads were 318 ± 18, 277 ± 16, and 305 ± 15 days, respectively, and did not differ significantly from one another. The mean accumulated dose at death for each group in the same order was 1300, 2444, and 3858 rads, respectively.

It was quite obvious from the results of this study that a simple ERD model is not applicable to even a limited range of exposure conditions. Figure 2 shows an attempt to anticipate what might be expected with the simple ERD model used (see legend) and the assumption that 1 rad of gamma-ray exposure shortens the life span of the mouse by 0.093 day (5). Early mortality in the 200-ERD level (Fig. 1) was due to a high incidence of thymomas early in the study. It may be that gamma-ray doses given at the 200-ERD level were optimum for provoking thymic carcinomas and that doses at the 300-ERD level were therapeutic as well. It appears from the results of this investigation that the model used overestimates the irreparable irradiation effect (often referred to as "radiation aging") but does not sufficiently consider radiation-induced diseases which lead to early mortality. Continuing investigations should be helpful in designing more useful mathematical models for anticipating radiation injury and repair.

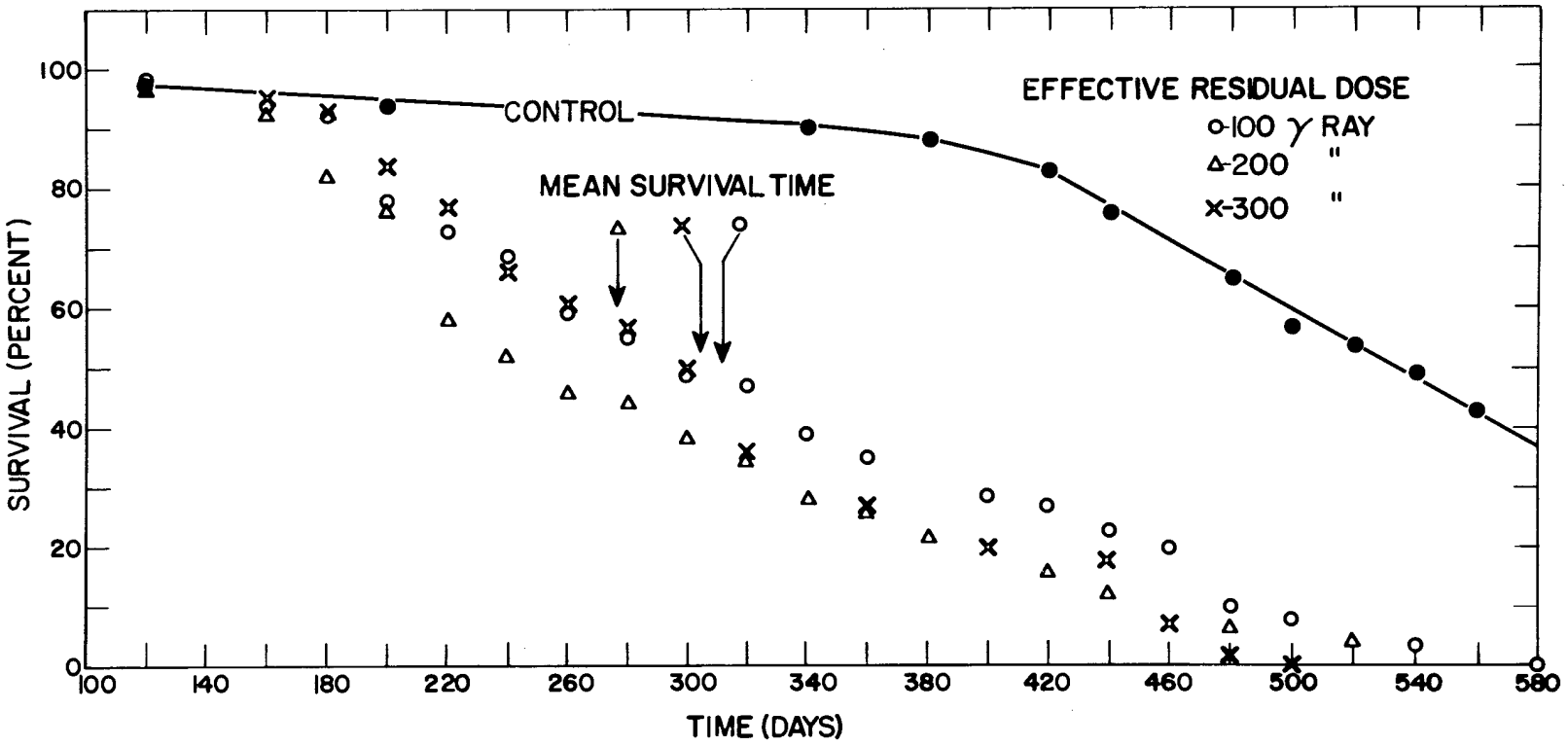

Fig. 1. Survival for 3 groups of mice assigned to 100-, 200-, or 300-rad effective residual dose levels.

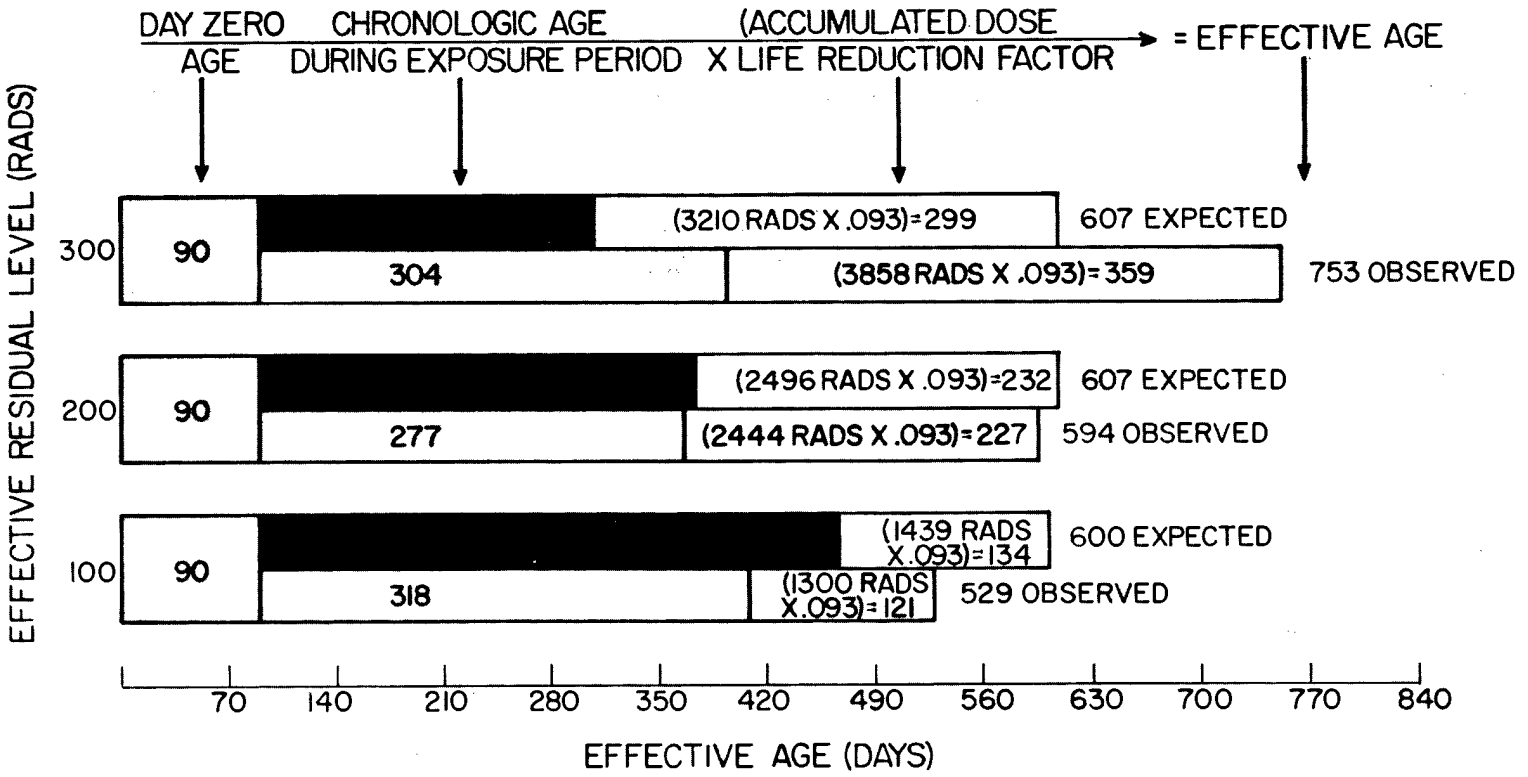

Fig. 2. Predicted versus observed effective mean age at death for 3 groups of mice on 100-, 200-, and 300-rad MP ERD gamma-ray exposure schedules. Exposures were made using the mathematical model,

$$A_i = L\,[\gamma_i + R_i e^{-\eta \Delta t}],$$

where A_i = ERD at t_i; L = desired radiation level; γ_i = irreparable at t_i; R_i = reparable at $t_i = 1 - \gamma_i$; $\Delta t = t_i$ - (time of last exposure); an assumed repair half time of 7 days; a 5 percent irreparable injury component; and the radiation life reduction factor of 0.093 day/rad.

REFERENCES

(1) National Committee on Radiation Protection and Measurements, Exposure to Radiation in an Emergency, Report No. 29 (1962).

(2) J. F. Spalding, T. T. Trujillo, and W. L. LeStourgeon, Radiation Res. 15, 378 (1961).

(3) J. F. Spalding, V. G. Strang, and F. C. V. Worman, Radiation Res. 13, 415 (1960).

(4) J. F. Spalding, Los Alamos Scientific Laboratory Report LA-3432-MS (1965), p. 75.

(5) T. T. Trujillo, J. F. Spalding, and W. H. Langham, Radiation Res. 16, 144 (1962).

MAMMALIAN RADIOBIOLOGY SECTION

PUBLICATIONS AND ABSTRACTS OF MANUSCRIPTS SUBMITTED

ACUTE RADIO-SENSITIVITY AS A FUNCTION OF AGE IN MICE, J. F. Spalding, O. S. Johnson, and R. F. Archuleta. Nature 208, 905-906 (1965).

Abstracted in Los Alamos Scientific Laboratory Report LA-3432-MS (1965), p. 100.

REDUCTION IN LIFE EXPECTANCY AS A MEASURE OF RADIATION-INDUCED GENETIC DAMAGE IN MICE, J. F. Spalding and M. R. Brooks. Proc. Soc. Exp. Biol. Med. 119, 922-925 (1965).

Abstracted in Los Alamos Scientific Laboratory Report LA-3432-MS (1965), p. 101.

HERITABLE RADIATION EFFECTS ON MOUSE BODY AND ORGAN WEIGHTS, FAT DEPOSITION, CELLULAR ENZYMES, AND BLOOD, R. R. J. Chaffee, J. C. Hensley, and J. F. Spalding. Genetics 53, 875-882 (1966).

Six- to eight-month-old offspring of white mice whose male ancestors received whole-body X-ray exposures of 200 rads over 25 to 37 successive generations had lower body weights, less omental and uterine associated fat, but higher kidney weights than controls. There were no differences in the weights of the heart, liver, spleen or scapular brown fat pads. There were no differences in the mean weights for the two mouse lines at age 75 or 90 days; only body weights were measured on mice of this age. There were no differences in the oxidative enzyme systems assayed in adults.

The irradiated line mice had a lower total white blood cell

count which was primarily due to fewer lymphocytes. There was a somewhat higher erythrocyte mean cell volume in the irradiated line, but erythrocyte counts were not different. The amino acid composition of the hemoglobin in the two lines of mice was indistinguishable, but preliminary studies indicated that the electrophoretic migration patterns of the hemoglobins in the two lines may be quite different. Blood oxygen and CO_2 levels were different in the two lines, as was blood sodium, but blood glucose levels were the same. The results of these experiments should be useful in indicating where some definable and transmissible changes take place for future studies on mutagenic effects of irradiation.

COMPARATIVE REPOPULATION RECOVERY OF CIRCULATING ERYTHROCYTES FOLLOWING GRADED SECOND GAMMA-RAY EXPOSURES IN MICE, J. F. Spalding. Radiation Res. (in press).

Mice were exposed to either 200, 400, 600, or 800 rads of γ-rays (6 rads/min), and the injury and recovery pattern of the bone marrow was followed by RBC determinations for 90 days post exposure. Second exposures were given following the 90-day recovery period and were of the same magnitude as first exposures, but the dose groups were reversed so that each group received a total of 1000 rads. Comparative recovery patterns were done following second exposures to determine the extent of irreparable bone marrow injury from first exposures. Repopulation recovery of circulating erythrocytes failed to reveal an irreparable bone marrow lesion. Mice with second exposures were able to recover with the same resilience as from a single exposure.

REPRODUCTIVITY AND LIFE SPAN OF MOUSE POPULATIONS FROM 25 GENERATIONS OF IRRADIATED SIRES, J. F. Spalding, M. R. Brooks, and P. McWilliams. Genetics (in press).

Reproductive fitness (comparative litter data studies) and life span of nonirradiated offspring from 25 generations of X-irradiated progenitors was studied. Irradiated line mice showed decrements in fitness by producing and weaning fewer progeny, by exhibiting a greater tendency toward cannibalism and sterility, and by producing stillbirths in greater numbers than control line mice. Life span was not significantly changed by progenitor irradiation.

CHAPTER 5

MAMMALIAN METABOLISM SECTION

RESIDENCE TIME OF FALLOUT CESIUM-137 IN A CONTROL POPULATION FOLLOWING THE JULY 1964 PEAK (C. R. Richmond and J. E. London)

INTRODUCTION

Pronounced peaks in cesium-137 body burdens occurred following each of the major periods (1957-1958 and 1960-1961) of atmospheric weapons testing. The larger of the two, in July 1964, has been followed by gradually decreasing body burdens. It is now possible to quantitate the residence time for fallout cesium-137 so that meaningful predictions can be made.

METHODS AND RESULTS

Data on cesium-137 burdens were obtained from a group of laboratory personnel that are counted each month by whole-body assay. Burdens for a 20-month period following the July 1964 peak were fit by an iterative least-squares procedure programmed in FORTRAN IV for an IBM 7094 computer. Both linear and exponential models were used. Figure 1 shows the linear fit to the data points. The best fit equation is:

$$y = 120.81 - 2.59\ x, \qquad \text{(Eq. 1)}$$

where y is picocuries of cesium-137 per gram of potassium (pCi/g K) and x is months after July 1964. The data were also fit to a single exponential model (Fig. 2) and gave the equation:

$$y = 122.64\ e^{-0.027\ x}. \qquad \text{(Eq. 2)}$$

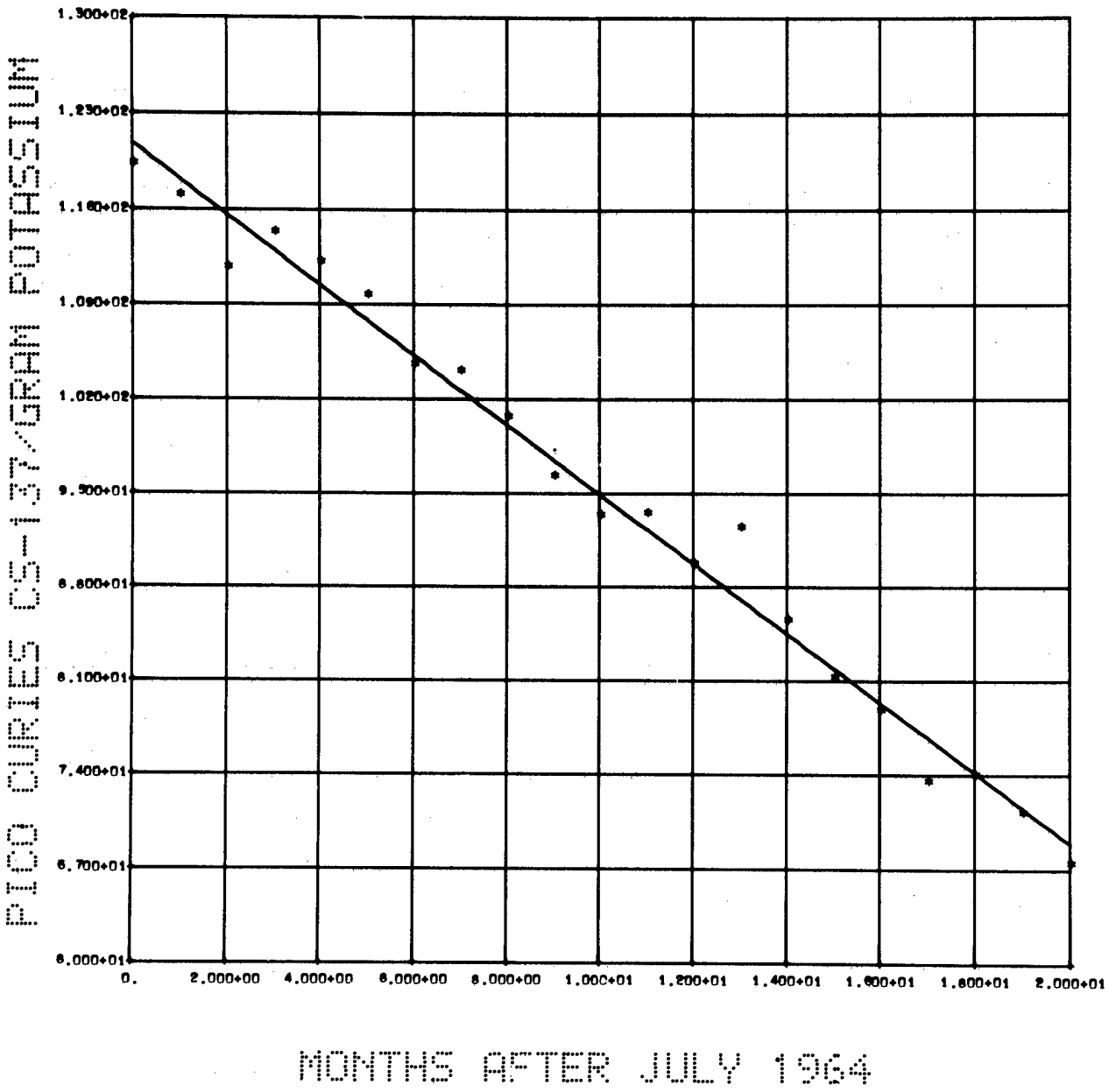

Fig. 1. Linear plot of cesium-137 body burdens from July 1964 to March 1966.

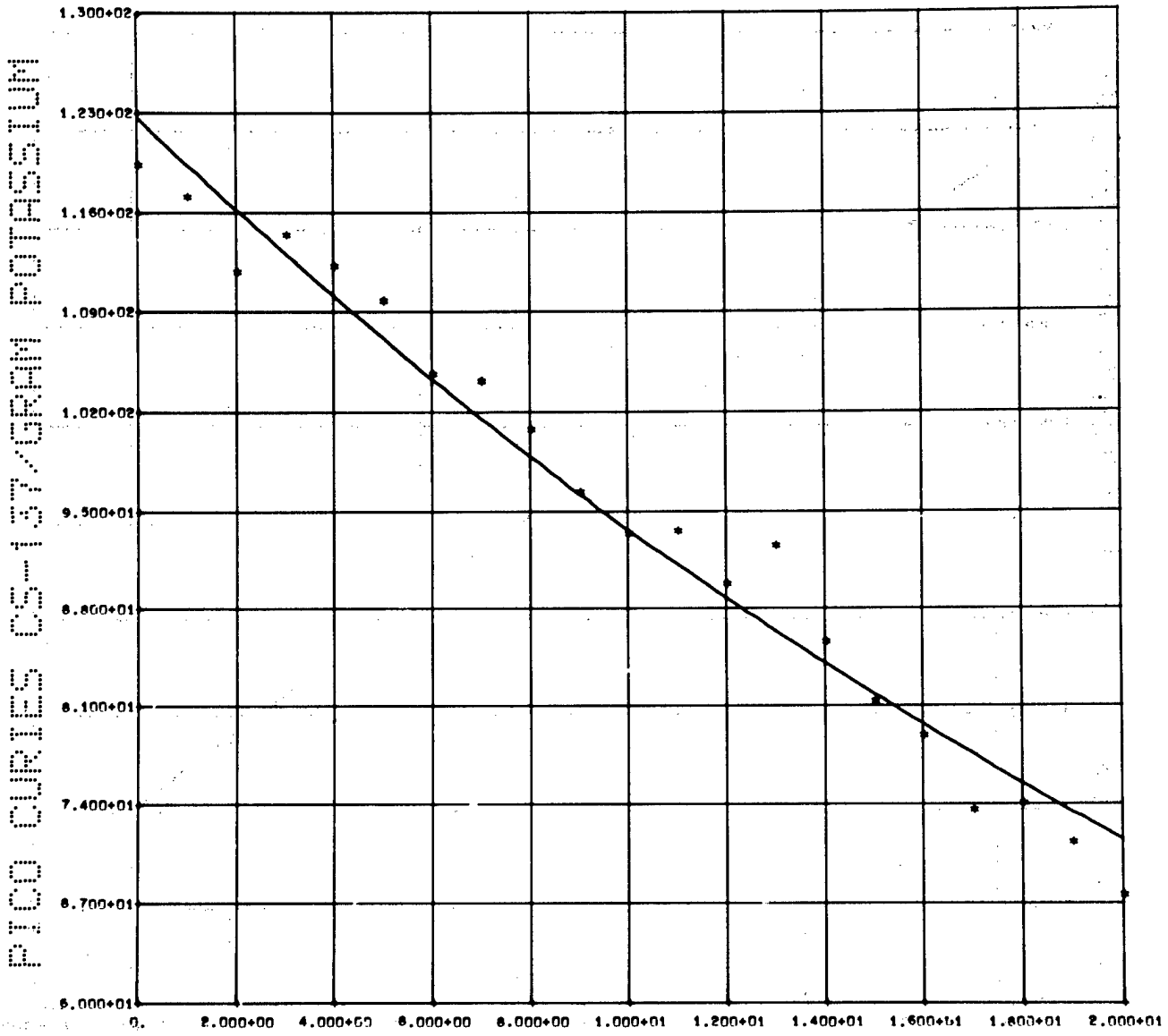

Fig. 2. Exponential plot of cesium-137 body burdens from July 1964 to March 1966.

DISCUSSION

Based on the criterion of smallest weighted variance, Eq. 1 describes the data slightly better than does Eq. 2. Using Eq. 1, the predicted burden for March 1966 of 69.0 pCi/g K agrees well with the observed value of 67.5. However, the linear model predicts a burden of essentially zero in roughly 4 years.

The exponential model predicts a level of 71.5 pCi/g K for March 1966, in good agreement with the observed value of 67.5. After 4 years about 33.6 pCi/g K, or about 25 percent of the July 1964 burden, would remain. Although the level predicted for June 1966 by the exponential model is only slightly higher than the observed value (65.9 versus 60.2), better agreement exists between the value predicted by the linear model and the observed model (59.6 versus 60.2 pCi/g K).

Using the rate constant obtained in Eq. 2 and propagating errors,* a half-time of 25.70 $\pm$ 1.02 months is obtained. The rate constant indicates a change of about 2.7 percent per month in body cesium-137 burden, as contrasted with 15 percent per month observed after a single intake of cesium-137.

It is expected, on the basis of exponential retention of cesium by man, that the linear fit to the observed data is fortuitous and will tend to underestimate future cesium-137 burden.

---

*$T = \ln 2/k$; $\sigma_t = (\ln 2)(\sigma_k)/(k)^2$.

CESIUM-137 CONTENT OF NEW MEXICO CONTROL SUBJECTS: JULY 1965 THROUGH JUNE 1966 (C. R. Richmond, J. E. London, and J. S. Wilson)

INTRODUCTION

This report covers systematic monthly measurements of the secular changes in whole-body cesium-137 burdens for the period July 1965 through June 1966 in a control group of about 30 subjects. The format has been changed to include statistical errors and results of body potassium measurements.

METHODS AND RESULTS

Whole-body activity measurements were made in HUMCO-II, a nearly 4π steradian geometry liquid scintillation counter. Each subject was measured for 200 seconds after donning a disposable paper suit; no showering was required. About 30 people from the monthly control group of 35 subjects were measured each month. The statistical error (standard error of the mean) for body potassium is about $\pm$ 3 g, or several percent of the body potassium content for an average adult male containing about 150 g potassium. Tables 1, 2, 3, and 4 give body cesium-137 and potassium, together with body weights, for monthly control subjects for the third and fourth quarters of 1965 and for the first and second quarters of 1966, respectively. The mean ($\bar{x}$), standard deviation (σ_i), standard error ($\sigma_{\bar{x}}$), and coefficient of variation ($\sigma_i/\bar{x}$) are given for each parameter.

Mean body weights were larger during the first two quarters of 1966 as compared with the last two quarters of 1965. This is related to replacement of 3 children in the sample with adults. The larger body weights are associated with smaller standard deviations as the sample now is comprised entirely of adults.

Cesium concentrations (pCi cesium-137 per g potassium) dropped from an average of 89.6 for the third quarter of 1965 to an average of 63.7 during the second quarter of 1966. These concentrations correspond to cesium-137 body burdens of 10.5 and 7.7 nCi for the third quarter of 1965 and the second quarter of 1966, respectively.

Figure 1 shows change in body cesium-137 for the 4 quarters reported here plus the 4 previous years. Monthly averages and standard errors are given. In general, levels are still decreasing since the July 1964 peak. This holds true for other groups being studied in the United States except for certain Alaskan natives who are expected to have higher burdens in 1966 as compared with 1965 (1).

DISCUSSION

Body burdens of cesium-137 continued to decrease throughout the second half of 1965 and the first half of 1966 in 30 New Mexico control subjects and are expected to continue to decrease provided no weapons are tested in the atmosphere. Isolated Chinese tests since the 1963 moratorium on atmospheric testing did not appear to disturb the trend.

REFERENCE

(1) W. Hanson, Eleventh Annual Health Physics Society Meeting, held in Houston, Texas (June 27-July 1, 1966); to be published in Proceedings.

TABLE 1. BODY CESIUM-137 AND POTASSIUM AND BODY WEIGHT DATA FOR MONTHLY CONTROL SUBJECTS DURING THE THIRD QUARTER OF 1965

	Weight (kg)	Potassium (g/kg)	Cesium-137 (pCi/g K)	Potassium (g)	Cesium-137 (nCi)	Cesium-137 (pCi/kg)
July 1965: n = 30						
Mean	60.87	1.947	89.82	118.23	10.68	174.61
σ_i*	16.01	0.272	23.53	35.28	4.36	51.54
$\sigma_{\bar{x}}$**	2.92	0.050	4.30	6.44	0.80	9.41
$\sigma_i/\bar{x}$	26.30	13.973	26.19	29.84	40.82	29.51
August 1965: n = 31						
Mean	61.57	1.891	92.96	116.02	10.75	174.08
σ_i	14.64	0.262	26.04	31.60	3.82	47.97
$\sigma_{\bar{x}}$	2.63	0.047	4.68	5.68	0.69	8.62
$\sigma_i/\bar{x}$	23.78	13.873	28.02	27.24	35.53	27.56
September 1965: n = 32						
Mean	61.42	1.939	85.68	118.49	10.11	164.17
σ_i	15.73	0.300	26.34	34.73	4.13	50.32
$\sigma_{\bar{x}}$	2.78	0.053	4.66	6.14	0.73	8.89
$\sigma_i/\bar{x}$	25.60	15.448	30.74	29.31	40.91	30.65

*$\sigma_i = \left[\frac{\Sigma (x - \bar{x})^2}{n - 1}\right]^{1/2}$.

**$\sigma_{\bar{x}} = \frac{\sigma_i}{n^{1/2}}$.

TABLE 2. BODY CESIUM-137 AND POTASSIUM AND BODY WEIGHT DATA FOR MONTHLY CONTROL SUBJECTS DURING THE FOURTH QUARTER OF 1965

	Weight (kg)	Potassium (g/kg)	Cesium-137 (pCi/g K)	Potassium (g)	Cesium-137 (nCi)	Cesium-137 (pCi/kg)
October 1965: n = 33						
Mean	61.43	1.970	81.30	120.34	9.88	159.33
σ_i*	15.35	0.292	20.72	34.37	3.80	45.48
$\sigma_{\bar{x}}$*	2.67	0.051	3.61	5.98	0.66	7.92
$\sigma_i/\bar{x}$	24.99	14.825	25.48	28.56	38.47	28.54
November 1965: n = 29						
Mean	64.16	1.933	78.87	124.39	9.73	150.50
σ_i	12.86	0.277	20.89	32.56	3.23	37.30
$\sigma_{\bar{x}}$	2.39	0.051	3.88	6.05	0.60	6.93
$\sigma_i/\bar{x}$	20.04	14.309	26.49	26.18	33.23	24.78
December 1965: n = 30						
Mean	62.31	1.927	73.56	120.45	8.91	141.30
σ_i	14.50	0.254	19.48	33.85	3.35	41.47
$\sigma_{\bar{x}}$	2.65	0.046	3.56	6.18	0.61	7.57
$\sigma_i/\bar{x}$	23.27	13.209	26.48	28.10	37.64	29.35

*See Table 1.

TABLE 3. BODY CESIUM-137 AND POTASSIUM AND BODY WEIGHT DATA FOR MONTHLY CONTROL SUBJECTS DURING THE FIRST QUARTER OF 1966

	Weight (kg)	Potassium (g/kg)	Cesium-137 (pCi/g K)	Potassium (g)	Cesium-137 (nCi)	Cesium-137 (pCi/kg)
January 1966: n = 29						
Mean	66.31	1.930	74.11	128.76	9.33	141.21
σ_i*	9.52	0.283	22.24	29.30	3.04	42.48
$\sigma_{\bar{x}}$*	1.77	0.052	4.13	5.44	0.56	7.89
$\sigma_i/\bar{x}$	14.36	14.642	30.01	22.76	32.55	30.08
February 1966: n = 31						
Mean	64.96	1.939	71.35	126.72	8.89	136.85
σ_i	10.13	0.260	20.06	29.12	2.77	38.37
$\sigma_{\bar{x}}$	1.82	0.047	3.60	5.23	0.50	6.89
$\sigma_i/\bar{x}$	15.59	13.391	28.11	22.98	31.15	28.03
March 1966: n = 30						
Mean	66.04	1.912	67.53	126.99	8.48	128.47
σ_i	9.18	0.265	17.58	27.41	2.63	36.24
$\sigma_{\bar{x}}$	1.68	0.048	3.21	5.00	0.48	6.62
$\sigma_i/\bar{x}$	13.09	13.864	26.04	21.59	30.99	28.21

*See Table 1.

TABLE 4. BODY CESIUM-137 AND POTASSIUM AND BODY WEIGHT DATA FOR MONTHLY CONTROL SUBJECTS DURING THE SECOND QUARTER OF 1966

	Weight (kg)	Potassium (g/kg)	Cesium-137 (pCi/g K)	Potassium (g)	Cesium-137 (nCi)	Cesium-137 (pCi/kg)
April 1966: n = 29						
Mean	65.72	1.874	66.99	123.97	8.18	124.76
σ_i*	9.18	0.277	17.83	27.98	2.61	36.46
$\sigma_{\bar{x}}$*	1.70	0.051	3.31	5.20	0.49	6.77
$\sigma_i/\bar{x}$	13.97	14.765	26.61	22.57	31.92	29.22
May 1966: n = 27						
Mean	65.04	1.864	63.85	121.81	7.64	118.33
σ_i	8.97	0.263	17.36	26.22	2.29	35.07
$\sigma_{\bar{x}}$	1.73	0.051	3.34	5.05	0.44	6.75
$\sigma_i/\bar{x}$	13.79	14.123	27.19	21.53	29.97	29.63
June 1966: n = 28						
Mean	65.58	1.883	60.22	124.36	7.37	112.87
σ_i	9.07	0.269	17.86	28.36	2.50	36.03
$\sigma_{\bar{x}}$	1.71	0.051	3.37	5.36	0.47	6.81
$\sigma_i/\bar{x}$	13.83	14.293	29.66	22.81	33.86	31.95

*See Table 1.

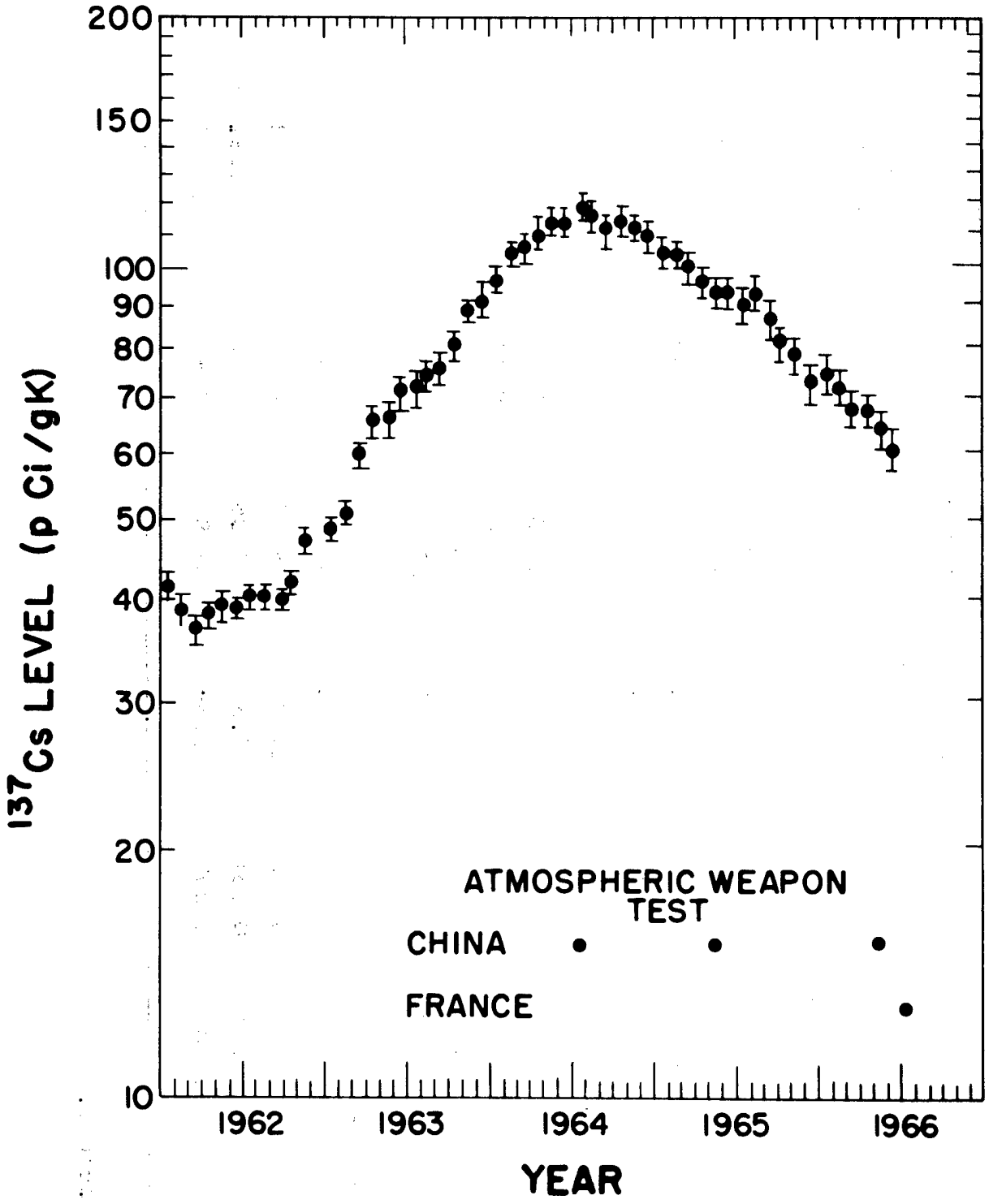

Fig. 1. Cesium-137 body burdens of monthly control subjects.

LOSS OF WHOLE-BODY CESIUM-137 IN HUMANS (J. E. Furchner, J. E. London, G. A. Drake, and C. R. Richmond)

INTRODUCTION

A detailed short-term record of whole-body activity of cesium-137 in humans is of interest for comparison with acute administration data and with data gathered at longer intervals (1). Abrupt changes in whole-body activity may be detected and recorded when assay times are separated by short intervals and thus provide a monitor for intake levels.

METHODS

Measurements have been made for 180 days in HUMCO II. Four 100-second counts were made on the subjects at least 3 times per week. Two males and 1 female were assayed during a 6-month period, and 2 females were assayed for about 100 days. The activities measured in all subjects but one were assumed to be from ingested fallout cesium. In the other, the residual activity from a deliberately acquired burden resulted in a 2 to 4 times greater amount than in the other subjects. The raw counting data were processed by computers programmed to give units of radioactivity and estimates of precision of the assay. The relative standard deviation of the body burdens was about 7.5 percent.

RESULTS AND DISCUSSION

The results are presented in Table 1 and in Fig. 1; the straight lines are least-squares best fits to the data. The upper lines (lines 1 and 2) and data points represent the activity of a standard counted before and after the subjects. The broken line (line 1) is the expected change in activity for an isotope with a 30-year half-life. The solid line (line 2) is a linear least-squares fit to the data. A single exponential fit to the same data gives a half-time of about 15 years. Neither of these slopes is significantly different from zero ($p > 0.01$), which is consistent with the relatively short period of measurement.

TABLE 1. WHOLE-BODY CESIUM-137 IN HUMANS

Subject Number*	Sex	Weight (kg)	Cesium-137 (pCi/g K)	Body Burden (nCi)	Linear Rate Constant	Half-Time (days)**
3	M	73	150-100	25.2	0.0488	305
4	F	71	80-69	11.3	0.0142	460
5	M	72	67-58	10.6	0.0119	505
6	F	50	65-61	6.5	0.0086	530
7	F	53	57-50	5.1	0.0040	780

*The number corresponds with the number in Fig. 1.

**Derived from fit to an exponential function.

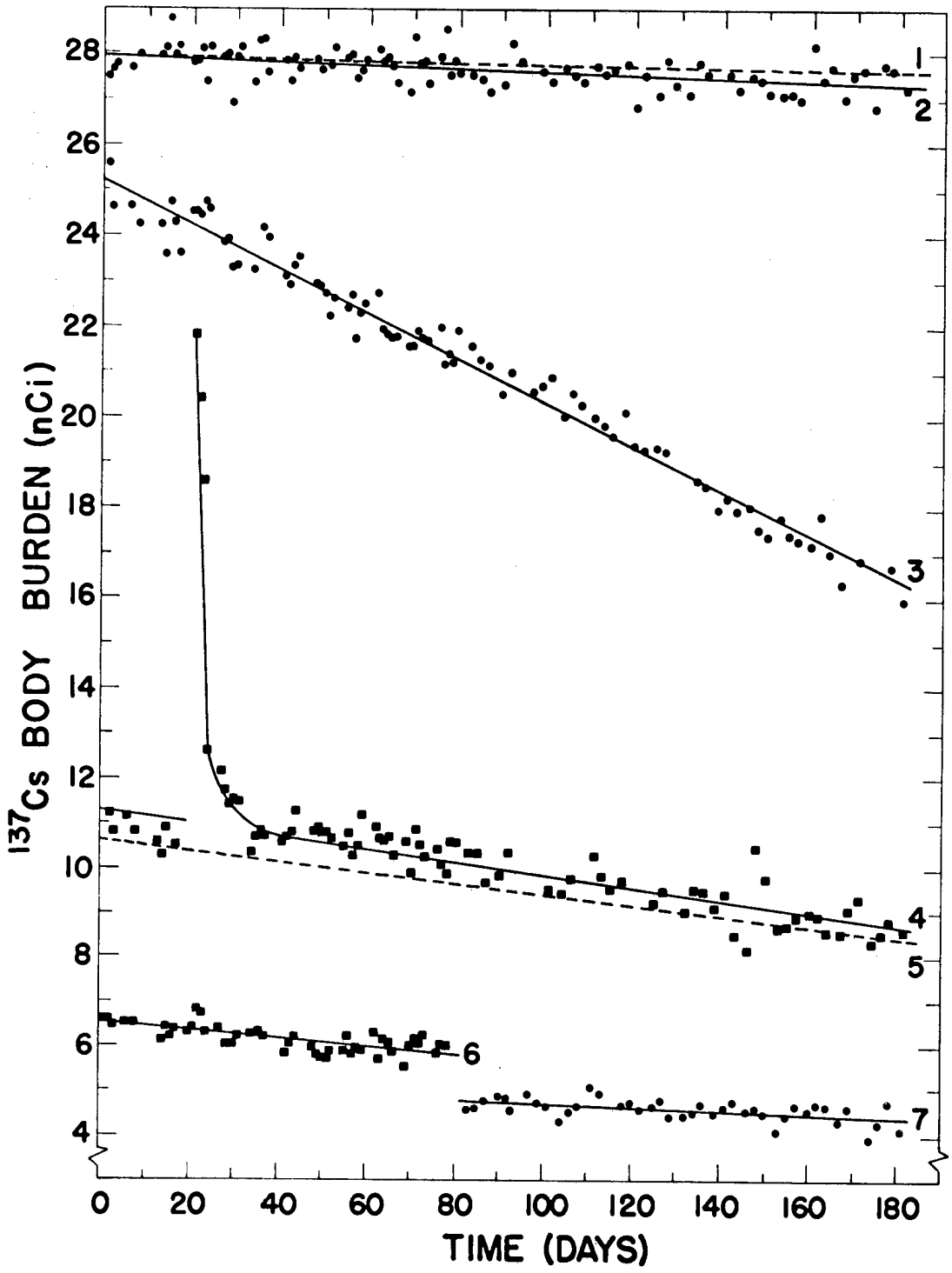

Fig. 1. Linear plot of changes in whole-body burden of cesium-137. Exponential expressions also fit the data.

Line 3 is the linear best fit to data obtained from a subject deliberately exposed to a single low-level dose of cesium-137. The apparent linear rate of loss does not exclude an exponential fit to the data. Lines 4 and 5 are the best fits to data from a female (line 4) externally contaminated with a small amount of niobium-95 at about the 20th day and a male (line 5) with an approximately equal body burden of cesium-137. Data points from the female only are shown. The similarity in excretion rates is clear. Lines 6 and 7 are plots best fitting the data of 2 females. The low total cesium-137 in these subjects is largely due to their size (about 50 kg versus about 70 kg for the other 3 subjects).

The data shown in Fig. 1 can also be described by an exponential expression, and half-times so derived are given in Table 1. The changing whole-body activities are due to ingestion and excretion of cesium-137 and obviously do not represent an equilibrium condition. The half-times in Table 1 are all much greater than the approximate 150-day half-time reported after acute administration to humans. The general decline in activity is due to a decrease in amount ingested, indicating a decreasing food contamination. The reasons for the rate differences among the subjects are not clear but are most likely due to individual variations.

No seasonal variations are apparent in the 6 months (November to May) covered by these data. A somewhat similar decline in whole-body activity, with no seasonal fluctuation, has been found in a larger group counted less frequently (2).

REFERENCES

(1) C. R. Richmond, J. E. London, and J. S. Findlay, Los Alamos Scientific Laboratory Report LA-3432-MS (1965), pp. 36-40.

(2) C. R. Richmond and J. E. London, this report, pp. 166-169.

RETENTION OF CESIUM-137 BY THE WHITE-TAILED RAT (J. E. Furchner, G. A. Drake, and C. R. Richmond)

INTRODUCTION

Metabolic data from experimental animals are used to estimate maximum permissible concentrations of radionuclides in water. Extrapolations are made from data obtained from mice, rats, dogs, and monkeys to man. The addition of the white-tailed rat (Mystromys albicaudatus) to this list is being considered, and various physiological parameters are being measured. At present, no respiratory diseases have been found in the colony. This fact and a reputed 2- to 7-year life span make the white-tailed rat attractive as an experimental animal.

METHODS

Three groups, each consisting of 4 male white-tailed rats 6 months old, were anesthetized and given about 0.5 μCi cesium-137 chloride per rat. Three routes of administration were used: oral, gastric intubation; intravenous, jugular sinus; and intraperitoneal. Little or no differences in absorption and retention of cesium due to route of administration are found in rats or mice, and none were anticipated in these animals. Six male Sprague-Dawley rats 6 months old and weighing about 350 g were injected with 0.5 μCi of the same cesium-137 solution. All animals were assayed periodically for 80 days, by which time whole-body activity had fallen to less than 1 percent of the administered dose. The data were collected by 4π liquid scintillation detectors and were analyzed by electronic computers programmed to fit summed exponential expressions to the data.

RESULTS AND DISCUSSION

Table 1 gives the parameters of the exponential expressions fit to the data. The half-times for the I. P. white-tailed rats seem to be greater than the other 2 groups, but less remains in the long component. The equilibrium factors, which are an estimate of the body burden in terms of daily intake under conditions of chronic exposure to a constant

level of contamination, therefore, are essentially the same for all routes. It is assumed that no difference in retention resulted from the route of administration. The smooth curves in Fig. 1 are plots of the retention functions given in Table 1. At 80 days the differences among the group average values are less than 0.1 percent of the initial dose, and the range of values is less than 0.5 percent.

To test the applicability of these data to the interspecific relation used to make estimates of equilibrium levels for humans, a portion of the best-fit line calculated from cesium-137 retention data in mice, rats, monkeys, dogs, and humans is plotted in Fig. 2 along with data points for Sprague-Dawley rats and RF mice used in determination of the line (1). The white-tailed rat data do not deviate from the relation calculated for the other 5 species. The point for the rat also shows little difference from data collected more than 5 years ago. This indicates a consistency in data collection and analysis and in the validity and stability of the relation between body weight and equilibrium factors.

REFERENCE

(1) C. R. Richmond, J. E. Furchner, and W. H. Langham, Los Alamos Scientific Laboratory Report LAMS-2627 (1961), pp. 175-182.

TABLE 1. EFFECTIVE RETENTION PARAMETERS FOR CESIUM-137 ADMINISTERED TO WHITE-TAILED AND ALBINO (SPRAGUE-DAWLEY) RATS

Route	a_1*	k_1	a_2	k_2	a_3	k_3	Body Weight (g)	EF**
White-Tailed Rats								
Oral	13.34	1.6675 (0.42)***	28.31	0.3667 (1.89)	58.34	0.07248 (9.56)	133	8.90
Intravenous	20.47	1.6626 (0.42)	20.16	0.3103 (2.23)	59.37	0.07781 (8.91)	133	8.40
Intraperitoneal	23.63	0.6625 (1.05)	27.63	0.1606 (4.32)	48.74	0.07006 (9.89)	150	9.44
Sprague-Dawley Rats								
Intraperitoneal	18.31	1.4796 (0.47)	23.63	0.1456 (4.76)	58.06	0.05345 (12.97)	367	12.61

*Percent retention, $R_t = \sum_{i=1}^{n} a_i e^{-k_i t}$, where t is time in days.

**The equilibrium factor, $EF = \int_0^\infty R_t \, dt/100$.

***Figures in parentheses are half-times in days.

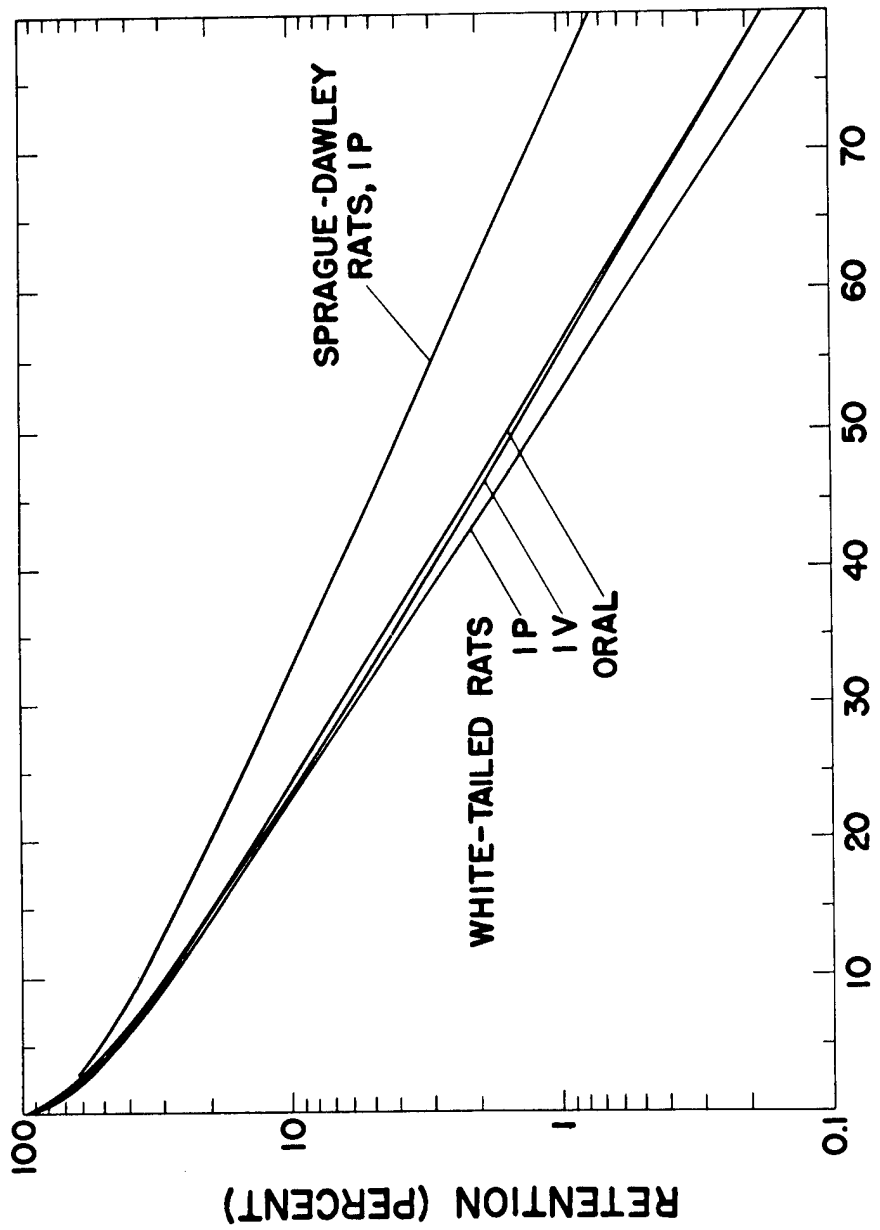

Fig. 1. Effective retention of cesium-137 by white-tailed rats (Mystromys albicaudatus) after oral, intraperitoneal, and intravenous administration.

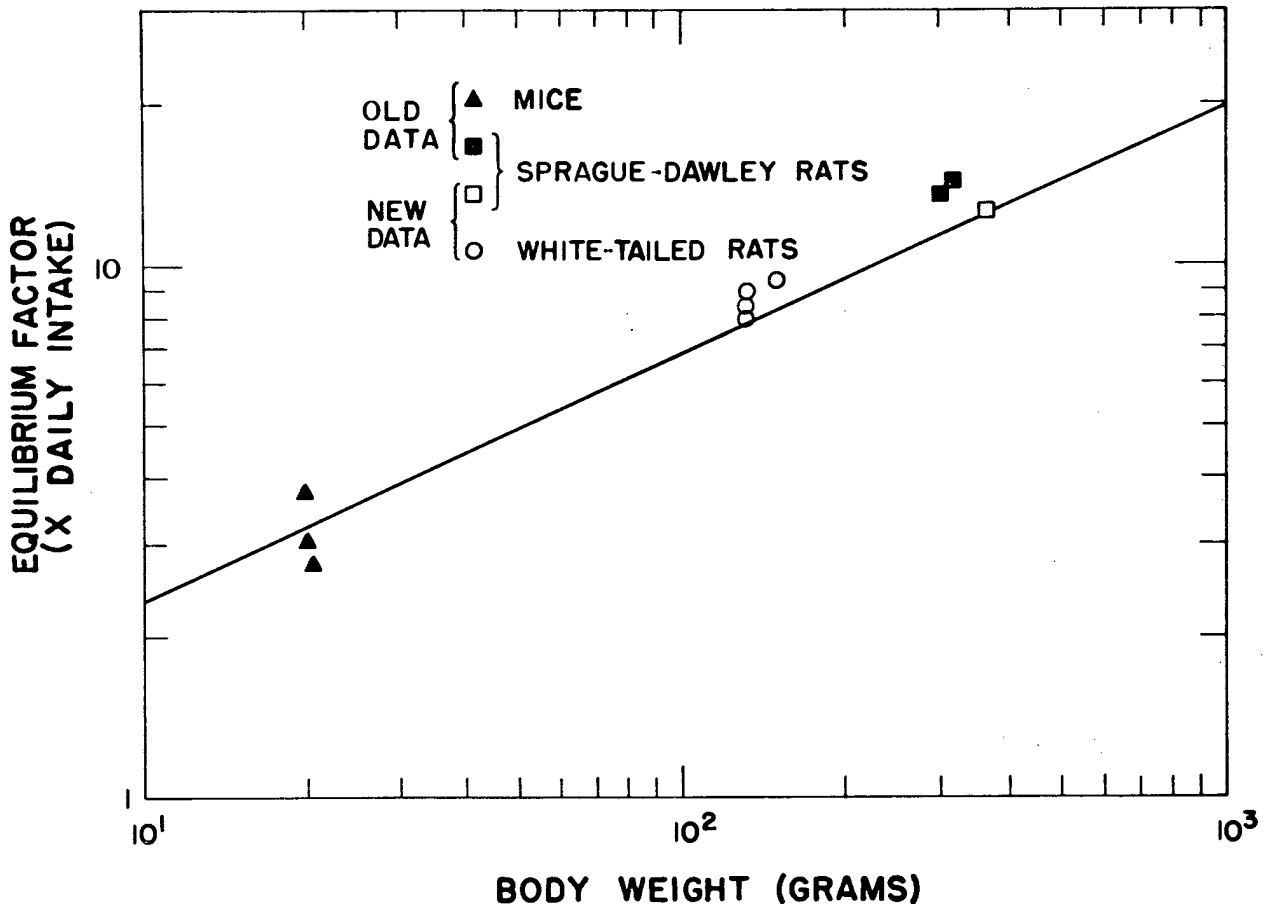

Fig. 2. A portion of the curve showing the relation between body weight and equilibrium factor calculated in 1961 (1). The closed points are the original data; open points are from this report.

RETENTION OF SILVER-110 BY MICE (J. E. Furchner, G. A. Drake, and C. R. Richmond)

INTRODUCTION

The retention of radiosilver in mice was measured as part of the continuing program aimed at establishing a relation between whole-body weights of laboratory mammals and retention parameters for various radionuclides. The whole-body retention of silver-110 in rats has been reported (1).

METHODS

Female RF mice about 8 weeks old and weighing about 22 g were used. Approximately 0.4 μCi silver-110 nitrate was injected into each of 48 mice by either the intravenous, intraperitoneal, or oral route. Twelve mice were injected via the surgically exposed external jugular sinus, and 12 were injected via the tail vein. The oral dose was administered with a stomach tube. All mice except the I. P. group were lightly anesthetized at the time of administration. The body burden of each mouse was assayed within 30 minutes of injection in LASAC III, a 4π liquid scintillation counter. The oral mice were assayed for 4 days. The other groups were assayed periodically for about 70 days. At about 20 days, each of the I. V. and I. P. groups was assayed as a unit by placing the mice in a cardboard container and measuring the activity of the group in HUMCO II, a large 4π liquid scintillation counter. Assay in HUMCO was continued for about 5 months. The data were analyzed electronically by conventional programs.

RESULTS AND DISCUSSION

The results are given in Table 1 and in Figs. 1 and 2. The data were fit to the sum of 4 exponentials in each group except the oral group. The parameters of the retention functions, in terms of percent of injected dose, are given in Table 1. The LASAC III data for the group injected via the tail vein are given in Fig. 1. Each data point represents the count minus background for 1 mouse on the day indicated on the abscissa. The smooth curve is a plot of retention

TABLE 1. EFFECTIVE WHOLE-BODY RETENTION OF SILVER-110 BY MICE AFTER ORAL, INTRAPERITONEAL, AND INTRAVENOUS ADMINISTRATION

	a_1*	k_1	a_2	k_2	a_3	k_3	a_4	k_4	EF**
Oral (A)	99.14	5.5134	0.86	0.4402	--	--	--	--	0.20
I. P. (A)	58.91	3.1637	38.69	0.7231	1.60	0.1501	0.80	0.01056	1.63
I. P. (B)	54.97	3.6559	42.46	0.7559	1.86	0.0894	0.71	0.00810	1.80
Tail (A)	41.81	3.3650	52.22	0.8360	5.00	0.1551	0.97	0.01330	1.80
Tail (B)	36.00	5.6834	58.61	0.8729	4.63	0.1364	0.76	0.00997	1.84
Jugular Sinus (B)	60.18	1.4452	37.96	0.6011	1.35	0.0988	0.51	0.00962	1.71

(A) Data from LASAC only.

(B) Data from LASAC and HUMCO.

*Constants of the retention function, $R_t = \sum_{i=1}^{n} a_i e^{-k_i t}$, where the units of a_i are percent and k_i are 1/day.

**$EF = \int_0^\infty R_t \, dt/100$.

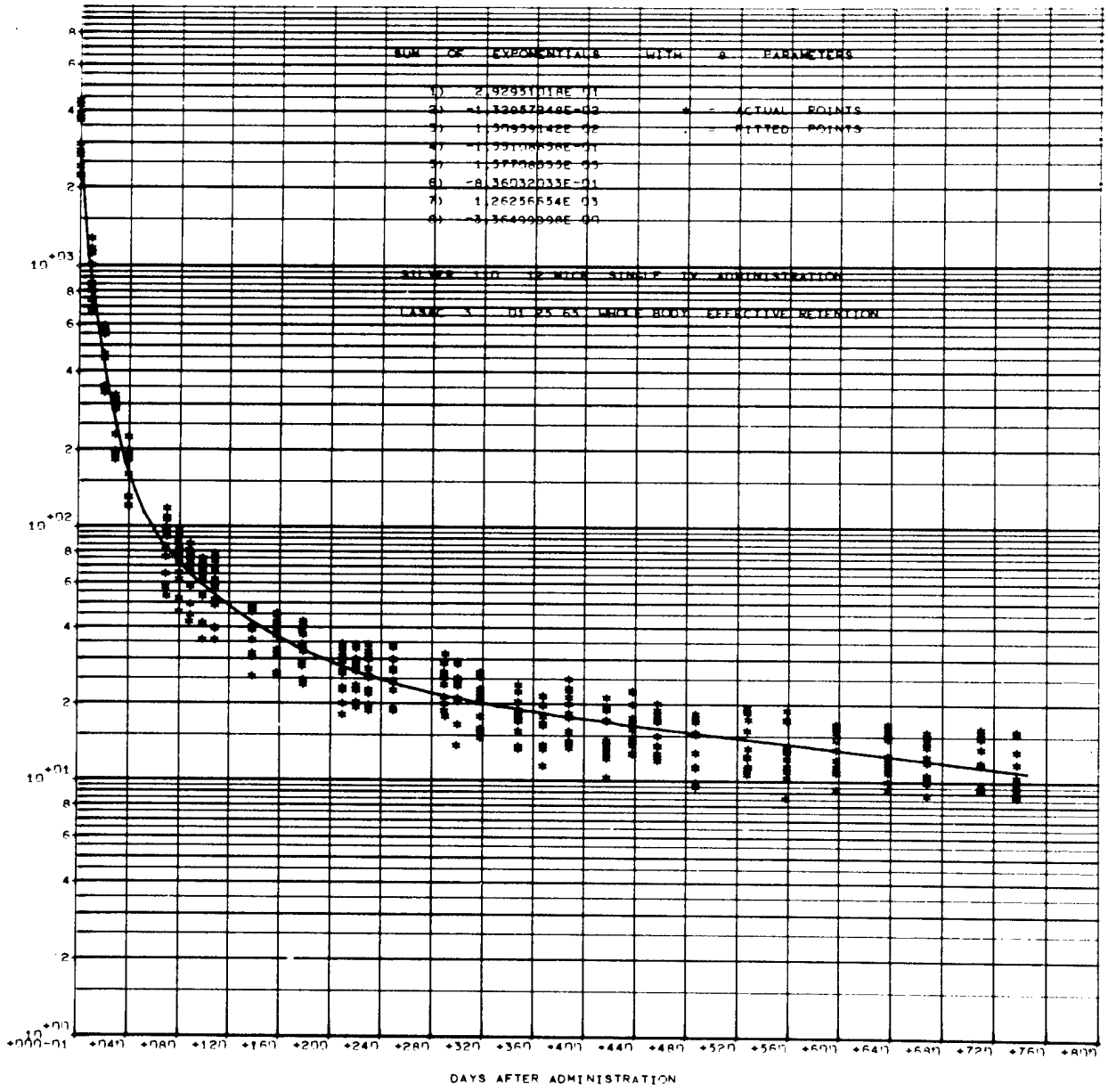

Fig. 1. Whole-body effective retention of silver-110 in mice after injection in the tail vein. The smooth curve is the best fit to all data points given.

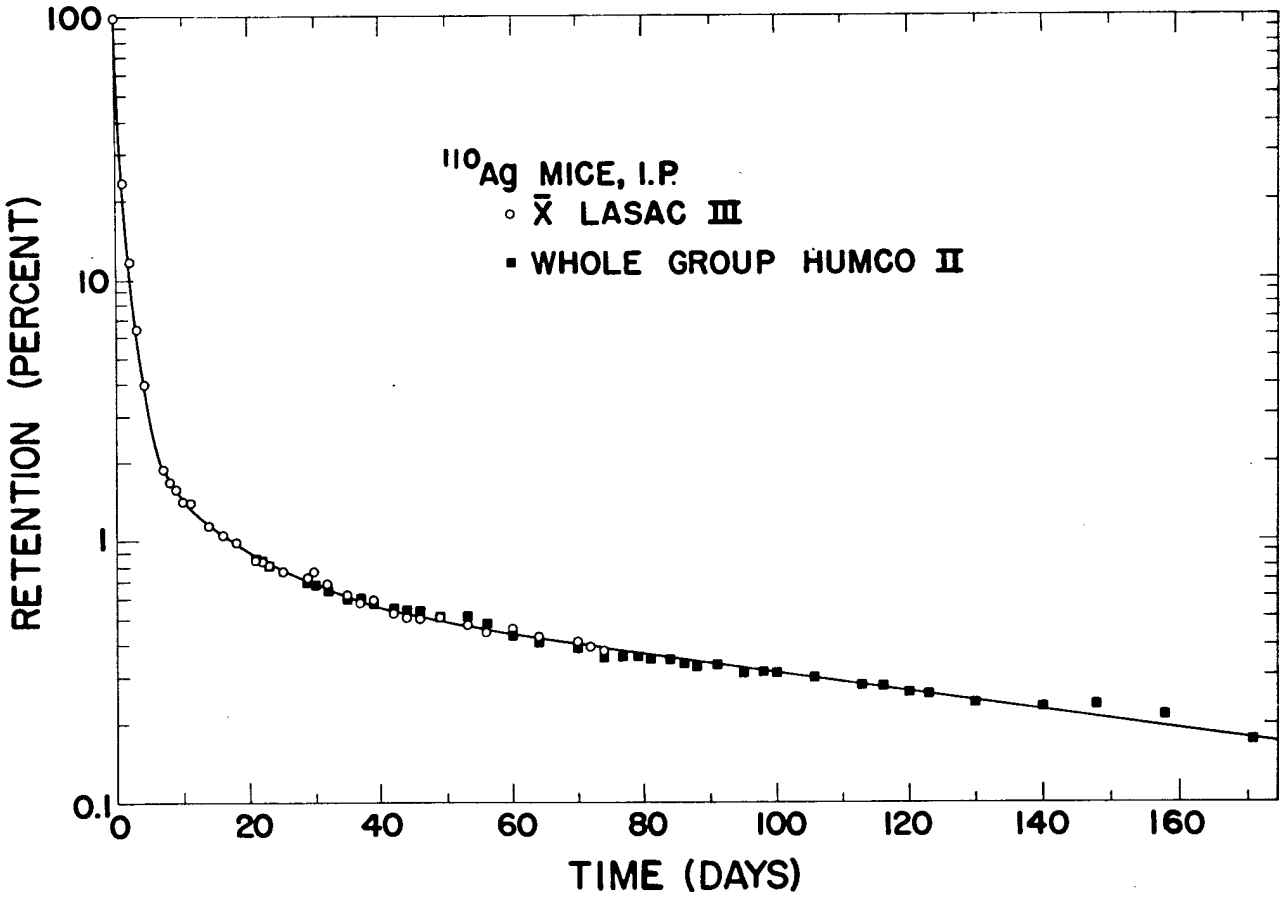

Fig. 2. Whole-body effective retention of silver-110 in mice after intraperitoneal injection. The open circles represent average values of 12 determinations. The closed squares represent the values of 12 mice assayed simultaneously.

function derived by computer. In Fig. 2 the data for the I. P. group, collected in both LASAC III and HUMCO II, are presented as percent of injected dose. The open circles are average values for 12 mice counted separately in LASAC III. The closed squares are derived from the group counted as a unit. The smooth curve is a plot of the best fit retention function given in Table 1 for the I. P. mice.

The data are fit by the sum of 4 exponentials when counted for 70 days in LASAC only and when counted for an additional 100 days in HUMCO, and only small increases in equilibrium factors result from assay in the two systems. When assay of silver-110 retention in rats was extended by similar use of two counting systems, it was possible to add a fourth exponential component to the three that described retention measured in a single system. The mice lost about half the administered dose at a very rapid rate not seen in rats. Mice lost 99 percent of the administered dose in about 18 days, whereas the rats required about 30 days. The amount of silver absorbed, whatever the route of administration, is small, and massive dosages are necessary to attain significant levels.

Almost the entire oral dose was lost with a half-time of about 1/8th day. The little that remained after the first day was lost with a half-time of about 1.5 days. The body burden under conditions of chronic oral ingestion would be only about 1/5th of the daily dose.

REFERENCE

(1) J. E. Furchner, G. A. Drake, and C. R. Richmond, Los Alamos Scientific Laboratory Report LA-3132-MS (1964), pp. 93-99.

EFFECTIVE RETENTION OF SILVER-110 BY DOGS AFTER ORAL ADMINISTRATION (J. E. Furchner, G. A. Drake, and C. R. Richmond)

INTRODUCTION

The parameters describing retention of silver-110 by dogs were determined as a portion of the program for establishing interspecific relations based on weight and integral of retention parameters. Data for rats have been previously reported (1), and similar data for mice are elsewhere in this report (2). Retention data for both mice and rats after oral administration were collected for less than a week as the whole-body activity decreased to less than 1 percent of the administered dose. However, dogs retained more than 1 percent of the daily dose for at least 4 weeks. Counting was continued for about 20 weeks in an attempt to determine if such low counts would give returns commensurate with the effort.

METHODS

The dose was administered to 4 male beagles with an average weight of 13.5 kg (range 12 to 16 kg) and an average age of 5.5 years. Each dog received a sugar cube on which 0.6 μCi of silver-110 as the nitrate had been allowed to dry. The dogs were assayed for activity shortly before and within 30 minutes of administration of the dose. The activity was measured in HUMCO II for 100-second periods until day 8; thereafter each dog was counted for 200 seconds. The data were processed by standard methods.

RESULTS AND DISCUSSION

The parameters of the retention functions derived from the data are given in Table 1. The intercept constants (a_i) have been converted from counts to percent to facilitate comparisons. About 90 percent of the dose was lost very rapidly, indicating an absorption of about 10 percent, a much larger absorption than that found in mice (less than 1 percent) and in rats (about 4 percent).

About 70 percent of the absorbed dose had a half-time of

TABLE 1. RETENTION OF SILVER-110 AFTER ORAL ADMINISTRATION TO DOGS

Dog Number	a_1*	k_1	a_2	k_2	a_3	k_3	EF**
37	84.31	3.789	12.31	0.0807	3.37	0.0183	3.59
39	92.84	6.758	4.33	0.0907	2.83	0.0115	3.07
41	92.90	7.354	5.16	0.1089	1.94	0.0234	1.43
65	90.83	3.309	5.37	0.0828	3.80	0.0286	2.26

*Retention, $R_t = \sum_{i=1}^{n} a_i e^{-k_i t}$.

**Equilibrium factor, $EF = \int_0^{\infty} R_t \, dt/100$.

about 1 month. The data are plotted in Fig. 1 as percent of administered dose, along with an average retention function (smooth curve). Although curves were fit to the data at extended times, the scatter is such that little significance should be attached to the half-time of 30 days. The whole-body retention of dogs injected intravenously with silver-110 will be measured as a function of time. The long components of the excretion curve will be compared with the long component found in this report.

REFERENCES

(1) J. E. Furchner, G. A. Drake, and C. R. Richmond, Los Alamos Scientific Laboratory Report LA-3132-MS (1964), pp. 93-99.

(2) J. E. Furchner, G. A. Drake, and C. R. Richmond, this report, p. 186.

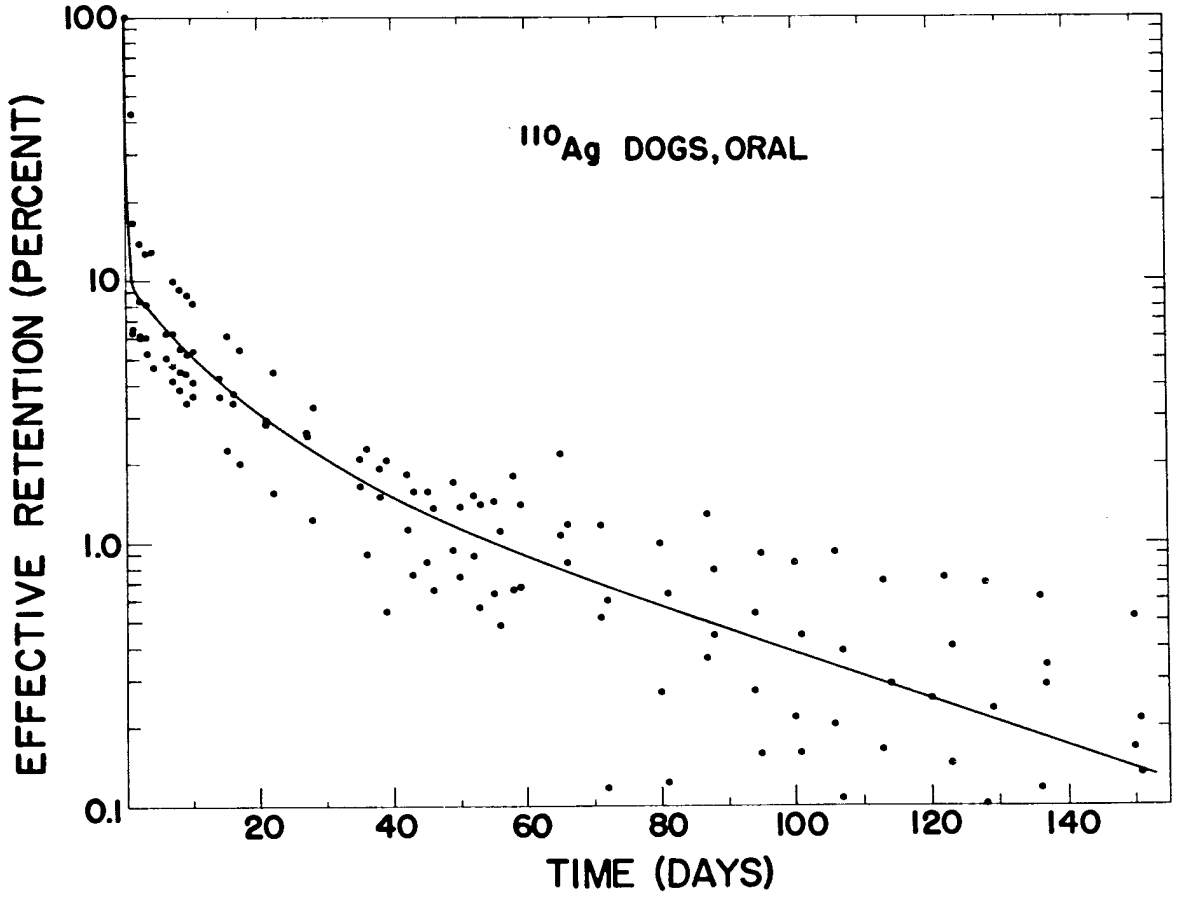

Fig. 1. Retention of silver-110 by dogs after oral administration. Note that the points tend to be smoothly curvilinear above 1 percent and to have a random-appearing scatter at lesser values.

WHOLE-BODY RETENTION OF CADMIUM-109 BY MICE FOLLOWING ORAL, INTRAPERITONEAL, AND INTRAVENOUS ADMINISTRATION (C. R. Richmond, J. S. Findlay, and J. E. London)

INTRODUCTION

The purpose of this work was to establish long-term whole-body retention of cadmium in a mammalian species. Although cadmium is characterized by its virtual absence of metabolic turnover, it does exert influence upon the metabolism of other elements (e.g., zinc). Cadmium-109 is a biospheric contaminant.

METHODS AND RESULTS

Female RF strain mice, about 80 days old, were each given about 0.2 μCi carrier-free cadmium-109 (1.3-year half-life) by either oral (I. G.), intraperitoneal (I. P.), or intravenous (I. V., lateral tail vein) administration. Cadmium-115 (45-day half-life) is normally used as a radioactive tracer for cadmium; this work employed cadmium-109 because of its longer physical half-life of about 1.3 years. A dual-crystal (sodium iodide) detector with 0.005-in. thick aluminum windows was used in conjunction with a multichannel pulse-height analyzer to measure the 22-kev silver X rays which arise from electron capture during cadmium-109 decay. The crystals, each 8 in. in diameter by 4 in. thick, were separated by 2 in. during the counting procedure. Each mouse was placed in a small cardboard box along the axis of the crystals. This system offers an efficient and reproducible counting geometry.

Each animal was measured for several minutes at the times indicated in the figures. Appropriate standards (mock mouse) and backgrounds were also measured. Data were corrected for drifts and changes in the electronics system relative to time zero by the following:

$$(ER)_n = A_n \, (S_i/S_n \, e^{\lambda n}),$$

in which ER is effective retention, A and S are the respective animal and standard count rates, i is the initial

measurement, n is the time of interest, and λ is the physical decay constant. An energy interval of 12.5 kev on either side of the 22-kev photopeak was used in the data analysis.

Figure 1 shows effective retention for 8 mice for about 360 days following oral intubation. The initial burden drops several orders of magnitude over several days as the result of loss through the gastrointestinal tract. Absorption is of the order of 1 percent. Cadmium-109 is retained with only slow turnover following absorption. The early loss is characterized by a half-time of about 0.3 day, whereas subsequent loss is controlled by at least one exponential loss governed by a biological half-life of more than 200 days.

Figure 2 shows effective retention of intraperitoneally-injected cadmium-109 by 6 mice for about 440 days. The solid line represents a tentative fit to the data (for day zero to day 440) using a linear combination of three exponential terms having effective half-times of 0.4, 42.3, and 313.3 days. In general, the ranking of each animal remains the same within the group. The last data points represent a mean biological retention of 59.7 percent.

Figure 3 shows effective retention of intravenously-injected cadmium-109 by 12 mice for about 425 days. The retention pattern is much different than that observed following intraperitoneal injection. The half-lives which compose effective retention are roughly 0.5, 34.1, and 213 days. The largest reservoir contains some 80 percent of the label, as compared with 98 percent for intraperitoneal injection. Average biological retention for the intravenous group on day 423 is 18.55 percent. The difference in retention patterns depending on route of administration is real and has been verified by supplemental experiments.

DISCUSSION

Carrier-free cadmium-109 is not readily absorbed following oral intubation. The fraction going into the blood (f_1) is of the order of 1 to 2 percent. Whole-body retention data measured out to about 400 days indicate multi-exponential loss from three compartments. Effective half-lives for the major retention component will be at least 200 to 300 days, depending on the mode of administration. These values are

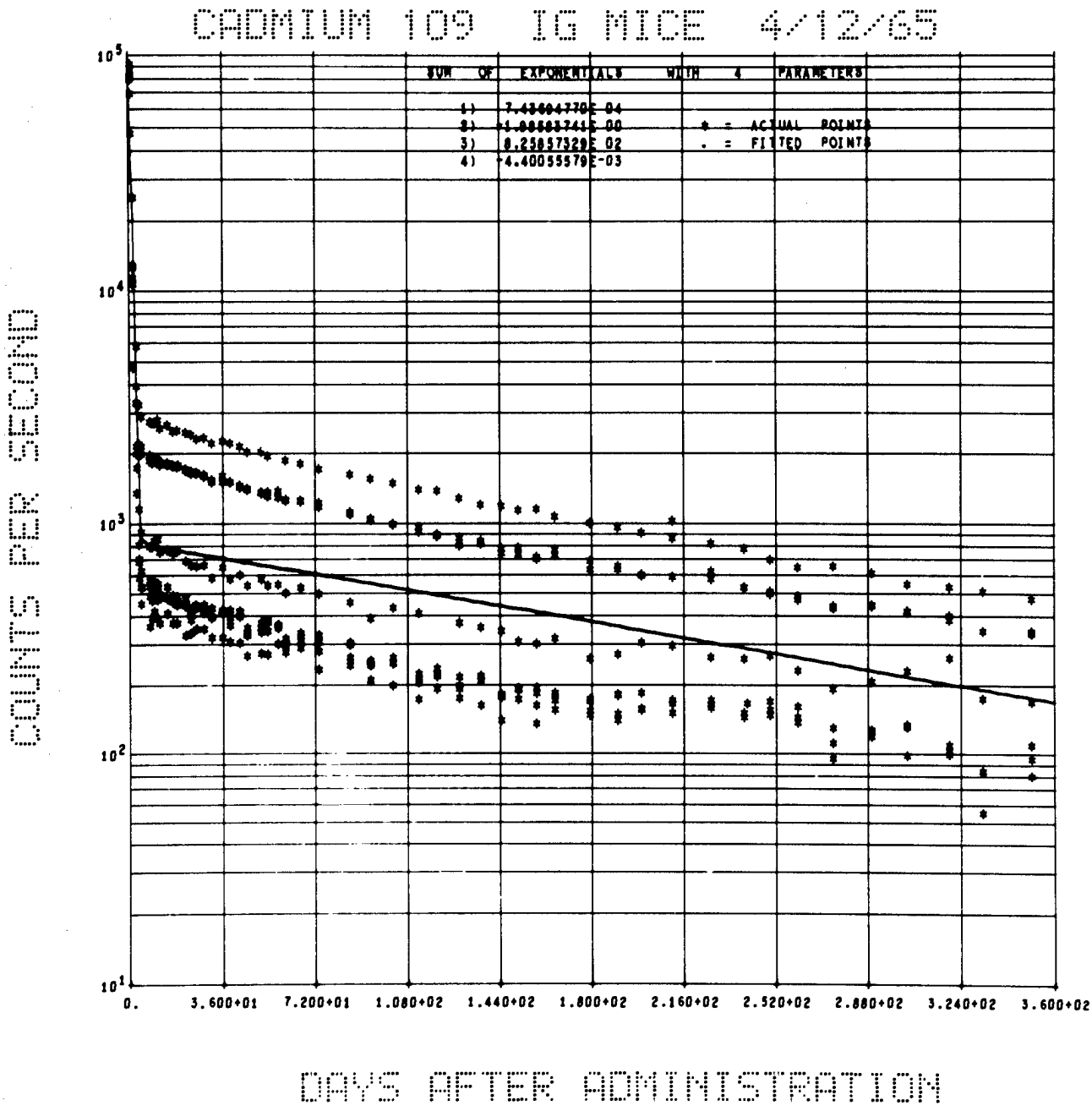

Fig. 1. Effective retention of carrier-free cadmium-109 by mice following oral intubation.

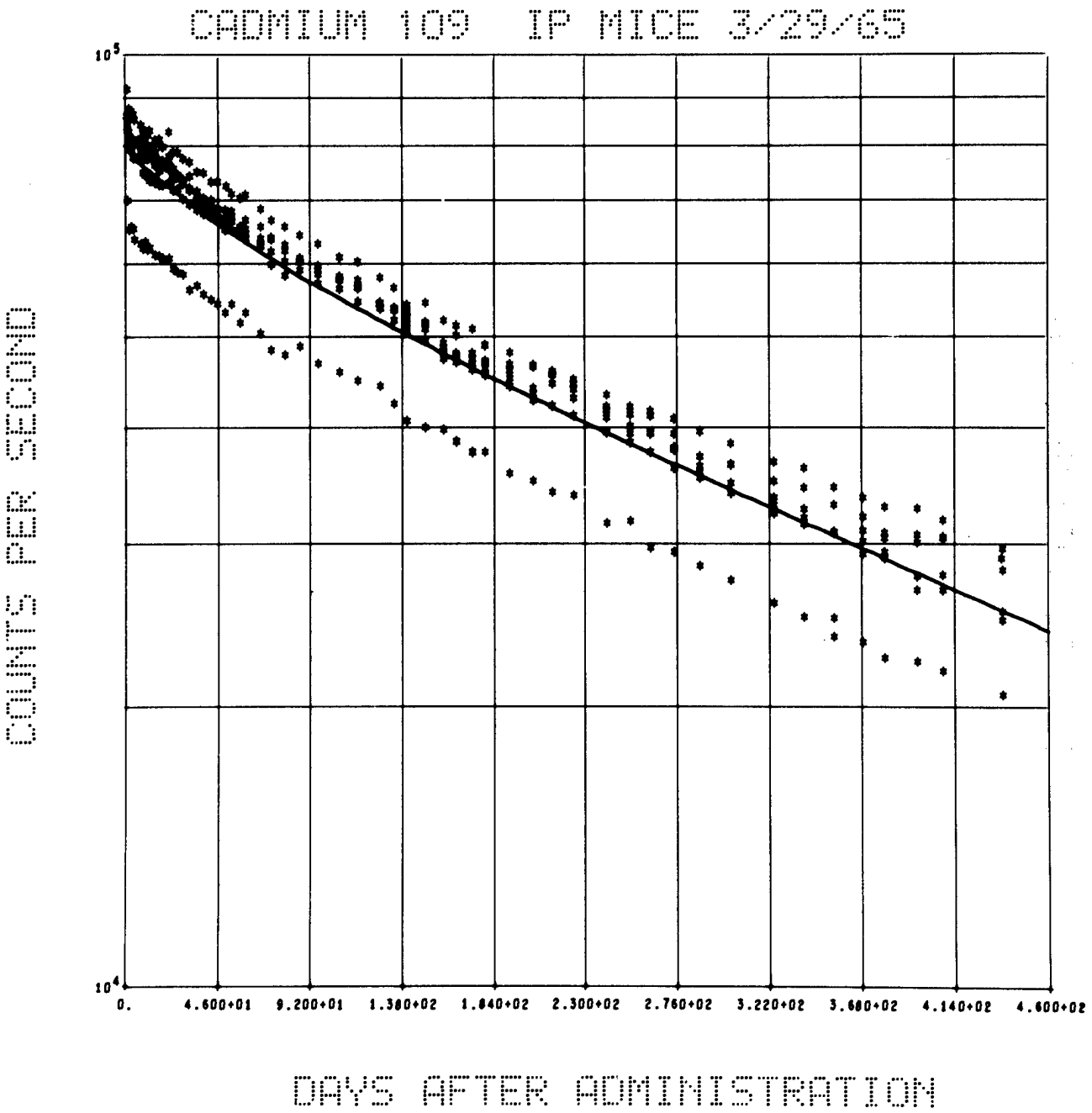

Fig. 2. Effective retention of carrier-free cadmium-109 by mice following intraperitoneal injection.

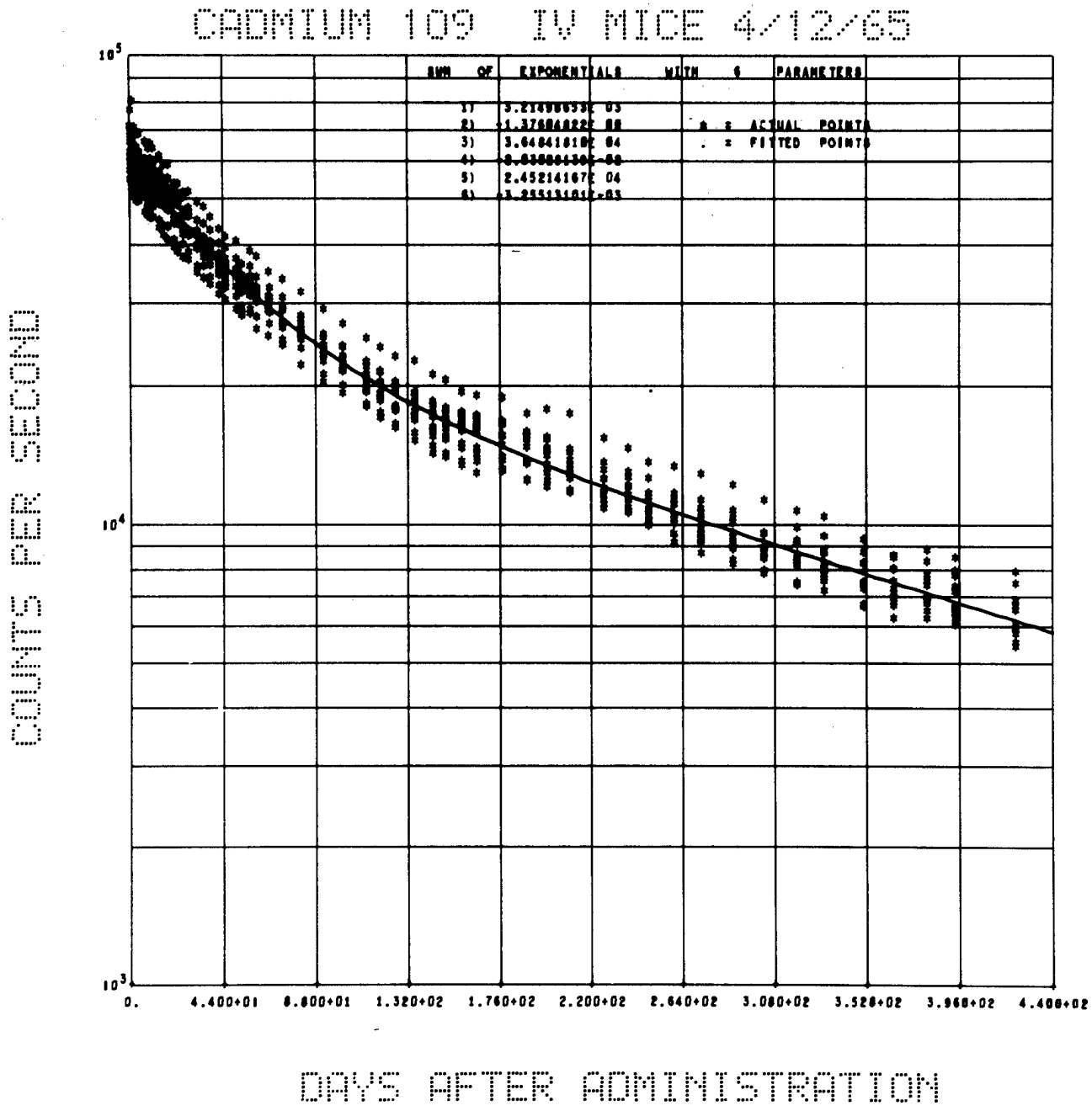

Fig. 3. Effective retention of carrier-free cadmium-109 by mice following intravenous injection.

considerably greater than that of 140 days currently listed by the ICRP (1). Retention might be considerably greater in a larger species. Because of the weak electromagnetic radiations emitted (22 kev), work in larger animals will probably be done by excretion analyses. The real difference in retention patterns depending on mode of parenteral administration is probably due to cadmium being bound to organic materials, notably proteins, in the peritoneal cavity with subsequent slow release into the systemic circulation.

REFERENCE

(1) P. W. Durbin, K. G. Scott, and J. G. Hamilton, University of California Radiation Laboratory Report UCRL-3607 (1956).

WHOLE-BODY RETENTION OF BARIUM-133 BY MONKEYS (C. R. Richmond and J. E. London)

INTRODUCTION

The purpose of this work was to quantitate the long-term retention of barium-133 by a primate species. Previous studies using rodents and dogs have indicated little absorption from the gut, followed by very slow turnover from the body. As is commonly true for materials that are only slowly lost from the body, retention could be described either by a linear sum of exponentials or by a power function. Barium is metabolized in much the same way, at least qualitatively, as is strontium. Retention can be studied for a large portion of the animal's life span because of slow turnover of barium and long physical half-life of barium-133 (i.e., about 8 years).

METHODS AND RESULTS

Each of 4 adult male Macaca speciosa monkeys was given about 420 nCi of high specific activity barium-133 as the chloride by intravenous injection. Sterile nonpyrogenic solution (1.5 ml; pH 5.5) was injected into the saphenous vein while the animal was under phencyclidine hydrochloride* (1 mg/kg; I. M.). Each monkey received about 0.3 μg barium with the tracer injection. Body weight data for each animal are given in Table 1. Commercial monkey food** and water were allowed ad libitum.

All whole-body radioactivity measurements were made in HUMCO II, a 4π steradian detector containing 440 gallons of liquid scintillator solution around a 10.4-cubic foot (6- by 1.5-foot) cylindrical counting chamber. Measurements were made about 30 minutes after tracer injection and at the times calculated to the nearest minute as shown in Fig. 1. Because multiple Compton scattering is involved in energy deposition within the scintillator, a large energy interval of 70 to 800 kev was used. The count rate data in Fig. 1 have been

---

*Serynal (Parke, Davis and Company, Detroit, Michigan).

**Purina (St. Louis, Missouri).

TABLE 1. BODY WEIGHTS AND PERCENT BIOLOGICAL RETENTION OF BARIUM-133 ON DAY 214 FOR MONKEYS GIVEN A SINGLE INTRAVENOUS INJECTION

Animal Number	Initial Weight (kg)	Weight on Day 214 (kg)	Biological Retention on Day 214 (percent)
6	12.5	13.1	21
10	7.4	9.5	34
11	13.0	13.0	25
16	10.3	13.2	43

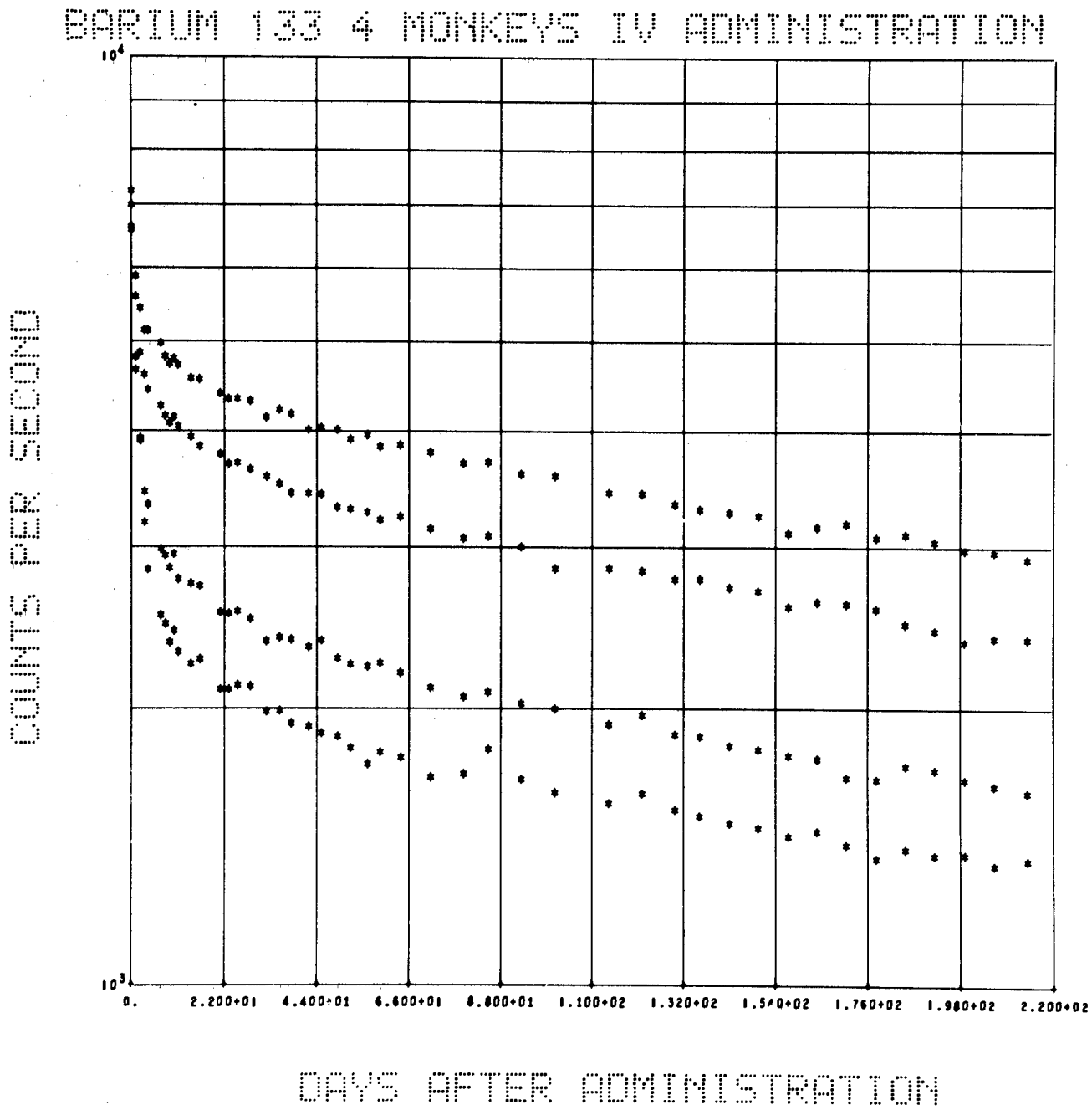

Fig. 1. Whole-body effective retention of high specific activity barium-133 by monkeys following intravenous injection.

corrected for background and pre-experimental gamma-ray activity over the energy interval of interest. No attempts have been made to fit the data because of the changing nature of the retention function.

Retention drops rapidly for several days after injection, probably as the result of early clearance from the blood. The rate of change in whole-body retention decreases with time, and it is difficult to establish if retention becomes monotonic during the 220-day period. A factor of 2 variation exists among the injected activities remaining in the animals on day 214. Table 1 gives body weights and percent biological retention for each animal on day 214.

Qualitatively, the retention data are similar to those obtained in the dog following oral administration of barium-133 for the absorbed portion of the administered dose (Fig. 2). Measurements will be made weekly throughout the year so that long-term whole-body retention can be quantitated in a primate species and compared with strontium retention.

DISCUSSION

Whole-body retention of high specific activity barium-133 by 4 monkeys for 214 days following a single intravenous injection is presented. Retention changes with time and does not appear to be monotonic over the 214 days. About half the dose is cleared by the body in the first week; retention varies from 21 to 43 percent on day 214.

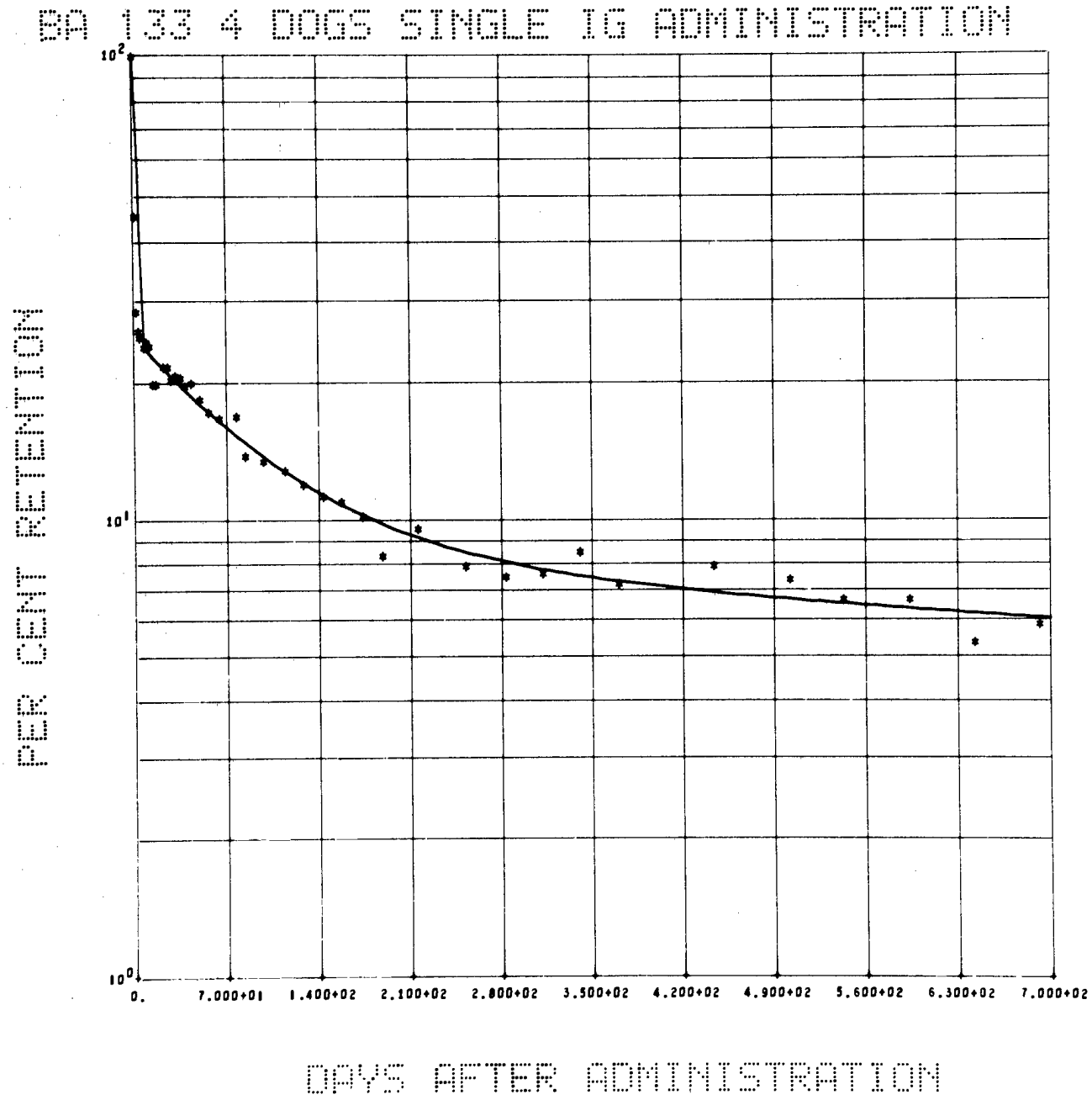

Fig. 2. Whole-body retention of high specific activity barium-133 by beagles following oral administration.

EVALUATION OF DETECTOR VARIANCE (J. E. Furchner, G. A. Drake, and P. C. McWilliams*)

INTRODUCTION

One of the assumptions implicit in computer programs used in this Laboratory for determining retention parameters is that the counting variations follow a Poisson distribution and that no further variations be considered in assigning weights to the counts. When the assumption is valid, the count rates are weighted by the inverse of the variance of the count rate:

$$\text{Variance} = \frac{R_s}{t_s} + \frac{R_b}{t_b} ,$$

where R_s is the count rate of the sample plus background, R_b is the count rate of the background, t_s is the measurement time for the sample, and t_b is the measurement time for the background. The weighted variance of the data set has a chi-squared distribution with an expected value of 1 $[E(\chi)^2 = 1]$. Because many data sets yielded values for this statistic between 10 and 100, an attempt was made to devise a more suitable system of assigning weighting factors.

METHODS AND RESULTS

A group of 18 cesium-137 samples, ranging between 80 and 8000 counts/sec was assayed daily in LASAC III, a 4π liquid scintillation gamma-ray detector. Each sample count was of 100 seconds duration, and a total of 20 assays for each sample was collected during a period of 4 weeks. A similar group of 15 samples ranging between 3 and 1000 counts/sec was assayed in a twin-crystal gamma-ray spectrometer. In this case, the counts were of 1 minute duration. An analysis of variance was made on count rates of each sample, and

---

*Group T-1 of the Theoretical Division, Los Alamos Scientific Laboratory.

Fig. 1 shows a plot of the variance as a function of the logarithm of the count rate.

Two sets of data for retention of cesium-137 in rats, which had been fit to 3 exponentials by the computer using the inverse of the variances, were re-analyzed using the above. The parameters resulting from the two weighting systems are compared in Table 1.

DISCUSSION

The weighted variances resulting from the new weights appear to be more satisfactory than those resulting from the presently used system. The equilibrium factors, which afford an estimate of body burden when exposed to a constant daily dose, were not affected by the weighting. The largest changes in rate constants (k_1 and k_2 for rat No. 3) resulting from the changed weights occurred in those constants with the larger relative standard deviations; the better fitting portion of the curve was less susceptible to changes imposed by changed weights.

These results suggest a careful evaluation of the variance of the detection system. It appears that 20 consecutive counts of a standard made without removing it from the detector have a variance in keeping with a Poisson distribution; however, when the same sample is counted daily for 1 month, larger displacements about a mean occur. The means and variances of two samples counted 20 times on 20 different days were 86.24 (21.89) and 490.64 (47.37). When the same samples were counted 20 times on the same day, the means and variances were 86.52 (2.36) and 488.25 (5.36). Day-to-day variations occur in spite of daily calibration. Because retention is measured over periods extending to years, these variations may necessitate adjustment of weights. Further evaluations of counter variances will be made.

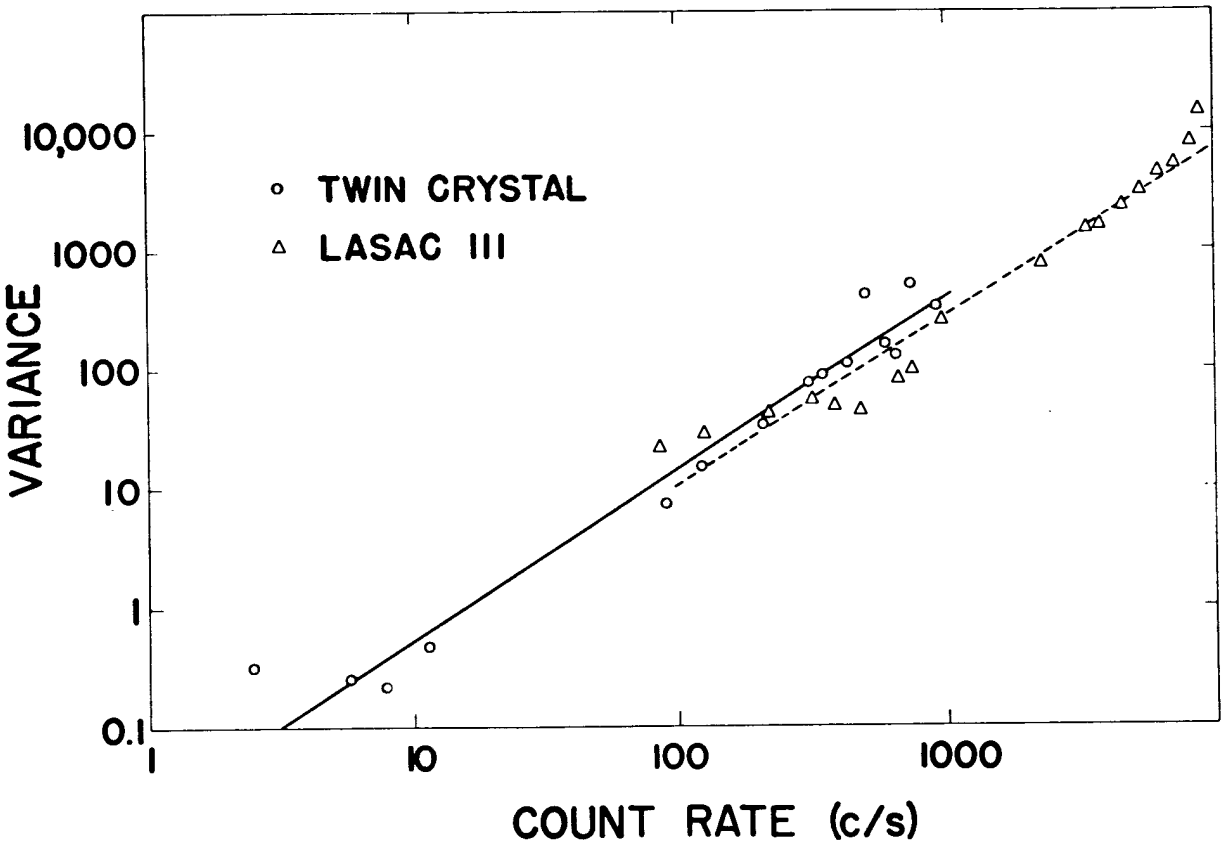

Fig. 1. Variance as a function of count rate. The straight lines are eye-fit to the data.

TABLE 1. EFFECTS OF WEIGHTING SYSTEMS ON RETENTION PARAMETERS

Parameter	Poisson Weights	Empirical Weights
Rat No. 3		
a_1*	630 (0.325)**	1024 (0.208)
a_2	967 (0.174)	719 (0.231)
a_3	4154 (0.015)	4002 (0.028)
k_1	2.35 (0.636)	1.19 (0.321)
k_2	0.366 (0.238)	0.205 (0.340)
k_3	0.0604 (0.010)	0.0593 (0.013)
EF+	12.5	12.5
WV‡	26.4	0.94
Rat No. 5		
a_1	936 (0.037)	933 (0.045)
a_2	1267 (0.479)	1188 (0.428)
a_3	1775 (0.356)	1858 (0.288)
k_1	0.822 (0.062)	0.824 (0.075)
k_2	0.0894 (0.174)	0.0914 (0.168)
k_3	0.0535 (0.078)	0.0540 (0.064)
EF	12.2	12.2
WV	3.71	0.18

*a_1 and k_1 are parameters of the retention function, $R_t = \sum_{i=1}^{n} a_i e^{-k_i t}$.

**Figures in parentheses are the relative standard deviation, $\frac{\sigma_x}{\bar{x}}$.

+Equilibrium factor, EF = $\int_0^\infty R_t \, dt$.

‡Weighted variance, WV = $\Sigma (y - \hat{y})^2 w$, where y is the observed rate, $\hat{y}$ is the calculated rate, and w is the weighting factor.

MAMMALIAN METABOLISM SECTION

PUBLICATIONS AND ABSTRACTS OF MANUSCRIPTS SUBMITTED

ENHANCEMENT OF CESIUM-137 EXCRETION BY RATS MAINTAINED CHRONICALLY ON FERRIC FERROCYANIDE, C. R. Richmond and D. E. Bunde. Proc. Soc. Exp. Biol. Med. 121, 644-670 (1966).

Effects of ferric ferrocyanide (Prussian blue, PB) on retention and excretion patterns of cesium-137 given intravenously to rats were investigated. Concentrations of 0, 0.025, 0.25, and 2.5 g/l. were given continuously via drinking water for 60 days. All measurements of radioactivity were made in a 4π steradian geometry liquid scintillation counter, and the data were fitted to a retention model based on a linear combination of three exponential terms. Concentrations of 0.25 and 2.5 g/l. were effective in reducing the body burdens of cesium-137 relative to control animals. The beneficial decrease in body burden resulted from both reduced fractional deposition in and increased biological turnover from the major retention component. Cesium secreted into the gut is bound by PB and is prevented from reentering the body for recirculation and deposition. Interrupting the enteral cycle reduced the urinary-to-fecal excretion ratio by a factor of 20. A kinetic approach for assessing total integrated effect of drug treatment in tracer experiments is presented. The integrated effect of PB treatment at the 2.5 g/l. concentration represented a reduction of about 60 percent in the total area under the retention curve compared with that of controls. The effective half-life for the largest retention component was 14.1 days for the control group and 8.8 days for the 2.5 g/l.-treated group.

HALF-LIFE OF IODINE-125, C. R. Richmond and J. S. Findlay. Health Phys. 12, 865 (1966).

The physical half-life (T_r) was measured for two iodine-125 sources measured over a 143-day period. The detecting system

was comprised of two 8-in. diameter by 4-in. thick sodium iodide (Tl) crystals housed in a 7-in. thick steel shield. Each crystal face was covered with 0.005-in. thick aluminum. A multichannel pulse-height analyzer was used to measure the activity in an energy interval of 36 kev around the 27-kev X-ray peak. Each source was about 140 nCi iodine-125. The data were fit in the normal plane by an iterative least squares technique programmed for an IBM 7094 computer. No logarithmic transformations of the dependent variable were made.

Sample 1 yielded a T_r of 58.72 + 0.10 days (mean + σ) with a weighted variance of 1.2, and the corresponding T_r value for sample 2 was 58.80 + 0.08 days with a weighted variance of 1.18. Measured values were compared with values obtained from other sources.

COMPARATIVE METABOLISM OF RADIONUCLIDES IN MAMMALS. III. RETENTION OF MANGANESE-54 BY FOUR MAMMALIAN SPECIES, J. E. Furchner, C. R. Richmond, and G. A. Drake. Health Phys. (in press).

Abstracted in Los Alamos Scientific Laboratory Report LA-3432-MS (1965), p. 55.

LONG-TERM IN VIVO RETENTION OF CERIUM-144 BY BEAGLES, C. R. Richmond and J. E. London. Nature (in press).

Cerium-144, a high yield (about 5 percent) product of nuclear fission, is readily detected in nuclear debris and in foods and animal bones. It has been detected also in pulmonary lymph nodes and lungs of man. This report summarizes whole-body retention data for a single injection of 28 μCi cerium-144 (as $CeCl_3$) in equilibrium with praseodymium-144. Measurements were made over a period of 1050 days in each of 4 adult male beagles. A large-volume liquid scintillation counter (HUMCO-II) was the detector system.

A sum of two exponentials was required to fit the time-course of retention. The major retention component corresponded to a biological half-life of roughly 10 years. For cases involving internal deposition of cerium-144 in humans, it would be conservative to assume that physical decay alone would account for changes in the cerium-144 body burden.

CESIUM-137 BODY BURDENS IN MAN: 1956-1966, C. R. Richmond. Radiation Res. (submitted).

This report is a recapitulation of cesium-137 body burdens measured in a control group of about 30 subjects at the Los Alamos Scientific Laboratory for the years 1956-1966. An estimate of total body radiation dose resulting from the decade of exposure to cesium-137 is about 8.4 mrems, roughly 5 percent of that resulting from potassium-40 radiation in the body for the same period. For periods of maximum cesium-137 burdens, the cesium-to-potassium dose ratio was about 0.10. Observed data are compared with cesium-137 burdens reported from other laboratories.

MOVEMENT OF DISCRETE PARTICLES IN THE 100- TO 200-MICRON DIAMETER RANGE THROUGH THE GASTROINTESTINAL TRACT OF LABORATORY ANIMALS AND MAN, C. R. Richmond and J. E. Furchner. To be presented at the Symposium on Gastrointestinal Radiation Injury, to be held at the Battelle-Northwest Laboratories, Richland, Washington (September 25-28, 1966); to be published in the Proceedings.

The possibility of atmospheric reentry and burnup of nuclear rocket propulsion reactors and auxiliary power supplies and attendant biological problems prompted this investigation. Consideration of radiation dose from an insoluble discrete radioactive particle temporarily residing in the lumen of the gut requires a knowledge of the time-course of retention by specific segments of the gastrointestinal tract. Unfortunately, lack of agreement on the average time required for any material to pass through the gastrointestinal tract is augmented by the great variability in dietary and defecation habits among people. This specific problem is complicated by the densities of the particles (10 to 19) involved. For example, entrapment between villi or failure to move against gravity (e.g., up the ascending colon or out of the gastric fundus) have been suggested as mechanisms which might cause prolonged transit times for small high-density particles.

Gamma-ray spectrometry was used to identify electromagnetic radiations from ceramic spheres containing manganese-54 and from uranium carbide fuel cores. The uranium carbide particles were about 170 microns in diameter with a density of

10.8; the ceramic spheres were about 150 microns in diameter with a density of 3.0. Information obtained from 156 individual particles given subjects yielded an average gross transit time of 34.5 hours (range 14 to 72). No effect of density on transit time was observed. On the average, particles were passed in the second stool sample. Time of ingestion was found to affect transit time in all individuals.

Chronic feeding of labeled particles to experimental animals showed a relatively rapid movement through the stomach and small intestine, followed by a hold-up in the cecum and temporary storage in the large intestine. For the dog, particles remained in the cecum and large intestine for 50 to 70 percent of the total transit time.

This work suggests that small high-density uranium carbide fuel cores (nonfissioned) are not preferentially retained by the gastrointestinal tract.

CHAPTER 6

BIOPHYSICS SECTION

IN VIVO MEASUREMENT OF PLUTONIUM-239 LUNG BURDENS IN HUMANS
(P. N. Dean and J. H. Larkins)

INTRODUCTION

The effort to develop a facility for measuring lung burdens of plutonium-239 (1) is continuing. A prototype detector has demonstrated a capability of detecting small amounts ($\sim$5 to 10 nCi) of plutonium. To increase geometrical efficiency, a new counter was designed and is being constructed.

METHODS

Construction of the prototype counter has been described (1). The new counter arrangement consists of 2 identical counters (each 6 in. wide, 12 in. long, and 5 in. thick) suspended in such a manner that one counter can be positioned over each lobe of the lung. Internal construction is the same as for the prototype except that the anticoincidence (AC) and main sections are separated by a 0.015-in. thick sheet of stainless steel. This change was made to prevent charge leakage between the two sections of the counter. The entrance window is a 1/16-in. thick sheet of polyethylene coated on the inner surface with a 70-micron thick layer of aluminum.

RESULTS AND DISCUSSION

The performance of the prototype detector was first measured using a gas filling of 90 percent argon and 10 percent methane. Figure 1 shows the background of the detector with and without AC in operation. The count rate in the

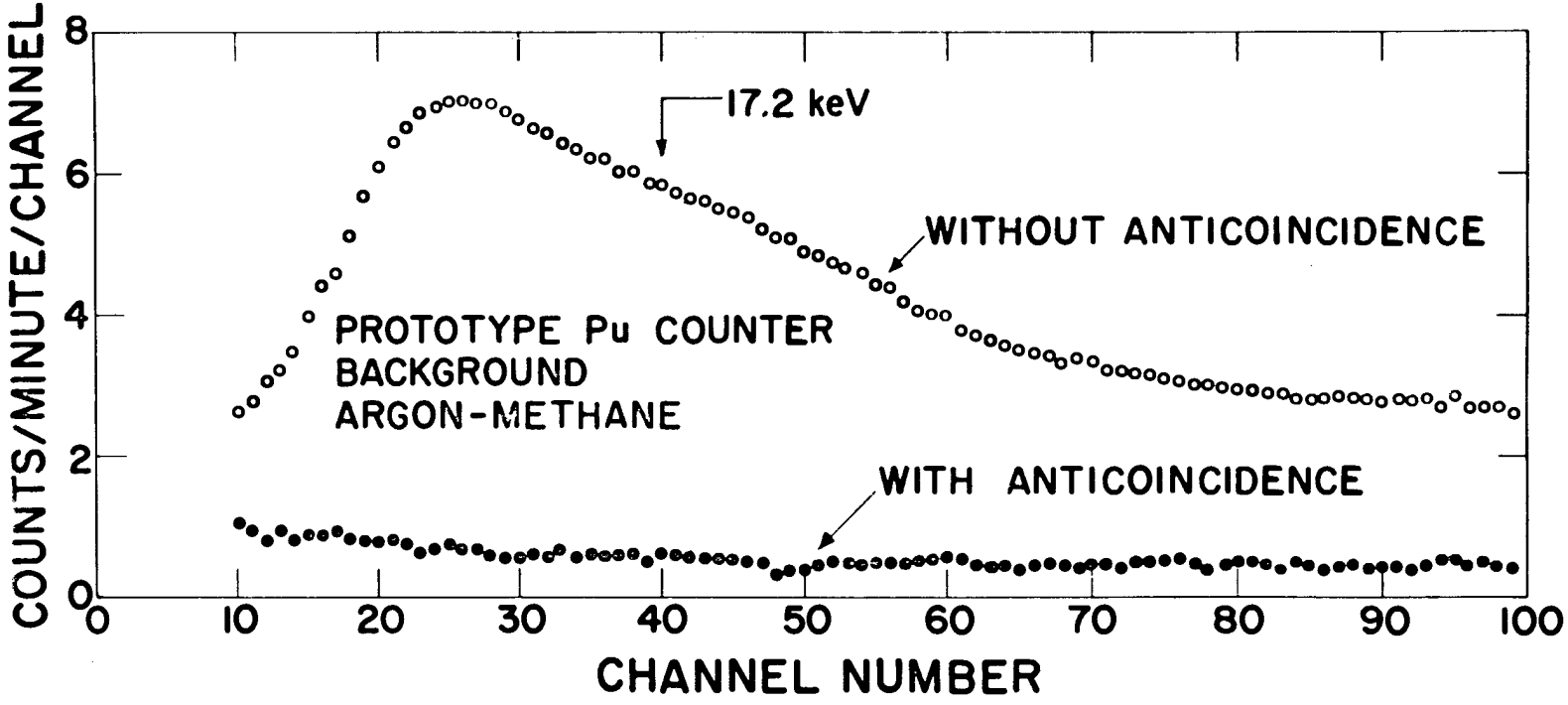

Fig. 1. Background of prototype counter filled with 90 percent argon and 10 percent methane gas mixture, with and without AC.

energy band of 11.5 to 23 kev is 17 cpm with AC and 150 cpm without it (an 89 percent reduction with AC). Figure 2 is the spectrum obtained using a thin source of plutonium-239. The calculated absorption efficiency is 20 percent for the 17.2-kev X ray and 40 percent for the 13.6-kev X ray. Resolution of the 17.2-kev X ray is 13.5 percent.

To improve the efficiency of the counter, it was next filled with a mixture of 90 percent xenon and 10 percent methane. Calculated efficiencies for the 13.6- to 17.2- and 20.5-kev X rays were 95, 85, and 65 percent, respectively. Experimentally, counting efficiency for a plutonium-239 source with no absorber has increased by a factor of 4.5 over the argon-methane filling. Figure 3 shows the background with and without AC shielding for the xenon-methane mixture. The background in the 11.5- to 23-kev band is 236 cpm without AC. With AC it is 130 cpm, a reduction of only 55 percent. This relatively high background is attributed to poor AC shielding at low pulse-height, due primarily to charge leakage between the two sections of the counter. Figure 4 is the spectrum of plutonium-239 with no absorber. Resolution of the 17.2-kev line is 16 percent. The minimum detectable amount (MDA) is estimated to be 6 nCi with a 60-minute counting time. This number is arrived at by measuring the counting efficiency of a point source 10 cm from the counter window with a 2.5-cm thick plastic absorber and using the equation,

$$MDA = \frac{3}{s}\left(\frac{b}{t}\right)^{1/2},$$

where s is the efficiency in cpm/μc, b is background counting rate, and t is counting time.

Several laboratory personnel who have shown high urine concentrations of plutonium were counted with the xenon-methane gas mixture. Figure 5 is the net spectrum of one of them. The background used was the spectrum of an uncontaminated individual of similar stature. There is no evidence of any plutonium X rays within the limit of detection of the counter, which has been the case with all of the workers counted.

An extensive calibration of the prototype counter was not attempted. Upon completion of construction of the new pair

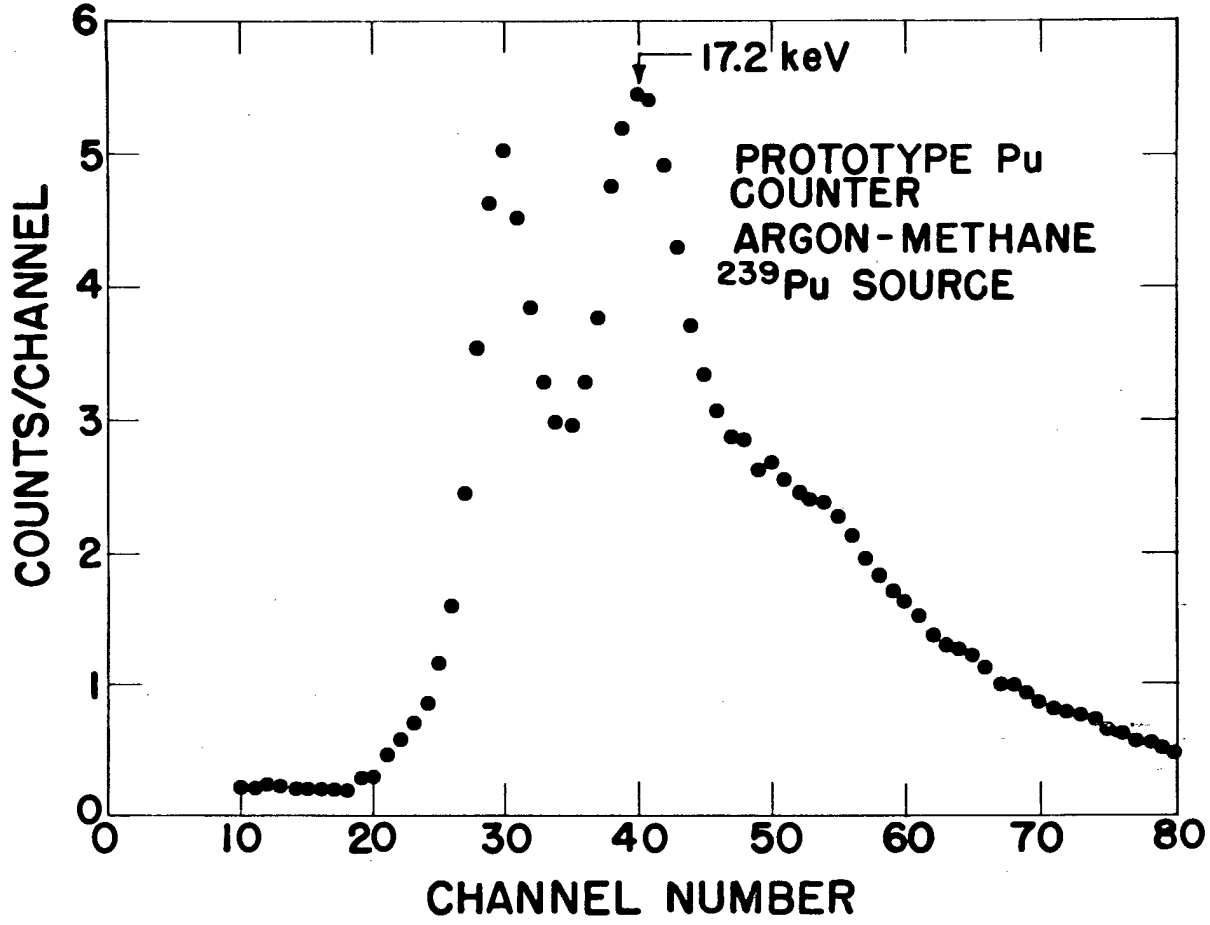

Fig. 2. X-ray spectrum of thin layer of plutonium-239 as measured with argon-methane gas mixture in prototype counter.

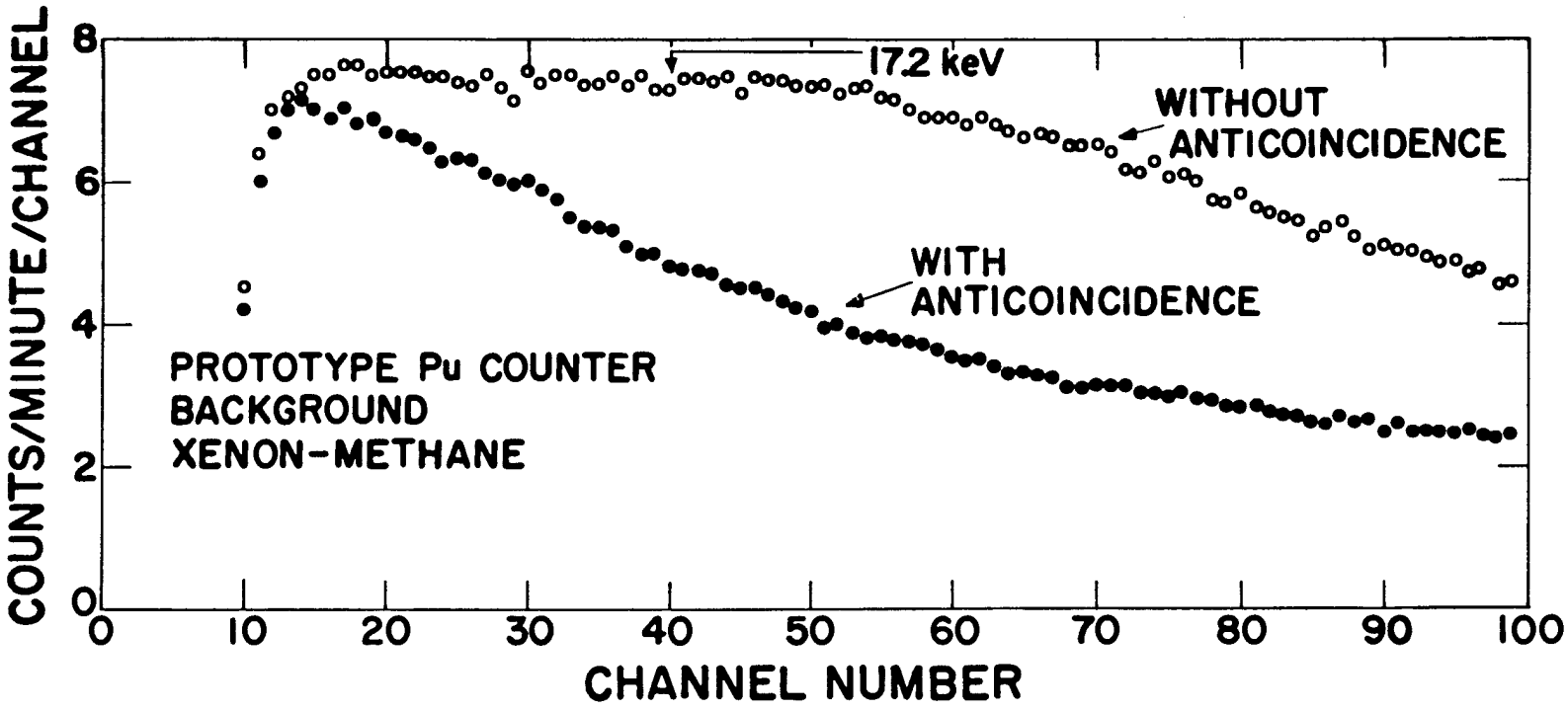

Fig. 3. Background of prototype counter filled with 90 percent xenon and 10 percent methane gas mixture, with and without AC.

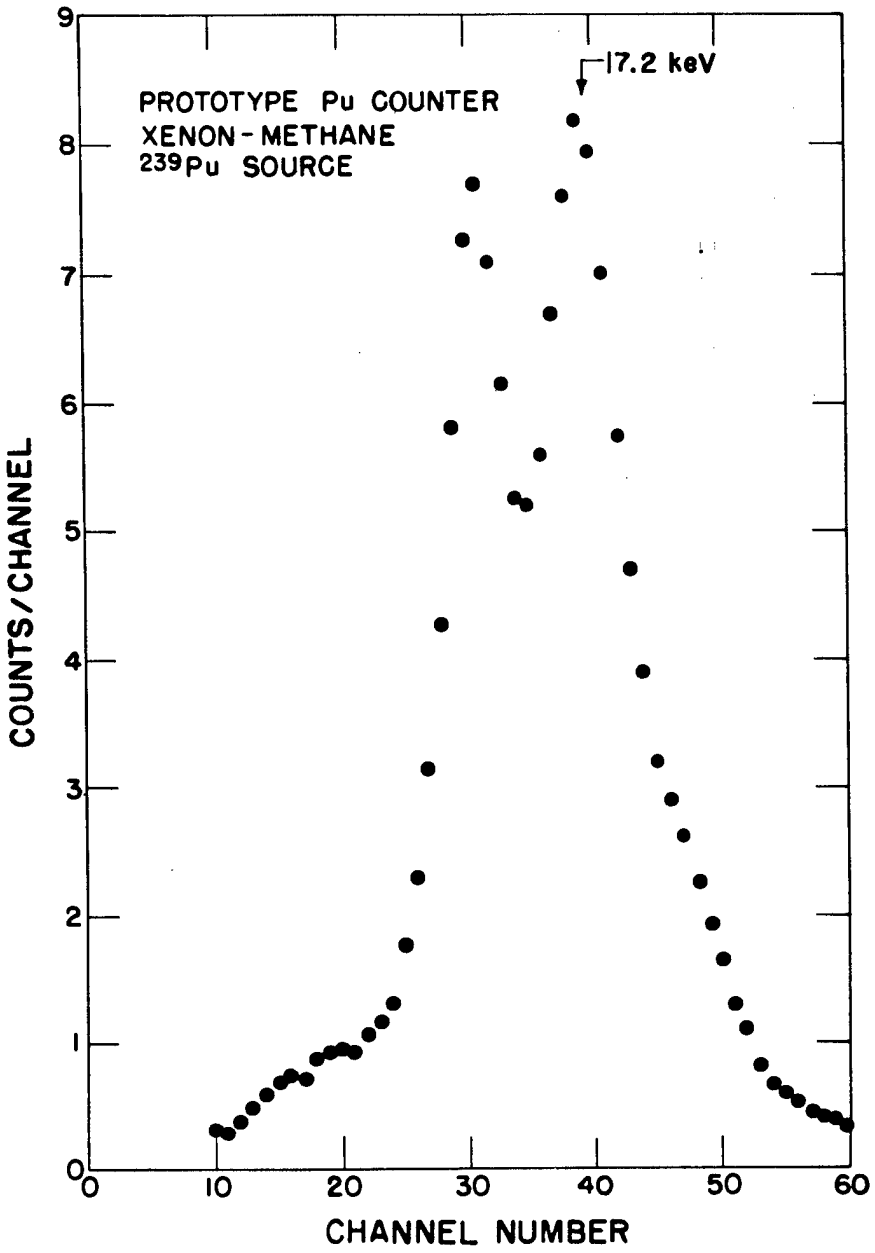

Fig. 4. X-ray spectrum of point source of plutonium-239 as measured with xenon-methane gas mixture in prototype counter.

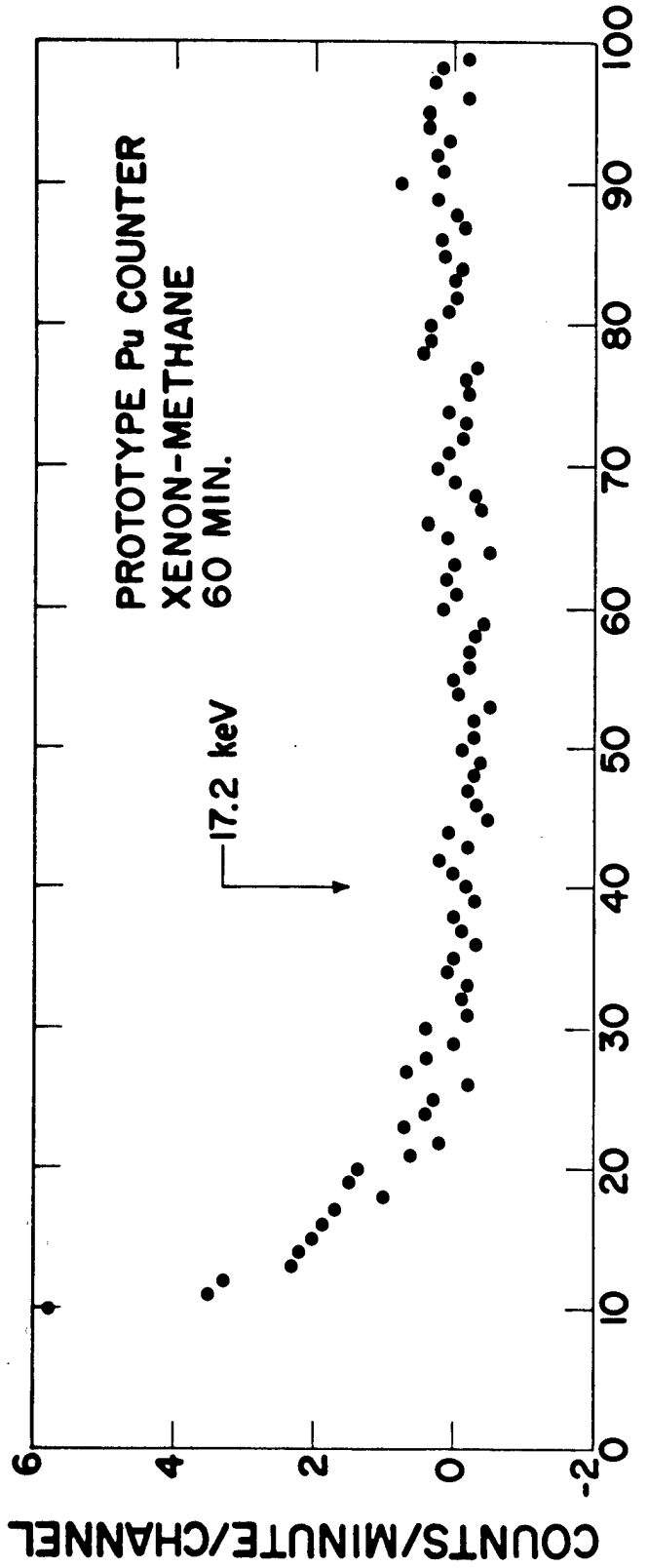

Fig. 5. Spectrum of human subject as measured with the prototype proportional counter with xenon-methane gas mixture.

of counters, a calibration program will be started. Chest phantoms of the same size and shape as a typical human chest and having similar absorption characteristics for low-energy photons could be used. Plutonium sources of different geometries could be inserted into various locations in the chest. Mixtures of isotopes with both X and gamma rays and having short biological half times could be inhaled by volunteer subjects. The amount of each isotope would be determined by counting the gamma rays with conventional whole-body counting techniques. The X rays could then be used to calibrate the proportional counter. These two methods seem to be the most promising and will be used at this Laboratory.

REFERENCE

(1) P. N. Dean and J. H. Larkins, Los Alamos Scientific Laboratory Report LA-3432-MS (1965), p. 119.

FURTHER DEVELOPMENT OF THE CELL SEPARATOR (M. J. Fulwyler)

INTRODUCTION

Refinement of the cell separator, the operation of which has been described earlier (1,2), is expected to result in an instrument suitable for routine application to a variety of biological and nonbiological problems. Preliminary application has been made to separation of human leucocytes (3), mouse bone marrow cells (4), and several other cell types.

RESULTS AND DISCUSSION

As shown in Fig. 1, recent improvements in the device permit simultaneous separation of 4 discrete volume fractions of a distribution. The dotted line indicates the volume distribution of polystyrene spheres (diameter 7 to 14 microns) prior to separation. The remaining 4 curves represent the distribution of each of the 4 separated fractions. The separator has been used to isolate volume fractions of normal human leucocytes (5) and leucocytes from some abnormal states (6).

The entire separator mechanism may be sterilized by autoclaving. The pressure reservoir may be heated or cooled as needed to maintain the cell suspension at a desired temperature. These improvements will permit experiments in which it is desired to recover and to culture sterile, separated volume-fractions of living cells.

Improved electronics incorporating an anticoincidence circuit have been designed and built and are being tested. The anticoincidence circuit will sense the time between passage of particles through the Coulter aperture. This circuit will prevent separation, should two particles pass through the aperture so close in time that they might be collected in the same group of deflected droplets. This and other improvements are expected to increase the analysis rate of the separator from 10^5 to perhaps 2 to 4 x 10^5 particles/min, which will greatly enhance the usefulness of the device for certain biological experiments.

Described elsewhere in this report (7) are efforts to develop a sensor of cell optical properties. Such a sensor may have great value in electronically resolving cells of differing morphological character.

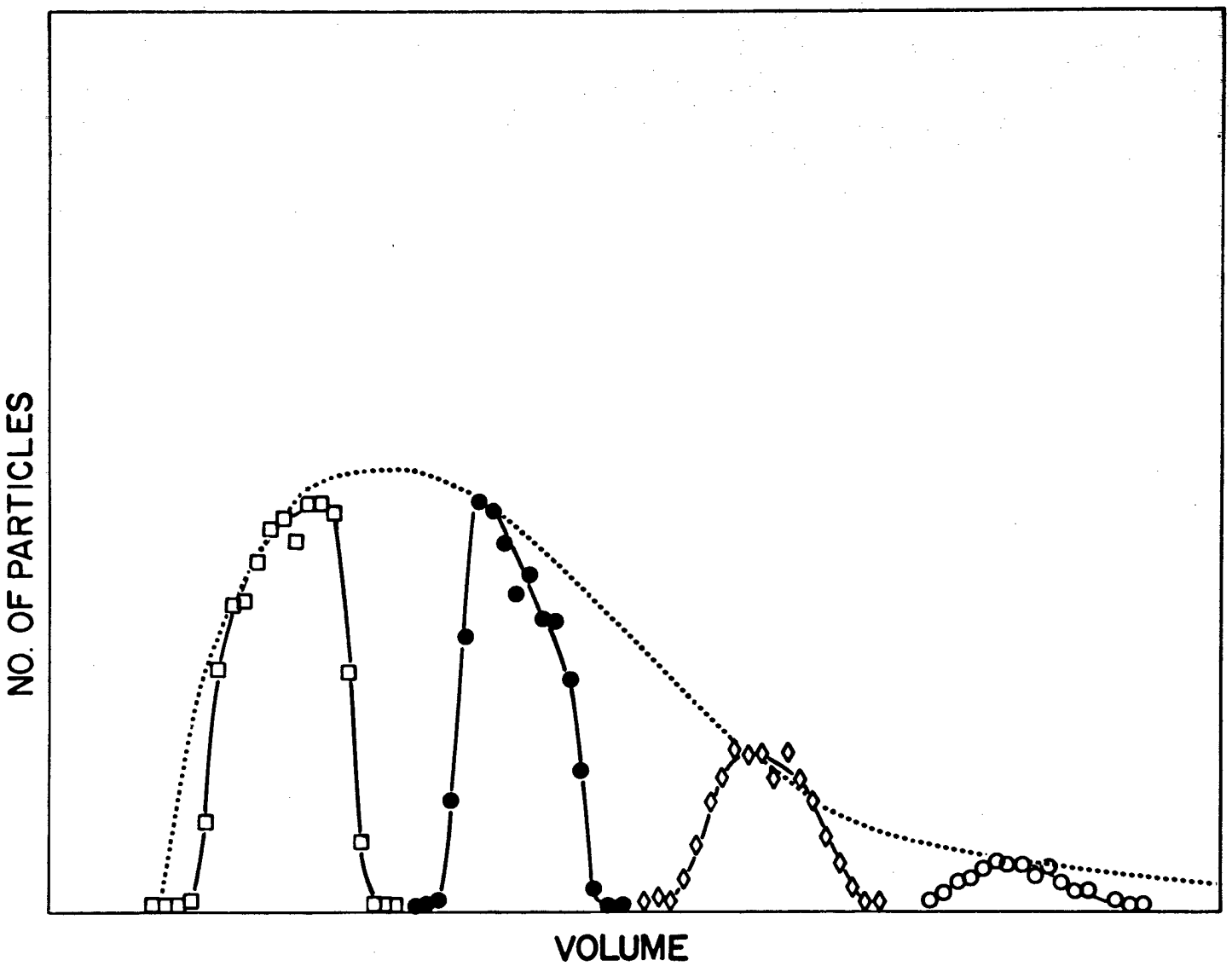

Fig. 1. Simultaneous separation of 4 discrete volume fractions from a distribution of polystyrene spheres ranging in diameter from 7 to 14 microns.

REFERENCES

(1) M. J. Fulwyler, Science 150, 910 (1965).

(2) M. J. Fulwyler, Los Alamos Scientific Laboratory Report LA-3432-MS (1965), p. 114.

(3) M. A. Van Dilla and J. M. Hardin, this report, p. 234.

(4) M. A. Van Dilla, J. M. Hardin, and C. F. Bidwell, this report, p. 239.

(5) M. A. Van Dilla, M. J. Fulwyler, and I. U. Boone, submitted to Science.

(6) I. U. Boone, M. J. Fulwyler, and M. W. Stewart, In Proceedings of the American Association for Cancer Research 7, 8 (1966), 57th Annual Meeting, Denver, Colorado. Abstract No. 28.

(7) M. A. Van Dilla, this report, p. 225.

DETECTION OF BIOLOGICAL CELLS BY LIGHT-SCATTERING (M. A. Van Dilla)

INTRODUCTION

The phenomena of light-scattering and absorption by biological cells and their fluorescence when stained suitably are of great value in studying the properties of both normal and pathological cells. A study of light-scattering by single cells has been started; future adaptation to the electronic cell separator developed by Fulwyler (1) and dual-sensor systems may be feasible. The optical components of two commercial optical blood cell counters have been modified to yield pulse-height distributions for several types of inert particles and biological cells and these compared with volume distributions from a Coulter spectrometer. These data have enough interesting features to make it worthwhile to proceed with the design of a more flexible and suitable light-scatter sensor. This development, which uses a laser light source and attempts at optimal stray light control, is currently in progress.

METHODS

The most straightforward experimental approach to the problem of cell detection by light-scattering was to take advantage of existing commercial optical blood cell counters. The photomultiplier circuit of a Sanborn-Frommer blood cell counter was modified to allow pulse-height analysis of the output. The pulses generated by cells traversing the illuminated region of the scattering chamber were amplified and analyzed by the same electronic equipment used with the Coulter sensor (2). The resulting pulse-height distributions for leucocytes obtained by saponin lysis of diluted whole blood and erythrocytes are shown in Fig. 1. These distributions are quite different from those obtained with a Coulter spectrometer (see below), and hence something other than volume is being sensed.

Inherent disadvantages in the Sanborn-Frommer scattering chamber made it worthwhile to look for a design better suited to our needs. A new unit recently marketed by Vickers Instruments Ltd. seemed promising in this respect, since it generated a cell suspension stream of small diameter (about 100 microns), each cell of which traversed the illuminated region before exiting

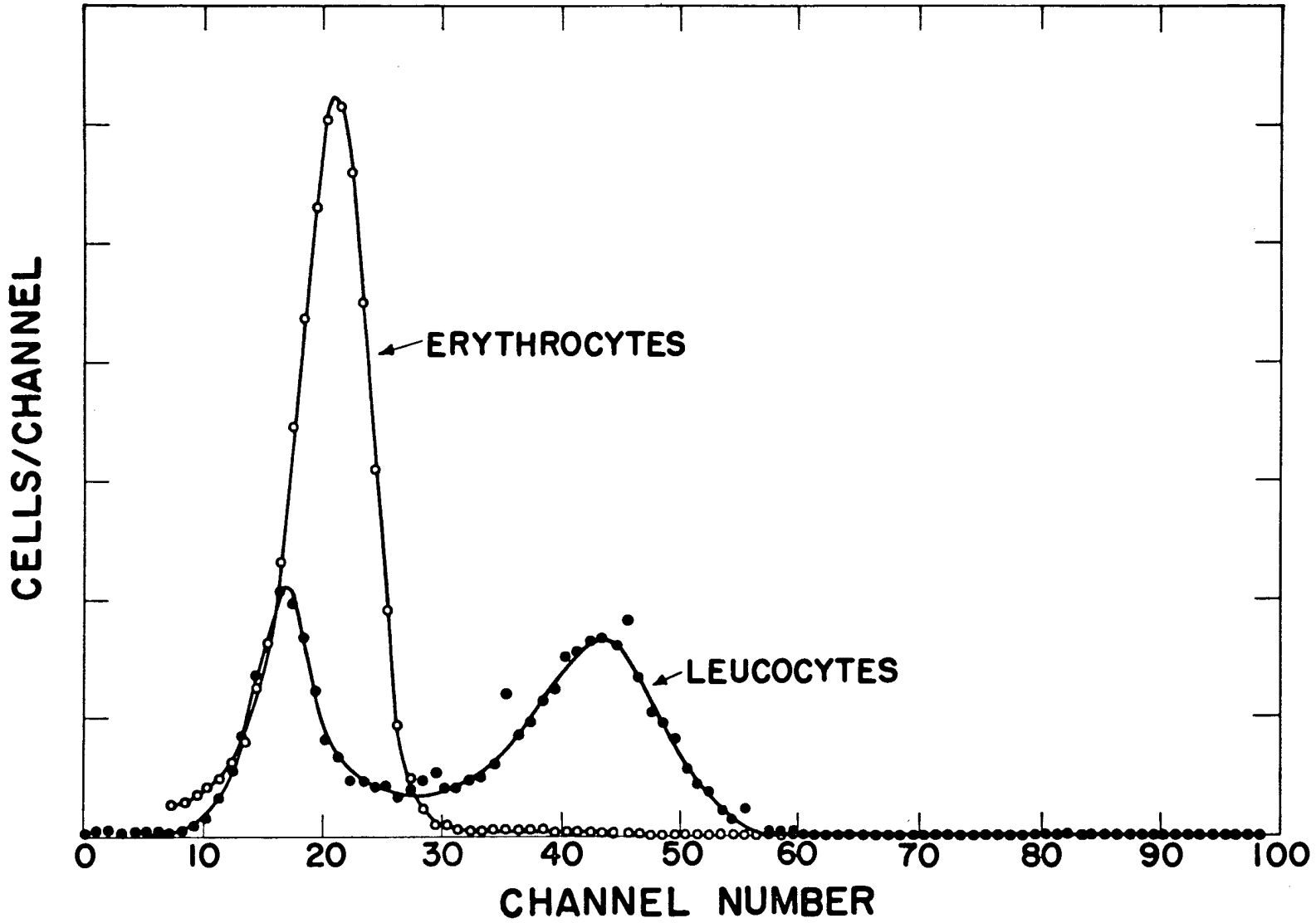

Fig. 1. Pulse-height distribution of normal erythrocytes and leucocytes obtained with a modified Sanborn-Frommer counter.

through a small aperture (about 500 microns diameter). With the photomultiplier circuit modified as in the case of the Sanborn-Frommer counter and the same amplifier and analyzer, pulse-height distributions generated by leucocytes, erythrocytes, ragweed pollen, and paper mulberry pollen were compared with those from a Coulter spectrometer (Figs. 2, 3, 4, and 5). The interesting features of these data, combined with the limitations of the Vickers system for our purposes, led to the design of a system using a helium-neon laser light source, the Vickers scattering chamber, and arrangement to allow variation of scattering angle. This experiment is currently in progress.

RESULTS AND DISCUSSION

First results with the Sanborn-Frommer detector are shown in Fig. 1. The erythrocyte peak shape resembles that obtained with the Coulter spectrometer. Both are approximately Gaussian with a standard deviation of about 15 percent. However, the leucocyte peaks obtained with the optical detector are spread further apart than in the volume spectrum. In addition, the lymphocyte and erythrocyte peaks in the optical spectrum have similar mean values, whereas the lymphocyte mean volume is known to be about triple the erythrocyte mean volume from the Coulter spectra (see below). These results indicate that the light-scatter sensor is detecting different cellular properties than the Coulter sensor and hence would seem worthy of further study. However, design of the Frommer scattering chamber, although suitable for red cell enumeration, was not suitable for our purposes. Its limitations are that only a small fraction of the cells are detected, that stray light due to dirt on the windows is hard to control, and that future adaptation to the cell separator or dual-sensor arrangements seems very difficult.

The Vickers instrument, based on Crosland-Taylor's design (3), seemed to offer a way to circumvent many of these difficulties. Here a sheath flow of distilled water carries a cell suspension stream across the scattering chamber and out through a small aperture (about 500 microns diameter). The cell stream exits axially, while the sheath flow exits peripherally through the remainder of the aperture. Just before exiting, the cell stream diameter is about 100 microns; the dark-field image of a slit illuminated by a tungsten filament lamp is focused on the stream at this point. Thus every cell is counted, stray light generated by dirt on windows is reduced, and the possibility exists of converting the exit aperture into a Coulter

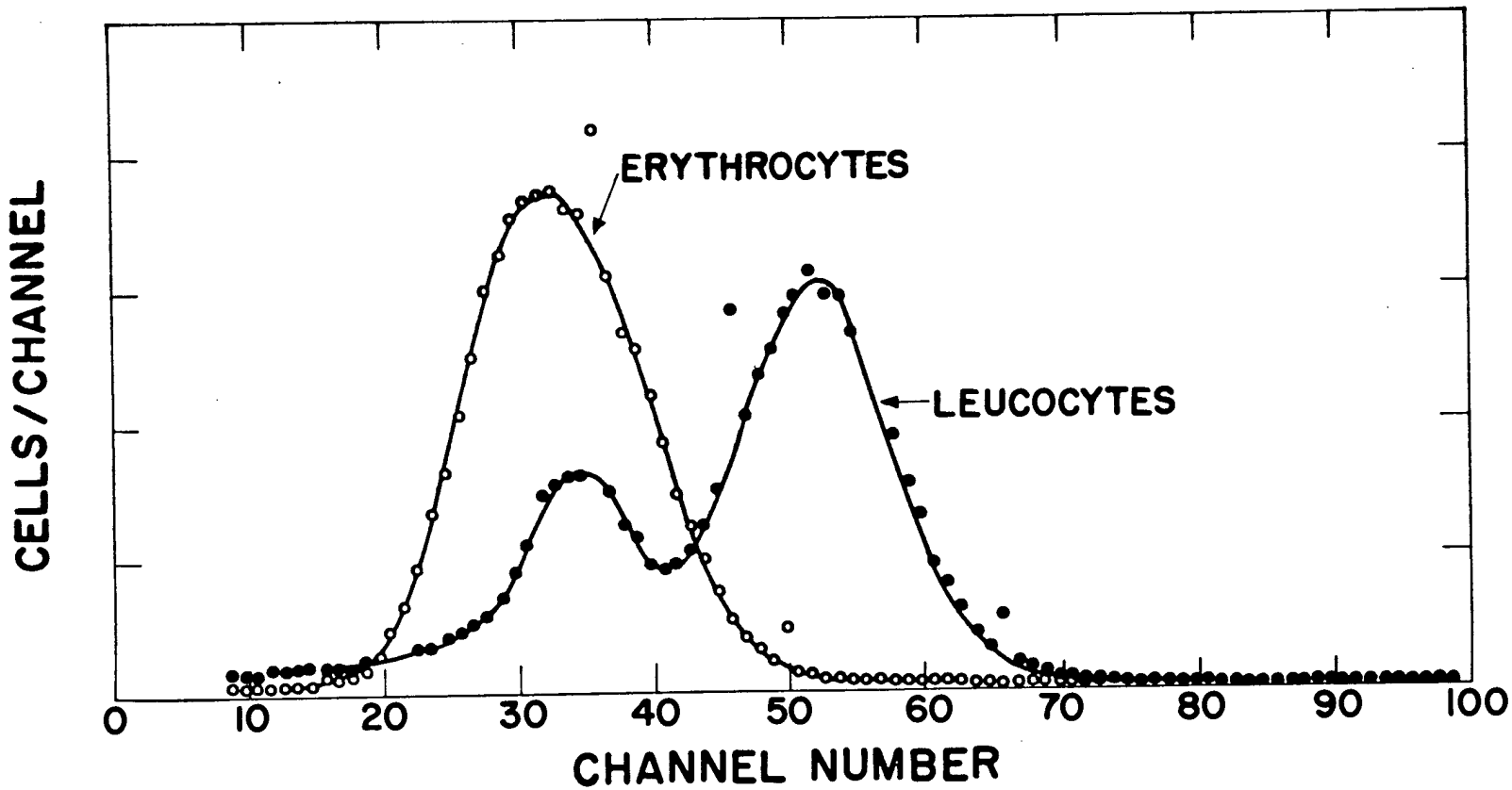

Fig. 2. Pulse-height distribution of normal erythrocytes and leucocytes obtained with a modified Vickers counter.

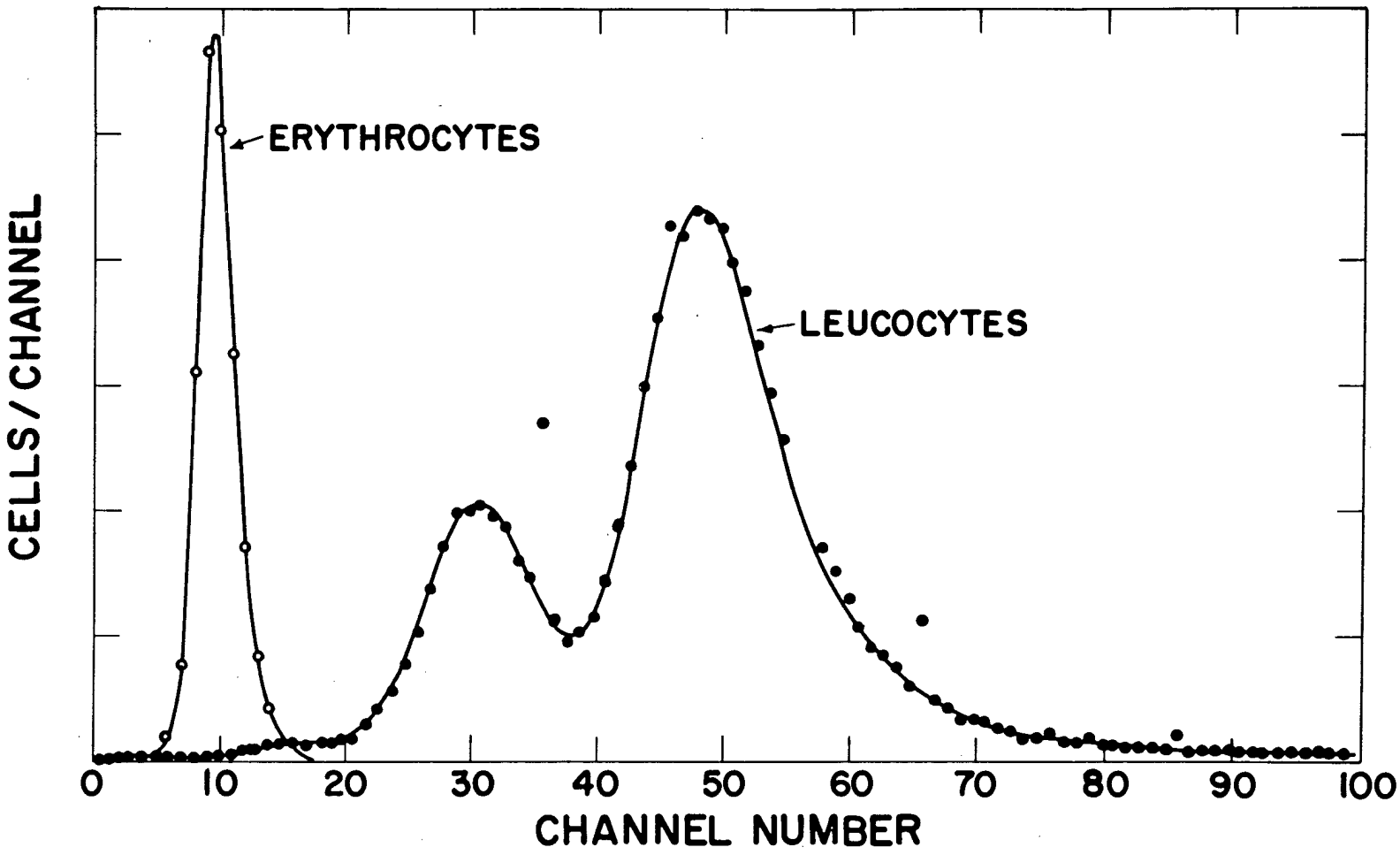

Fig. 3. Pulse-height (volume) distribution of normal erythrocytes and leucocytes obtained with a Coulter spectrometer.

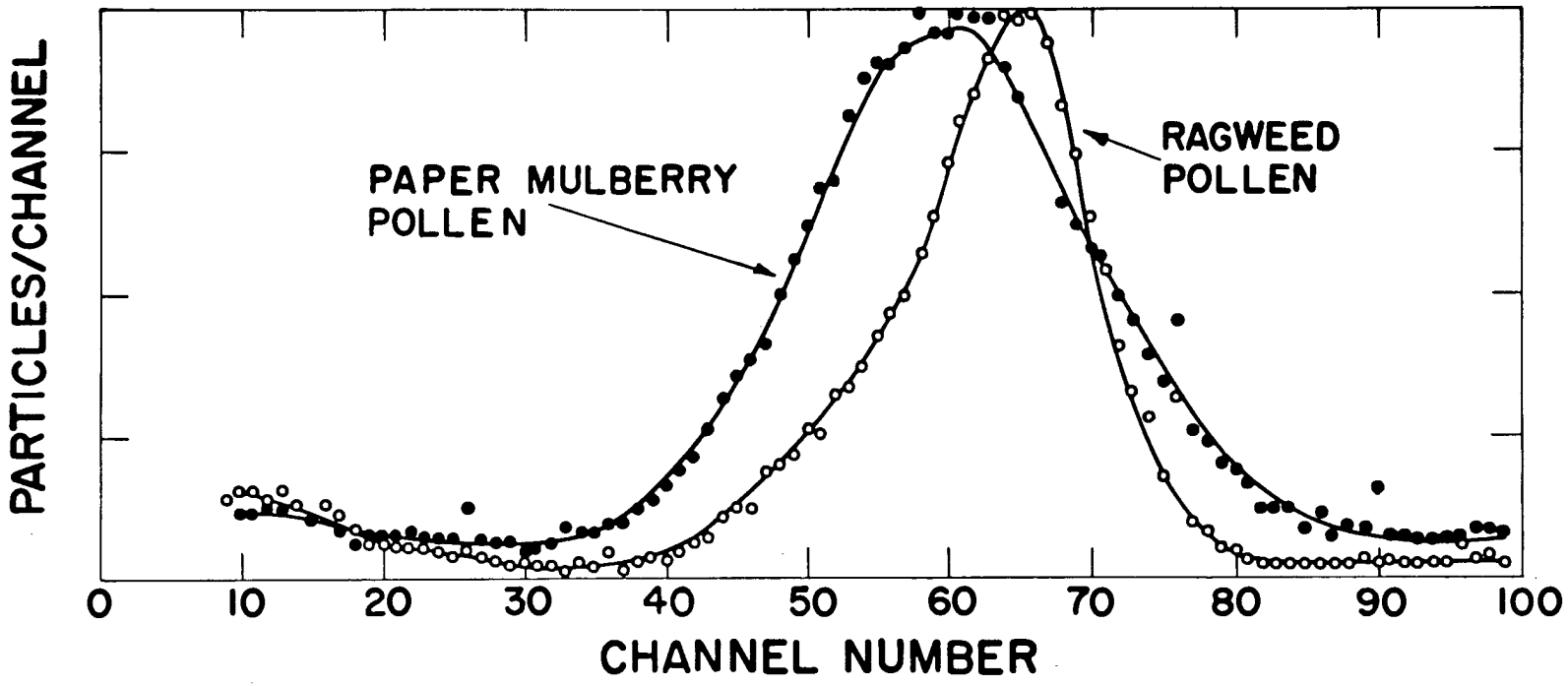

Fig. 4. Pulse-height distribution of ragweed and paper mulberry pollens obtained with a modified Vickers counter.

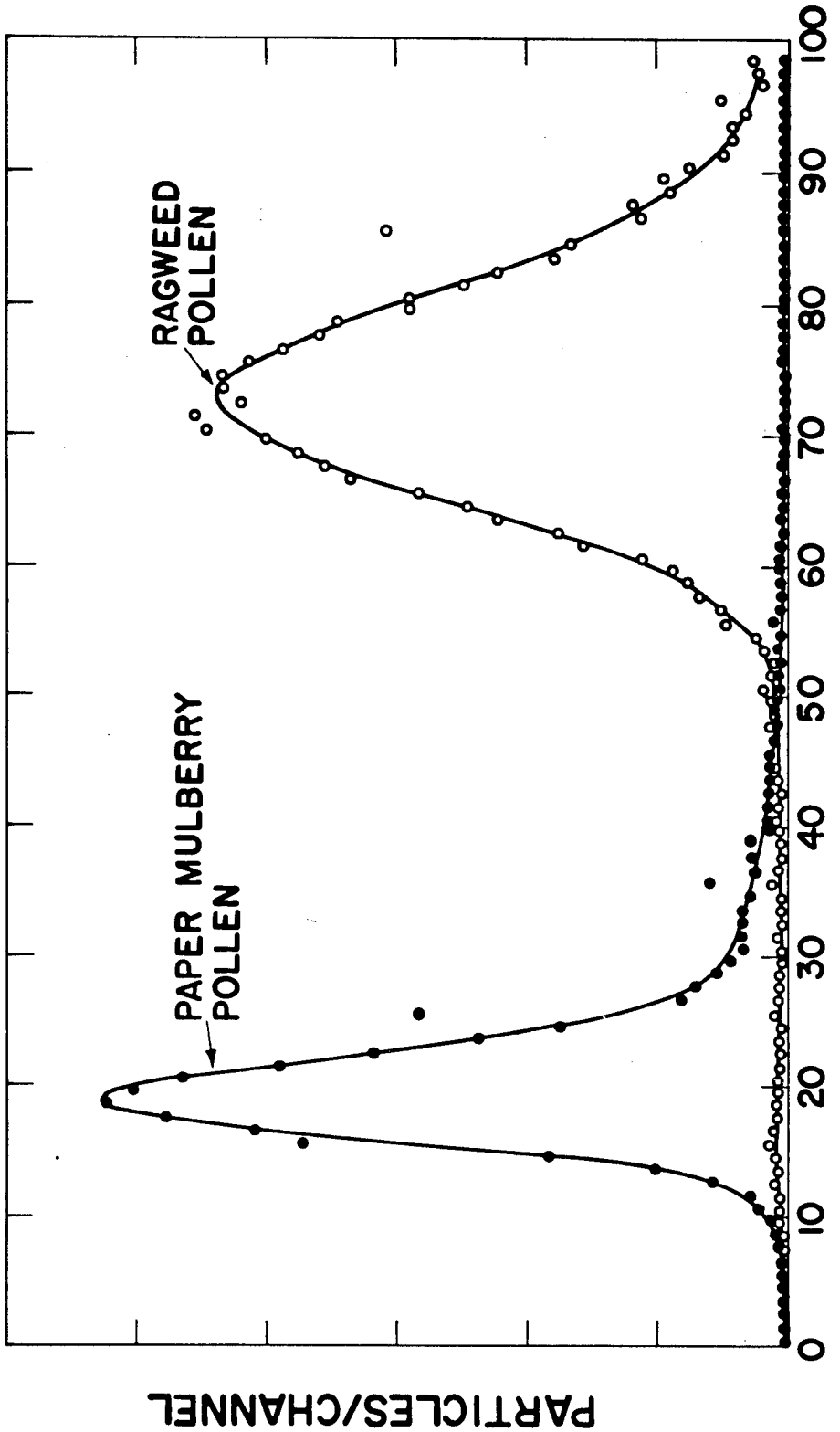

Fig. 5. Pulse-height (volume) distribution of ragweed and paper mulberry pollens obtained with a Coulter spectrometer.

sensor. With this sensor the pulse-height distributions shown in Figs. 2, 3, 4, and 5 were obtained. Now the shape of the leucocyte distribution agrees quite well with the volume distribution, but again the optical sensor shows little difference between lymphocytes and erythrocytes. In addition, the erythrocyte standard deviation is now larger (about 21 percent) than that observed with either the Coulter or Sanborn-Frommer sensor. This may be a cell orientation effect due to the disc shape of the red cell. In all three sensors the fluid flow pattern would be expected to cause the red cell axis to line up perpendicular to the flow direction. In the Sanborn-Frommer sensor this would result in fixed orientation to the light beam, and in the Coulter sensor independence of orientation. However, in the Vickers sensor red cells would be expected to orient with respect to the beam edgewise, broadside, or an angle in between, thus producing a wider pulse-height distribution. The difference between the leucocyte spectra from the two optical sensors was quite unexpected but may have to do with the angle of acceptance of scattered light. This question will be investigated with the more flexible experimental arrangement discussed below.

In Figs. 4 and 5 we see again a striking difference between the volume spectrum (Coulter sensor) and light-scatter spectrum (Vickers sensor) of two different particles, this time ragweed and paper mulberry pollens. This emphasizes the point that different particle properties are being detected. The theory of light-scattering by particles large compared to the wavelength of the incident light (4,5) applies to all particles and cells discussed above; the ratio of particle diameter to wavelength is about 20 to 1. In this case the concepts of physical optics apply, and incident light interacts with the particle by ordinary processes of reflection, refraction, and diffraction. All of the light incident on the particle is removed from the beam by reflection from the surface, refraction, traversal of the interior (with some absorption), and exiting through the opposite surface. These processes cause large-angle deviations from the incident beam direction. An equal amount of light is diffracted, but this light is confined to small angles (about 3 to 4°). Thus the angle subtended by the photomultiplier is probably quite important in determining what cellular properties are being sensed. This point is under investigation with an experimental system which uses a laser light source (Spectra-Physics, Model 130 B) and the Vickers scattering chamber arranged to allow variation of scattering angle.

REFERENCES

(1) M. J. Fulwyler, Science 150, 910 (1965).

(2) M. A. Van Dilla and J. F. Spalding, Nature (in press).

(3) P. J. Crosland-Taylor, Nature 171, 37 (1953).

(4) H. C. Van de Hulst, In Light Scattering by Small Particles, Chapter 8, John Wiley and Sons, Inc., New York (1957), pp. 103-111 and 172-224.

(5) J. R. Hodkinson, In Proceedings of the National Conference on Aerosols, Liblice, Czechoslovakia (October 8-13, 1962), Czechoslovak Academy of Sciences (1964), pp. 181-194.

VOLUME DISTRIBUTION OF NORMAL HUMAN ERYTHROCYTES AND LEUCOCYTES (M. A. Van Dilla and J. M. Hardin)

INTRODUCTION

Leucocytes have been concentrated from the whole blood of normal individuals, their volume measured, and the resulting data subjected to computer analysis. Each peak of the bimodal volume distribution can be well fitted by a skewed normal distribution -- the same function that gives a good fit to erythrocyte volume distribution data. The coefficient of variation of each leucocyte peak and erythrocyte peak is close to 15 percent; this is about what has been observed for several types of mammalian cells in tissue culture at division or just after division. The leucocyte peak at larger volume has a tail that cannot be fitted, suggesting a different population. Subsequent studies showed this tail highly enriched in monocytes.

METHODS AND RESULTS

Erythrocyte distributions were obtained from whole blood diluted in physiological saline buffered at pH 7.3 in the way previously described (1). An aperture 40 microns in diameter and 190 microns long and an aperture current of 100 μA were used. The leucocytes were concentrated from whole blood by the method of Herbeuval et al. (2) and were measured under the same conditions. A computer program described by Dean (3) was used to fit the experimental data. Normal, log-normal, and skewed-normal functions were tried; the latter function gave the best fit for both erythrocyte and leucocyte data. The program reads-in the data, fits the peaks, prints out the parameters of the function, and plots the data points and computed function. Typical graphical computer outputs are shown in Fig. 1 (erythrocyte volume distribution) and in Fig. 2 (leucocyte volume distribution). In these plots, channel number is proportional to cell volume; the constant of proportionality for Fig. 1 was made one-fourth that for Fig. 2 so that both distributions would fall in mid-scale. Parameters of the computed functions are listed in Table 1, where σ/m is the coefficient of variation (i.e., ratio of standard deviation to mean) and γ is the coefficient of skewness (4).

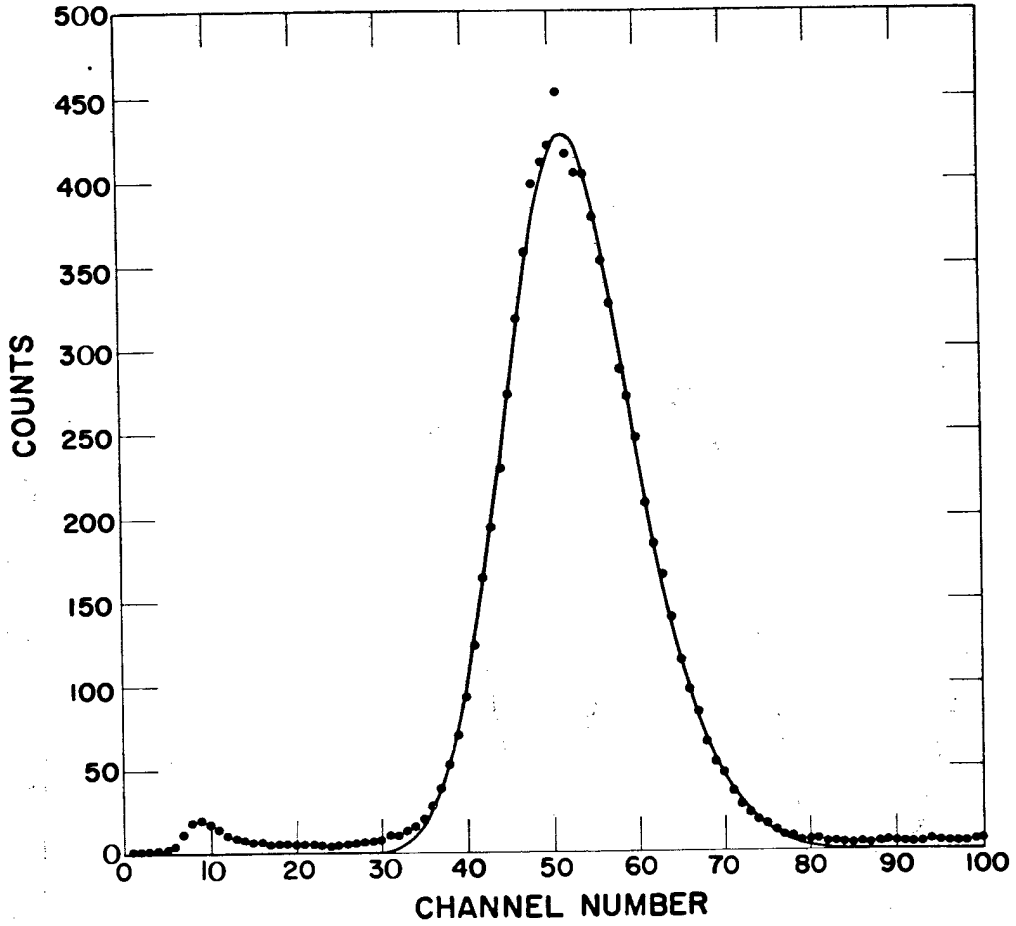

Fig. 1. Volume distribution of erythrocytes from a normal adult.

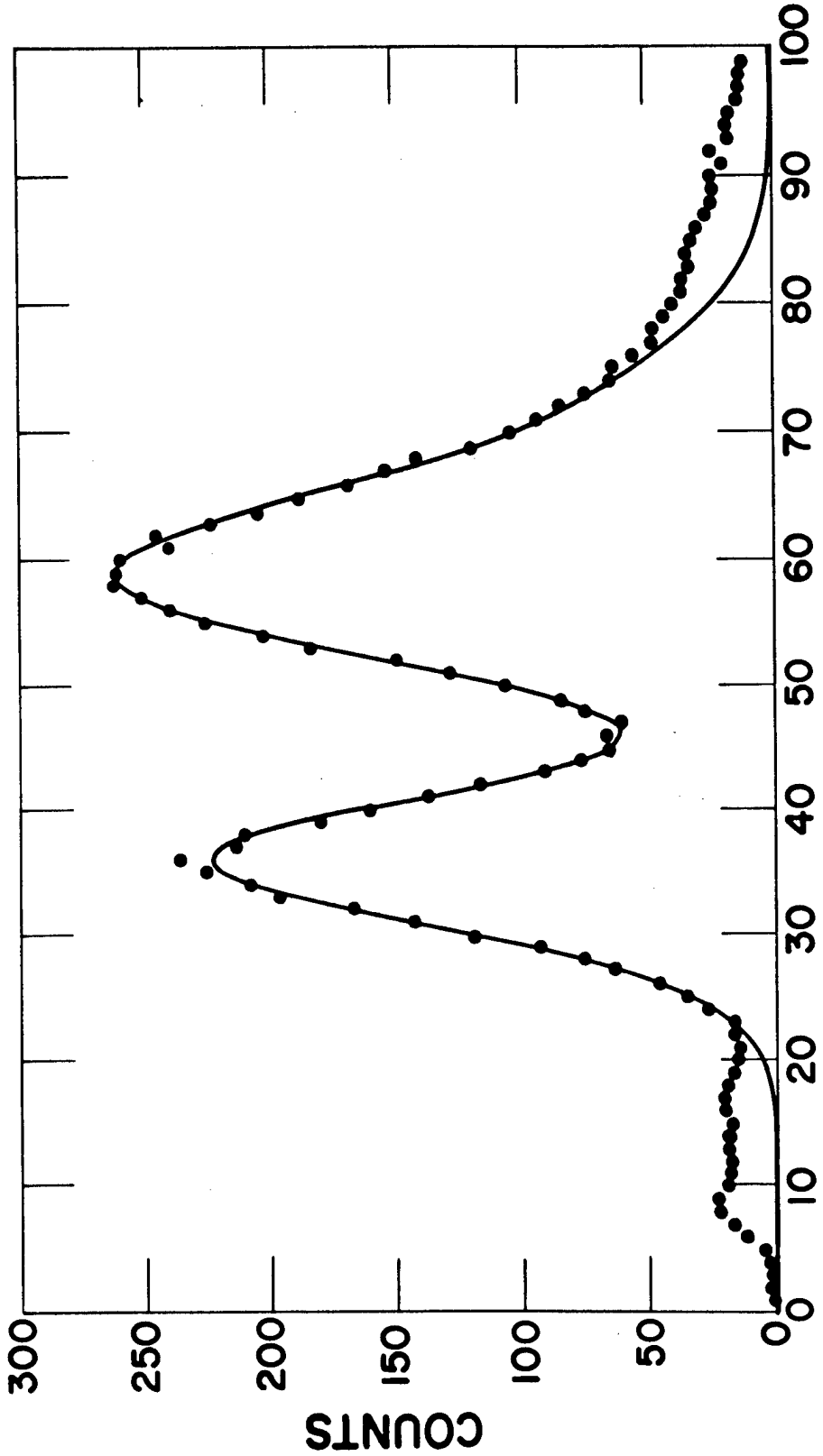

Fig. 2. Volume distribution of leucocytes from a normal adult.

TABLE 1. PARAMETERS OF COMPUTED SKEWED NORMAL DISTRIBUTION FUNCTION WHICH BEST FITS BLOOD CELL DATA FOR A NORMAL ADULT

Cell Type	σ/m (percent)	γ	Mean Volume Relative to Erythrocytes
Erythrocyte	14	0.40	1.0
Leucocyte (peak 1)	13	0.23	2.6
Leucocyte (peak 2)	15	0.67	4.6

DISCUSSION

Experiments with the cell separator (5) have shown that the leucocyte peak with the smaller mean volume is due mostly to lymphocytes and that the other peak is due mostly to granulocytes with the large-volume tail (not fitted) highly enriched in monocytes. Thus, we see that volume distributions of normal erythrocytes, lymphocytes, and granulocytes are quite similar in shape, with similar coefficients of variation and asymmetry. Lymphocytes are larger than erythrocytes by a factor of about 2.5 and granulocytes by a factor of about 4.5. Data on several other normal adults are very similar, so that the results presented above are typical.

It was a surprise to find similar distributions for diverse cell types of quite different morphology and function and, in the case of lymphocytes, site of origin. Data of E. C. Anderson of this Laboratory on CHO, HeLa, and mouse L cells indicate that the volume distributions of these mammalian cells at division and when in the steady state have coefficients of variation of about 15 percent. Studies by Kubitschek (6) on cell generation rates show a coefficient of variation of 10 to 20 percent for several widely different kinds of cells. It is conceivable, therefore, that there exists a generalization which states that cells of a given

type cannot be too dissimilar in size (coefficient of variation about 15 percent) when growing in the steady state (i.e., volume distribution constant). The mechanism is unknown.

REFERENCES

(1) M. A. Van Dilla, N. J. Basmann, and M. J. Fulwyler, Los Alamos Scientific Laboratory Report LA-3132-MS (1964), pp. 182-204.

(2) R. Herbeuval, H. Herbeuval, and J. Duheille, Triangle 4, 47 (1963).

(3) P. N. Dean, Los Alamos Scientific Laboratory Report LA-3440 (1966).

(4) F. E. Croxton and D. J. Cowden, eds., Applied General Statistics, Prentice-Hall, Englewood Cliffs, New Jersey (1958), pp. 617-619.

(5) M. J. Fulwyler, Science 150, 910 (1965).

(6) H. E. Kubitschek, Exp. Cell Res. 26, 439 (1962).

VOLUME DISTRIBUTION OF MOUSE BONE MARROW CELLS (M. A. Van Dilla, J. M. Hardin, and C. F. Bidwell)

INTRODUCTION

Bone marrow plays a vital role in the biological effects of radiation and recovery from radiation injury. Much can be learned from study of the circulating blood cells (1,2), but study of the source of these cells in the bone marrow is of primary importance whenever possible. A recent paper by Lee and Richards (3) describes bone marrow cell volume distributions for normal and irradiated mice which contrast with the results obtained at this Laboratory, as described below.

METHODS AND RESULTS

An amount of blood equal to 2 percent of body weight was taken by orbital bleeding from 15 RF female mice, and volume distributions of the circulating blood cells and femoral bone marrow cells were measured at daily intervals thereafter for 5 days. The animals were 3 to 4 months old; average weight was 25 g. Bone marrow cells were obtained from the femur by cutting the ends off and flushing physiological saline buffered at pH 7.3 through each shaft with a No. 23 needle on a 2-ml syringe to yield 5 ml of cell suspension. Passage through the needle several times was sufficient to break up clumps with no apparent damage to the cells. Dilution by a factor of 25,000 was followed by a 1-minute measurement of volume distribution of cells from each femur in a Coulter spectrometer (4). Whole blood was diluted by a factor of 10^5 and measured in the same way. Blood smears were examined for reticulocytes using standard techniques.

Circulating cell volume distributions were fit by a skewed Gaussian function using computer methods (5). The data for the initial 2 percent bleeding of the 15 animals are shown in Table 1. The parameters of the fitted functions are area (proportional to cell count), mean channel number (proportional to mean cell volume), standard deviation, and skewness coefficient (upon which the asymmetry of the distribution depends). Accurate calibration of channel number in terms of volume in cubic microns was not undertaken. An approximate calibration with Dow monodisperse polyvinyltoluene latex spheres yielded a conversion factor of 0.91 μ^3/channel,

TABLE 1. PARAMETERS OF ERYTHROCYTE VOLUME DISTRIBUTION OF 15 NORMAL MICE

Mouse No.	RBC (in 10^6 cells/mm^3)	Mean Channel Number	Standard Deviation (channels)	Skewness Coefficient
1	10.30	42.4	6.32	0.316
2	11.90	43.4	6.84	0.237
3	9.58	41.9	6.19	0.256
4	10.70	43.2	6.48	0.246
5	9.70	42.5	6.31	0.292
6	9.71	42.2	6.15	0.240
7	10.50	43.5	6.41	0.250
8	10.60	42.6	6.15	0.293
9	9.42	42.9	6.39	0.304
10	10.50	42.2	6.14	0.295
11	11.00	42.2	6.11	0.284
12	9.81	43.4	6.25	0.272
13	9.28	43.2	6.23	0.271
14	10.40	43.1	6.24	0.250
15	9.92	42.3	6.15	0.280
Mean	10.20	42.8	6.29	0.269
1 (2 hours)	8.67	52.9	7.93	0.180

so that channel number 42.8 = 39 μ^3. Table 1 also shows the deleterious effect on erythrocytes of standing in the saline counting solution for 2 hours, emphasizing the point that the counting suspension should be measured quickly after preparation.

Anemia caused by bleeding stimulated a macrocytosis illustrated in Figs. 1 and 2. Figure 1 shows the circulating erythrocytes 3 days after bleeding compared with a control. Figure 2 shows the variation of erythrocyte volume distribution parameters with time after bleeding and also the reticulocyte count as percent of circulating cells determined from the stained slides.

The volume distribution of normal mouse bone marrow cells is shown in Fig. 3, along with the normal erythrocyte volume distribution. Bleeding stimulated the marked changes shown in Fig. 4. All bone marrow cell distributions represent a standard dilution of cells from a single femur measured under standard conditions so that the vertical scales are identical.

DISCUSSION

The control erythrocyte volume distribution data are notably homogeneous. Thus, mean channel number averaged over the 15 mice is 42.8 $\pm$ 0.52, or a coefficient of variation (i.e., percent standard deviation) of about 1 percent. Hence, mean erythrocyte volumes are very tightly distributed for this group of animals. Inspection of Table 1 shows further that the other parameters of the cell distribution function also show little variance, with the exception of area (i.e., red cell count). This exception may be due to the fact that red cell count is directly proportional to fluid content of the blood; total red cell mass would be a more meaningful quantity but much more difficult to measure accurately.

Figure 1 shows that the effect of bleeding is a macrocytosis, as reported by Brecher and Stohlman (6). A similar effect has been noted following radiation-induced bone marrow arrest (1,2). Figure 2 shows that the skewness coefficient is the parameter most correlated with degree of reticulocytosis; variation of this parameter with time after bleeding closely parallels variation of the reticulocyte fraction seen in stained preparations. The standard deviation is also correlated with reticulocyte count; mean channel number (not plotted) shows a less striking correlation.

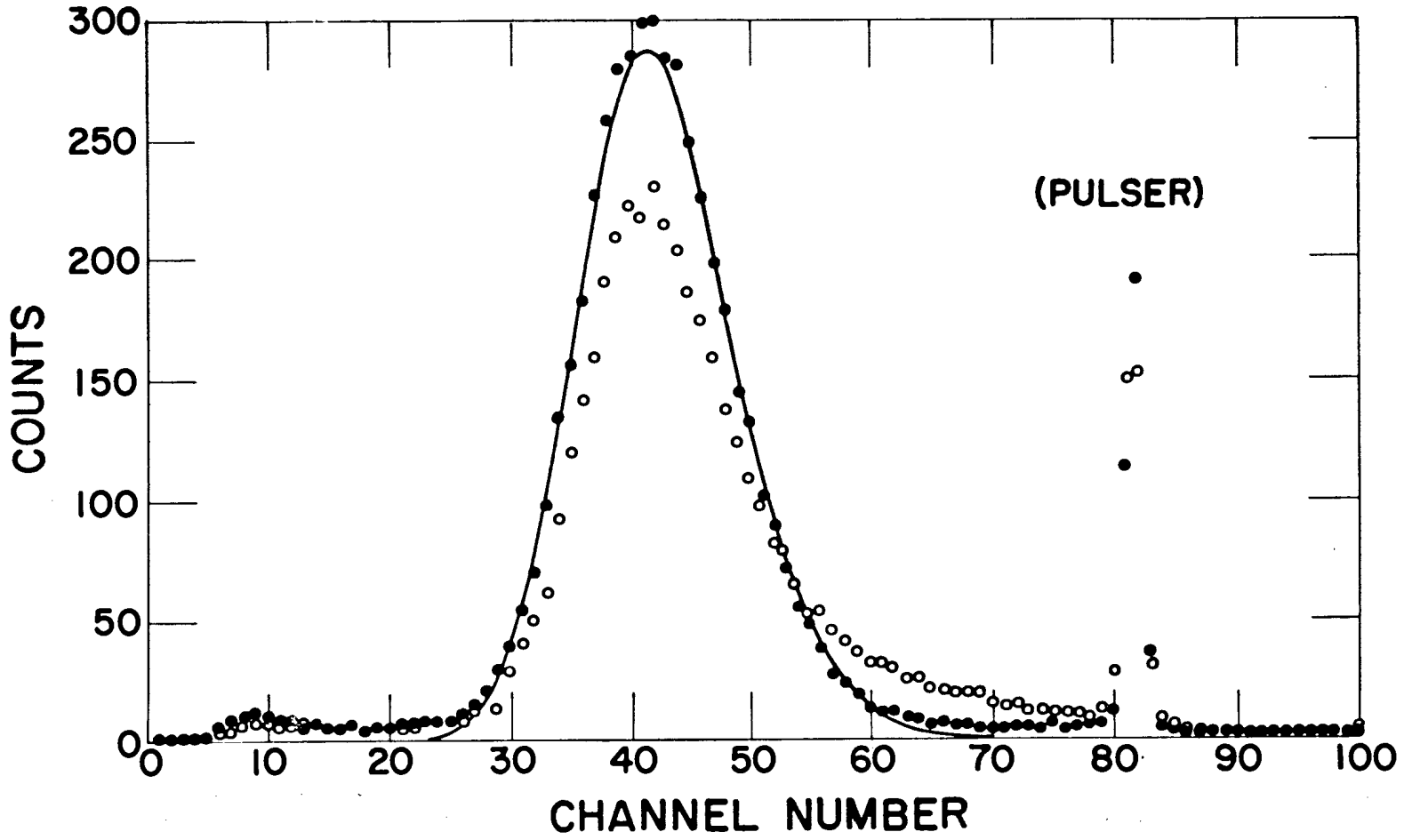

Fig. 1. Erythrocyte volume distribution of a mouse 3 days after bleeding (●) compared with control (O); solid line is computer fit of control data.

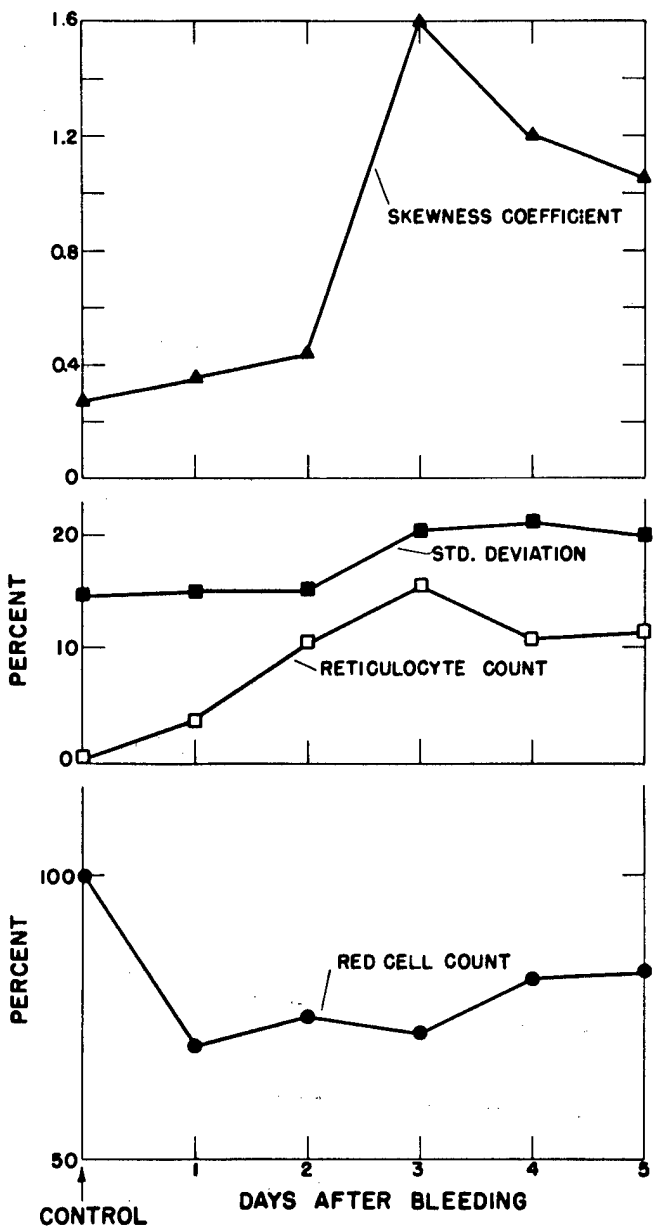

Fig. 2. Dependence of parameters of erythrocyte volume distributions on time after bleeding. Skewness coefficient is dimensionless. Standard deviation is expressed as percent of mean red cell volume. Reticulocyte count is expressed as percent of total red cells. Red cell count is expressed as percent of control value.

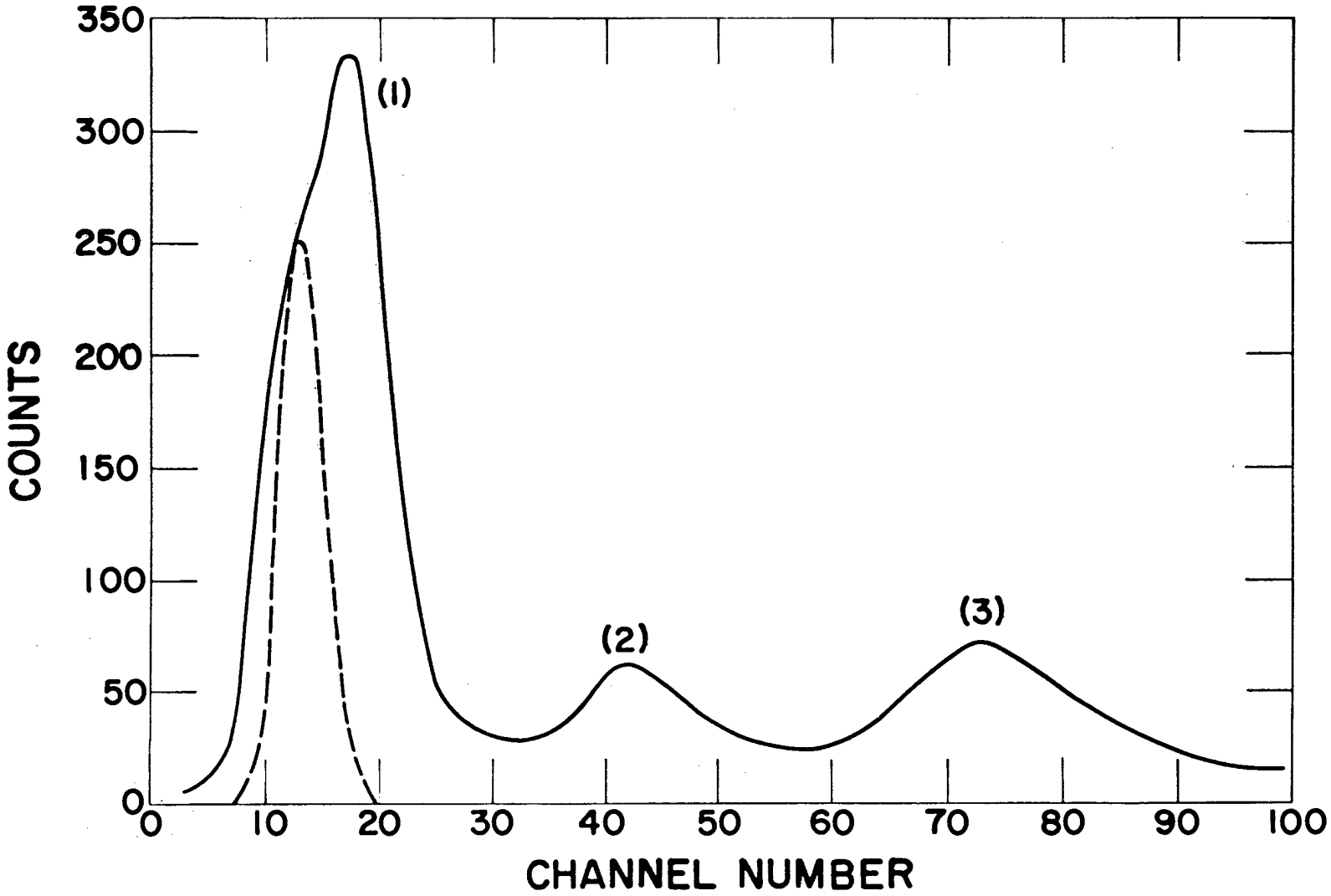

Fig. 3. Normal bone marrow cell volume distribution (———) compared with circulating erythrocyte distribution (-----).

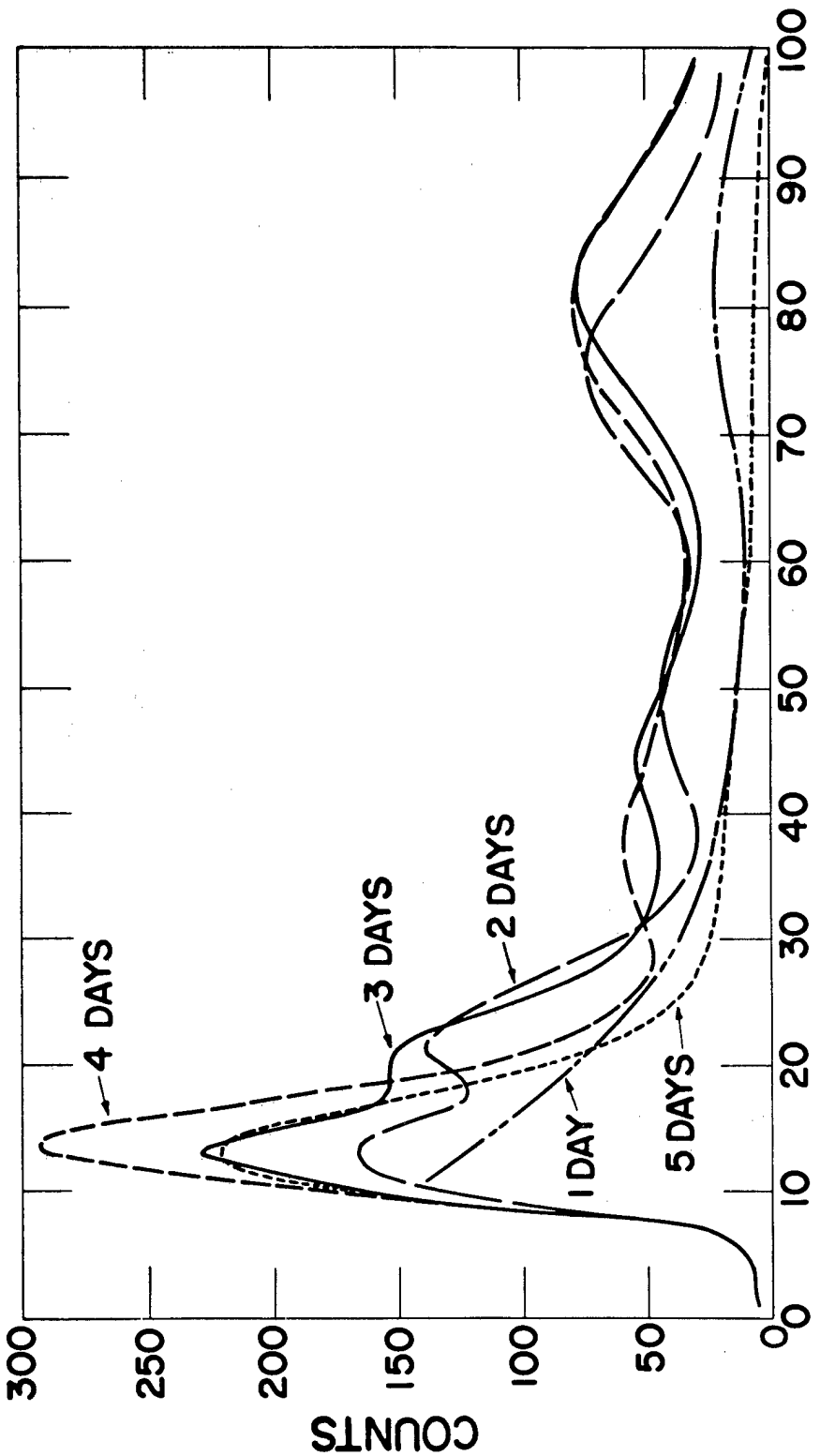

Fig. 4. Changes with time in volume distribution of bone marrow cells induced by bleeding (0.5 ml).

Normal bone marrow cell distribution (Fig. 3) has 3 peaks. The first (at minimum volume) is very broad and appears composite, perhaps a mixture of circulating erythrocytes and late marrow cells of the erythroid series. The cell types comprising the other 2 peaks are not obvious, but it seems likely that they are more immature precursors of the erythroid and granulocytic series. A comparison between Fig. 3 and the comparable data of Lee and Richards (3) shows marked differences. Their control distribution does not show a peak corresponding to our peak 1; they say these cells are excluded, since they were mostly erythrocytes mixed with a great deal of debris. Nor is there a peak corresponding to our peak 2. Their only peak (at 40 threshold units) corresponds to our peak 3.

The reason for these differences is not clear. Lee and Richards also report that their only peak disappears with whole-body X-ray doses of 100 r and over, in contradiction of their data on "cellular dry mass and the percent of radiation-induced giant cells." They attribute this to "changes in conductivity of the cell caused by cell membrane injury from irradiation." We have some, although certainly inconclusive, evidence to the contrary in our mouse bone marrow arrest experiments (1,2); after doses of 1600 rads spread over a 2-week period, no such effects could be observed on macrocytic reticulocytes or erythrocytes.

Bone marrow cell distributions undergo considerable change after bleeding (Fig. 4). Peak 1 disappears at 1 day and then shows a bimodal structure which suggests a mixture of circulating erythrocytes (channel 13) and marrow reticulocytes or late normoblasts (channel 21). Two cell groups of similar volume were observed in the circulating blood of mice in the bone marrow arrest experiments (1,2) and were identified as erythrocytes and macrocytic reticulocytes by microscopic examination. If the morphology of the erythrocytic and granulocytic series and the myeloid-to-erythroid ratio in mice are similar to humans, then perhaps peak 2 is predominantly erythrocytic and peak 3 predominantly granulocytic. Experiments with the cell separator (7) are planned to clarify this situation.

REFERENCES

(1) M. A. Van Dilla, N. J. Basmann, J. M. Hardin, and J. F. Spalding, Los Alamos Scientific Laboratory Report LA-3432-MS (1965), pp. 102-106.

(2) M. A. Van Dilla and J. F. Spalding, Nature (in press).

(3) H. Lee and V. Richards, Nature 205, 821 (1965).

(4) M. A. Van Dilla, N. J. Basmann, and M. J. Fulwyler, Los Alamos Scientific Laboratory Report LA-3132-MS (1964), pp. 182-204.

(5) P. N. Dean, Los Alamos Scientific Laboratory Report LA-3440 (1966), pp. 17-34.

(6) G. Brecher and F. Stohlman, Jr., In Erythropoiesis (L. O. Jacobson and M. Doyle, eds.), Grune and Stratton, New York (1962), pp. 216-221.

(7) M. J. Fulwyler, this report, p. 222.

AMINO ACID ANALYSIS BY COMPUTER (P. N. Dean and C. N. Roberts)

INTRODUCTION

Quantitative analysis of mixtures of amino acids has been considerably simplified by application of automatic data acquisition and analysis techniques to the data obtained from automatic amino acid analyzers. Manual calculation of the areas of the elution peaks by "dot" counting is tedious, time-consuming, and relatively inaccurate when peaks overlap. A system has been devised which will punch the data directly onto paper tape for analysis by computer. A computer program calculates the absorbance area of each of the peaks, compares the results with a standard calibration, and prints out the final results as μmoles and μmole percent of each of the acids. A typical analysis requires approximately 4.5 minutes of IBM-7030 (STRETCH) computer time.

METHODS

The usual method of data readout from an amino acid analyzer is via a multipoint strip chart recorder. Three curves are plotted alternately, point by point. These correspond to transmission of the 570-, 440-, and suppressed 570-mμ light beams through a mixture of ninhydrin reagent and column effluent. The analog signal, corresponding to the pen displacement of the recorder at each data point, is converted to a digital form and recorded on punched paper tape. Data on the paper tape are then read onto magnetic tape and processed by a computer. The computer program converts the transmission to absorption and fits the peaks corresponding to the different amino acids by the method of least squares with the function,

$$Y_i = \frac{A}{\sqrt{2\pi}\,\sigma}(1 - B)\exp\left[-\frac{1}{2}\left(\frac{X_i - \mu}{\sigma}\right)^2\right] + a + b\,X_i + c\,X_i^2,$$

with $B = \frac{\alpha_3}{2}\left[\frac{X_i - \mu}{\sigma} - \frac{1}{3}\left(\frac{X_i - \mu}{\sigma}\right)^3\right]$, where Y_i is the absorbance

at time X_i, μ is the arithmetic mean of the function corresponding to time of detection of the acid, σ is the standard deviation, A is the area of the peak, and α_3 is the coefficient of skewness. Base line changes are compensated for by including the second-order polynomial with coefficients a, b, and c. As many as three peaks are fitted simultaneously, depending on the amount of overlap between peaks. Methionine sulfoxide is not fitted as a peak; it is taken to be the difference between measured spectrum and spectrum computed for aspartic acid, including the region of the methionine sulfoxide peak. Any peak which is not present in the observed spectrum can be omitted from the calculation. The proline peak is calculated from the 440-mμ curve, since it is more prominent at this wavelength.

The procedure of calculation is first to obtain the area for each peak of a standard solution (typically, 0.16 μmole of each amino acid). This yields a calibration factor for each amino acid in μmoles/unit area of absorbance. The analysis is performed at present for only the 19 acids listed in Table 1. The peak areas present in a sample run are calculated and multiplied by the appropriate calibration factors, yielding the number of μmoles of each amino acid present in the sample.

RESULTS AND DISCUSSION

Table 1 gives the results of an analysis of a histone sample. The μmoles of ammonia are calculated but are not included in the μmole percentages. The μmoles of methionine sulfoxide are calculated and listed but are included with the methionine for total μmoles and μmole percent. Half-cystine was not present in the sample and is listed as zero amount. The alternate or suppressed 570-mμ curve was not used; it would be used only if a given peak exceeded the range of the 570-mμ curve. The spectrum is divided into 11 parts for calculation, including the proline peak. Figures 1 through 11 show experimental spectra (open circles) and computer calculated spectra (solid lines). The abscissa is the time of emergence of the peak in minutes and the ordinate is absorption. The time required by the computer to perform this analysis was 4.2 minutes. The areas were computed with an accuracy of $\pm$ 0.1 percent or better. Thus, with its ability to compensate for skewing of peaks due to hold-up in the column or for other reasons and to correct for base line changes on other than a straight line basis, computer analysis has proven to have considerable advantage over hand calculations.

TABLE 1. AMINO ACID ANALYSIS OF SAMPLE HISTONES[a]

Peak No.	Time (min)	Amino Acid	Peak Area	μMoles	μMole Percent
1	42	Lysine	2.751	0.185	12.8
2	49	Histidine	0.306	0.024	1.6
3	57	Ammonia	2.26	0.179	--
4	87	Arginine	1.482	0.108	7.4
5	0	Methionine sulfoxide	0.02	0.002	--
6	72	Aspartic acid	1.316	0.107	7.4
7	85	Threonine[b]	0.93	0.076	5.3
8	91	Serine[c]	0.965	0.077	5.3
9	105	Glutamic acid	1.836	0.147	10.1
10	113	Proline[d]	0.264	0.088	6
11	141	Glycine	1.748	0.139	9.6
12	149	Alanine	2.06	0.162	11.1
13	0	Half-Cystine	0	0	0
14	185	Valine	1.101	0.087	6
15	216	Methionine[e]	0.149	0.013	0.9
16	228	Isoleucine	0.758	0.058	4
17	235	Leucine	1.399	0.106	7.3
18	272	Tyrosine	0.478	0.037	2.5
19	280	Phenylalanine	0.493	0.038	2.6
			Total percent		100
			Total μmoles		1.45

[a]At 570 mμ, 1.432 mg was hydrolyzed in 0.41 ml 6 N HCl, dried in the oven, stored in vacuum over Drierite, diluted with 6.14 ml sample dilutor, 1 ml onto each column.

[b]Corrected for 5 percent loss.

[c]Corrected for 10 percent loss.

[d]Proline peak read from 440-mμ curve.

[e]Sum of methionine and methionine sulfoxide.

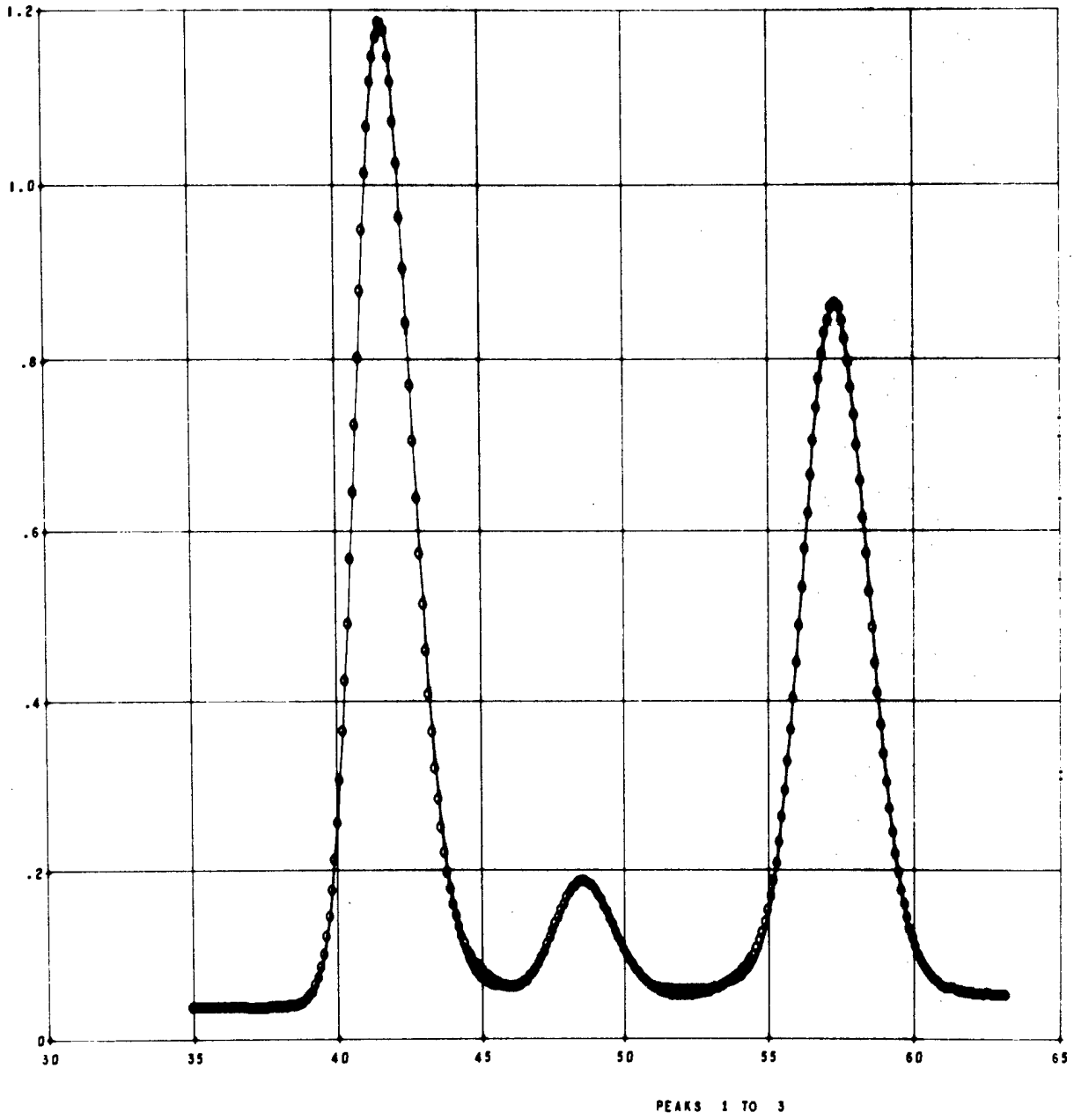

Fig. 1. Peaks 1 to 3: lysine, histidine, and ammonia.

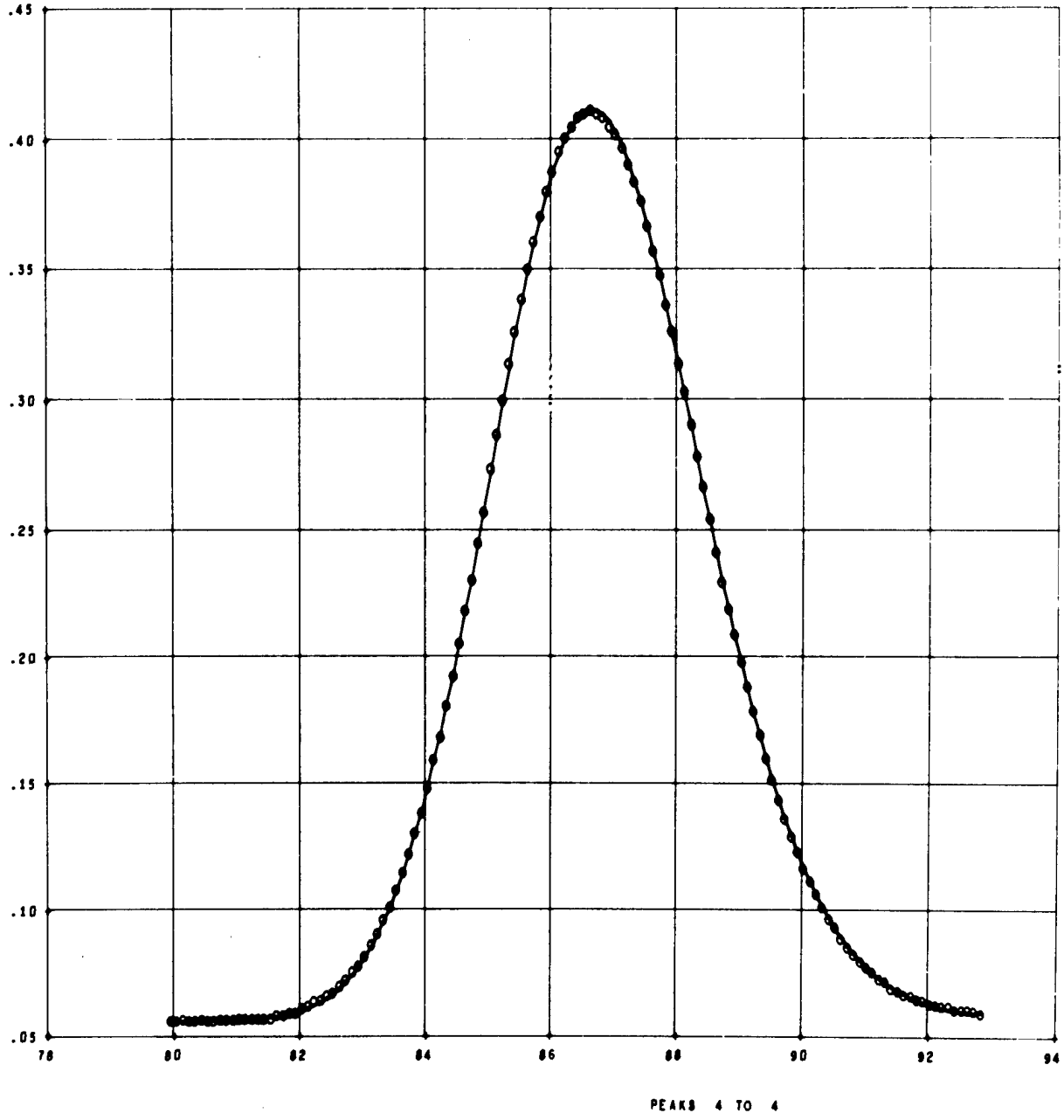

Fig. 2. Peak 4: arginine.

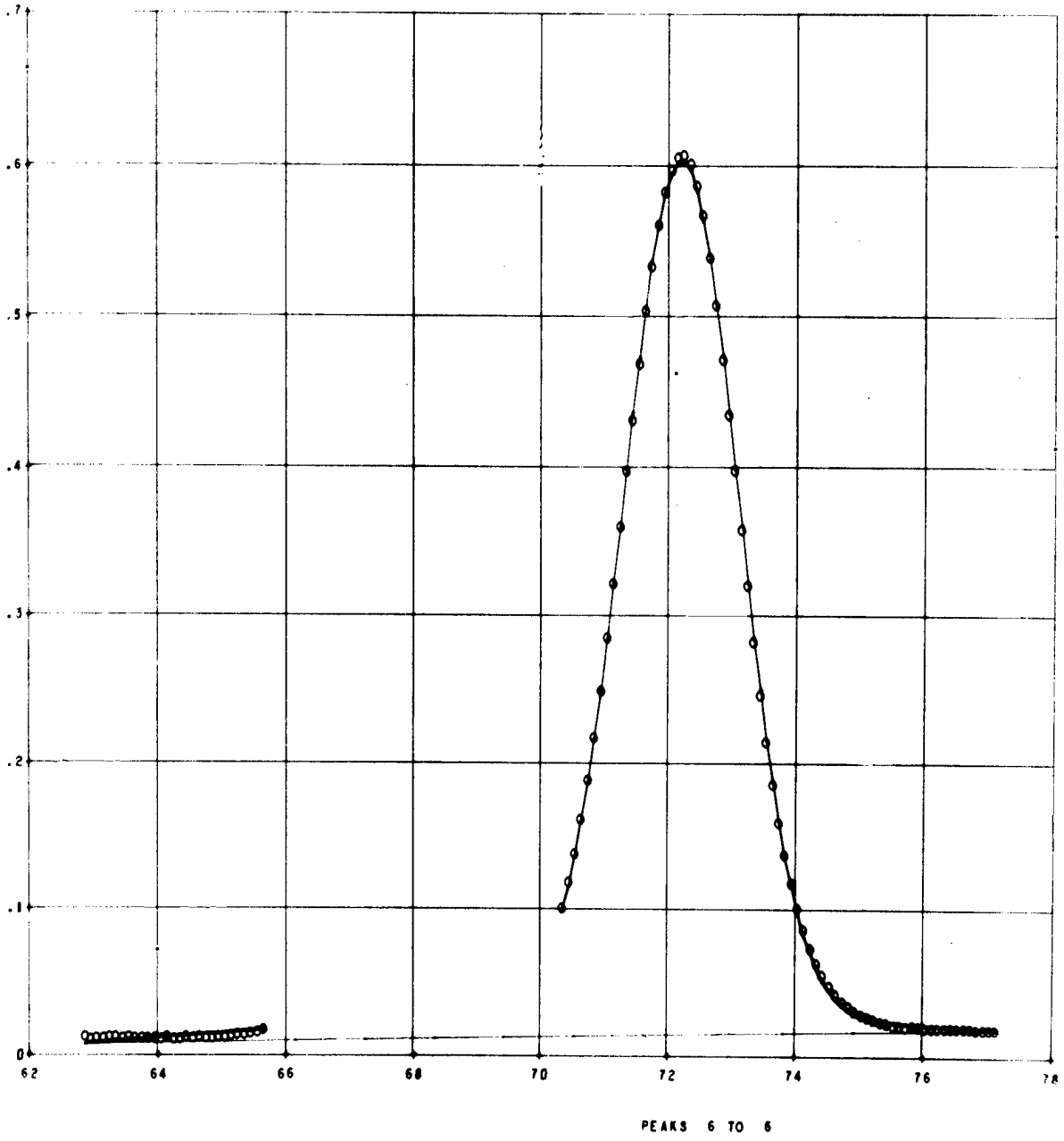

Fig. 3. Peak 6: aspartate.

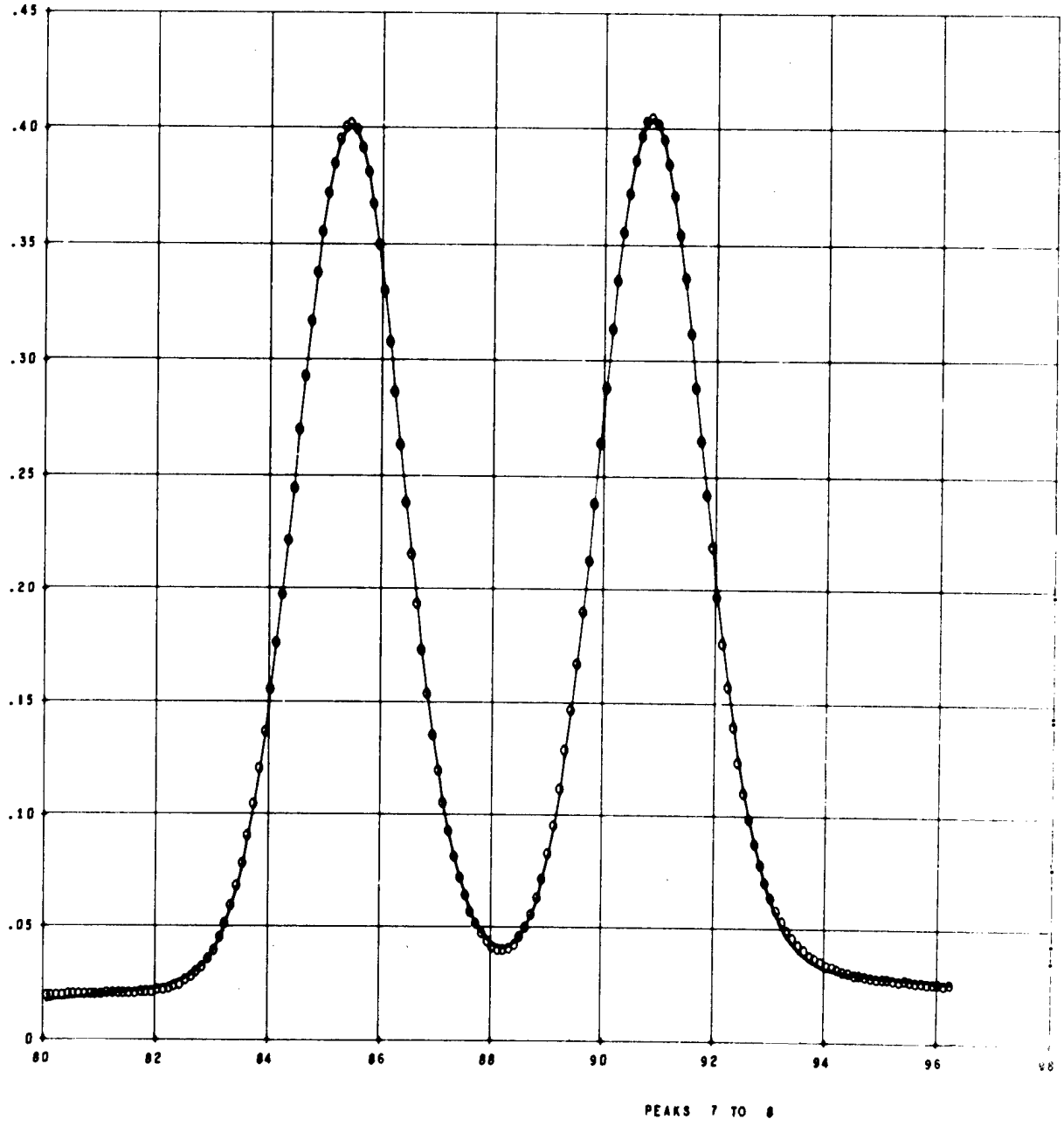

Fig. 4. Peaks 7 and 8: threonine and serine.

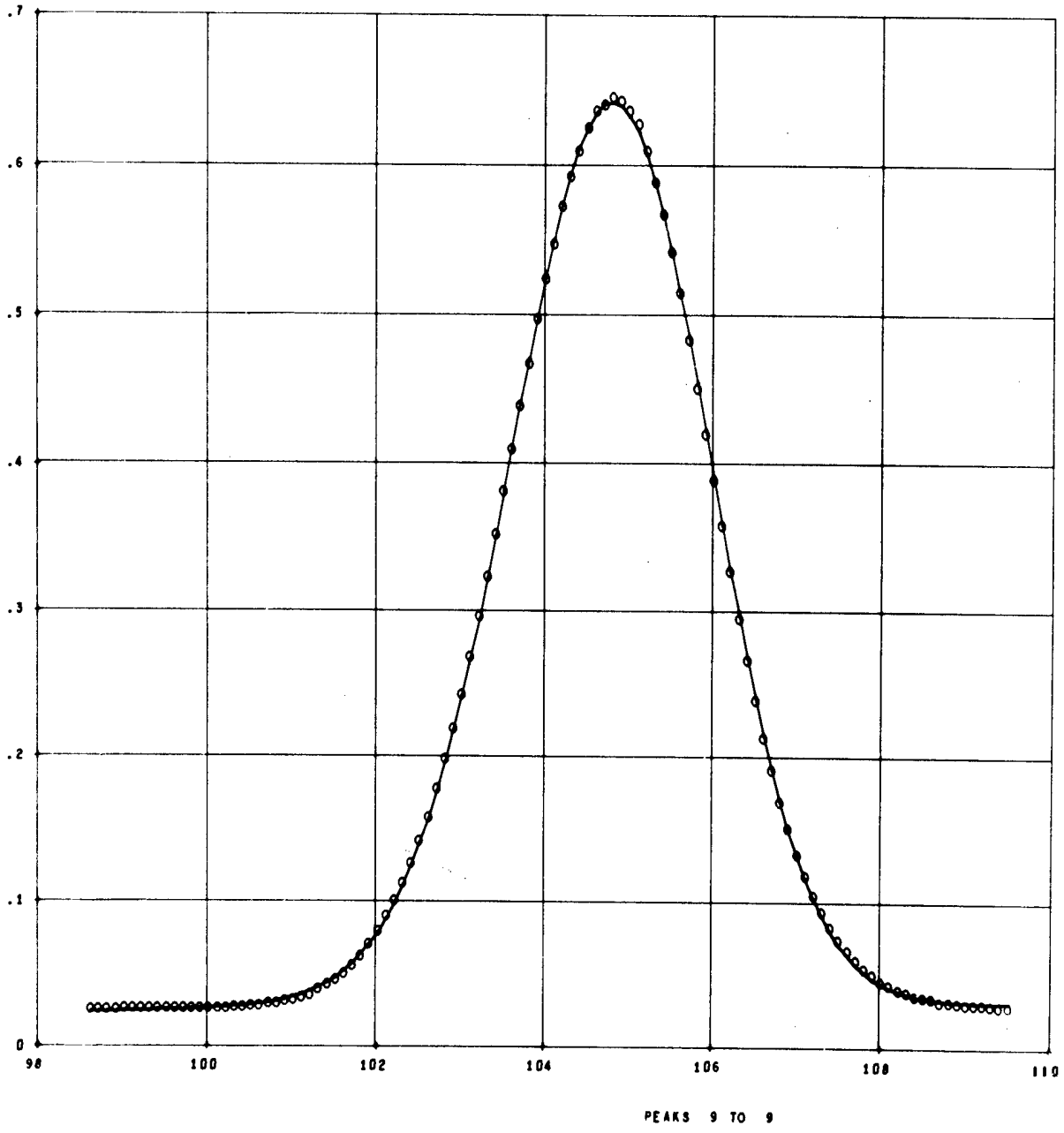

Fig. 5. Peak 9: glutamate.

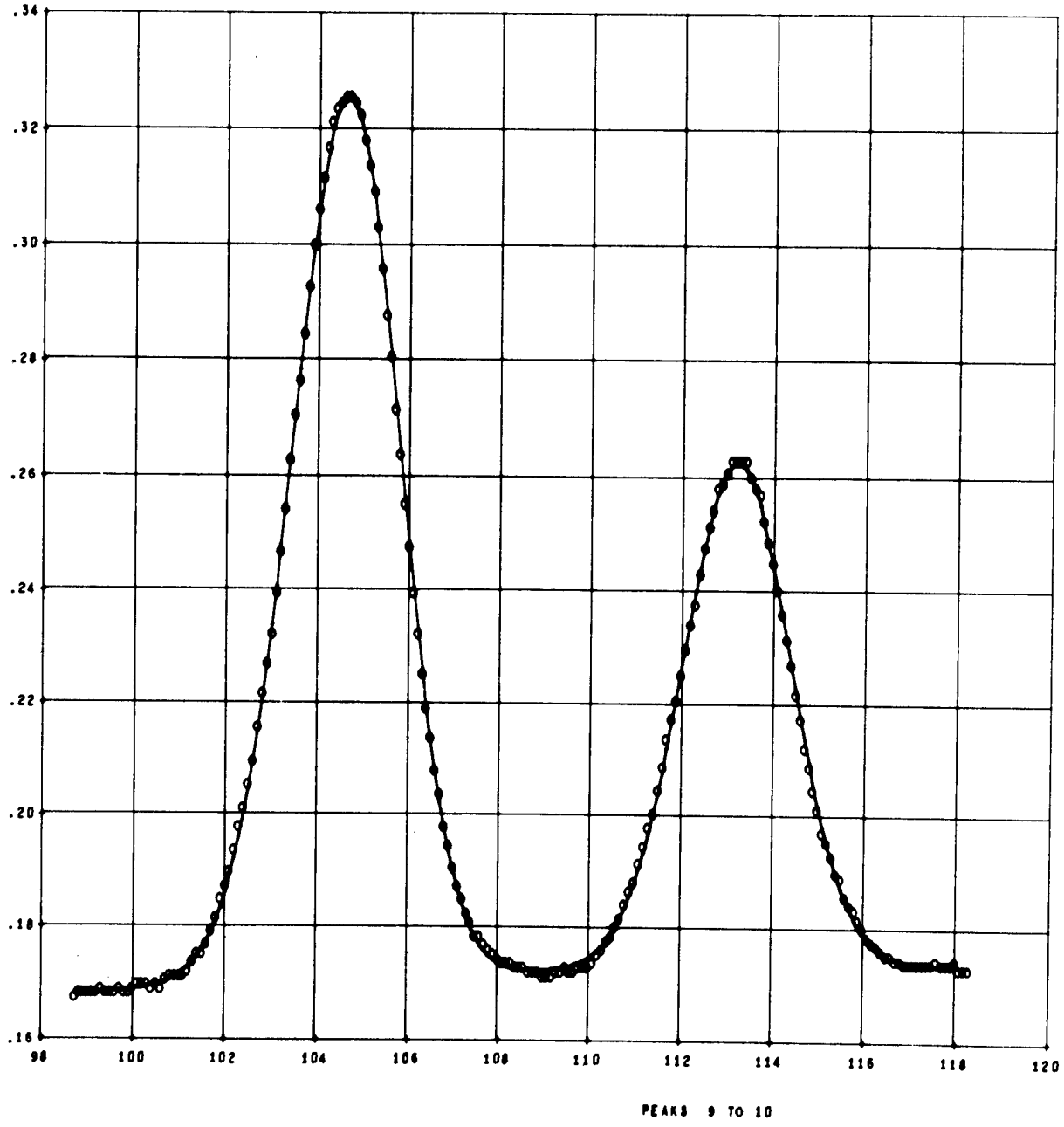

Fig. 6. Peaks 9 and 10 (440 mμ): glutamate and proline.

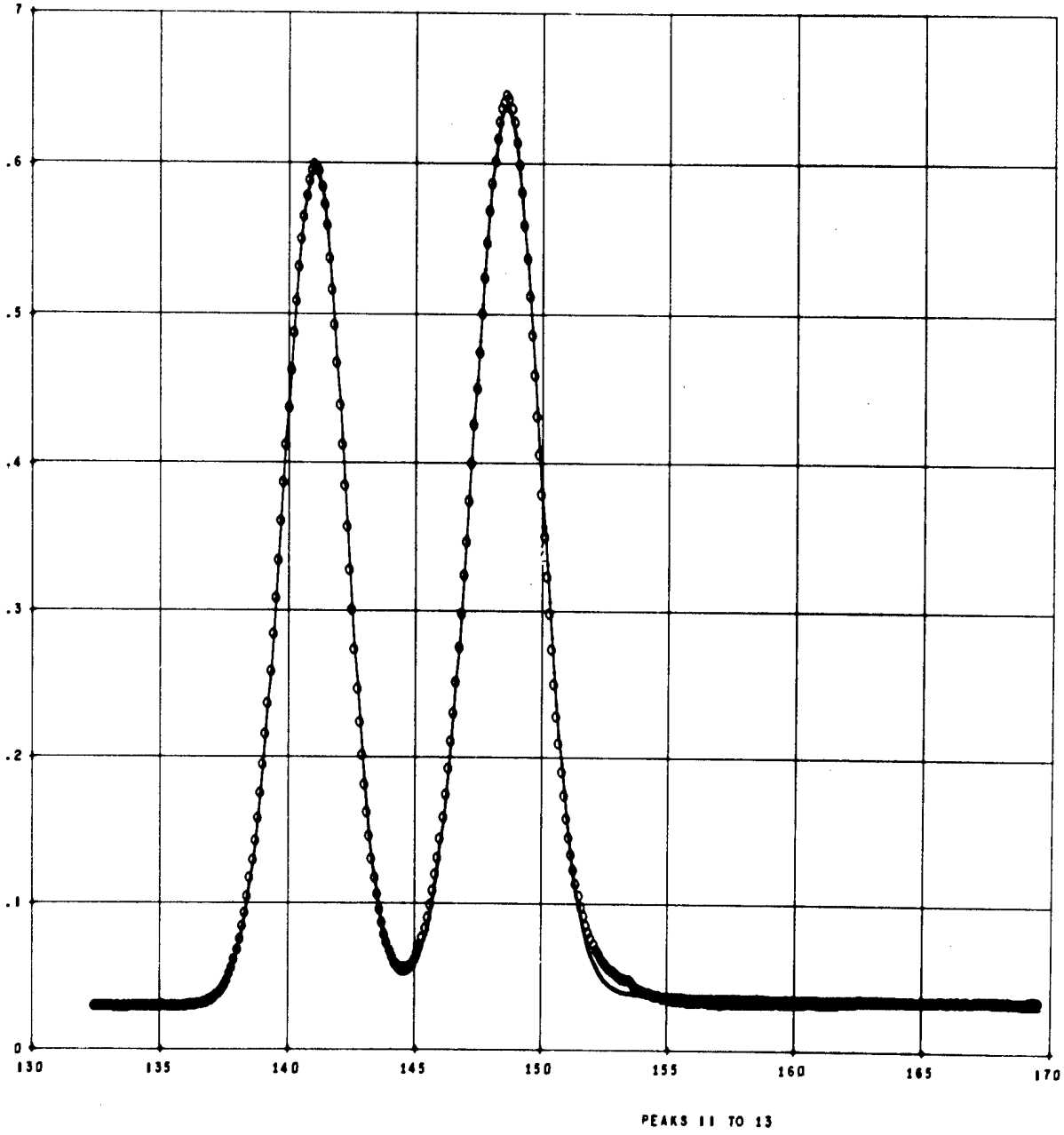

Fig. 7. Peaks 11 to 13: glycine, alanine, and half-cystine.

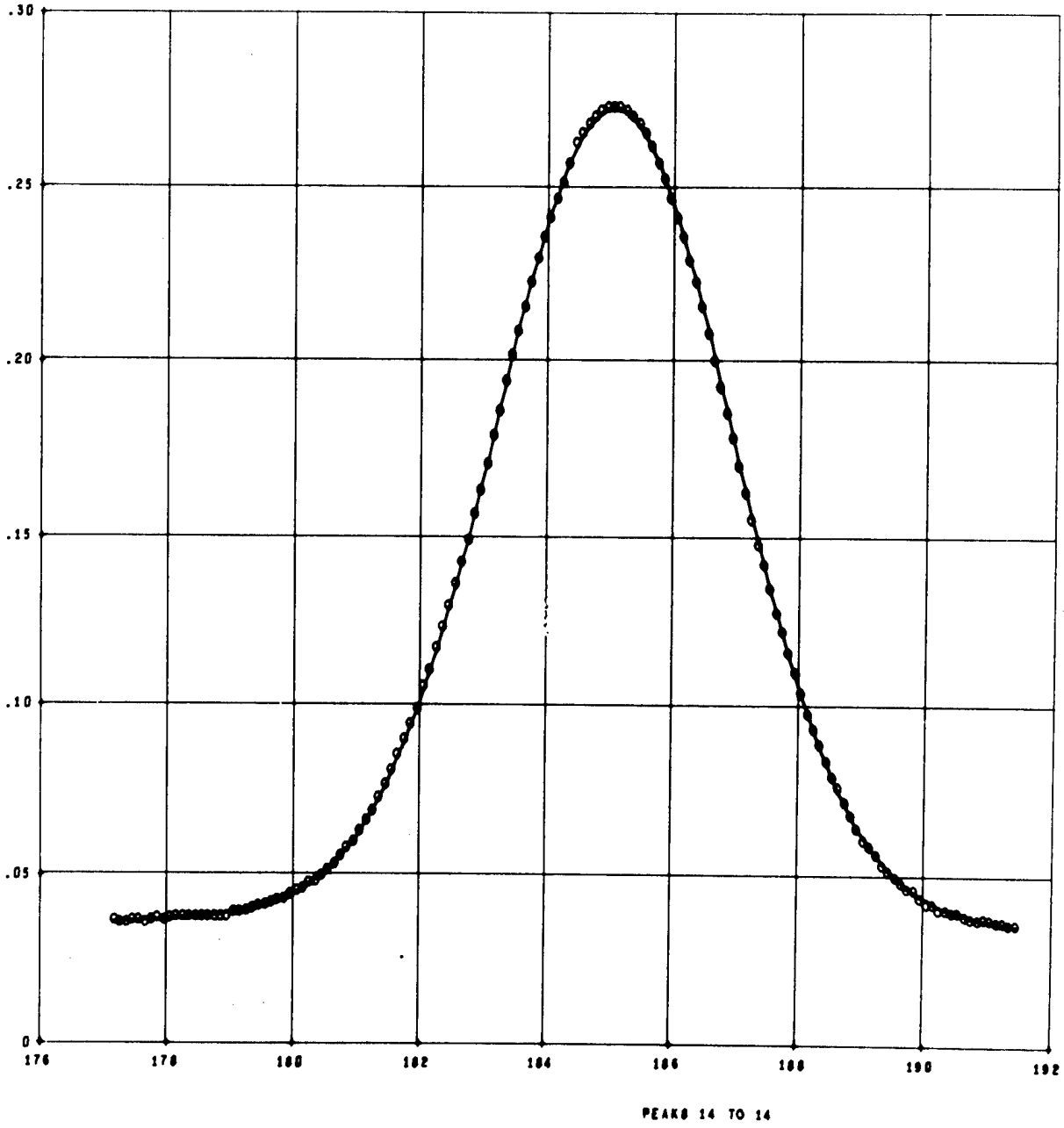

Fig. 8. Peak 14: valine.

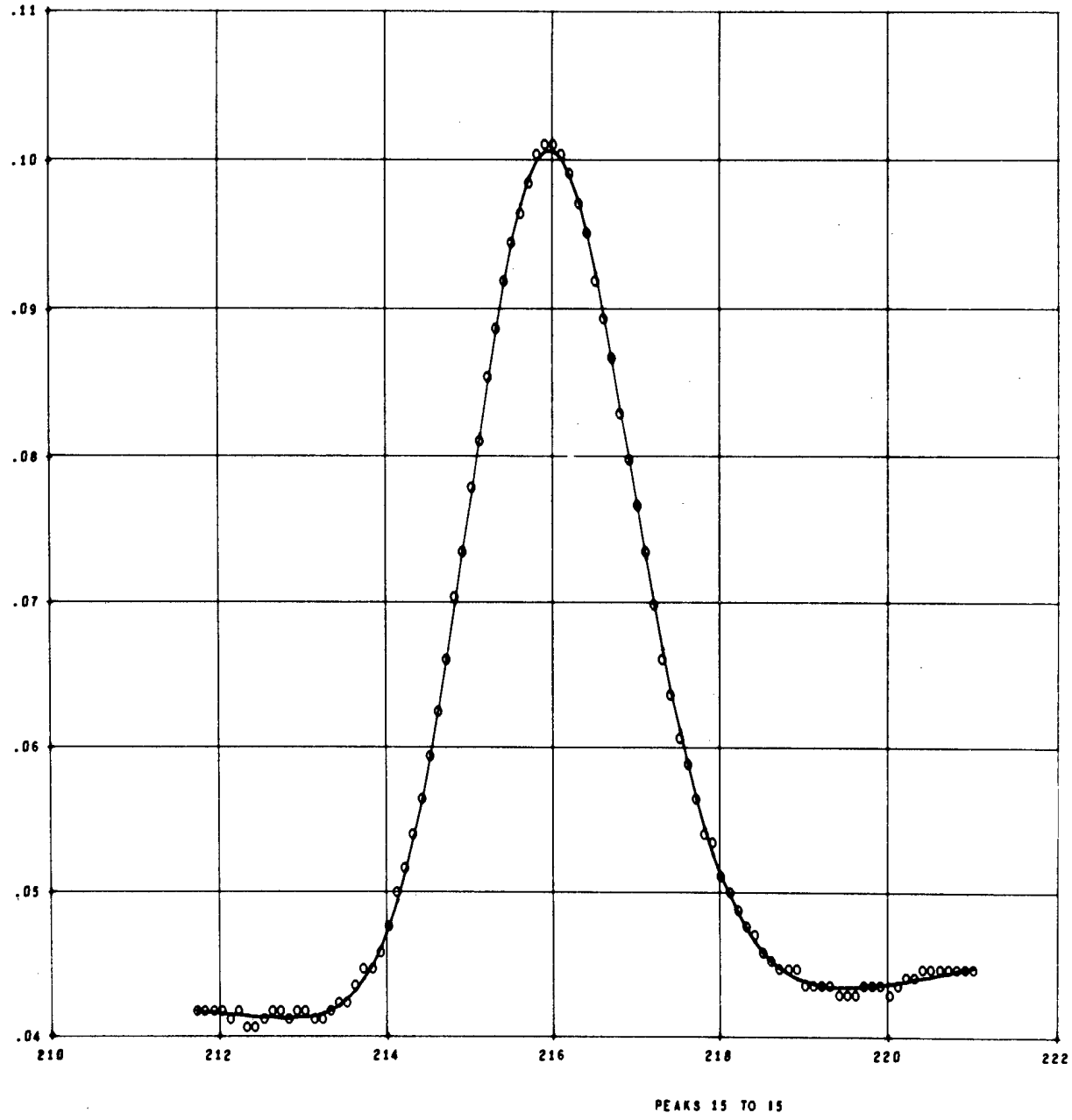

Fig. 9. Peak 15: methionine.

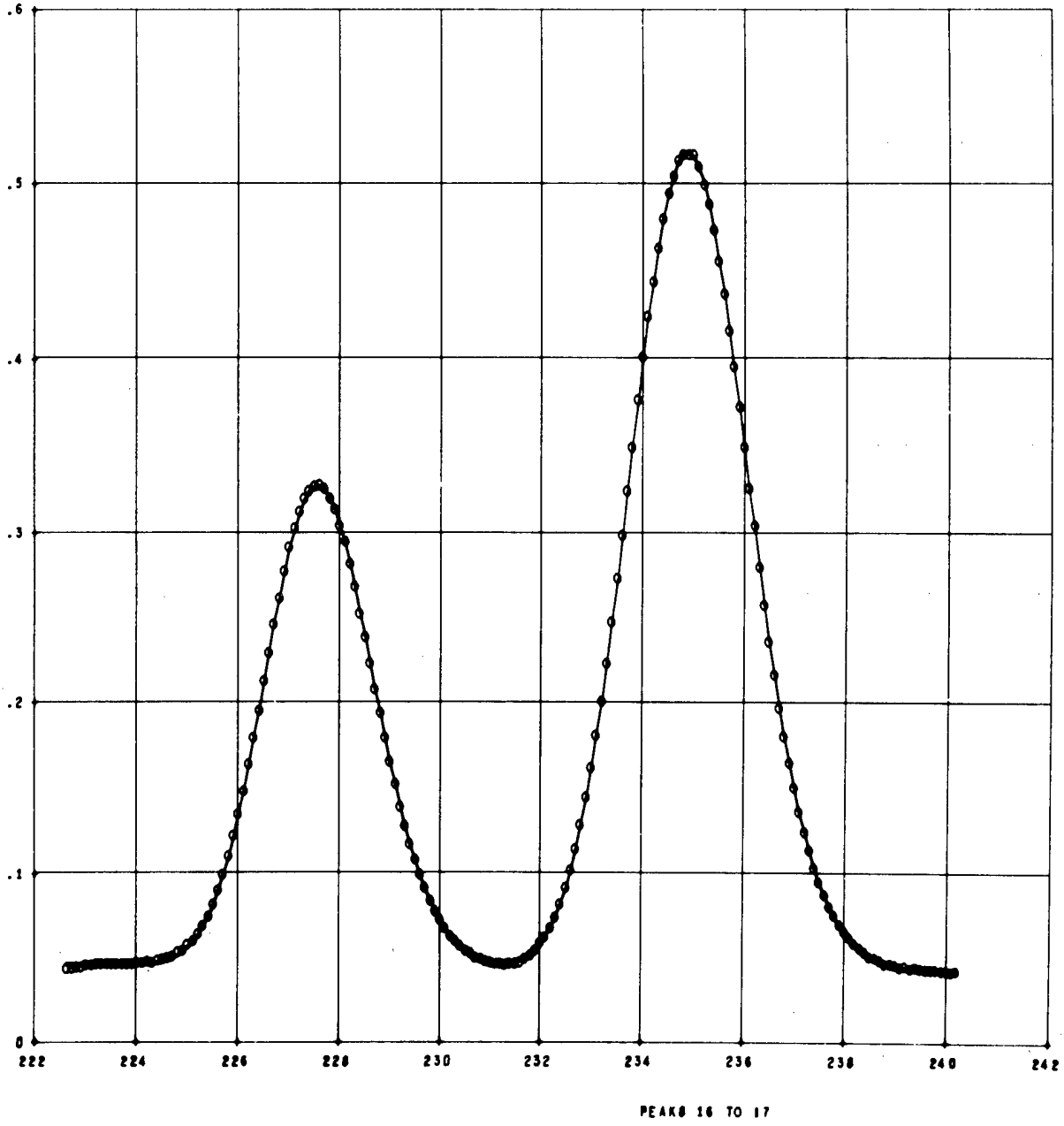

Fig. 10. Peaks 16 and 17: isoleucine and leucine.

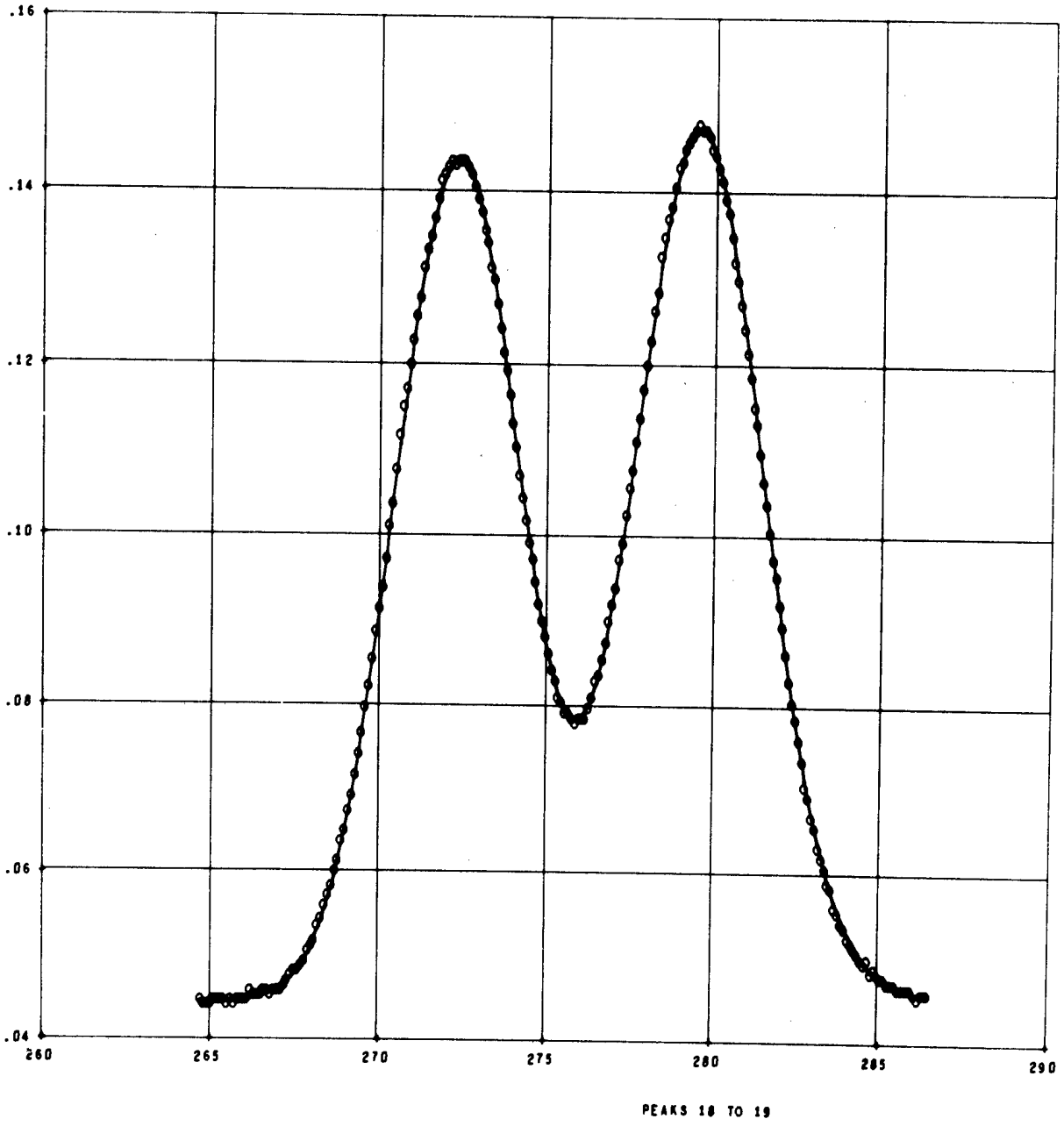

Fig. 11. Peaks 18 and 19: tyrosine and phenylalanine.

BIOPHYSICS SECTION

PUBLICATIONS AND ABSTRACTS OF MANUSCRIPTS SUBMITTED

SOME BIOLOGICAL ASPECTS OF RADIOACTIVE MICROSPHERES, W. H. Langham, C. R. Richmond, J. C. Hensley, P. N. Dean, and M. A. Van Dilla. Los Alamos Scientific Laboratory Report LA-3365-MS (August 23, 1965).

Abstracted in Los Alamos Scientific Laboratory Report LA-3432-MS (1965), p. 128.

COMPUTER REDUCTION OF METABOLIC DATA OBTAINED FROM SCINTILLATION COUNTERS, P. N. Dean. Los Alamos Scientific Laboratory Report LA-3298 (November 15, 1965).

Abstracted in Los Alamos Scientific Laboratory Report LA-3432-MS (1965), p. 128.

ELECTRONIC SEPARATION OF BIOLOGICAL CELLS BY VOLUME, M. J. Fulwyler. Science 150(3698), 910-911 (1965).

Abstracted in Los Alamos Scientific Laboratory Report LA-3432-MS (1965), p. 129.

AUTOMATIC DATA ACQUISITION, REDUCTION AND ANALYSIS, P. N. Dean and C. R. Richmond. In Radioisotope Sample Measurement Techniques in Medicine and Biology, International Atomic Energy Agency, Vienna (1965), pp. 139-168.

Abstracted in Los Alamos Scientific Laboratory Report LA-3432-MS (1965), p. 127.

COMPUTER ANALYSIS OF CELL VOLUME DISTRIBUTIONS, P. N. Dean. Los Alamos Scientific Laboratory Report LA-3440 (February 7, 1966).

Two computer programs have been written to analyze cell volume distributions measured with a Coulter type of cell spectrometer. One of the programs, called AVØL, is used to calculate the mean cell volume of any type of distribution and to plot the data in various formats. The other program, called CELVØL, uses an iterative least-squares technique to fit either normal, log-normal, or skewed-normal distributions to the data. Either single- or double-peak distributions can be fitted. The program also converts the results of the fit to cell concentration in each peak in cells per cubic millimeter, standard deviation in cubic microns, and mean cell volume in cubic microns. For red blood cells the mean cell volume is also calculated from the hematocrit and included in the data output listing.

ISOLATION OF NORMAL AND ABNORMAL CIRCULATING CELLS BY AN ELECTRONIC PARTICLE SEPARATOR, I. U. Boone, M. J. Fulwyler, and M. W. Stewart. Proceedings of the American Association for Cancer Research 7, 8 (April 1966), 57th Annual Meeting, Denver, Colorado. Abstract No. 28.

Separation of discrete cellular fractions of normal and abnormal WBC and abnormal circulating cells on the basis of cell volume has been undertaken using an electronic particle separator (Fulwyler, Science 150:910, 1965). Cell volume distribution is first obtained using a modified Coulter aperture, and cells are subsequently isolated in droplets of suspending medium which are charged and deflected according to sensed volume. Circulating normal WBC were separated into lymphocyte-, granulocyte- and monocyte-rich fractions. Mononuclear cells from patients with infectious mononucleosis were separated into four distinct fractions and subsequently lymphocytes from at least two fractions cultured in artificial medium. Viability of separated cells was proven by obtaining chromosomes with usual techniques used in cultured cells. The technique has been further extended to isolation and concentration of large abnormal hematopoietic elements and cancer cells from peripheral blood of a patient with terminal neuroblastoma.

THE CELL SEPARATOR -- DESIGN AND USAGE, M. J. Fulwyler. Radiation Res. 27, 501 (1966). Abstract No. Ca-4.

An electronic device has been developed that is capable of separating particles (suspended in a conducting liquid) on the basis of volume. Particle volume is sensed by a Coulter aperture. The suspension is ejected from a nozzle as a fluid jet and is uniformly broken into droplets by high frequency vibrations produced by a piezoelectric crystal. It takes 250 μsec for a particle to travel from the volume-sensing point to the jet separation point, where it is caught in a forming droplet. At the time of formation droplets are given an electric charge predetermined from the measured volume of the contained particle. The charged droplets pass through an electrostatic field and are deflected in proportion to their charge. The deflected droplets are collected in a series of vessels.

Volume fractions of mouse lymphoma cells randomly growing in suspension culture have been separated, and mixtures of chicken and human red blood cells have been quantitatively separated. Volume fractions have been isolated from normal human white blood cells and from white blood cells found in disease states such as leukemia and infectious mononucleosis. Application is being made to bone marrow cytology using mice. Tests with Chinese hamster ovary cells showed 98 percent viability and normal growth rate after passing through the device.

The separation principle may be extensible to the separation of particles on the basis of any electronically measurable property such as ultraviolet absorption or fluorescence. We are investigating such sensors.

ERYTHROCYTE VOLUME DISTRIBUTION DURING RECOVERY FROM RADIATION-INDUCED BONE MARROW ARREST, M. A. Van Dilla and J. F. Spalding. Nature (in press).

It has been shown that macrocytosis follows erythropoietic stimulation by phenylhydrazine anemia, bleeding, or administration of erythropoietin. Here we report that bone marrow arrest induced by whole-body radiation also produces a similar macrocytosis in mice. It was observed in the course of the experiment that the volume of mouse red cells decreases as they age.

VOLUME DISTRIBUTION AND SEPARATION OF NORMAL HUMAN LEUCOCYTES, M. A. Van Dilla, M. J. Fulwyler, and I. U. Boone. Science (submitted).

The volume distribution of human leucocytes has been obtained using a modification of the Coulter counter. The position of lymphocytes, granulocytes, and monocytes within this distribution has been determined by morphological examination following isolation of cell groups of desired volume with an electronic cell separator.